

THE ENANTIOSELECTIVE SYNTHESIS OF 2-INDOLYL-1-NITRO
DERIVATIVES AND BODIPY DYES IN THE PRESENCE OF CHIRAL
BIFUNCTIONAL SQUARAMIDE ORGANOCATALYSTS

A THESIS SUBMITTED TO
THE GRADUATE SCHOOL OF NATURAL AND APPLIED SCIENCES
OF
MIDDLE EAST TECHNICAL UNIVERSITY

BY

ESRA DÜNDAR

IN PARTIAL FULFILLMENT OF THE REQUIREMENTS
FOR
THE DEGREE OF DOCTOR OF PHILOSOPHY
IN
CHEMISTRY

AUGUST 2022

Approval of the thesis:

**THE ENANTIOSELECTIVE SYNTHESIS OF 2-INDOLYL-1-NITRO
DERIVATIVES AND BODIPY DYES IN THE PRESENCE OF CHIRAL
BIFUNCTIONAL SQUARAMIDE ORGANOCATALYSTS**

submitted by **ESRA DÜNDAR** in partial fulfillment of the requirements for the degree of **Doctor of Philosophy in Chemistry, Middle East Technical University** by,

Prof. Dr. Halil Kalıpçılar
Dean, Graduate School of **Natural and Applied Sciences**

Prof. Dr. Özdemir Doğan
Head of the Department, **Chemistry**

Prof. Dr. Cihangir Tanyeli
Supervisor, **Chemistry, METU**

Examining Committee Members:

Prof. Dr. Özdemir Doğan
Chemistry, METU

Prof. Dr. Cihangir Tanyeli
Chemistry, METU

Prof. Dr. Adnan Bulut
Chemistry, Kırıkkale University

Assoc. Prof. Dr. Yunus Emre Türkmen
Chemistry, Bilkent University

Assoc. Prof. Dr. Salih Özçubukçu
Chemistry, METU

Date: 08.08.2022

I hereby declare that all information in this document has been obtained and presented in accordance with academic rules and ethical conduct. I also declare that, as required by these rules and conduct, I have fully cited and referenced all material and results that are not original to this work.

Name Last name : Esra Dündar

Signature :

ABSTRACT

THE ENANTIOSELECTIVE SYNTHESIS OF 2-INDOLYL-1-NITRO DERIVATIVES AND BODIPY DYES IN THE PRESENCE OF CHIRAL BIFUNCTIONAL SQUARAMIDE ORGANOCATALYSTS

Dündar, Esra
Doctor of Philosophy, Chemistry
Supervisor: Prof. Dr. Cihangir Tanyeli

August 2022, 163 pages

In our research group, chiral bifunctional squaramides with different basic units have been synthesized and evaluated in various asymmetric reactions. To test the catalytic activity of organocatalysts, Friedel-Crafts alkylation of indoles with nitroolefins was selected as a model reaction in the first part of the study. 19 different 2-indolyl-1-nitro derivatives were synthesized with up to >99% ee in the presence of sterically encumbered *tert*-butyl substituted squaramide/quinine. Besides, 2-adamantyl squaramide/quinine was evaluated in the addition of BODIPY core to isatin derivatives which will be the *first example* of this kind of enantioselective addition in literature. 6 novel chiral BODIPY dyes were synthesized with up to 60% ee, and their spectroscopic and chiroptical properties were investigated. In the final chapter, a point chiral at boron and carbon BODIPY was synthesized with a two-pot, one-step synthesis-an interrupted Knoevenagel condensation. ECD spectra of the dye showed a strong Cotton effect in the visible region. However, this dye showed weak fluorescence emission due to partly vibrational relaxations and bent-shaped molecular geometry.

Keywords: Enantioselective Synthesis, Organocatalysis, Friedel-Crafts Alkylation,
BODIPY Dyes, Squaramides

ÖZ

2-İNDOLİL-1-NİTRO TÜREVLERİNİN VE BODIPY BOYALARININ KİRAL BİFONKSİYONEL SKUARAMİT ORGANOKATALİZÖRLER İLE ENANTİYOSEÇİCİ SENTEZİ

Dündar, Esra
Doktora, Kimya
Tez Yöneticisi: Prof. Dr. Cihangir Tanyeli

Ağustos 2022, 163 sayfa

Araştırma grubumuzda, farklı bazik birimlere sahip kiral bifonksiyonel skuaramitler sentezlenmiş ve çeşitli asimetrik reaksiyonlarda değerlendirilmiştir. Bu organokatalizörlerin katalitik aktivitesini test etmek için, çalışmanın ilk kısmında, indollerin nitroolefinlerle Friedel-Crafts alkilasyonu model reaksiyon olarak seçilmiştir. 19 farklı 2-indolil-1-nitro türevi, *tert*-bütil skuaramit/kinin varlığında >99% enantiyoseçicilik ile sentezlenmiştir. Ayrıca, 2-adamantil skuaramit/kinin, literatürde bu tarz enantiyoseçici katılmanın ilk örneği olacak olan BODIPY yapısının isatin türevlerine katılmasında değerlendirilmiştir. 6 özgün kiral BODIPY boyası 60% enantiyoseçicilik ile sentezlenmiştir ve bu boyaların spektroskopik ve kayroptik özellikleri araştırılmıştır. Son bölümde, bor ve karbonda kiral merkezleri olan BODIPY tek step-yarıda kesilmiş Knoevenagel yoğunlaşması ile sentezlenmiştir. Boyanın ECD spektrumu görünür bölgede güçlü Cotton etkisi göstermiştir. Bununla birlikte, bu boya, kısmen titreşimli gevşemeler ve bükülmüş şekilli moleküler geometri nedeniyle zayıf floresan emisyonu göstermiştir.

Anahtar Kelimeler: Enantiyoseçici Sentez, Organokatalizör, Friedel-Crafts Alkilasyonu, BODIPY Boyaları, Skuaramitler

"Kadınlarımız için asıl mücadele alanı, asıl zafer kazanılması gereken alan, biçim ve kılıkta başarıdan çok; ışıkla, bilgi ve kültürle, gerçek faziletle süslenip donanmaktır."

Mustafa Kemal ATATÜRK
Saygı ve özlemle...

ACKNOWLEDGMENTS

Ph.D. has been a major part of my life, and coming to end will be a milestone. During this long journey, I have so many great people around me; now the time is gratitude.

Firstly, I would like to express my deepest gratitude to my supervisor Prof. Dr. Cihangir Tanyeli, for his support, encouragement, guidance, and motivation during this study and the about life. He is a second father to me because I have felt at home all the time since I became a member of Tanyeli's research group. I will be extremely grateful for giving me a chance to work with him in this kind of environment.

A very special thanks goes to Assoc. Prof. Dr. Murat Işık for involving me in the collaboration study and for his guidance and encouragement. He had a great contribution to this study because I have learned much valuable information about BODIPY structures from him. I am also grateful for both academic and non-academic support.

I would like to thank my thesis monitoring committee members, Prof. Dr. Özdemir Doğan and Assoc. Prof. Dr. Yunus Emre Türkmen for their feedback, suggestions, and their time throughout this study. Also, I would like to thank Prof. Dr. Adnan Bulut and Assoc. Prof. Dr. Salih Özçubukçu for their time and comments about this thesis.

I share most of my time with all Tanyeli group members with former and older ones. I am very grateful to all of them. Among them, one of my favorite person is Zeynep Dilşad Susam. She is my companion on this journey, and she is also one of my best friends. So, I am extremely grateful for her friendship, help, support, and any contribution to my study as well as my life. Also, I would like to express my great thanks to Ezgi Bayer Kömüşdoğan for her close and intimate friendship. She was always there for anything I need. Besides, a special thank you goes to all D-254 members.

During this study, I conduct many analyses, and there were great people for helping me with the analyses and the instruments. The first person I would like to thank is also a nice friend, Perhan Öztürk Düzenli, for CD measurements and discussions about analyses. She is also one of my close friends from the department and organic laboratory. Also, I would like to thank Elif Demir Arabacı for helping with CV and DPV analyses, Güzide Aykent for conducting LC-MS analysis, and Mehrdad Forough for teaching me to calculate the fluorescence quantum yield.

I am also grateful to specifically the 3rd floor of D-block and also all members of the department for sharing everything, including chemicals, glassware, and instruments. Also, Leyla Sevindik, Mehmet Dede, Eda Durkan and Şaban Geliş are the great people who finds solutions to my problems all the time.

I would like to thank Zeynep Erdoğan (UNAM) for HRMS experiments and TÜBİTAK for all the financial support (217Z035 and 120Z951).

Apart from the department, I have so many great friends which supported me all the time. A very special thank you goes to Günnur and Serkan Ekinci for their great friendship, support, encouragement, and motivation since we became friends. Also, I am also thankful to Ayşegül Hisar Telli and Nurdan Öney for their close and intimate friendship as well as moral support during this study.

I would like to thank my two families, Kanberoğlu and DüNDAR, for their support and pray all the time. Another special thank you to my sisters Kübra and Büşra as well as my brother Mahmut Can. I am so glad to have them in my life.

In the last, the biggest and special thank you for my dear husband, Dr. Semih Alper DüNDAR. He witnessed all stages of my Ph.D. from proficiency exam to conducting experiments and also writing thesis. He was always by my side whenever I need. Not only he came with me to the library to study but also, he helped me making a column chromatography. He had so much contribution to this study Also, he believed in me, supported and motivated me all the time. I am extremely grateful for his presence.

TABLE OF CONTENTS

ABSTRACT.....	v
ÖZ	vii
ACKNOWLEDGMENTS.....	x
TABLE OF CONTENTS	xii
LIST OF TABLES	xv
LIST OF FIGURES	xvi
LIST OF SCHEMES	xxii
LIST OF ABBREVIATIONS	xxiv
CHAPTERS	
1 INTRODUCTION.....	1
1.1 The Organocatalysis in Asymmetric Synthesis.....	1
1.1.1 Bifunctional Organocatalysis	4
1.1.2 Squaramides in Bifunctional Organocatalysis.....	4
1.2 Friedel-Crafts Alkylation Reactions.....	10
1.2.1 Enantioselective Friedel-Crafts Alkylation of Indole with Nitroolefins	11
1.2.2 The Importance of 2-Indolyl-1-nitro Derivatives.....	13
1.3 Fluorescence Spectroscopy.....	15
1.3.1 BODIPY Dyes as Fluorescent Compounds.....	16
1.4 The Aim of the Study	23
2 RESULTS and DISCUSSION	27
2.1 The Synthesis of 2-AminoDMAP and Quinine Based Bifunctional Squaramide Organocatalysts	27
2.2 Evaluation of Bifunctional Organocatalysts in the Friedel-Crafts Alkylation of Indoles 33 with Nitroolefins 16.....	29
2.2.1 Optimization Studies	29
2.2.2 Scope of Friedel-Crafts Alkylation	33

2.3 Evaluation of Bifunctional Organocatalysts in the Enantioselective Addition of BODIPYs to Isatins.....	37
2.3.1 Synthesis of Starting Materials	37
2.3.2 Optimization Studies for Enantioselective Addition of BODIPYs to Isatins	38
2.3.3 Scope of Enantioselective Addition of BODIPYs to Isatins	43
2.3.4 Spectroscopic and Chiroptical Properties	45
2.4 Synthesis of Novel BODIPY Chiral at Boron and Carbon.....	49
2.4.1 Spectroscopic Properties	53
2.4.2 Resolution of BODIPY 96	56
2.4.3 Chiroptical and Electrochemical Properties of BODIPY 96	58
2.4.4 Stability Tests.....	60
3 EXPERIMENTAL	63
3.1 Materials and Methods.....	63
3.2 General Procedure for Friedel-Crafts Alkylation of Indoles 33 with Nitroolefins 16	64
3.2.1 Synthesis of 3-(2-nitro-1-phenylethyl)-1H-indole 34aa	65
3.2.2 Synthesis of 3-(1-(4-methoxyphenyl)-2-nitroethyl)-1H-indole 34ab	66
3.2.3 Synthesis of 3-(2-nitro-1-(p-tolyl)ethyl)-1H-indole 34ac	66
3.2.4 Synthesis of 3-(1-(4-chlorophenyl)-2-nitroethyl)-1H-indole 34ad	67
3.2.5 Synthesis of 3-(1-(4-bromophenyl)-2-nitroethyl)-1H-indole 34ae	67
3.2.6 Synthesis of 3-(1-(furan-2-yl)-2-nitroethyl)-1H-indole 34af	68
3.2.7 Synthesis of 3-(2-nitro-1-(thiophen-2-yl)ethyl)-1H-indole 34ag.....	68
3.2.8 Synthesis of 3-(1-(2-chlorophenyl)-2-nitroethyl)-1H-indole 34ah.....	69
3.2.9 Synthesis of 3-(1-(2-methoxyphenyl)-2-nitroethyl)-1H-indole 34ai	69
3.2.10 Synthesis of 3-(1-(3-bromophenyl)-2-nitroethyl)-1H-indole 34aj.....	70
3.2.11 Synthesis of 3-(1-(3-methoxyphenyl)-2-nitroethyl)-1H-indole 34ak	70
3.2.12 Synthesis of 3-(1-(2,4-dichlorophenyl)-2-nitroethyl)-1H-indole 34al.....	71
3.2.13 Synthesis of 3-(1-(2,5-dimethoxyphenyl)-2-nitroethyl)-1H-indole 34am ...	72
3.2.14 Synthesis of 3-(1-(2-(benzyloxy)phenyl)-2-nitroethyl)-1H-indole 34an.....	72
3.2.15 Synthesis of 5-(benzyloxy)-3-(2-nitro-1-phenylethyl)-1H-indole 34ba	73

3.2.16 Synthesis of 7-(benzyloxy)-3-(2-nitro-1-phenylethyl)-1H-indole 34ca.....	74
3.2.17 Synthesis of 7-bromo-3-(2-nitro-1-phenylethyl)-1H-indole 34da.....	74
3.2.18 Synthesis of 3-(1-(4-methoxyphenyl)-2-nitroethyl)-1-methyl-1H-indole 34eb	75
3.2.19 Synthesis of 2-(2-nitro-1-phenylethyl)-1H-pyrrole 86.....	75
3.3 Synthesis of BODIPYs 53	76
3.4 General Procedure for Addition of BODIPYs 53 to Isatin Derivatives 72	78
3.4.1 Synthesis of chiral BODIPY 73aa.....	78
3.4.2 Synthesis of chiral BODIPY 73ab.....	79
3.4.3 Synthesis of chiral BODIPY 73ac	80
3.4.4 Synthesis of chiral BODIPY 73ad.....	80
3.4.5 Synthesis of chiral BODIPY 73ae	81
3.4.6 Synthesis of chiral BODIPY 73be.....	82
3.5 Procedure for Synthesis of BODIPY 96.....	83
3.5.1 The reaction intermediate 95	84
3.6 The experimental calculation of fluorescence quantum yield.....	84
4 CONCLUSION	87
REFERENCES	89
APPENDICES	
A. NMR SPECTRA.....	97
B. HPLC CHROMATOGRAMS	126
C. HRMS DATA	156
D. X-RAY DATA	160
CURRICULUM VITAE	163

LIST OF TABLES

TABLES

Table 1. Catalyst and Catalyst Loading Screening ^a	30
Table 2. Solvent Screening ^a	32
Table 3. Additional Screening ^a	33
Table 4. Derivatization Study ^a	34
Table 5. Catalyst Screening ^a	39
Table 6. Solvent Screening ^a	40
Table 7. Concentration Screening and Catalyst Loading ^a	42
Table 8. Derivatization Study ^a	44
Table 9. Optical characterization of BODIPY 96 in various solvents	54
Table 10. Electrochemical Properties of BODIPY 96	60

LIST OF FIGURES

FIGURES

Figure 1. Representative examples of chiral amines	3
Figure 2. Examples of hydrogen-bonding catalysts	3
Figure 3. Ditopic binding (left) and H-bonding patterns (right) in squaramides	5
Figure 4. Resonance structures of thio(urea) and squaramides	6
Figure 5. The distance between N-H (left) & convergent orientation of N-H (right)	6
Figure 6. Activation of different functional groups by squaramides.....	7
Figure 7. Chiral bifunctional 2-aminoDMAP/squaramides	8
Figure 8. Chiral bifunctional quinine/squaramides 28-30	9
Figure 9. 2-indolyl-1-nitro intermediates 41	14
Figure 10. Examples of THBCs and Tryptamines	15
Figure 11. IUPAC numbering for compounds 45, 46 & 47	16
Figure 12. Functionalization of BODIPY core.....	17
Figure 13. Chiral BODIPYs containing chiral carbon atoms.....	20
Figure 14. Optically active BODIPYs linked with optically active molecules	20
Figure 15. Axially-chiral BODIPYs	21
Figure 16. ¹ H NMR Spectrum of compound 73aa	43
Figure 17. UV-vis absorption spectra of BODIPY 53a , <i>N</i> -Me isatin 72a , and BODIPY 73aa	46
Figure 18. UV-vis absorption and fluorescence emission spectra of 73aa (2μM). 46	
Figure 19. Comparison of quantum yields of 73aa and fluorescein	47
Figure 20. UV-vis absorption spectra of derivatives 73	47
Figure 21. Fluorescence emission spectra of derivatives 73	48
Figure 22. ECD spectra of 73aa in different concentrations	49
Figure 23. ¹ H NMR Spectrum of BODIPY 96 in CDCl ₃	51
Figure 24. LC-MS analysis at t ₁ : 1 min	52
Figure 25. LC-MS analysis at t ₁ : 60 min	52

Figure 26. Proposed reactive intermediate.....	53
Figure 27. Spectroscopic analyses of BODIPY 96	54
Figure 28. X-Ray Structure of BODIPY 96	56
Figure 29. The separation of enantiomers of BODIPY 96 on chiral HPLC.....	57
Figure 30. The HPLC chromatogram of fast-eluting enantiomer.....	57
Figure 31. The HPLC chromatogram of slow-eluting enantiomer.....	57
Figure 32. ECD and UV spectra of enantiomers of BODIPY 96	59
Figure 33. CV (left) and DPV (right) of BODIPY 96	59
Figure 34. LC-MS analysis after TFA addition.....	61
Figure 35. Time-dependent fluorescence intensity profile of BODIPY 96	61
Figure A. 1. ¹ H NMR spectrum of 34aa	97
Figure A. 2. ¹³ C NMR spectrum of 34aa	97
Figure A. 3. ¹ H NMR spectrum of 34ab	98
Figure A. 4. ¹³ C NMR spectrum of 34ab	98
Figure A. 5. ¹ H NMR spectrum of 34ac	99
Figure A. 6. ¹³ C NMR spectrum of 34ac	99
Figure A. 7. ¹ H NMR spectrum of 34ad	100
Figure A. 8. ¹³ C NMR spectrum of 34ad	100
Figure A. 9. ¹ H NMR spectrum of 34ae	101
Figure A. 10. ¹³ C NMR spectrum of 34ae	101
Figure A. 11. ¹ H NMR spectrum of 34af	102
Figure A. 12. ¹³ C NMR spectrum of 34af	102
Figure A. 13. ¹ H NMR spectrum of 34ag	103
Figure A. 14. ¹³ C NMR spectrum of 34ag	103
Figure A. 15. ¹ H NMR spectrum of 34ah	104
Figure A. 16. ¹³ C NMR spectrum of 34ah	104
Figure A. 17. ¹ H NMR spectrum of 34ai	105
Figure A. 18. ¹³ C NMR spectrum of 34ai	105
Figure A. 19. ¹ H NMR spectrum of 34aj	106
Figure A. 20. ¹³ C NMR spectrum of 34aj	106

Figure A. 21. ^1H NMR spectrum of 34ak	107
Figure A. 22. ^{13}C NMR spectrum of 34ak	107
Figure A. 23. ^1H NMR spectrum of 34al	108
Figure A. 24. ^{13}C NMR spectrum of 34al	108
Figure A. 25. ^1H NMR spectrum of 34am	109
Figure A. 26. ^{13}C NMR spectrum of 34am	109
Figure A. 27. ^1H NMR spectrum of 34an	110
Figure A. 28. ^{13}C NMR spectrum of 34an	110
Figure A. 29. ^1H NMR spectrum of 34ba	111
Figure A. 30. ^{13}C NMR spectrum of 34ba	111
Figure A. 31. ^1H NMR spectrum of 34ca	112
Figure A. 32. ^{13}C NMR spectrum of 34ca	112
Figure A. 33. ^1H NMR spectrum of 34da	113
Figure A. 34. ^{13}C NMR spectrum of 34da	113
Figure A. 35. ^1H NMR spectrum of 34eb	114
Figure A. 36. ^{13}C NMR spectrum of 34eb	114
Figure A. 37. ^1H NMR spectrum of 86	115
Figure A. 38. ^{13}C NMR spectrum of 86	115
Figure A. 39. ^1H NMR spectrum of 73aa	116
Figure A. 40. ^{13}C NMR spectrum of 73aa	116
Figure A. 41. ^1H NMR spectrum of 73ab	117
Figure A. 42. ^{13}C NMR spectrum of 73ab	117
Figure A. 43. ^1H NMR spectrum of 73ac	118
Figure A. 44. ^{13}C NMR spectrum of 73ac	118
Figure A. 45. ^1H NMR spectrum of 73ad	119
Figure A. 46. ^{13}C NMR spectrum of 73ad	119
Figure A. 47. ^1H NMR spectrum of 73ae	120
Figure A. 48. ^{13}C NMR spectrum of 73ae	120
Figure A. 49. ^1H NMR spectrum of 73be	121
Figure A. 50. ^{13}C NMR spectrum of 73be	121

Figure A. 51. ^1H NMR spectrum of 95	122
Figure A. 52. ^{13}C NMR spectrum of 95	122
Figure A. 53. ^1H NMR spectrum of BODIPY 96	123
Figure A. 54. ^{13}C NMR spectrum of BODIPY 96	123
Figure A. 55. ^1H - ^1H COSY NMR spectrum of BODIPY 96	124
Figure A. 56. HMBC NMR spectrum of BODIPY 96	124
Figure A. 57. HSQC NMR spectrum of BODIPY 96	125
Figure B. 1. HPLC chromatogram of <i>rac</i> - 34aa	126
Figure B. 2. HPLC chromatogram of enantiomerically enriched 34aa	126
Figure B. 3. HPLC chromatogram of <i>rac</i> - 34ab	127
Figure B. 4. HPLC chromatogram of enantiomerically enriched 34ab	127
Figure B. 5. HPLC chromatogram of <i>rac</i> - 34ac	128
Figure B. 6. HPLC chromatogram of enantiomerically enriched 34ac	128
Figure B. 7. HPLC chromatogram of <i>rac</i> - 34ad	129
Figure B. 8. HPLC chromatogram of enantiomerically enriched 34ad	129
Figure B. 9. HPLC chromatogram of <i>rac</i> - 34ae	130
Figure B. 10. HPLC chromatogram of enantiomerically enriched 34ae	130
Figure B. 11. HPLC chromatogram of <i>rac</i> - 34af	131
Figure B. 12. HPLC chromatogram of enantiomerically enriched 34af	131
Figure B. 13. HPLC chromatogram of <i>rac</i> - 34ag	132
Figure B. 14. HPLC chromatogram of enantiomerically enriched 34ag	132
Figure B. 15. HPLC chromatogram of <i>rac</i> - 34ah	133
Figure B. 16. HPLC chromatogram of enantiomerically enriched 34ah	133
Figure B. 17. HPLC chromatogram of <i>rac</i> - 34ai	134
Figure B. 18. HPLC chromatogram of enantiomerically enriched 34ai	134
Figure B. 19. HPLC chromatogram of <i>rac</i> - 34aj	135
Figure B. 20. HPLC chromatogram of enantiomerically enriched 34aj	135
Figure B. 21. HPLC chromatogram of <i>rac</i> - 34ak	136
Figure B. 22. HPLC chromatogram of enantiomerically enriched 34ak	136
Figure B. 23. HPLC chromatogram of <i>rac</i> - 34al	137

Figure B. 24. HPLC chromatogram of enantiomerically enriched 34al	137
Figure B. 25. HPLC chromatogram of <i>rac</i> - 34am	138
Figure B. 26. HPLC chromatogram of enantiomerically enriched 34am	138
Figure B. 27. HPLC chromatogram of <i>rac</i> - 34an	139
Figure B. 28. HPLC chromatogram of enantiomerically enriched 34an	139
Figure B. 29. HPLC chromatogram of <i>rac</i> - 34ba	140
Figure B. 30. HPLC chromatogram of enantiomerically enriched 34ba	140
Figure B. 31. HPLC chromatogram of <i>rac</i> - 34ca	141
Figure B. 32. HPLC chromatogram of enantiomerically enriched 34ca	141
Figure B. 33. HPLC chromatogram of <i>rac</i> - 34da	142
Figure B. 34. HPLC chromatogram of enantiomerically enriched 34da	142
Figure B. 35. HPLC chromatogram of <i>rac</i> - 34eb	143
Figure B. 36. HPLC chromatogram of enantiomerically enriched 34eb	143
Figure B. 37. HPLC chromatogram of <i>rac</i> - 86	144
Figure B. 38. HPLC chromatogram of enantiomerically enriched 86	144
Figure B. 39. HPLC chromatogram of <i>rac</i> - 73aa	145
Figure B. 40. HPLC chromatogram of enantiomerically enriched 73aa	145
Figure B. 41. HPLC chromatogram of <i>rac</i> - 73ab	146
Figure B. 42. HPLC chromatogram of enantiomerically enriched 73ab	146
Figure B. 43. HPLC chromatogram of <i>rac</i> - 73ac	147
Figure B. 44. HPLC chromatogram of enantiomerically enriched 73ac	147
Figure B. 45. HPLC chromatogram of <i>rac</i> - 73ad	148
Figure B. 46. HPLC chromatogram of enantiomerically enriched 73ad	148
Figure B. 47. HPLC chromatogram of <i>rac</i> - 73ae	149
Figure B. 48. HPLC chromatogram of enantiomerically enriched 73ae	149
Figure B. 49. HPLC chromatogram of <i>rac</i> - 73be	150
Figure B. 50. HPLC chromatogram of enantiomerically enriched 73be	150
Figure B. 51. HPLC Chromatogram of (-)-BODIPY 96 at 50 °C	151
Figure B. 52. HPLC Chromatogram of (-)-BODIPY 96 at 75 °C	152
Figure B. 53. HPLC Chromatogram of (-)-BODIPY 96 at 100 °C	153

Figure B. 54. HPLC Chromatogram of (-)-BODIPY 96 at 125 °C.....	154
Figure B. 55. HPLC Chromatogram of (-)-BODIPY 96 at 150 °C.....	155
Figure C. 1. Mass Spectrum of 34an	156
Figure C. 2. Mass Spectrum of 34ca	156
Figure C. 3. Mass Spectrum of 34da	157
Figure C. 4. Mass Spectrum of 73aa	157
Figure C. 5. Mass Spectrum of 73ab	157
Figure C. 6. Mass Spectrum of 73ac	158
Figure C. 7. Mass Spectrum of 73ad	158
Figure C. 8. Mass Spectrum of 73ae	158
Figure C. 9. Mass Spectrum of 73be	159
Figure C. 10. Mass Spectrum of 95	159
Figure C. 11. Mass Spectrum of 96	159

LIST OF SCHEMES

SCHEMES

Scheme 1. Diels-Alder reaction catalyzed by imidazolidone organocatalyst 4	1
Scheme 2. The first organocatalytic intermolecular aldol reaction	2
Scheme 3. The first example of bifunctional organocatalysis	4
Scheme 4. The first example of bifunctional squaramide catalyzed Michael addition	5
Scheme 5. The synthesis of bifunctional squaramide	8
Scheme 6. Conjugate addition of dibenzoylmethane (26) to nitroolefins 16	9
Scheme 7. Michael addition of 1-nitropropane (31) to nitroolefins 16	10
Scheme 8. FCA of indoles 33 with nitroolefins 16	11
Scheme 9. FCA of indole (33a) with <i>trans</i> - β -nitrostyrene (16a)	11
Scheme 10. A literature comparison of FCA of indole (33a) with <i>trans</i> - β -nitrostyrene (16a) in organocatalysis	13
Scheme 11. Knoevenagel condensation of BODIPY 48 with 4-(dimethylamino)benzaldehyde (49).....	18
Scheme 12. The synthetic pathways of BODIPY 53a	19
Scheme 13. The enantioselective studies of BODIPY dyes	22
Scheme 14. The purpose of the first chapter of the thesis	24
Scheme 15. The purpose of the second chapter of the thesis.....	24
Scheme 16. The purpose of the third chapter of the thesis	25
Scheme 17. Synthesis of squaramides 78	27
Scheme 18. Synthesis of 2-aminoDMAP/squaramides 23-25	28
Scheme 19. Synthesis of quinine/squaramides 28-30	29
Scheme 20. Pyrrole (85) as an indole derivative in the FCA.....	36
Scheme 21. Proposed transition state for FCA of indole (33a) with <i>trans</i> - β -nitrostyrene (16a)	37
Scheme 22. Synthesis of BODIPY Dyes	37
Scheme 23. Synthesis of Isatin derivatives 72	38

Scheme 24. Future studies with 73aa	45
Scheme 25. The two-pot, one-step synthesis of BODIPY 96	50

LIST OF ABBREVIATIONS

ABBREVIATIONS

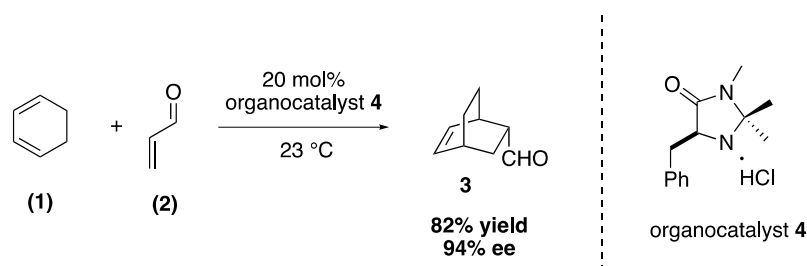
SOMO	singly occupied molecular orbital
DMAP	4-dimethylamino pyridine
FCA	Friedel-Crafts alkylation
THBC	tetrahydro-beta-carboline
BODIPY	difluoroboron dipyrromethene
BNP	binaphthyl
ECD	electronic circular dichroism
MBH	Morita-Baylis-Hillman
PET	positron emission tomography
OLED	organic-light emitting diode
NLO	nonlinear optic
ETM	electron-transporting material
PSC	perovskite solar cell
DIAD	diisopropyl azodicarboxylate
DPPA	diphenyl phosphoryl azide
CPL	circularly polarized luminescence
DPV	differential pulse voltammetry

CHAPTER 1

INTRODUCTION

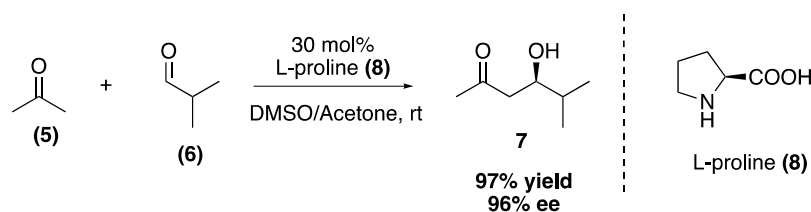
1.1 The Organocatalysis in Asymmetric Synthesis

The concept of organocatalysis was first defined as "using small molecules to catalyze organic reactions to synthesize optically active or chiral compounds" by MacMillan in 2000. Also, MacMillan et al. documented the first enantioselective organocatalytic Diels-Alder reaction of cyclohexa-1,3-diene (**1**) and acrolein (**2**) catalyzed by imidazolidinone **4** as an organocatalyst (Scheme 1).¹



Scheme 1. Diels-Alder reaction catalyzed by imidazolidone organocatalyst **4**

Another precious work in the organocatalysis field was conducted by List et al. in 2000. The first intermolecular aldol reaction between acetone (**5**) and isobutyraldehyde (**6**) was catalyzed by L-proline (**8**) (Scheme 2). This aldol reaction showed the benefits of an organocatalyst as being nontoxic, inexpensive, containing no metal, small molecule, and no requirement for inert conditions. Specific to proline, it was readily available in both enantiomeric forms and water-soluble, which could be easily extracted.²



Scheme 2. The first organocatalytic intermolecular aldol reaction

As a necessary conclusion from List's study, L-proline (**8**) was an organocatalyst that fulfills most of the prerequisites indicated with "green and sustainable" chemistry.³ The pioneers of asymmetric organocatalysis, Benjamin List and David MacMillan, were awarded the Nobel Prize in Chemistry in 2021 for their precious contribution to the development of asymmetric organocatalysis.⁴

From a mechanistic point of view, the organocatalysts activate the electrophile or nucleophile or both electrophile and nucleophile simultaneously. Also, the organocatalysts provide an asymmetric environment to get a chiral product due to the reaction.⁵ One type of organocatalysis classification conducted by Berkessel and Gröger is based on the interaction with the substrate, and they could be either covalent or non-covalent catalysis.⁶ In covalent catalysis, organocatalytic modes are activated through enamine, iminium, dienamine, SOMO, carbene, and Lewis base. Conversely, hydrogen-bonding and Brønsted acid activation, Brønsted base, bifunctional activation, and phase-transfer are three types of non-covalent organocatalytic modes of activation.⁷ A different kind of classification conducted by List depends on the acidity or basicity of the catalytic cycle, including Lewis acid/base and Brønsted acid/base catalysis.⁸ Moreover, the last type of classification conducted by MacMillan is considered from a different perspective which is generic activation modes of organocatalysts.⁹

One of the most commonly used activation modes is **enamine catalysis**, in which enolizable aldehyde and ketones could be functionalized in the alpha position with different electrophiles.¹⁰ Moreover, **iminium activation catalysis** is another

fundamental mode that a considerable variety of nucleophile-electrophile interactions such as cycloadditions, nucleophilic additions, attacks by bases, and decarboxylation could be foreseen.¹¹ L-proline¹²⁻¹⁴ (**8**) and (*S*)-phenylalanine^{15,16} (**9**) are chiral amines used in enamine activation catalysis, and the diarylprolinol silyl ethers^{17,18} **10** and aromatic diamines such as BINAM^{19,20} **11** are used for iminium activation catalysis (Figure 1).

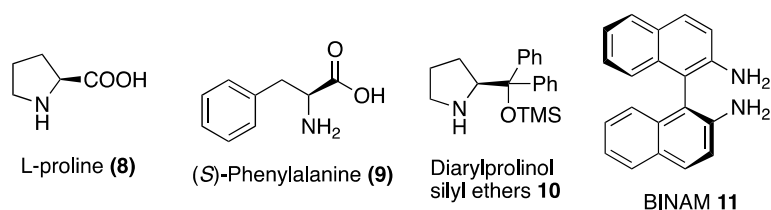


Figure 1. Representative examples of chiral amines

As an essential sub-class of non-covalent catalysis, **hydrogen-bonding catalysis** is a powerful tool to catalyze a wide range of enantioselective reactions by being responsible for activating electrophiles with their unique functional group structure of organocatalysts.^{21,22} Chiral thio(urea)s²³ **12**, diols²⁴ **13**, and phosphoric acids^{25,26} **14**, **15** are the most widely used hydrogen-bonding catalysts (Figure 2).

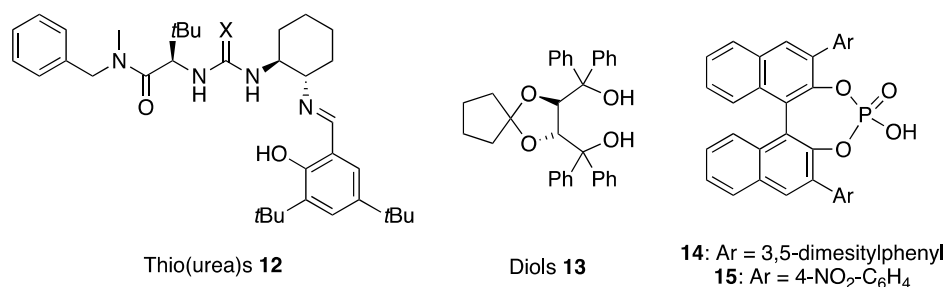
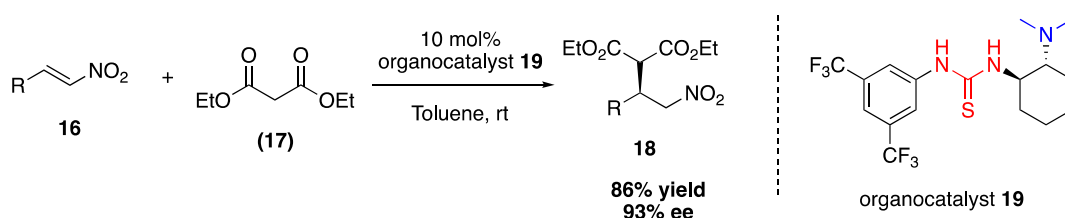


Figure 2. Examples of hydrogen-bonding catalysts

1.1.1 Bifunctional Organocatalysis

Bifunctional organocatalysis is the most substantial concept for developing efficient chiral catalysts by making bifunctionality one of the most effective sites in asymmetric catalysis.²⁷ The pioneering studies in bifunctionality were conducted by Wynberg and his co-workers. In their studies, the cinchona alkaloid-derived acid-base bifunctional organocatalyst bearing an OH unit at the C-9 position often showed good catalytic activity in terms of enantioselectivity than those counterparts not having an OH unit at the C-9 position. Unfortunately, these early attempts were not good enough to accomplish the reactions with high enantioselectivities.²⁸

In 2003, Takemoto and his co-workers developed the most critical study in the bifunctionality area. In their research, the Michael addition of diethyl malonate (**17**) to nitroolefins **16** was catalyzed by the bifunctional thiourea organocatalyst **19** with high enantioselectivities (Scheme 3). For the mechanistic view, the thiourea part, which is the acidic part of the organocatalyst, activates the electrophile, and the tertiary amino group as the basic unit activates the nucleophile simultaneously.²⁹

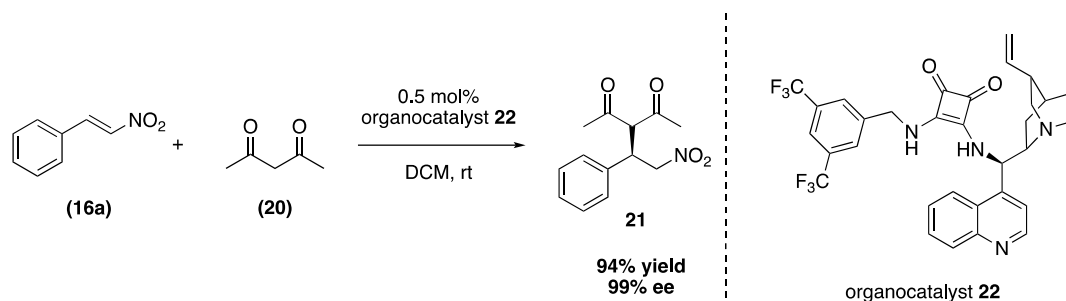


Scheme 3. The first example of bifunctional organocatalysis

1.1.2 Squaramides in Bifunctional Organocatalysis

Bifunctional squaramides, one of the most influential sub-classes of hydrogen-bonding catalysts, have been emerged to make asymmetric induction for synthesizing optically active compounds.³⁰ The pioneering study was conducted by Rawal and his co-workers in 2008 with the usage of cinchona-derived squaramide **22** as a bifunctional organocatalyst in the Michael addition of 2,4-pentanedione (**20**)

to *trans*- β -nitrostyrene (**16a**) (Scheme 4). Although it was the first study, the cinchona-derived squaramide **22** showed excellent catalytic activity in terms of enantioselectivity and chemical yield values.³¹



Scheme 4. The first example of bifunctional squaramide catalyzed Michael addition

Compared to their closest analogs, thio(urea)s, the functionality of squaramides has a significant difference in terms of duality, rigidity, H-bond spacing, angle, and pKa. Firstly, ion- and H-bonding duality is one of the most specific differences between squaramides and thio(urea)s. Squaramides have unique properties, ditopic binding (Figure 3, left), recognizing anions and cations in which thio(urea)s have limited ability.³² The reason for ion duality is explained by the increased aromaticity in the complexes in which squaramides form with several anions and cations. This bifunctional ditopic binding is used for designing ditopic receptors.³³ In addition to ditopic binding, squaramides have bifunctional H-bonding property, containing two N-H protons as H-bond donors and two carbonyl groups as H-bond acceptors. Also, one N-H and one carbonyl group are thought of as another H-bond donor/acceptor pattern (Figure 3, right).³⁴

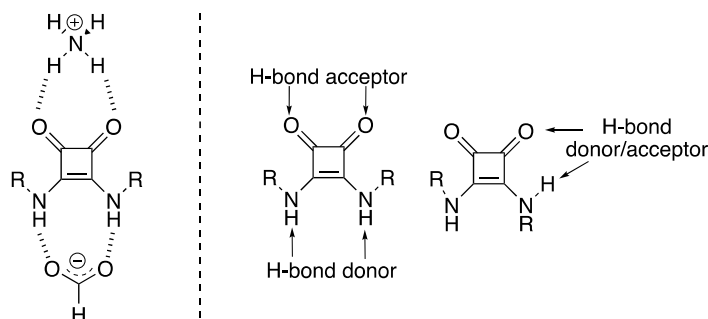


Figure 3. Ditopic binding (left) and H-bonding patterns (right) in squaramides

Secondly, squaramides are rigid compounds due to their structural features. The squaramides are the vinylogous amides which are nitrogenated derivatives of squaric acids, while their thio(urea) counterparts are (thio)amides. The functional parts in the structures restrict the rotation of the C-N bond by delocalizing the lone pair of nitrogen atoms through the carbon-oxygen double bond in the resonance structures in both analogs. Besides, in squaramides, the subscription of the partially aromatic cyclic unit enables the further delocalization of the structure. The aromaticity of these analogs is supported by the nucleus-independent chemical-shift method, a computational technic which specifies that these compounds provide all prerequisites for aromaticity (Figure 4).³²

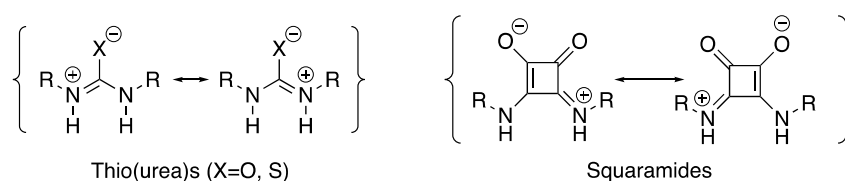


Figure 4. Resonance structures of thio(urea) and squaramides

Thirdly, the distance and spacing between two N-H protons is another significant difference between the thioureas and squaramides. The distance in thiourea is calculated as $\sim 2.1 \text{ \AA}$ by Takemoto³⁵ while in squaramide as $\sim 2.7 \text{ \AA}$ by Rawal³¹ (Figure 5, left, respectively). Another unique difference in improving H-bonding properties observed in squaramides is the H-bond angle which folded by 6° because of the square geometric structure of the cyclobutenedione ring. The angle difference causes a convergent orientation of N-H protons, which cannot be observed in thiourea analogs (Figure 5, right, respectively).^{31,32}

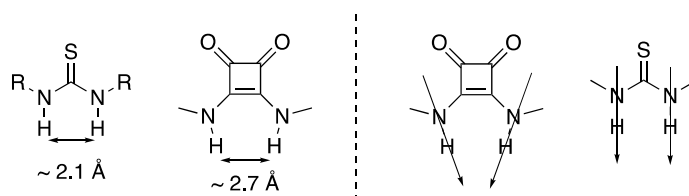


Figure 5. The distance between N-H (left) & convergent orientation of N-H (right)

Finally, the last difference between squaramides and thioureas is pKa values. In 2010, Cheng et al. first measured the pKa values of the most widely known thiourea catalysts based on the correlations of pKa values, activity, and enantioselectivity. Their study shows that faster reactions and better enantioselectivities are obtained with the more acidic thioureas.³⁶ After that, Schreiner also determined the pKa values of the most popular thio(urea)s with Bordwell's method.³⁷ For the squaramides, a similar study was conducted by Cheng et al. in 2014 with 18 different squaramides. Also, they compared the acidity of squaramides and their thiourea analogs by deducing that squaramides are more acidic due to having lower pKa values than the thioureas.³⁸

Generally, squaramides provide stronger H-bonding in compounds containing nitro, carbonyl, imino, and nitrile functionalities, etc. (Figure 6).³⁹

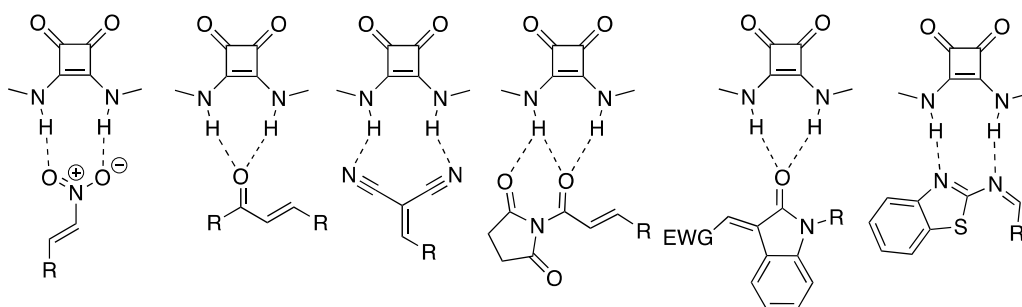
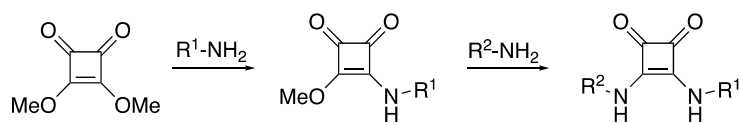


Figure 6. Activation of different functional groups by squaramides

Besides all these properties, the easy preparation of squaramides is another advantage. The synthesis procedure starts with the substitution of dimethyl squarate followed by a second substitution of a chiral primary amine to get the bifunctional squaramide (Scheme 5). In some cases, purification techniques are not needed due to the precipitation of catalysts in the solution. Moreover, when the combination of squaramide moiety with the chiral scaffold carrying a basic part results in the chiral bifunctional H-bonding organocatalyst.⁴⁰



Scheme 5. The synthesis of bifunctional squaramide

Up to now, a wide range of bifunctional squaramide organocatalysts are synthesized and evaluated in different types of reactions such as Michael additions, aldol, Mannich, Friedel-Crafts alkylation, Morita-Baylis-Hillman, Strecker, aza-Henry, cascade, and domino type reactions.^{30,32,39,40}

1.1.2.1 2-AminoDMAP and Quinine Based Bifunctional Squaramides in Tanyeli's Research Group

In 2015, Tanyeli et al. reported a new class of organocatalysts named as chiral bifunctional 2-AminoDMAP/squaramides with the cooperation of 2-aminoDMAP unit as a "superbase" and sterically encumbered squaramide motif as H-bond donor (Figure 7).

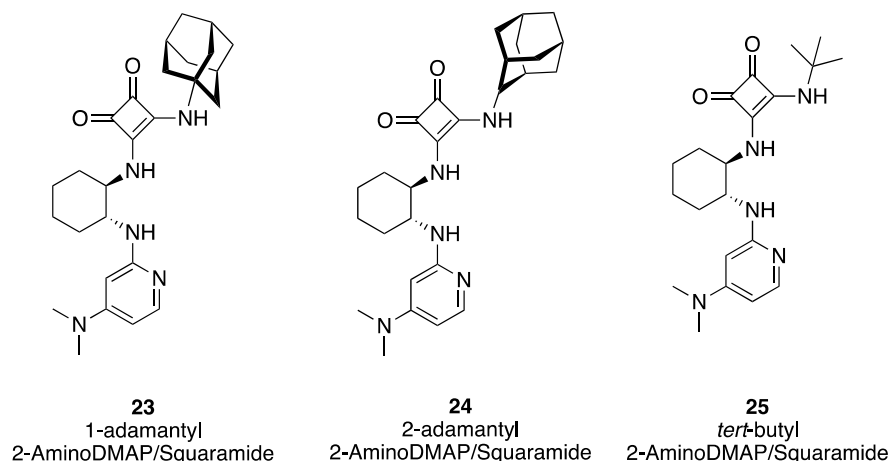
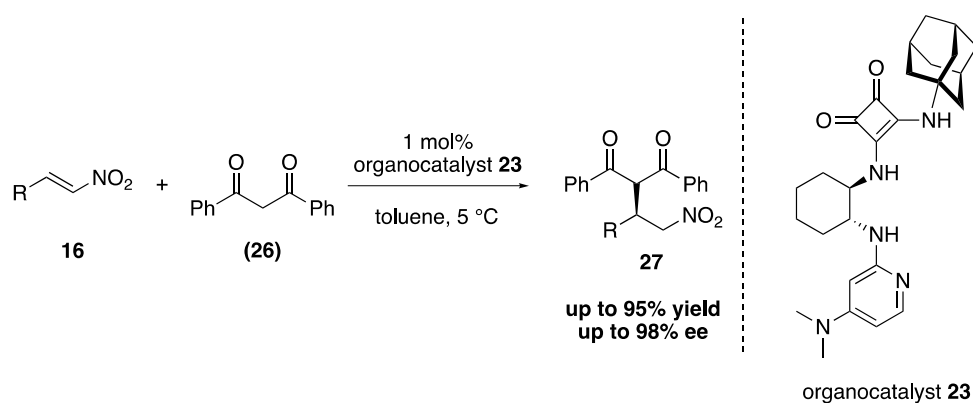


Figure 7. Chiral bifunctional 2-aminoDMAP/squaramides

Moreover, the catalytic activity of these organocatalysts was tested in the Michael addition of dibenzoylmethane (**26**) to various nitroolefins **16** with the usage of only 1 mol% catalyst loading (Scheme 6). 15 different derivatives were synthesized up to 98% enantioselectivities and 95% chemical yields in the presence of sterically encumbered 1-adamantyl substituted 2-aminoDMAP/squaramide organocatalyst **23**.⁴¹



Scheme 6. Conjugate addition of dibenzoylmethane (**26**) to nitroolefins **16**

After one year, in 2016, Kanberoğlu et al. synthesized another new class of bifunctional squaramides which are quinine based as cinchona alkaloid derivatives. These new types are named quinine/squaramides, which contain the same sterically encumbered units such as 1 & 2-adamantyl and *tert*-butyl as acidic parts (Figure 8).

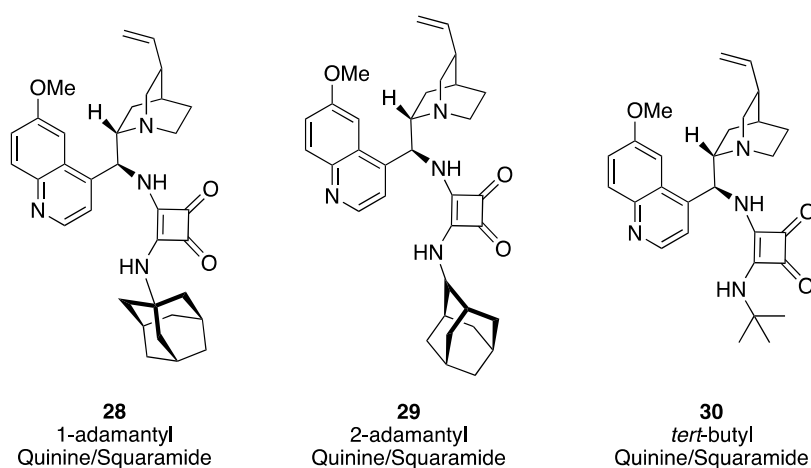
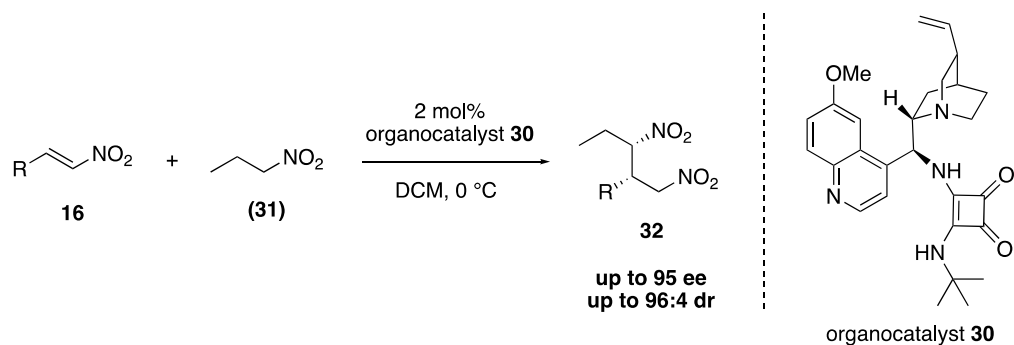


Figure 8. Chiral bifunctional quinine/squaramides **28-30**

After synthesizing organocatalysts, they were subjected to evaluate in the Michael addition of 1-nitropropane (**31**) to different nitroolefins **16**. Twelve different 1,3-dinitro products **32** are obtained up to 95% enantioselectivities and up to 96:4 diastereomeric ratio in the presence of 2 mol% *tert*-butyl quinine/squaramide **30** (Scheme 7).⁴²



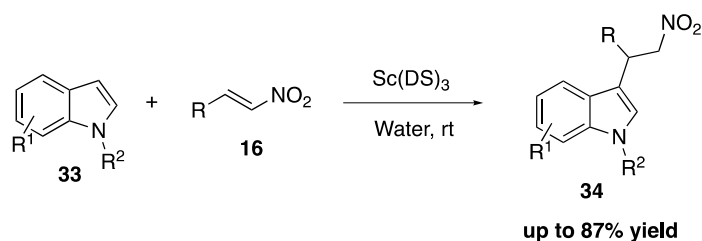
Scheme 7. Michael addition of 1-nitropropane (**31**) to nitroolefins **16**

In addition to these reactions, 2-aminoDMAP and quinine based squaramide organocatalysts have been evaluated for different types of reactions such as aza-Henry,⁴³ Friedel-Crafts alkylation,⁴⁴ Sulfa-Michael addition,⁴⁵ Mannich reactions,^{46,47} and domino type reactions.⁴⁸

1.2 Friedel-Crafts Alkylation Reactions

Friedel-Crafts reactions, discovered by Charles Friedel and James Mason Crafts in 1877, have a vast scope and occupy a prominent place in electrophilic reactions. Moreover, Friedel-Crafts reactions have two different categories: alkylation and acylation. Due to its vast diversity and types, Friedel-Crafts alkylation (FCA) is a substantial and significant reaction type to form a C-C bond in both aromatic and aliphatic systems in synthetic organic chemistry. In addition to all, the alkylation of aromatic compounds with an alkene is one of the most common application of Friedel-Crafts alkylation.⁴⁹

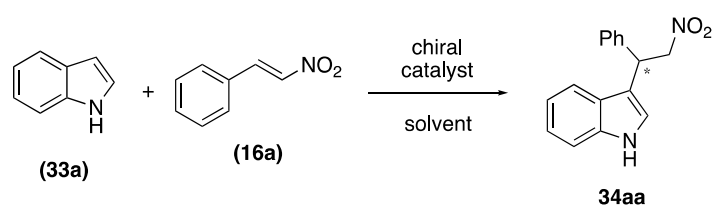
One of the early examples of alkylation of aromatic compounds with an alkene was come by Kobayashi et al. in 2000. In their study, Friedel-Crafts type conjugate addition of indole (**28**) to electron-deficient nitroolefins **16** was catalyzed by a surfactant-type Lewis acid, scandium tris(dodecyl sulfate), Sc(DS)₃ in water with good chemical yields (Scheme 8).⁵⁰



Scheme 8. FCA of indoles **33** with nitroolefins **16**

1.2.1 Enantioselective Friedel-Crafts Alkylation of Indole with Nitroolefins

The asymmetric version of Friedel-Crafts alkylation of indole (**33a**) with *trans*- β -nitrostyrene (**16a**) (Scheme 9) was tested by the mostly combination of ligands, and metal complexes,^{51–56} charged organocatalysts^{57–59} and inorganic materials.^{60,61}



Scheme 9. FCA of indole (**33a**) with *trans*- β -nitrostyrene (**16a**)

Moreover, the first organocatalytic literature example of Friedel-Crafts alkylation of indole (**33a**) with *trans*- β -nitrostyrene (**16a**) was accomplished by Ricci⁶² et al. in 2005. In the presence of 20 mol% simple thioureas **35**, 8 different 3-substituted

indole derivatives were synthesized with high enantioselectivities (up to 89% ee) and moderate yields (up to 88%) at -24 °C.

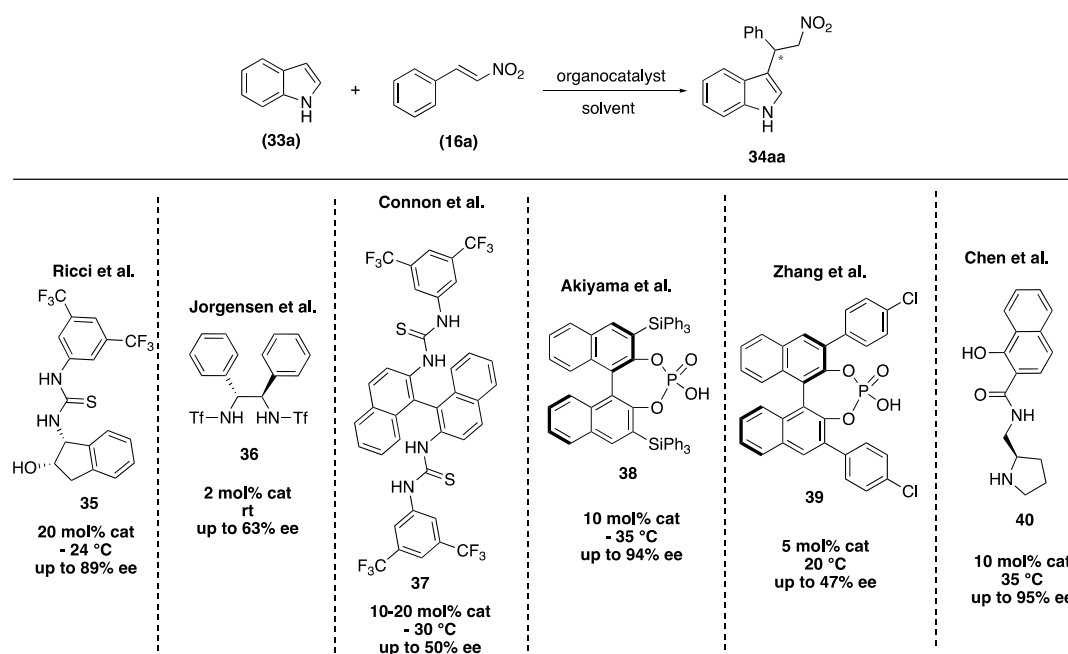
In the same year, Jørgensen⁶³ et al. used only 2 mol% H-bonding bis sulfonamides **36** as organocatalysts in the Friedel-Crafts alkylation of indole (**33a**) with *trans*- β -nitrostyrene (**16a**). They reached up to only 63% ee at room temperature. By using the recrystallization technique, the enantioselectivity of products was increased up to 99% ee.

After one year, in 2006, Connon⁶⁴ et al. evaluated their novel axially chiral bis-arythioureas **37** with the usage of 10-20 mol% catalyst loading in the FCA of indole (**33a**) with *trans*- β -nitrostyrene (**16a**). Although the chemical yield values were up to 98%, the enantioselectivity was obtained at only 50% among the 7 derivatives at -30 °C with long reaction durations (up to 287 h).

In 2008, chiral phosphoric acids **38** were evaluated in the FCA of indole (**33a**) with *trans*- β -nitrostyrene (**16a**) in harsh reaction conditions in which temperature at -35 °C and benzene as well as DCE as reaction solvents. Akiyama⁶⁵ et al. synthesized 14 different derivatives with up to 94% ee and moderate yields in the usage of 10 mol% catalyst loading.

In 2011, the FCA of indole (**33a**) with *trans*- β -nitrostyrene (**16a**) was catalyzed by 5 mol% chiral phosphoric acids **39** at 20 °C. Zhang et al. managed to reach up to only 47% ee and moderate yields with 23 different derivatives.⁶⁶

Another remarkable study came out in 2016 by Chen⁶⁷ et al. In their research, the FCA of indole (**33a**) with *trans*- β -nitrostyrene (**16a**) was catalyzed by novel chiral secondary amine-amide organocatalyst **40** with the usage of 10 mol% catalyst loading at 35 °C. 12 different derivatives were synthesized with enantioselectivities up to 95% and chemical yields (Scheme 10).



Scheme 10. A literature comparison of FCA of indole (**33a**) with *trans*- β -nitrostyrene (**16a**) in organocatalysis

1.2.2 The Importance of 2-Indolyl-1-nitro Derivatives

The outcome of the enantioselective Friedel-Crafts alkylation of indole (**33a**) with nitroolefins **16** is the chiral 2-indolyl-1-nitro derivatives **41**. The importance of these derivatives is attributed to two factors which one is the privileged structure of indole core in the pharmaceutical environment, fragrances, agrochemicals, pigments, and material science.^{68,69} Moreover, the second factor is the chemical diversity of the nitro group in nitroolefins due to their easy availability and transformation into different types of functional groups.⁷⁰

The chiral 2-indolyl-1-nitro derivatives **41** are fundamental building blocks for biologically active compounds such as melatonin analogs **42**, 1,2,3,4-tetrahydro- β -carbolines (THBCs) **43** and tryptamines **44** (Figure 9).⁷¹

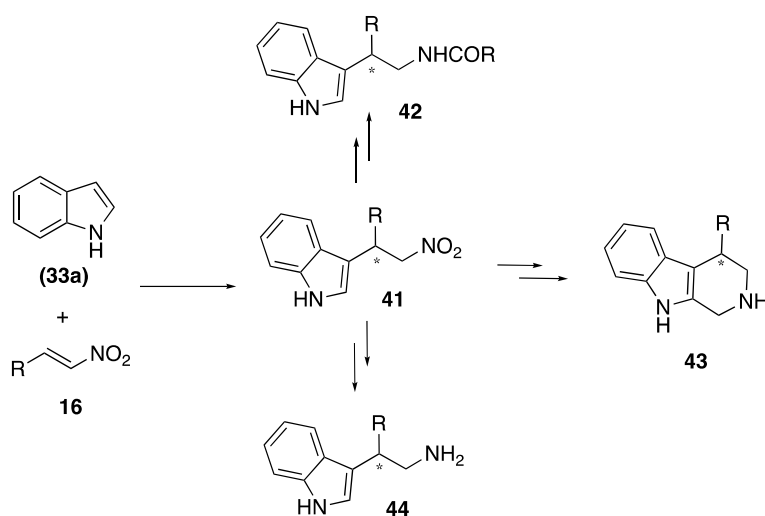


Figure 9. 2-indolyl-1-nitro intermediates **41**

Melatonin derivatives **42** are one of the most vital hormones secreted in the darkness, and it is responsible for regulating circadian rhythm and controlling associated diseases. In addition to the antioxidant property, it is also used to treat cancer and psychiatric disorder.⁷²

1,2,3,4-tetrahydro-β-carbolines (THBCs) **43** have a wide occurrence in nature and are synthetic compounds that could be synthesized with an enzymatic Pictet-Spengler cyclization in the presence of tryptamine or tryptophan and a carbonyl compound. Besides, THBCs **43** are key intermediates for alkaloids which are ajmalicine, strychnine, reserpine, tadalafil, eudistomin E, and trypargine (Figure 10). These alkaloids pharmacologically function as antihypertensive, pesticide, antimalarial, antiviral, and antitumor activities.^{73,74}

Tryptamines **44** are intermediates for triptans and tryptophans. Among these, triptans are synthesized as a partial agonist for the treatment and prophylaxis of migraine by pharmaceutical companies. The best-known example of triptans is sumatriptan. Moreover, tryptophan is a natural amino acid derivative that is essential for the human body to produce proteins (Figure 10).^{75,76}

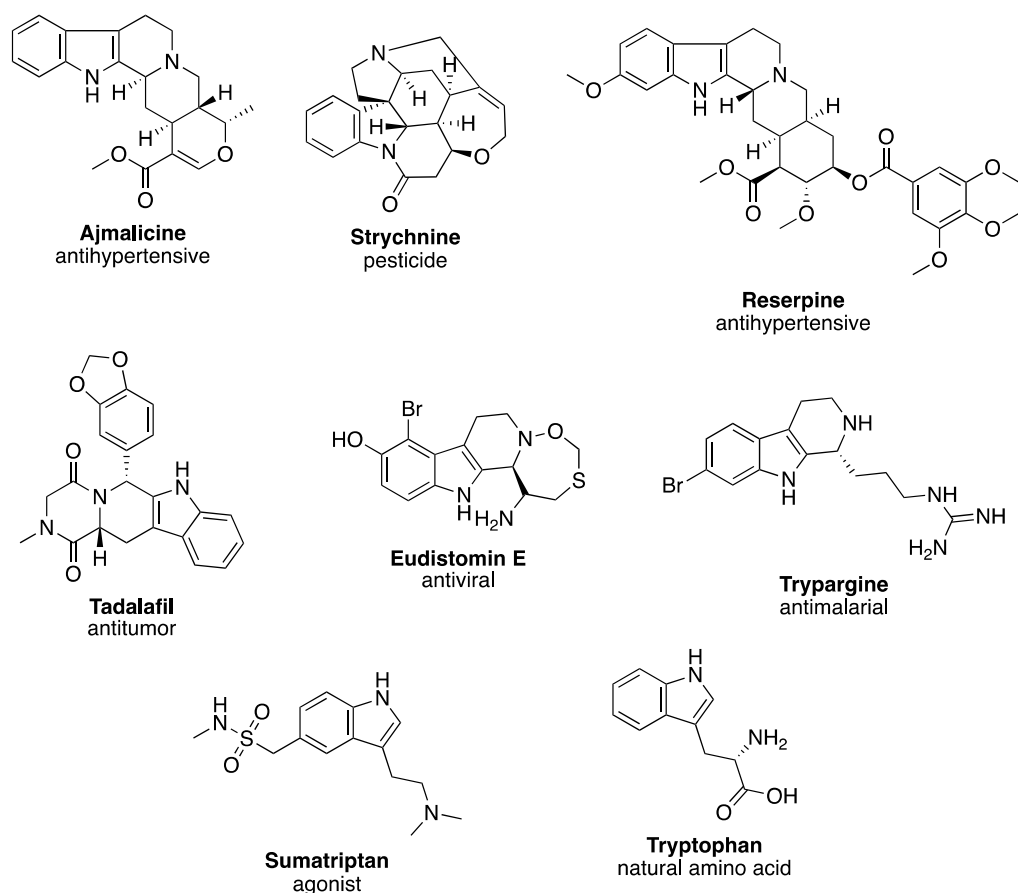


Figure 10. Examples of THBCs and Tryptamines

1.3 Fluorescence Spectroscopy

Fluorescence spectroscopy, with its indicators, sensors, probes, and imaging functions, has become an essential part of various fields of modern science, medicine, chemistry, biology, and materials science nowadays. Also, fluorescent techniques, which are highly sensitive and specific, offer many advantages such as excellent sampling capability, operationally simple, minimum disruptive, and versatility. Due to its broad benefits, fluorescence has a vital role in other measurement techniques that are microelectrodes, NMR, atomic absorption spectroscopy, and spectrophotometry.⁷⁷

1.3.1 BODIPY Dyes as Fluorescent Compounds

Among the all-fluorescent compounds, 4,4-difluoro-4-bora-3a,4a-diaza-s-indacene^{78,79} which is known commonly as BODIPY, difluoroboron *dipyrromethene*, is the most popular one. Although the first examples of BODIPY structures were reported by Treibs and Kreuzer⁸⁰ in 1968, the significant applications of these structures, such as biological labeling, laser dyes, sensors, and indicators, have been discovered entirely since the mid-1990s. The reason for this popularity and usage in various applications is the outstanding excellent chemical and physical properties of BODIPY dyes.⁷⁷

1.3.1.1 The Chemical and Physical Properties of BODIPY Dyes

The IUPAC numbering for BODIPY **45** and dipyrromethene **46** & dipyrromethane **47** is different but the same in *alpha*-, *beta*- and *meso*- positions (Figure 11).⁷⁸

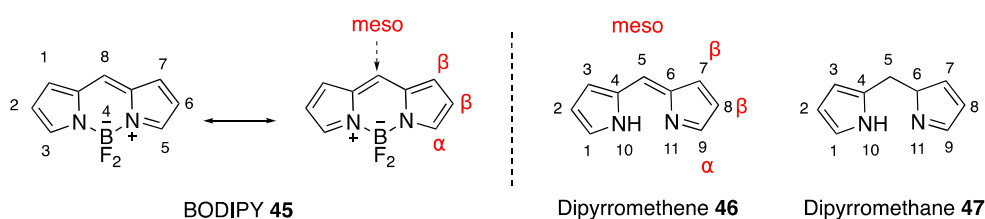


Figure 11. IUPAC numbering for compounds **45**, **46** & **47**

BODIPY **45** structure is considered as an example of a "rigid" molecule, and this rigidity restricts the rotation of the compound by resulting in unusually high fluorescence properties. Also, the conjugation of π -electrons in the dipyrromethene boron framework could be extended with the attachment of suitable groups onto both periphery or pyrrole parts.⁸⁰ In addition to high fluorescence quantum yields, BODIPY dyes have large molar absorptivity coefficients with their absorption & emission spectra located in the visible region, narrow emission bandwidths with high peak intensities, fluorescence lifetimes in the nanosecond range, and negligible

triplet-state populations. These dye structures have good solubility in all common solvents and remarkable redox characteristics. Moreover, BODIPYs are inert for chemicals and robust for light as well as resist toward self-aggregation in solution. All these spectroscopic and photophysical properties could be fine-tuned with the attachment of suitable groups to the core structure.⁸¹ From the chemical reactivity perspective, these BODIPY structures are functionalized at all positions which are 1, 2, 3, 5, 6, 7 of C-ring positions at pyrrole ring, *meso*- or 8-position, and boron atom (Figure 12).

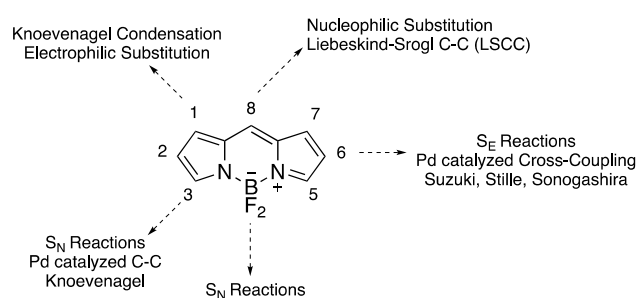
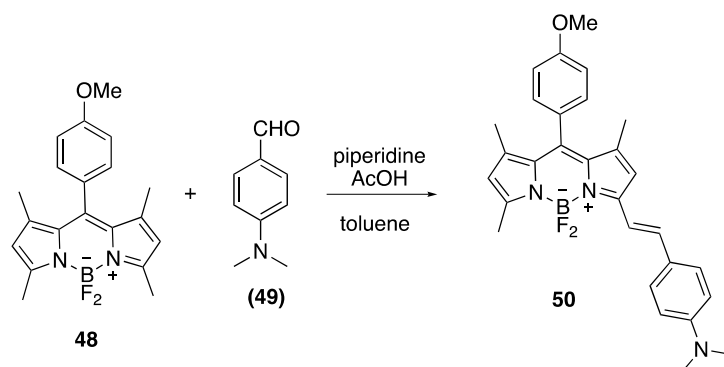


Figure 12. Functionalization of BODIPY core

2,6-positions which are free of substituents are susceptible to electrophilic substitution reactions in the presence of chlorosulfonic acid. Water-soluble BODIPY analogs,⁸² bromine^{83,84} and iodine⁸⁵ bearing BODIPY dyes are synthesized with this approach by occurring exclusively at 2,6-positions which is a valuable selective substitution.⁷⁹

Using the acidity of methyl groups on 3,5-positions of BODIPY dyes, these compounds could be subjected to addition-elimination reactions. Methyl groups at 3,5-positions are deprotonated in basic conditions and then added to an electron-rich aldehyde group, forming a styryl group.⁸⁶⁻⁸⁹ As a specific literature example, pH-dependent BODIPY **50** was synthesized with the Knoevenagel type condensation between the corresponding BODIPY **48** and 4-(dimethylamino)benzaldehyde (**49**) (Scheme 11).⁹⁰

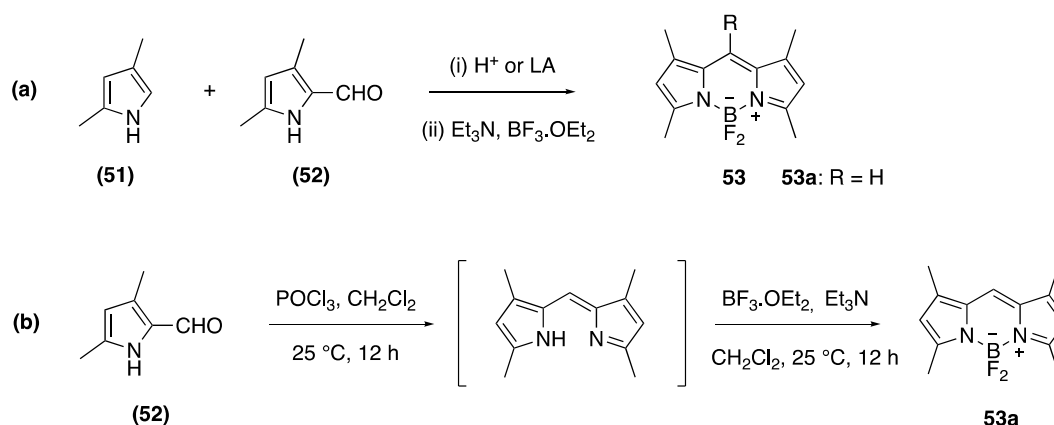


Scheme 11. Knoevenagel condensation of BODIPY **48** with 4-(dimethylamino)benzaldehyde (**49**)

Another mechanistic pathway is metal-catalyzed cross-coupling reactions, specifically palladium-catalyzed coupling reactions, to extend the conjugation of BODIPY dyes in which a halogenated group is directly attached to the core or aryl ring.⁹¹ Moreover, Heck, Suzuki, Sonogashira, or Stille type coupling reactions are used for the addition of ethyne, ethene, or aryl groups to the BODIPY core structure by remaining the B-F bond inert during the reaction.^{92,93}

With the nucleophilic substitution reactions, BODIPY dyes are derivatized from 8- or *meso*-positions in the presence of a variety of nucleophiles.^{94,95} Especially, 8-halogenated BODIPYs are excellent candidates for nucleophilic substitutions due to mild reaction conditions.⁹⁶ In addition to 8-position, fluorine atoms at boron could be substituted with aryl, alkyne, alkyl, alkoxide, and carboxylate groups.⁹⁷⁻¹⁰²

Although BODIPY structures have remarkable physical, chemical, and optical properties, only two synthetic methods are available to access these systems. BODIPY **53a** is obtained via condensation of a 3,5-dimethylpyrrole-2-carbaldehyde (**52**) with a 2,4-dimethylpyrrole (**51**) in the first method (Scheme 12, a).^{103,104} In the second synthesis procedure, condensation of only 3,5-dimethylpyrrole-2-carbaldehyde (**52**) in the presence of POCl₃ gives the desired BODIPY **53a** (Scheme 12, b).¹⁰⁵



Scheme 12. The synthetic pathways of BODIPY **53a**

1.3.1.2 The Chiral BODIPY Dyes

Due to tremendous chiroptical properties, optically active BODIPY dyes have many applications in optoelectronic devices, and are used as biological sensors. Mainly, optically active BODIPYs are divided into three subunits that differ in structures; (i) containing chiral carbon atoms, (ii) linking with optically active molecules, and (iii) axially chiral or stereogenic center at tetrahedral boron atom.¹⁰⁶ The first examples of optically-active BODIPYs **54**, which belong to the first subunit, are synthesized from the urobilin analogs.¹⁰⁷ Moreover, enantiopure aza crown ether-linked BODIPYs¹⁰⁸ **55** and containing chiral 1,2-diphenyl-1,2-ethanodiamine BODIPYs¹⁰⁹ **56** are given as another example for the same class (Figure 13).

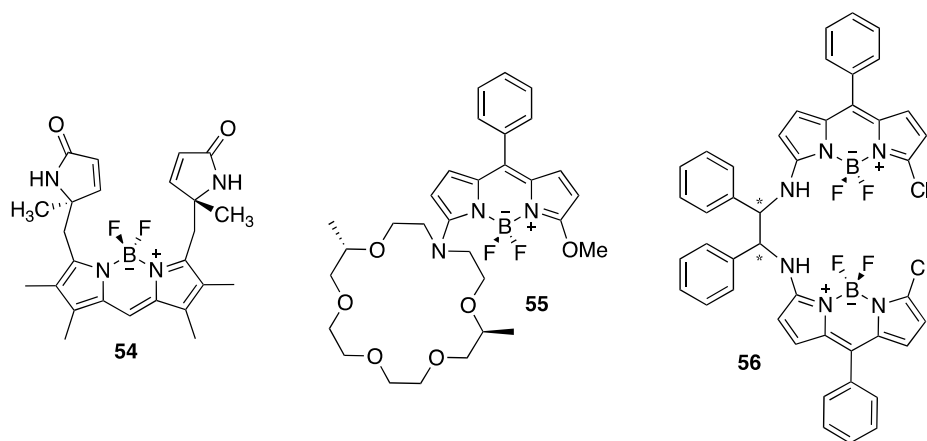


Figure 13. Chiral BODIPYs containing chiral carbon atoms

For the second type of chiral BODIPYs, binaphthyl (BNP) groups are commonly used as optically active molecules linked to BODIPY core structures. Daub and co-workers linked chiral BNP groups at the *meso*-position of the BODIPYs to get chiral BODIPYs **57**.^{110,111} Also, these BNP groups could be substituted from the 4-position, which is the boron atom of the core structure with Sonogashira coupling reactions. BODIPY **58** & **59** are two examples that having chiral BNP groups attached to boron atoms (Figure 14).^{112,113}

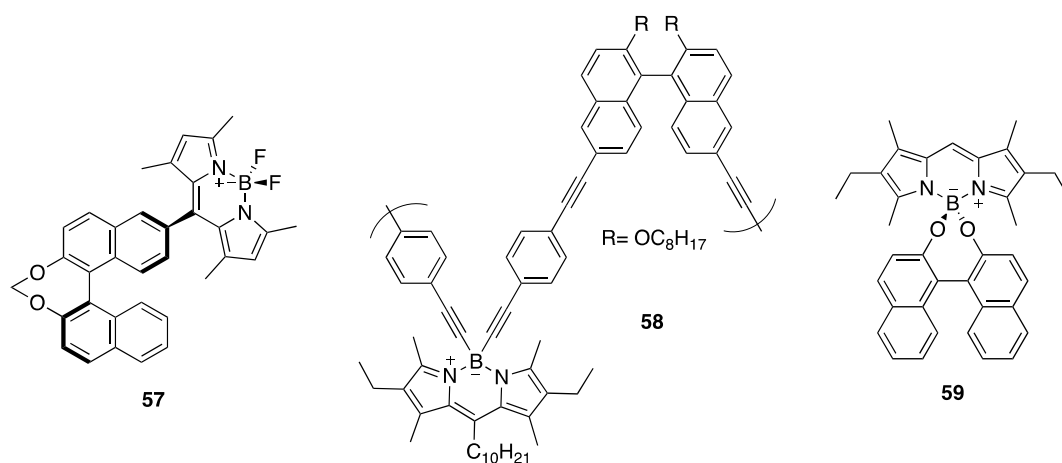


Figure 14. Optically active BODIPYs linked with optically active molecules

Axial chirality is observed in BODIPY molecules due to structural arrangement, although these compounds do not have a stereogenic center. Because of their chirality, their enantiomers are not superimposable with each other. BODIPY **60** shows “propeller-like” conformation, which is a requirement for axial chirality with the effect of steric hindrance between the large groups.¹¹⁴ As a different example for axial chirality, BODIPY **61** was reported by Hall and co-workers. Its separated enantiomers were showed mirror-image symmetry in CD spectra.¹¹⁵ Moreover, BODIPY dimer **62** and trimer **63** are also axially-chiral dyes with rotationally hindered structures reported by the Akkaya group (Figure 15).¹¹⁶

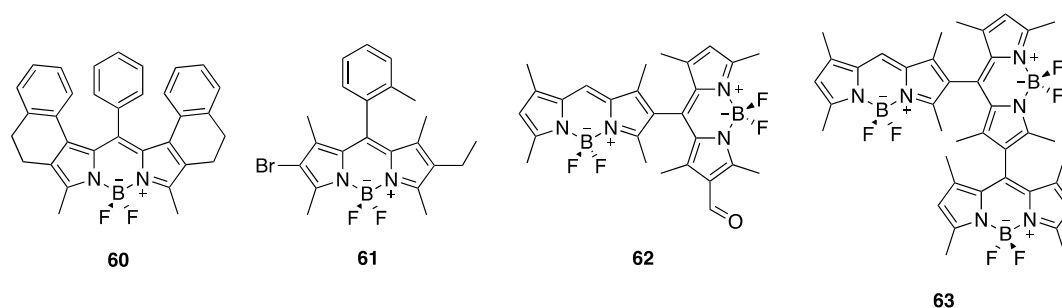
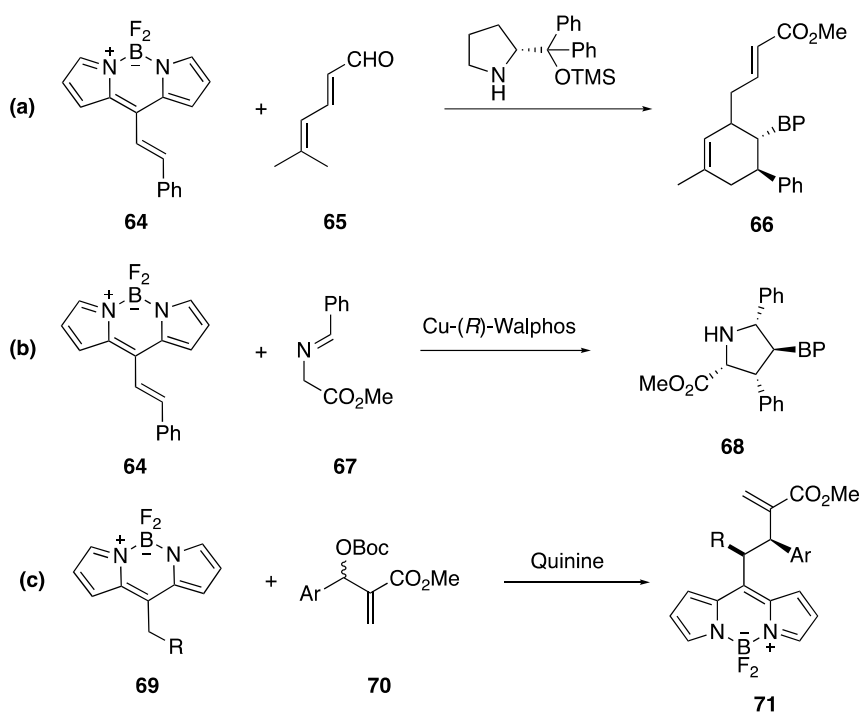


Figure 15. Axially-chiral BODIPYs

Although spectacular studies have been reported for synthesizing chiral BODIPY dyes, their asymmetric synthesis in the presence of chiral catalysts is very little known. Alemán and co-workers conducted the first studies. By using the EWG effect of BODIPY **64** in the activation of double bonds, they synthesized cyclohexyl derivatives **66** containing a BODIPY unit *via* trienamine catalysis with dienals **65** in 2019 (Scheme 13a)¹¹⁷ and pyrrolidine-based BODIPY dyes **68** by asymmetric copper-catalyzed [3+2] cycloaddition reactions with azomethine ylides **67** in 2020 (Scheme 13b).¹¹⁸ In addition to Alemán’s studies, different type of enantioselective work was conducted by Rios and co-workers in 2021. They added the alkyl BODIPYs **69** to Morita-Baylis-Hillman (MBH) carbonates **70** in the presence of cinchona alkaloids by using the methylene position of BODIPY as a nucleophile (Scheme 13c).¹¹⁹



Scheme 13. The enantioselective studies of BODIPY dyes

1.3.1.3 The Applications of BODIPY Dyes

Due to great structural versatility, excellent spectroscopic properties and photostability, high solubility in organic solvents, achiral and chiral BODIPY dyes have many applications in biological labeling, photodynamic therapy, dye lasers, chemosensors, and optoelectronic devices.¹⁰⁶

A typical fluorescent indicator equal to a detector, sensor, chemosensor, or probe combines with the binding site of an analyte with a fluorescent moiety. The function of this fluorophore is to translate the combination of analyte-fluorophore into a fluorescence output signal. In this way, essential and specific molecules could be detected, quantified, and imaged to understand the chemical and biological systems.⁷⁷

Moreover, positron emission tomography (PET) is one of the most critical molecular imaging techniques for diagnosing and treating diseases such as cancers by giving information about the biochemistry of the metabolism with the labeled radioisotopes. Fluorine-18 is widely used in PET scans due to its long enough half-time, suitable imaging characteristics, and decay pattern. On the other hand, fluorescent probes are used in optical imaging for tumor detection, image-guided surgery, and *in vivo* imaging studies due to their high spatial resolution and sensitivity and easy implementation. In the context of these two techniques, BODIPY dyes have a dual functionality such as PET tracers which contains fluorine-18 and optical fluorescent imaging probes.¹²⁰⁻¹²⁴

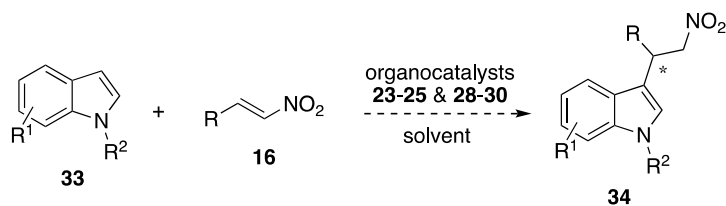
In addition to these, BODIPY dyes are used for optoelectronic applications such as organic light-emitting diodes (OLEDs), nonlinear optics (NLOs), sensing, hole-transporting materials (HTMs), and electron-transporting materials (ETMs) for perovskite solar cells (PSCs) and also, materials for ultrafast charge transfer. The advantage of the modification at almost every position and their comprehensive optical properties are used for these applications. Specifically, BODIPY structures are modified from the periphery position with bulky units for OLEDs to avoid the aggregation caused by quenching in the solid-state due to intermolecular π - π stacking.^{125,126}

1.4 The Aim of the Study

This thesis's main objective is to evaluate the chiral bifunctional 2-aminoDMAP **23-25** and quinine-based organocatalysts **28-30** (Figures 7 and 8, respectively) in different types of reactions and to synthesize the optically active novel compounds in the presence of these organocatalysts.

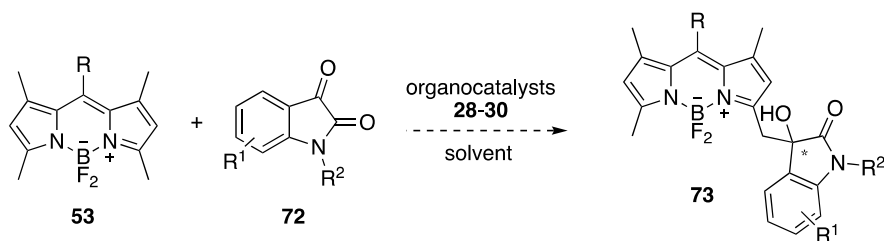
For these purposes, in the first chapter of the thesis, the chiral organocatalyst will be evaluated in the Friedel-Crafts alkylation of indoles **33** with nitroolefins **16** to synthesize 2-indolyl-1-nitro derivatives **34** (Scheme 14). Also, it is expected to find

ideal criteria for this reaction: the minimum catalyst loading in a short reaction duration with high chemical yield and enantioselectivities. After optimization studies, derivatization will be conducted with different indoles **33** and nitroolefins **16** in the most suitable condition. Besides, it is aimed to reach excellent reaction conditions and results better than the literature studies.



Scheme 14. The purpose of the first chapter of the thesis

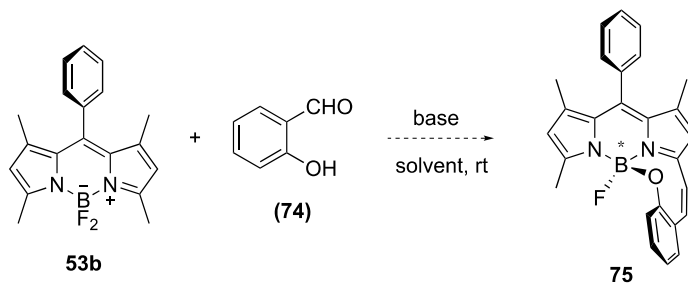
To test the catalytic activity of quinine-based bifunctional organocatalysts **28-30** in particular fields, chiral BODIPY dyes **73** will be synthesized with the enantioselective addition of BODIPY core **53** as a nucleophile to the electron-deficient isatin derivatives **72** as the first in the literature for the second chapter of the thesis (Scheme 15). After optimization and derivatization studies, the chiroptical properties of these novel BODIPY structures **73** will be analyzed with spectroscopic techniques such as UV-vis, CD, and fluorescence.



Scheme 15. The purpose of the second chapter of the thesis

To benefit deep insight from the structural chirality of BODIPY dyes, it is aimed to synthesize a helical BODIPY dye **75** with a collaborative study in the third part of the thesis. BODIPY **75** will be produced by a cascade which in the first step,

nucleophilic substitution at boron atom in *meso*-phenyl-BODIPY **53b** and then, Knoevenagel condensation with salicylaldehyde (**74**) in an intramolecular fashion (Scheme 16). After synthesizing the helical BODIPY **75**, its spectroscopic, chiroptical, and electrochemical properties will be analyzed.



Scheme 16. The purpose of the third chapter of the thesis

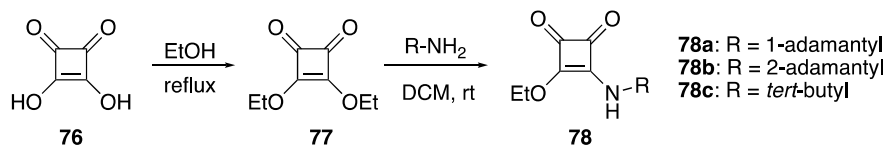
CHAPTER 2

RESULTS and DISCUSSION

2.1 The Synthesis of 2-AminoDMAP and Quinine Based Bifunctional Squaramide Organocatalysts

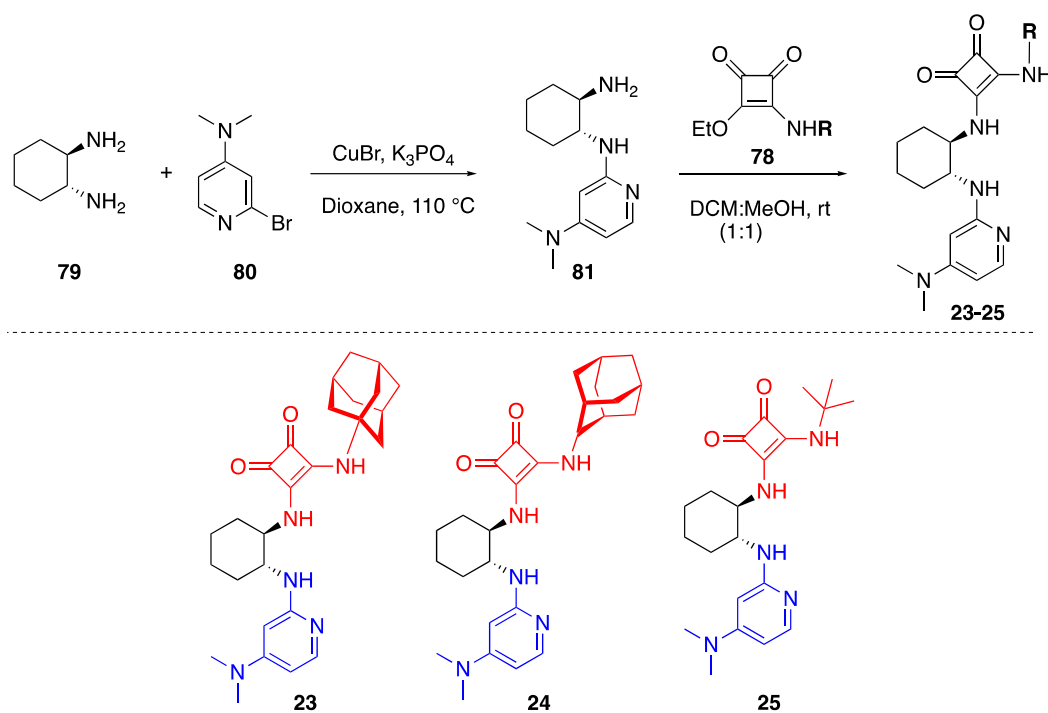
2-AminoDMAP and quinine-based bifunctional squaramide organocatalysts^{41,42} have been developed and synthesized in Tanyeli's research group. The main objective is to evaluate these bifunctional organocatalysts in different types of reactions with excellent enantioselectivities for the synthesis of optically active novel compounds. To construct these bifunctional squaramide organocatalysts, a sterically encumbered squaramide motif is chosen as Brønsted acidic part. These squaramide moieties, which possess bulky adamantyl and *tert*-butyl units, have two acidic hydrogens as an acidic counterpart for the target bifunctional organocatalysts.

Squaric acid **76** is used as a starting material to synthesize acidic units. By refluxing squaric acid **76** in absolute ethanol, diethyl squarate **77** is prepared. Then, commercially available 1-, 2-adamantyl, and *tert*-butyl amines are subsequently added in a 1:1 ratio to a reaction mixture in which dichloromethane (DCM) is a solvent at room temperature. The synthetic procedure³¹ of bulky squaramide moieties **78** is shown in Scheme 17.



Scheme 17. Synthesis of squaramides **78**

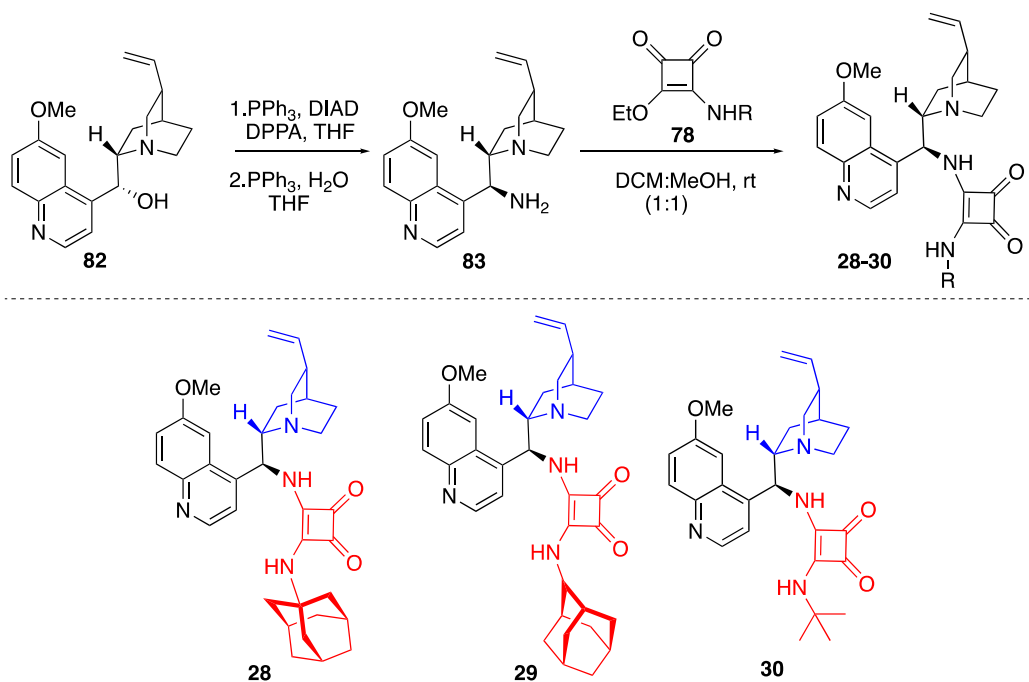
Moreover, 2-AminoDMAP and quinine are selected as "superbases" for the synthesis of bifunctional organocatalysts. For the 2-aminoDMAP case, C_2 -symmetric *trans*-cyclohexane-1,2-diamine **79** is chosen as the "privileged" chiral backbone. Then, chiral 2-aminoDMAP¹²⁷ **81** is constructed by anchoring Lewis base 2-bromoDMAP **80** motif on to C_2 -symmetric *trans*-cyclohexane-1,2-diamine **79** via direct selective mono-*N*-pyridilization in the presence of CuBr and K₃PO₄. After synthesis of acidic and basic units separately, chiral 2-aminoDMAP **81** and bulky squaramides **78** are simply mixed in DCM and methanol solvent combination at room temperature to get the chiral bifunctional 2-aminoDMAP/squaramides organocatalysts **23-25** (Scheme 18).



Scheme 18. Synthesis of 2-aminoDMAP/squaramides **23-25**

For the second type, quinine **82** is chosen as a chiral basic unit and it is converted to its amine analog which is quinine amine **83** by subsequent Mitsunobu and Staudinger reactions with the inversion of configuration at the stereocenter.¹²⁸ Then, with the same procedure as in the 2-aminoDMAP **81**, monosquaramides **78** are coupled with

quinine amine **83** in DCM and methanol combination at room temperature. Chiral bifunctional quinine/squaramides **28-30** are synthesized with high chemical yields (Scheme 19).

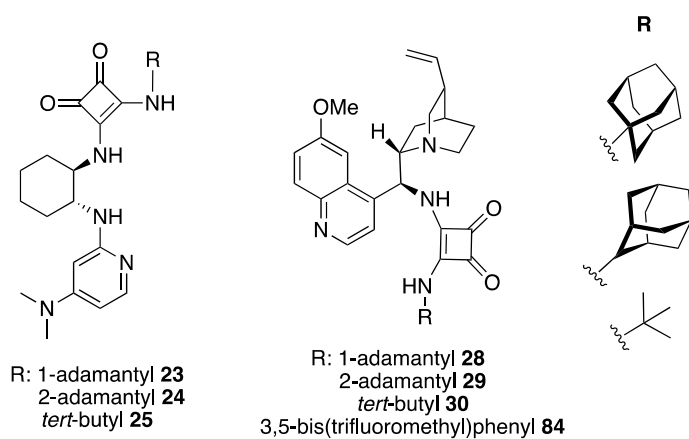
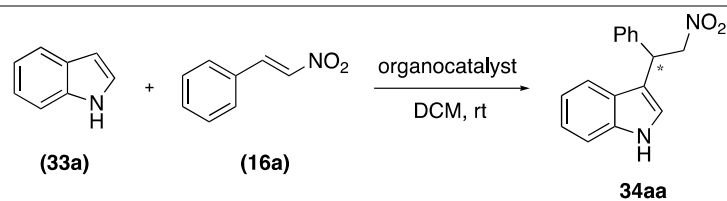


Scheme 19. Synthesis of quinine/squaramides **28-30**

2.2 Evaluation of Bifunctional Organocatalysts in the Friedel-Crafts Alkylation of Indoles **33** with Nitroolefins **16**

2.2.1 Optimization Studies

Due to the great importance of 2-indolyl-1-nitro derivatives in pharmaceutical chemistry, we decided to test the efficiency of bifunctional organocatalysts in the Friedel-Crafts alkylation of indoles **33** with nitroolefins **16**. We started optimization studies by screening all 2-aminoDMAP **23-25** and quinine-based **28-30** squaramide organocatalysts. Also, we wanted to check the catalytic performance of the literaturally available 3,5-bis(trifluoromethyl)phenyl substituted squaramide¹²⁹ **84** in the model reaction.

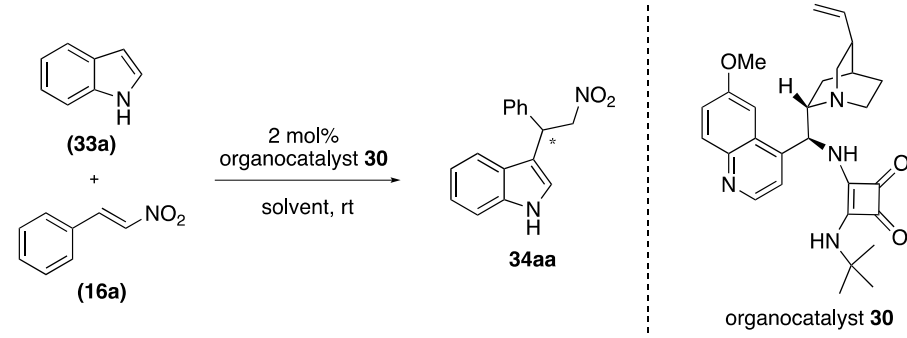
Table 1. Catalyst and Catalyst Loading Screening^a

Entry	Cat.	Cat. Load. (mol%)	Time (h)	Yield ^b (%)	ee ^c (%)
1	28	2	45	16	77
2	29	2	47	18	84
3	30	2	24	45	91
4	84	2	24	14	8
5	23	2	44	56	rac
6	24	2	44	42	12
7	25	5	48	55	15
8	28	5	45	20	81
9	29	5	45	19	88
10	30	5	24	38	89
11	30	10	24	54	91

^a Reaction conditions: indole (**33a**) (0.2 mmol), *trans*- β -nitrostyrene (**16a**) (0.2 mmol), DCM (0.5 mL, 0.4 M). ^b Isolated yields. ^c Determined by HPLC.

Six squaramides were tested with the usage of 2 mol% catalyst loading and DCM as solvent at room temperature in the 1:1 ratio of starting materials. Among the screened organocatalysts, quinine-based organocatalysts **28-30** except **84** afforded the product **34aa** with high enantioselectivity values (Table 1, entries 1-3) than the 2-aminoDMAP based ones **23-24** (2 mol%) and **25** (5 mol%) which gave nearly racemic products in the reaction (Table 1, entries 5-7). We continued to further optimization studies with quinine-based squaramides **28-30**. Due to low chemical yield values of 2 mol%, we increased the catalyst loading to 5 mol% (Table 1, entries 8-10). However, no improvement was observed in terms of chemical yield and reaction duration parameters comparing with 2 mol%. While a slight increase was beheld in ee values for organocatalyst **28** from 77% to 81% (Table 1, entries 1 & 8) and for organocatalyst **29** from 84% to 88% (Table 1, entries 2 & 9). On the other hand, organocatalyst **30** afforded the product **34aa** with the nearly same results with 2 mol% and 5 mol% (Table 1, entries 3 & 10) in terms of enantioselectivity, chemical yield, and reaction duration parameters. Also, we wanted to make a final check with 10 mol% catalyst loading for organocatalyst **30** and then, we again got the nearly same results (Table 1, entry 11). In the light of these data and due to atom economy, organocatalyst **30** with 2 mol% catalyst loading was chosen as the best for Friedel-Crafts alkylation of indole (**33a**) with *trans*- β -nitrostyrene (**16a**) in terms of enantioselectivity and chemical yield values (Table 1, entry 3).

After selecting the best organocatalyst and deciding its catalytic amount for the model reaction, other solvents which are chloroform, xylene, 1,4-dioxane, and toluene were examined to improve the enantioselectivity. Among the screened solvents, chloroform, xylene, and toluene brought about the product **34aa** with good ee values (Table 2, entries 2, 3, and 5, respectively). Unfortunately, 1,4-dioxane did not furnish the increment of enantioselectivity by giving the lowest value for the results (Table 2, entry 4). Also, no solvents increased the chemical yields of the product **34aa**. As a result of solvent screening, DCM proved to be the best solvent with 91% ee to be used in further trials for this FCA (Table 2, entry 1).

Table 2. Solvent Screening^a

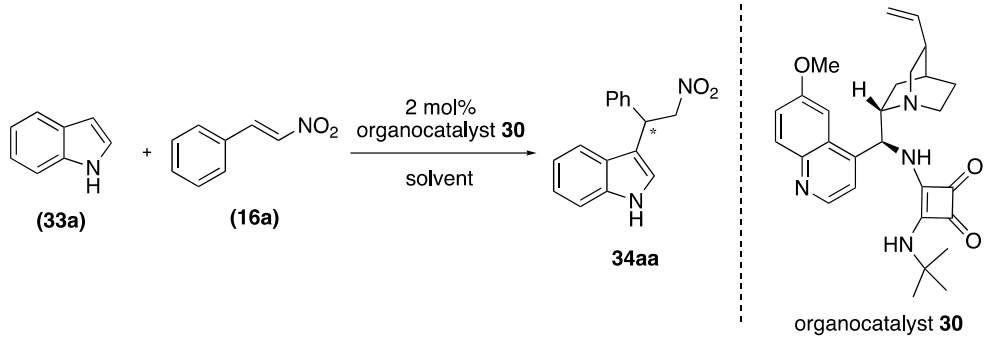
Entry	Solvent	Time (h)	Yield ^b (%)	ee ^c (%)
1	DCM	24	45	91
2	Chloroform	51	44	72
3	Xylene	44	24	78
4	1,4-Dioxane	92	trace	56
5	Toluene	51	26	82

^a Reaction conditions: indole (**33a**) (0.2 mmol), *trans*- β -nitrostyrene (**16a**) (0.2 mmol), Solvent (0.5 mL, 0.4 M). ^b Isolated yields. ^c Determined by HPLC.

To enhance both enantioselectivity and the chemical yield, we figured out that miscellaneous screenings had to be made, which are the effects of temperature, additive, and concentration. Due to low chemical yield values, the temperature was not decreased below room temperature. Then, it was examined only at 50 °C in the presence of toluene as a solvent because of the low boiling point of DCM (Table 3, entry 1). Also, the H⁺ sponge and NaOAc were used as basic additives for the activation of the nucleophile, indole (**33a**) in the model reaction (Table 3, entries 2-3, respectively). Finally, the concentration was increased to 1 M from 0.4 M was applied by decreasing the amount of solvent (Table 3, entry 4). With the all results, neither chemical yields nor enantioselectivities increased upon examining the effects of temperature, additive, and concentration.

Consequently, the optimized condition for this Friedel-Craft alkylation was set as the 2 mol% organocatalyst **30** in 0.4 M DCM as the reaction solvent at room temperature with no additives in the presence of a 1:1 ratio of starting materials which was found to be the best as 91% ee and 45% yield as in Table 1, entry 3.

Table 3. Additional Screening^a



Entry	Solvent	Conc.	Temp.	Additive	Time (h)	Yield ^b (%)	ee ^c (%)
1	Toluene	0.4 M	50°C	-	46	34	78
2	DCM	0.4 M	rt	H ⁺ spon.	2	32	71
3	DCM	0.4 M	rt	NaOAc	46	26	84
4	DCM	1 M	rt	-	48	23	88

^a Reaction conditions: indole (**33a**) (0.2 mmol), *trans*- β -nitrostyrene (**16a**) (0.2 mmol), Solvent (0.5 mL, 0.4 M & 0.2 mL, 1 M). ^b Isolated yields. ^c Determined by HPLC.

2.2.2 Scope of Friedel-Crafts Alkylation

With the optimized condition in hand, the scope of the stereoselective Friedel-Crafts alkylation reaction was explored using different nitroolefins **16** and indoles **33** in order to observe the effect of electron-donating and electron-withdrawing groups (Table 4).

Table 4. Derivatization Study^a

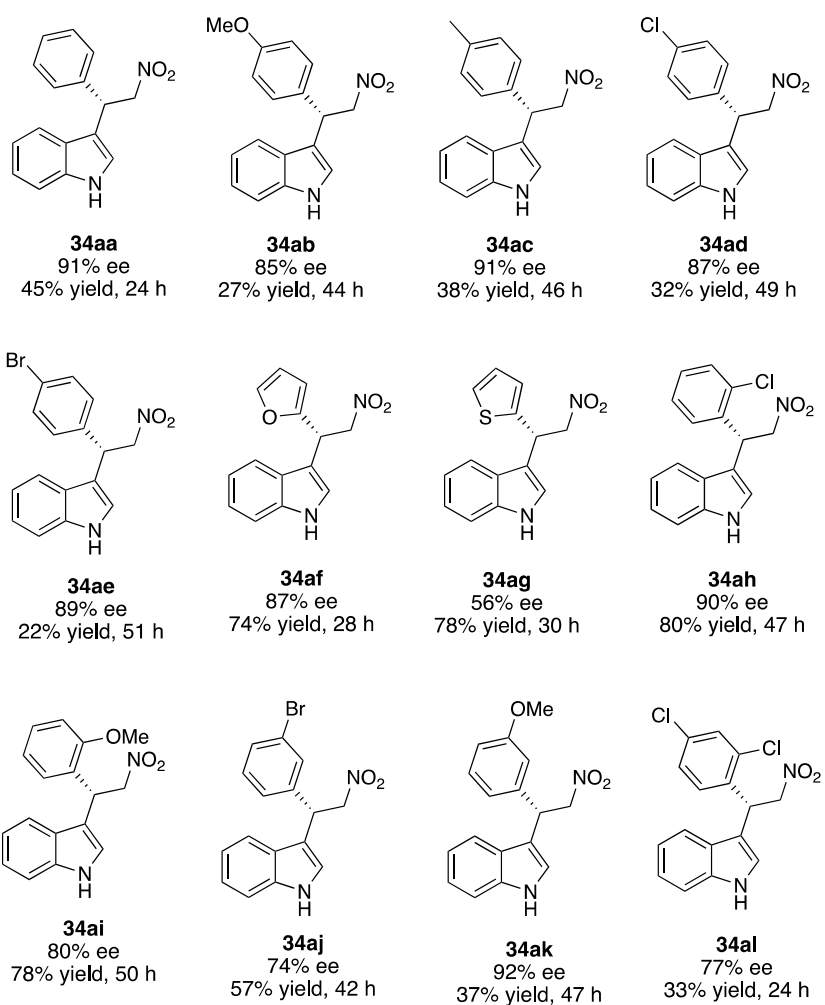
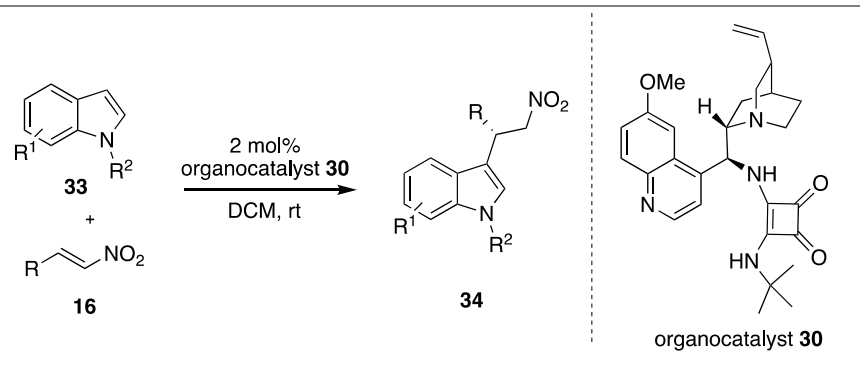
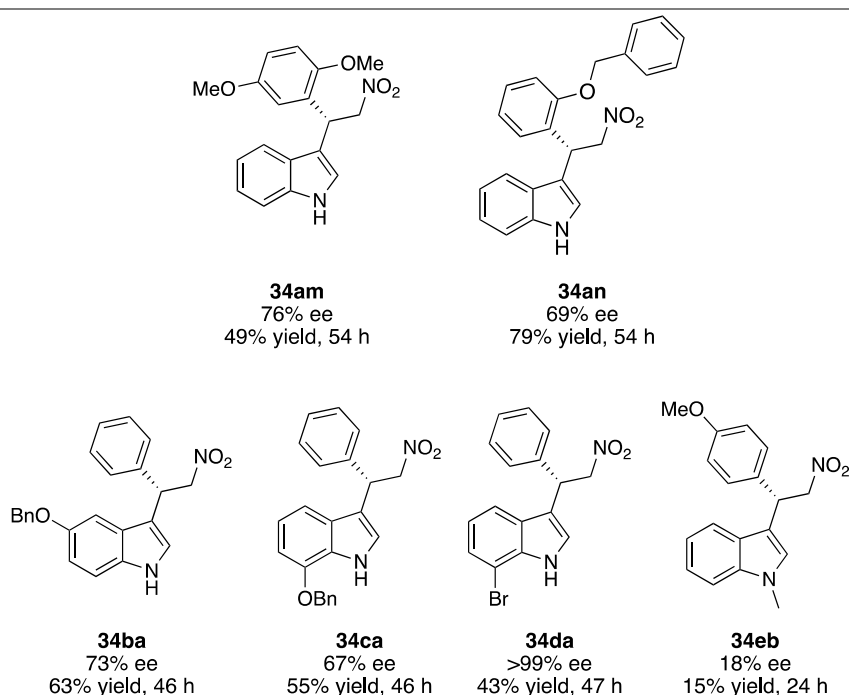
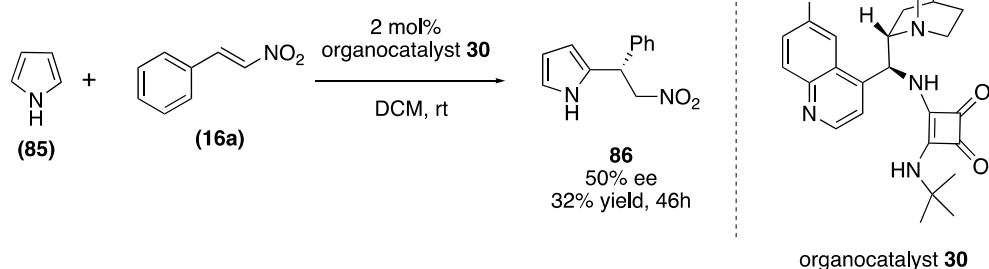


Table 4. Continued.^a

^a Reaction conditions: **33** (0.2 mmol), **16** (0.2 mmol), 2 mol% organocatalyst **30**, DCM (0.5 mL, 0.4 M) at rt.

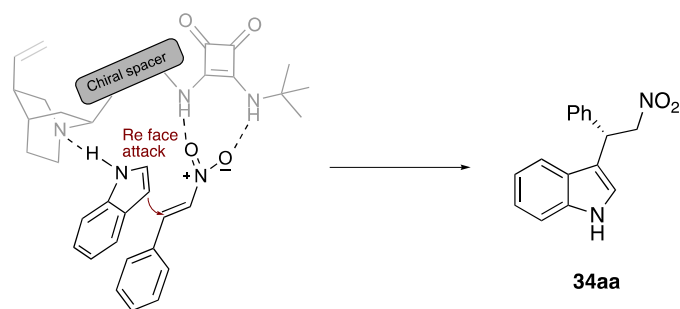
Among the all tested nitroolefin derivatives, the excellent enantiomeric excess were obtained with the unsubstituted-, **34aa** (91% ee), *p*-methyl, **34ac** (91% ee), *o*-chloro, **34ah** (90% ee), and *m*-methoxy, **34ak** (92% ee), derivatives regardless of their position or electronic nature of the substituent. On the other hand, thienyl substituted product, **34ag**, resulted in the lowest enantioselectivity value compared to the other nitroolefins. The remaining derivatives afforded the 2-indolyl-1-nitro products **34** with high enantioselectivities ranging between 69% to 89% and moderate chemical yields. When the results of the enantioselective FCA reaction were evaluated, it could be concluded that the stereoselectivity of this reaction was insensitive to the substitution pattern on the aromatic ring (*o*-, *m*-, or *p*-) of nitroolefins, as well as the electronic nature (Table 4, **34aa-34an**). Moreover, in order to widen the scope of the reaction, different indole derivatives **33** were tested in the optimized condition. Surprisingly, the 7-bromo substituted indole derivative (**33d**) attained the product

34da with excellent enantioselectivity, >99% ee, which is the highest value obtained for the derivatization part of the study. Also, 5-OBn and 7-OBn substituted indole derivatives (**33b-c**) afforded the products **34ba** and **34ca** with good outcomes in terms of enantioselectivity (73% and 67%, respectively) and chemical yields (63% and 55%). Unfortunately, *N*-Me substituted indole (**33e**) resulted in the lowest ee and yield values with the product **34eb**. The reason for this situation could be explained that the *N*-position was the coordination site of organocatalyst **30** and the indole (**33a**) as well as due to blocked by a methyl group caused the decrement of enantioselectivity and chemical yield values. In addition to these, pyrrole (**85**) was evaluated in the optimized condition as an indole derivative for the model reaction. The product **86** was attained with 50% ee and 32% yield (Scheme 20).



Scheme 20. Pyrrole (**85**) as an indole derivative in the FCA

The absolute configuration of the chiral product **34aa** was assigned as *S* based on a literature^{60,130–133} comparison of HPLC analysis and the rest of those were assigned by analogy. A transition state model was proposed to enlighten the source of chirality. In the transition state model, the deprotonation of indole (**33a**) was achieved by interaction via the H-bond by the quinuclidine nitrogen of the catalyst while the squaramide moiety activated the *trans*- β -nitrostyrene (**16a**), through double hydrogen bonding. Then, indole anion attacked the *Re* face of the activated nitroolefin affording the *S* configured product (Scheme 21).

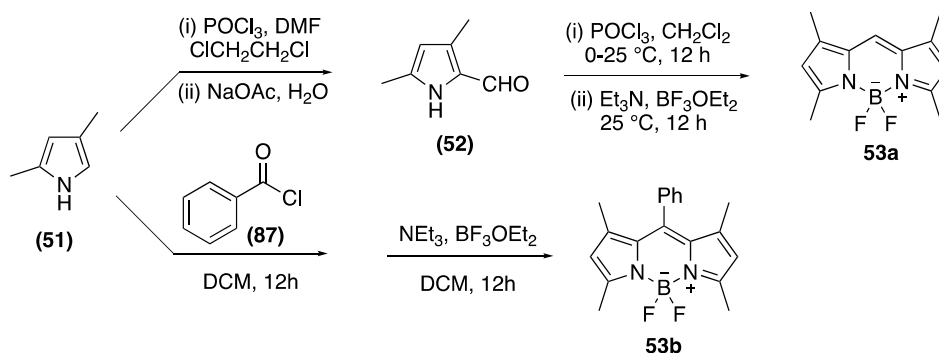


Scheme 21. Proposed transition state for FCA of indole (**33a**) with *trans*- β -nitrostyrene (**16a**)

2.3 Evaluation of Bifunctional Organocatalysts in the Enantioselective Addition of BODIPYs to Isatins

2.3.1 Synthesis of Starting Materials

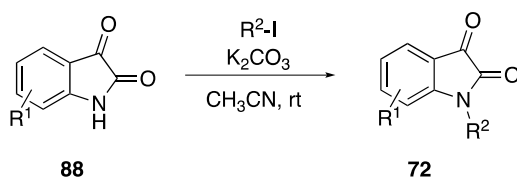
BODIPY structures have tremendous physical, chemical, and optical properties; unfortunately, their synthesis protocol is limited to a few methods. Here in this thesis, to synthesize BODIPY **53a**, firstly, 2,4-dimethylpyrrole (**51**) was transformed into its aldehyde analog **52** via Vilsmeier-Haack reaction in the presence of POCl₃ and DMF. Then, condensation of 3,5-dimethylpyrrole-2-carbaldehyde (**52**) afforded the desired BODIPY **53a** derivative by treating with POCl₃ and then, the addition of Et₃N and BF₃OEt₂ (Scheme 22).¹⁰⁵



Scheme 22. Synthesis of BODIPY Dyes

Moreover, the condensation of 2,4-dimethylpyrrole (**51**) with benzoyl chloride (**87**) resulted in the formation of a *meso*-phenyl derivative of BODIPY **53b** with a similar synthetic procedure (Scheme 22).¹³⁴

In addition to the synthesis of BODIPY dyes, *N*-alkylation, alkenylation, and benzylation of commercially available isatin derivatives **88**, were performed using corresponding alkyl, alkenyl, and benzyl halide (X= I, Br) in the presence of potassium carbonate as a base through *N*-substitution of amide moiety of isatin.¹³⁵



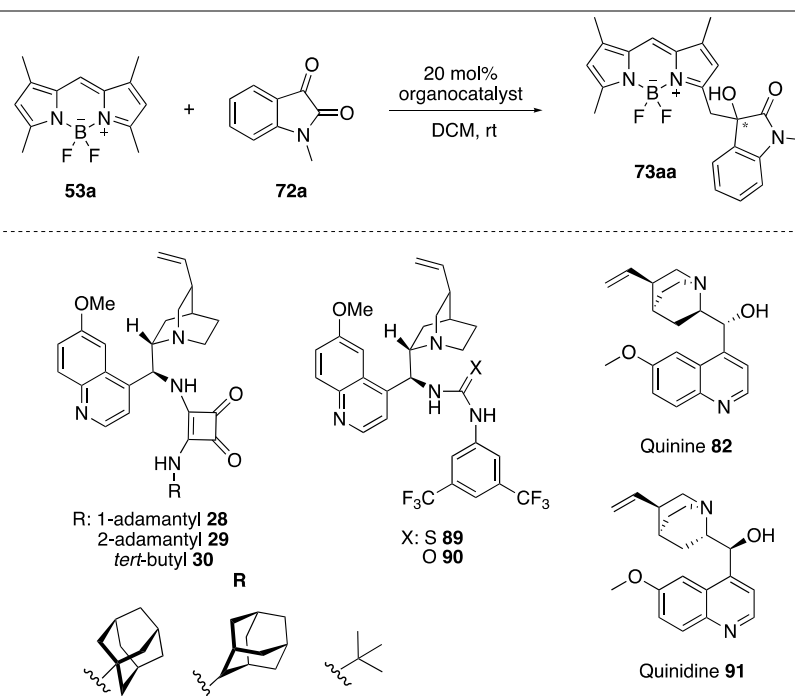
Scheme 23. Synthesis of Isatin derivatives **72**

2.3.2 Optimization Studies for Enantioselective Addition of BODIPYs to Isatins

Both the synthesis of optically active BODIPY dyes in the presence of chiral catalysts as a newly discovered area and excellent enantioselectivities in the first chapter of the thesis with quinine-based squaramides (Figure 8) directed us to synthesize the chiral BODIPY dyes in an asymmetric manner. Consequently, for the second chapter, it was aimed to get optically active BODIPY dyes with the enantioselective addition of BODIPYs **53** to isatin derivatives **72** in the presence of chiral bifunctional quinine-based organocatalysts. Isatin derivatives **72** were selected as electrophiles because these compounds were also very colorful dye structures. In addition to this, we were curious about the combination of these two dyes, enantiomerically enriched forms, and the chiroptical properties of the products. In order to initiate the optimization studies, quinine/squaramides **28-30**, quinine/thio(urea)s¹²⁸ **89-90** known in the literature, and commercially available quinine **82** and quinidine (**91**) were examined in the model reaction of addition of BODIPY **53a** to *N*-Me substituted isatin **72a**. The reaction conditions were set to the

usage of 20 mol% catalyst loading in DCM as the reaction solvent with a 1:1 ratio of starting materials at room temperature (Table 5).

Table 5. Catalyst Screening^a

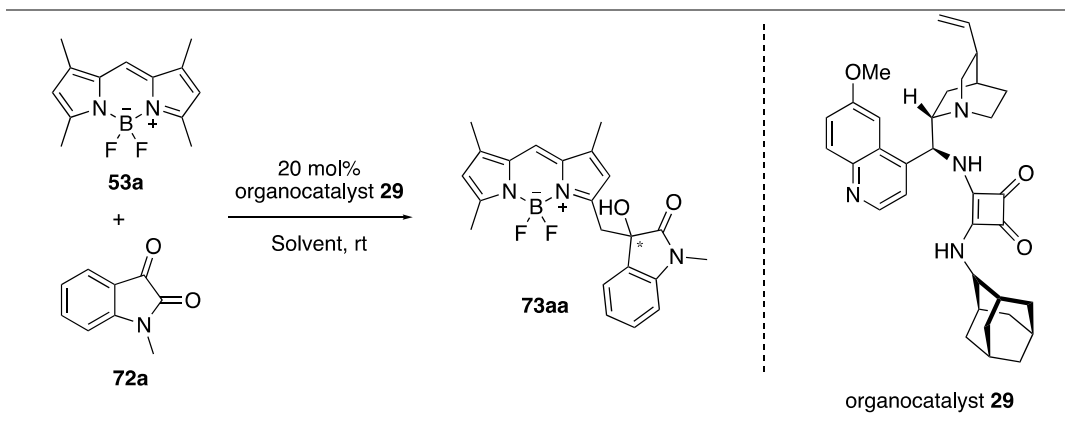


Entry	Organocatalyst	Time (day)	Yield ^b (%)	ee ^c (%)
1	28	11	7	17
2	29	6	6	38
3	30	6	8	23
4	89	10	17	30
5	90	10	40	18
6	82	6	27	6
7	91	8	26	4
8	29	14	10	51

^a Reaction conditions: BODIPY **53a** (0.1 mmol), *N*-Me Isatin **72a** (0.1 mmol), DCM (0.25 mL, 0.4 M). ^b Isolated yields. ^c Determined by HPLC. ^d *N*-Me isatin **72a** (0.2 mmol) is used.

The organocatalyst **29** was chosen as the best organocatalyst for this enantioselective addition, affording the desired product **73aa** with 38% enantioselectivity and 6% chemical yield (Table 5, entry 2). Although 38% ee seemed to be a low value, it encouraged us to go further because it was the first enantioselective result for this study and chemical yield was also low because of the formation of side products. In order to improve both enantioselectivity and chemical yield, we decided to increase the ratio of *N*-Me isatin **72a** to 2 equivalency. The change in the isatin ratio resulted in an increase in enantioselectivity from 38% to 51% and chemical yield from 6% to 10% (Table 5, entry 8). Hence, studies were continued with the 1:2 ratio of starting materials.

Table 6. Solvent Screening^a

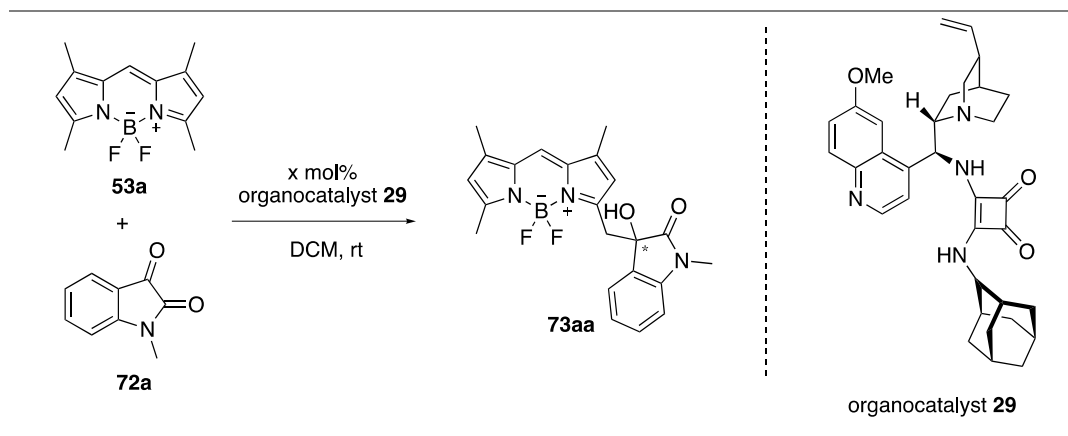


Entry	Solvent	Time (day)	Yield ^b (%)	ee ^c
1	DCM	14	10	51
2	Chloroform	9	10	38
3	1,2-DCE	7	13	40
4	Toluene	12	6	31
5	THF	7	16	25
6	Acetonitrile	6	9	rac
7	Dioxane	8	10	25

^a Reaction conditions: BODIPY **53a** (0.1 mmol), *N*-Me Isatin **72a** (0.2 mmol) Solvent (0.25 mL, 0.4 M). ^b Isolated yields. ^c Determined by HPLC.

After selecting the best organocatalyst and deciding the ratio of starting materials, the optimization studies were carried on for investigating the effect of solvent on the model reaction. Among the screened solvents, chlorinated ones, DCM, chloroform, and 1,2-DCE, gave the product **73aa** with higher enantioselectivities as 51%, 38% and 40% than the other solvents (Table 6, entries 1, 2, and 3, respectively). However, acetonitrile had no effect on the selectivity by affording the product **73aa** as a racemate (Table 6, entry 6). In addition to this, none of these solvents contributed to the increase in chemical yield of the product **73aa**. Thus, from the solvent screening, DCM was selected as the best solvent for this enantioselective addition (Table 6, entry 1).

The following parameter was the effect of concentration to be examined in the addition of BODIPY **53a** to *N*-Me isatin **72a**. Changing from 0.4 M to 0.2 M and 0.1 M caused a decrease in both enantioselectivities from 51% to 30% and 34%, and chemical yield values from 10% to 6% and 3% (Table 7, entries 1-3, respectively). On the other hand, when the concentration of BODIPY **53a** was set to 0.5 M, a slight increase was observed in the enantiomeric excess from 51% to 53% (Table 7, entries 1 and 4, respectively). As a result of concentration screening, 0.5 M was chosen as the most suitable concentration for BODIPY **53a** in the model reaction. Up to now, all screenings were conducted with 20 mol% catalyst loading and as a final parameter, the effect of catalyst loading on enantioselectivity was investigated. The reaction was carried out with 30 mol% and 10 mol% but unfortunately, the selectivity was found to be decreasing in both cases (Table 7, entries 5 and 6, respectively). In addition to these, due to low chemical yield values and long reaction durations, the 5, 2, and 1 mol% catalyst loadings were not tested in this enantioselective addition reaction. Besides, the effect of temperature was not surveyed in the optimization studies. The reasons could be explained as low chemical yield values and long reaction durations for low temperatures and also, the low boiling point of DCM, and probable low catalytic activity of organocatalyst **29** for high temperatures.

Table 7. Concentration Screening and Catalyst Loading^a

Entry	Catalyst Load.	Conc.	Time (day)	Yield ^b (%)	ee ^c
1	20 mol%	0.4 M	14	10	51
2	20 mol%	0.2 M	8	6	30
3	20 mol%	0.1 M	11	3	34
4	20 mol%	0.5 M	7	10	53
5	30 mol%	0.5 M	6	7	32
6	10 mol%	0.5 M	11	5	36

^a Reaction conditions: BODIPY **53a** (0.1 mmol), *N*-Me Isatin **72a** (0.2 mmol) ^b Isolated yields. ^c Determined by HPLC.

Consequently, the optimized condition for this enantioselective addition of BODIPY **53a** to *N*-Me isatin **72a** was decided as the 20 mol% organocatalyst **29** in 0.5 M DCM as the reaction solvent at room temperature in the presence of a 1:2 ratio of starting materials.

For the characterization of the novel compound **73aa**, as an illustrative example; ¹H NMR of the product **73aa** is given in Figure 16. In this NMR spectrum, the most indicative signal belongs to the OH group resonating at 3.86 ppm as a broad singlet. The disappearance of the broad singlet with the addition of D₂O is proved the OH group certainly. Also, the methylene protons at the conjunction point are

diastereotopic protons which give an AB system at around 3.30-3.60 ppm as doublets with $J = 15.0$ Hz.

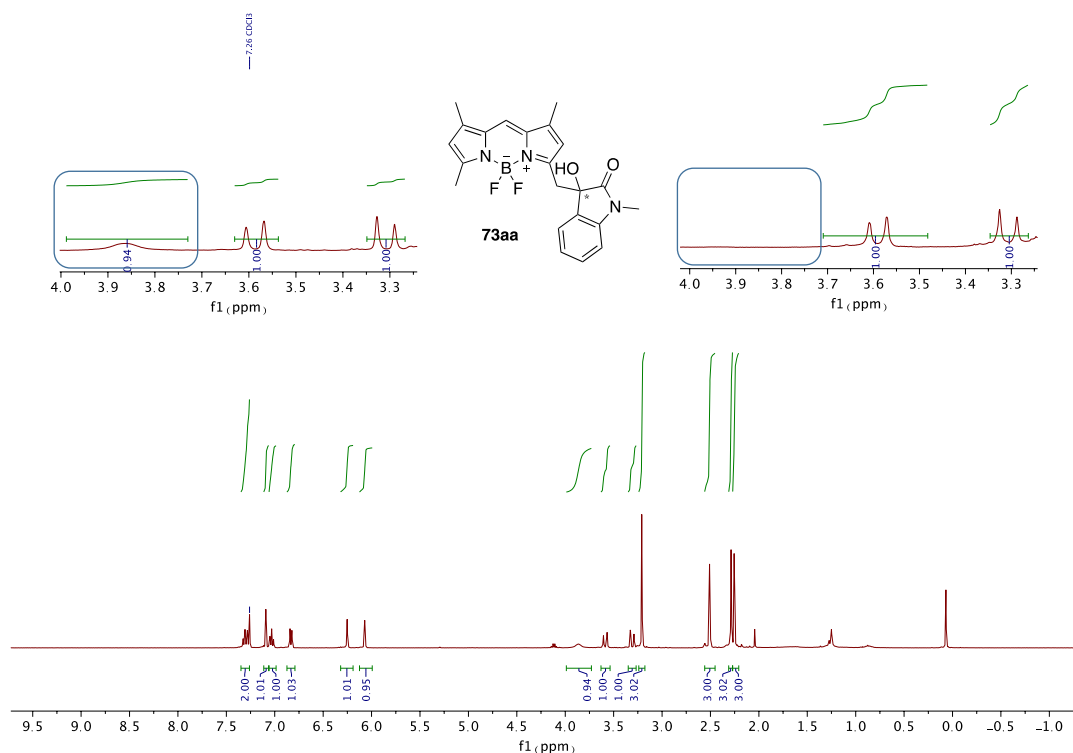


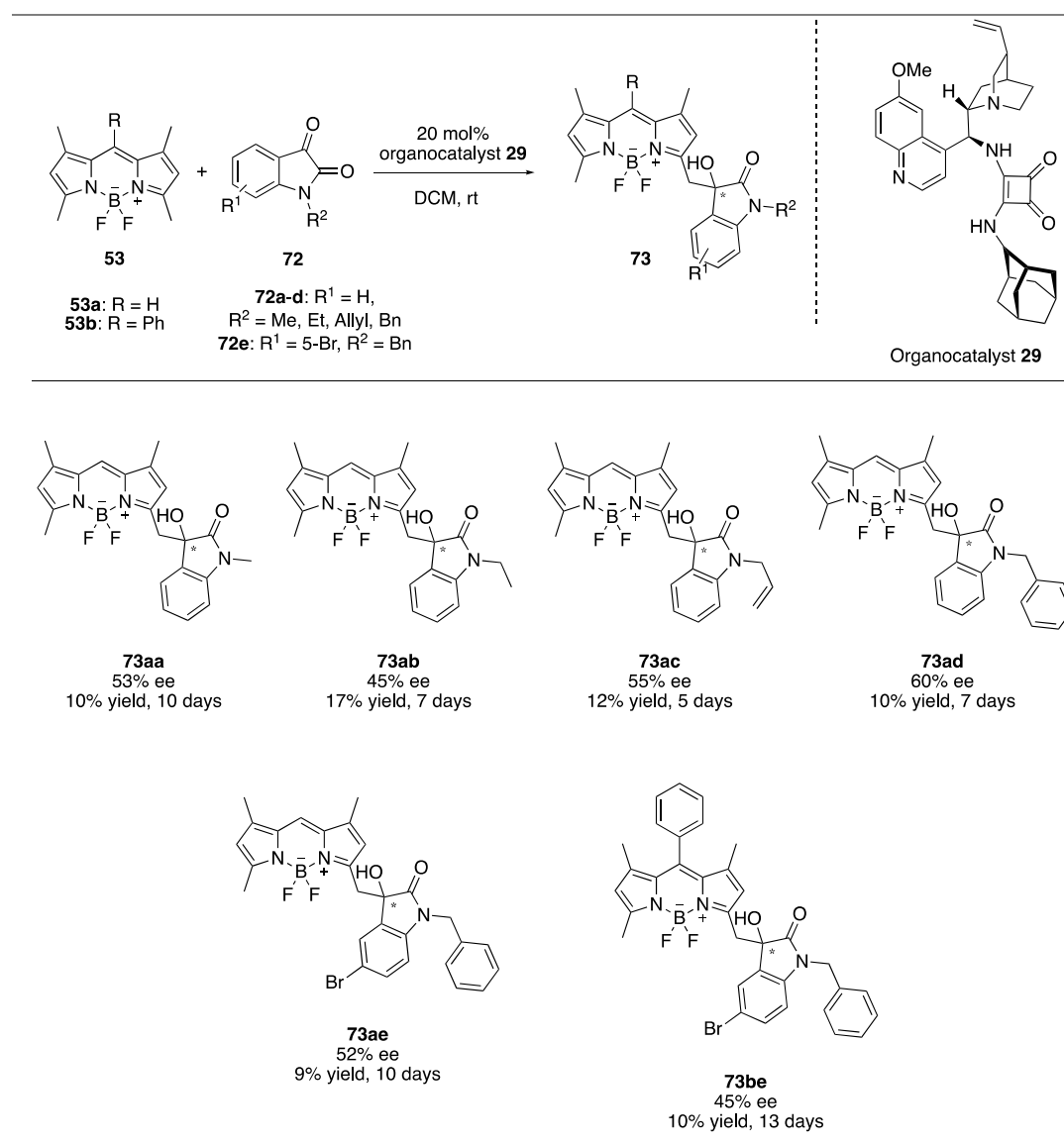
Figure 16. ^1H NMR Spectrum of compound **73aa**

2.3.3 Scope of Enantioselective Addition of BODIPYs to Isatins

In the optimized condition, six different chiral novel dyes **73** were synthesized by using different BODIPYs **53** and isatins **72**. For this part of the study, *N*-Me derived isatin **72a** was used in the model reaction in the optimization studies. Then, for the derivatization part, *N*-Et **72b**, *N*-allyl **73c**, and *N*-benzyl **73d** substituted isatins were tested firstly. Among these, *N*-benzyl substituted isatin afforded the product **73ad** with the highest enantioselectivity, 60% ee, and 10% isolated yield. After that, we decided to continue with *N*-benzyl substituted isatin derivatives. To discuss the effect of any group on the aromatic core of the isatin, 5-bromo substituted *N*-benzyl isatin **73e** was employed in the model reaction. However, no improvement was observed

in terms of both enantioselectivity and chemical yield. Finally, a *meso*-phenyl derivative BODIPY **53b** was used in this enantioselective addition. Unfortunately, the product **73be** gave the lowest ee value as 45% which was same for the *N*-Et substituted product **73ab**.

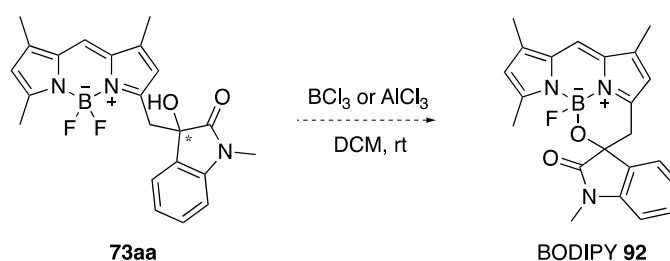
Table 8. Derivatization Study^a



^a Reaction conditions: BODIPY **53** (0.1 mmol), Isatin **72** (0.1 mmol), DCM (0.2 mL, 0.5 M).

Although both enantioselectivities were moderate (up to 60%) and chemical yield values were low (up to 17%), this study will be the *first example* of this kind of enantioselective addition of BODIPYs **53** to isatins **72**. Six different novels of BODIPY dyes **73** were synthesized in the presence of bifunctional organocatalyst **29** by using the acidity of proximal α -methyl groups at the 3,5 position of BODIPY **53** (Table 8).

After completing the derivatization, the cyclization studies will be conducted as future work to widen the scope of this enantioselective addition. The product **73aa** will be tested whether to give a cyclization product. This future work will be done with BCl_3 or AlCl_3 (Scheme 24).



Scheme 24. Future studies with **73aa**

2.3.4 Spectroscopic and Chiroptical Properties

To examine the spectroscopic properties, firstly, UV-vis analysis was conducted with the 10 μM CHCl_3 solutions of BODIPY **53a**, *N*-Me isatin **72a**, and the product **73aa**. The analysis showed that the compound **73aa** gave an absorption peak at 513 nm by shifting to red side with a 4 nm difference from BODIPY **53a** which absorbs at 509 nm (Figure 17).

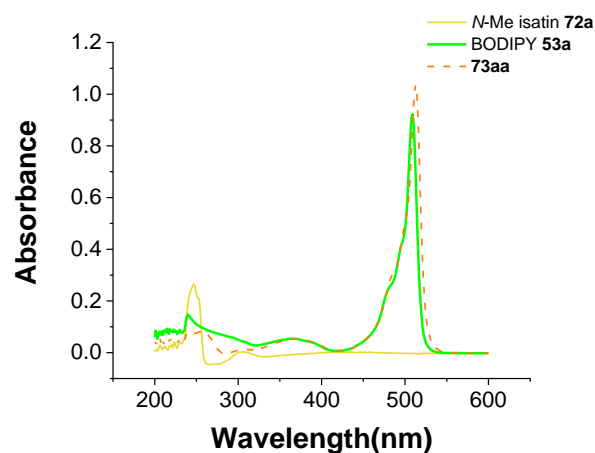


Figure 17. UV-vis absorption spectra of BODIPY **53a**, *N*-Me isatin **72a**, and BODIPY **73aa**

Then, another UV-vis and FL analysis was done to investigate the effect of solvent on product **73aa**. For that purpose, solutions were prepared at 2×10^{-6} M with solvents which were MeCN, CHCl_3 , DCM, *n*-hexane, and toluene (Figure 18). In both absorption and emission spectra, compound **73aa** showed very low solvent-dependent chromofluorogenicity by yielding small bathochromic shifts (about 10 nm) compared to BODIPY **53a**.

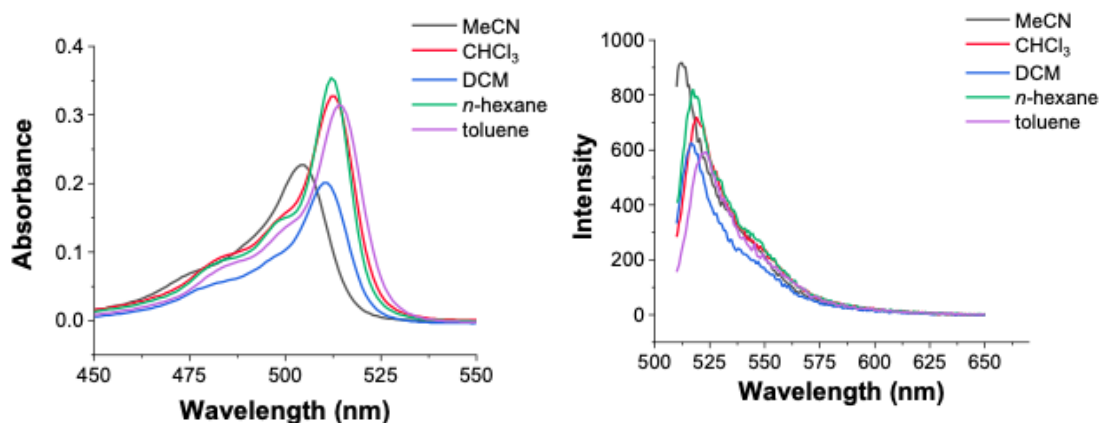


Figure 18. UV-vis absorption and fluorescence emission spectra of **73aa** ($2\mu\text{M}$).

In addition to low solvent-dependency, high emissions were observed in fluorescence analysis (In the analysis, the excitation and emission slits were set to 3.5 nm). To be a representative example, the fluorescence quantum yield of BODIPY **73aa** was calculated as 0.78 with the relative method¹³⁶ by taking the fluorescein as the standard (Figure 19).¹³⁷

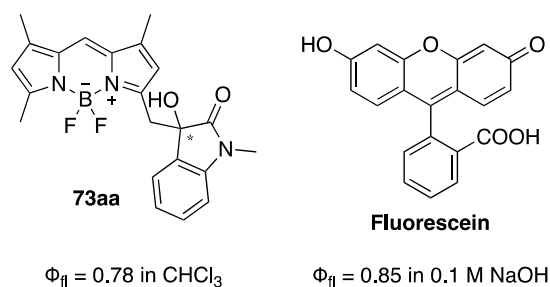


Figure 19. Comparison of quantum yields of **73aa** and fluorescein

Moreover, the photophysical properties of all six novel BODIPY dyes **73** were studied. Their absorption and emission spectra were measured at 1×10^{-6} M CHCl_3 solution. In all derivatives, the main absorption band centered between 512-513 nm was observed in UV spectra. It could be concluded that absorption maxima were red-shifted on those derivatives with substitution at the isatin core. Only *meso*-phenyl substituted BODIPY product **73be** was blue-shifted by giving maximum absorption at 506 nm (Figure 20).

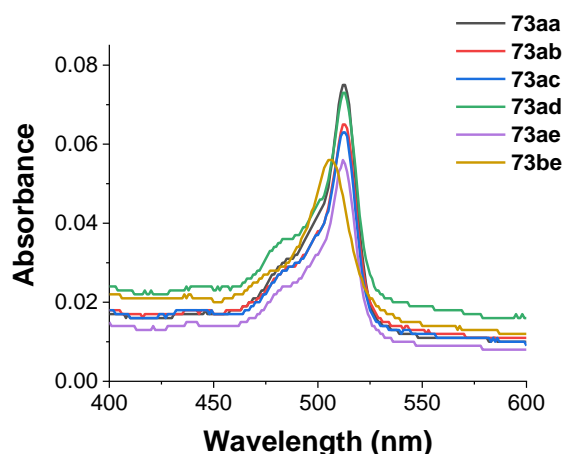


Figure 20. UV-vis absorption spectra of derivatives **73**

Moreover, the fluorescence emission spectra were recorded after excitation at absorption maxima from 450 to 650 nm with the same red shift effect as in the absorption spectra (In the fluorescence analysis, the excitation and emission slits were set to 5.0 nm). As in general, all derivatives gave high fluorescence emission intensity (Figure 21). However, among all derivatives, the emission intensity of *meso*-phenyl substituted BODIPY product **73be** was relatively low compared to other derivatives. The reason for the low emission value could be explained by the breaking down of the rigidity of the structure caused by the rotation of the phenyl group at the *meso*-position of the structure.

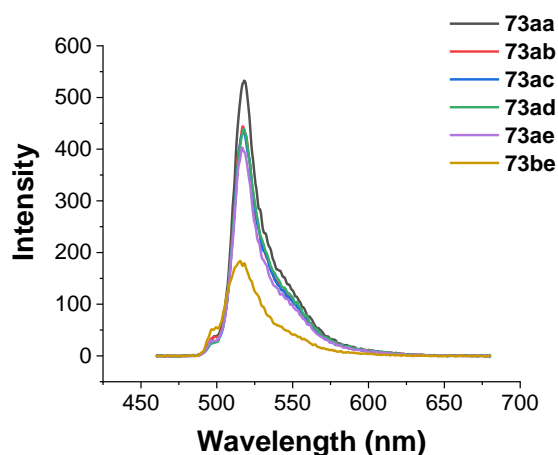


Figure 21. Fluorescence emission spectra of derivatives **73**

In order to study the chiroptical properties, ECD spectra of enantiomerically enriched product **73aa** were recorded with varying concentrations in the range of 1×10^{-5} , 2×10^{-5} , 5×10^{-5} , and 1×10^{-4} M in CHCl_3 solutions. In the ECD spectra, a very low signal was observed in the prepared concentrations (Figure 22). The reason for low ECD activity could be explained as the asymmetric unit was far from the boron dipyrromethene chromophore. Also another reason could be racemization in ECD due to the existence of both enantiomers with a 76.5:23.5 ratio.

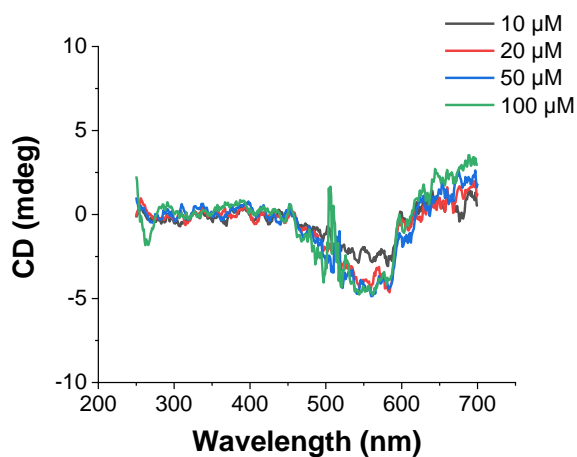
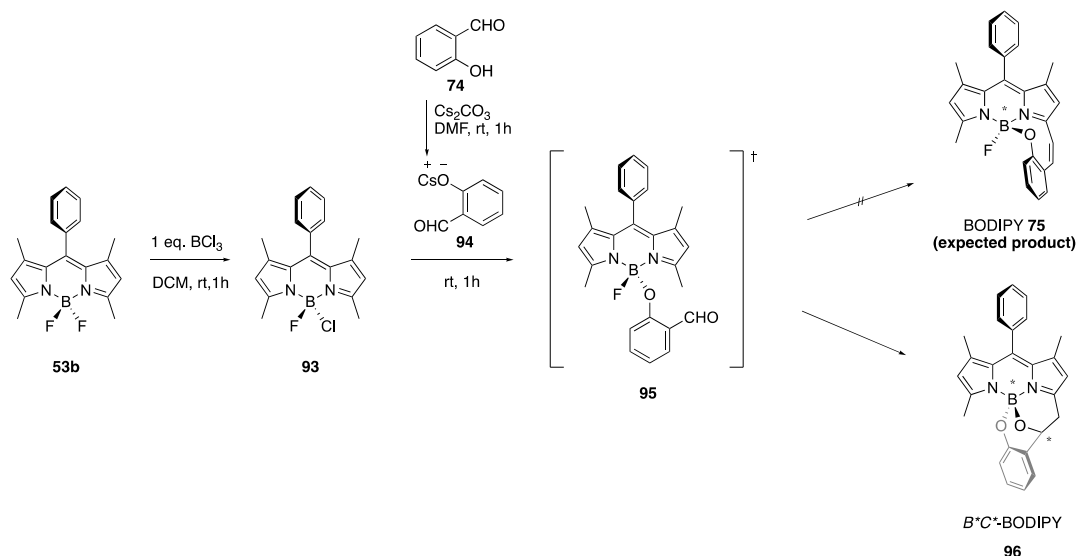


Figure 22. ECD spectra of **73aa** in different concentrations

2.4 Synthesis of Novel BODIPY Chiral at Boron and Carbon

BODIPY dyes are highly symmetrical structures that belong to the C_{2v} point group.¹⁰⁶ Hence, it is a challenge to induce chirality in those structures. Also, in point-chiral BODIPYs^{138,139} whose asymmetric unit is far from chromophore and those carrying a stereogenic boron atom,^{140,141} ECD activity is hardly observed. For these reasons, in the third part of the study, we aimed to synthesize a helically chiral BODIPY dye to benefit from structural chirality due to its high ECD and CPL activities¹⁴² and to investigate its spectroscopic, chiroptical, and electrochemical properties. With this purpose, the synthetic methodology was designed with the unique reactivities of BODIPY dyes in a cascade of nucleophilic substitution at boron followed by Knoevenagel condensation of α -methyl group with an unprecedented intramolecular fashion.¹⁴³ For that, the synthesis involved two pots in which the substitution of fluorine with chlorine¹⁴⁴ of BODIPY **53b**¹³⁷ took place in one pot, and the cesium salt of salicylaldehyde was prepared in the second pot. Then, mixing these two pots should give the expected helically chiral BODIPY **75**, but instead, we got a BODIPY point-chiral at boron and carbon, BODIPY **96**, with 18% isolated yield and some trace of its uncyclized precursor **95** (Scheme 25).



Scheme 25. The two-pot, one-step synthesis of BODIPY **96**

The molecular structure of BODIPY **96** was characterized by NMR (^1H , ^{13}C , COSY, HMBC, and HSQC), high-resolution mass spectrometry (HRMS), UV-visible (UV-vis), and X-ray single-crystal diffraction analysis. In the NMR spectra (Figure 23) of the BODIPY **96**, the characteristic peaks were the aliphatic protons which H_m and H_a were at the conjunction point. H_m and H_a were the diastereotopic protons, and with the neighboring proton, H_x , an AMX-type spin patterning was observed for couplings. H_m gave doublet at 2.95 ppm with a coupling constant $J_{\text{H}_a\text{-H}_m} = 18.5$ Hz. Also, H_a gave doublet of a doublet at 3.51 ppm with coupling constants $J_{\text{H}_a\text{-H}_m} = 18.5$ Hz and $J_{\text{H}_a\text{-H}_x} = 6.4$ Hz. In addition, H_x gave a singlet peak at 5.45 ppm. The significant difference in chemical shift values of diastereotopic protons, H_a and H_m , could be explained by the generated asymmetric centers, B^* and C^* , or chiral space. Although the geminal homonuclear coupling of diastereotopic protons, $J_{\text{H}_a\text{-H}_m} = 18.5$ Hz, and vicinal coupling, $J_{\text{H}_a\text{-H}_x} = 6.4$ Hz, were traceable from the cross-peaks in the ^1H - ^1H COSY spectrum (see page 124, Appendices A), no vicinal coupling between H_m and H_x was observed most probably because of the 78° dihedral angle.

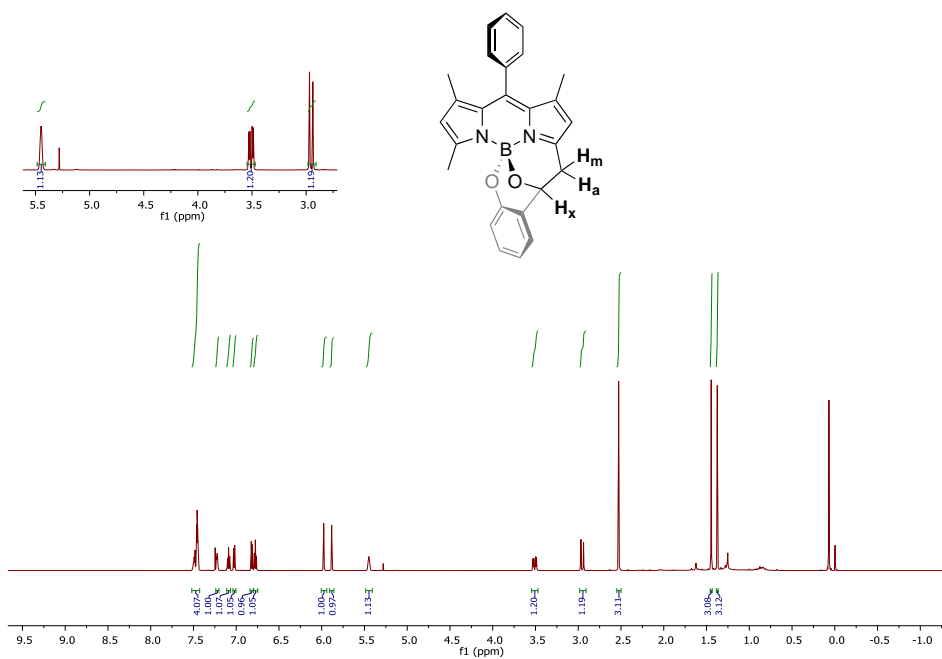


Figure 23. ^1H NMR Spectrum of BODIPY **96** in CDCl_3

In addition, due to two stereocenters of BODIPY **96**, four diastereomers were expected to form in the reaction medium. To clarify this, LC-MS analyses were conducted with several aliquots of 1 mL from the reaction mixture at times t_1 : 1min, t_2 : 15 min, t_3 : 30 min, and t_4 : 60 min. But, LC-MS analysis showed the exclusive formation of one diastereomer. Also, at t_1 : 1min, the mass of BODIPY **96** was observed on the chromatogram, meaning that the reaction was almost instantaneous (Figure 24).

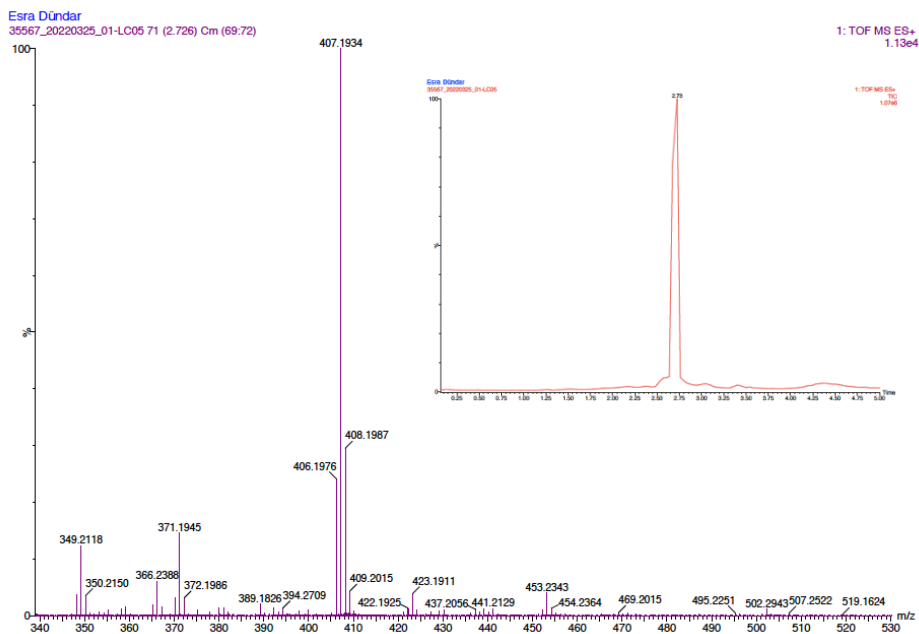


Figure 24. LC-MS analysis at t_1 : 1 min

However, the reaction time was set to 60 min. (1h) since the optimum reaction time as it allows a smoother chromatographic separation (Figure 25).

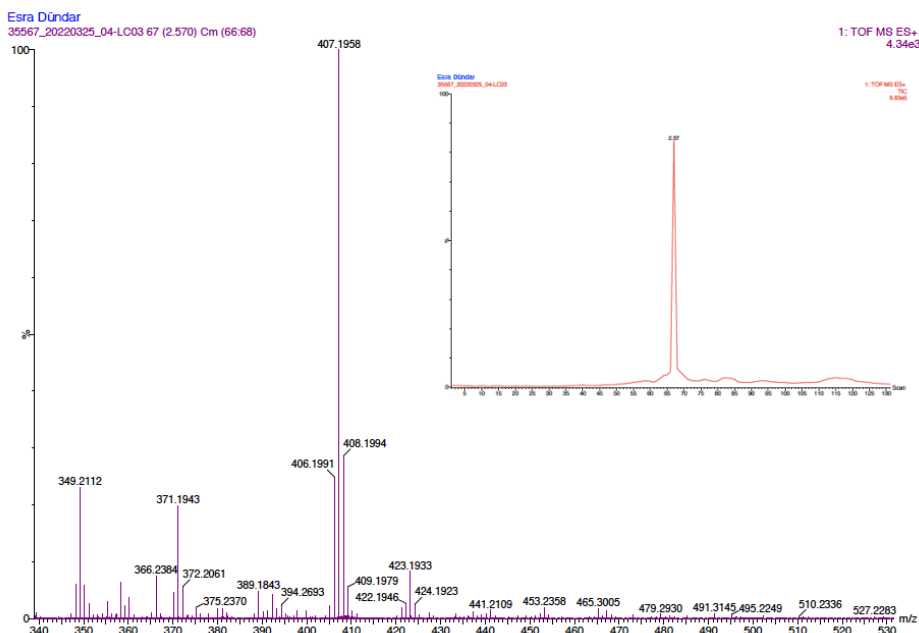


Figure 25. LC-MS analysis at t_1 : 60 min

The formation of other diastereomer was not observed since the reaction mechanism would be energetically disfavored because of the large strain. As a result of this, the enantiomers had a relative configuration of either R, R, or S, S.

In the reaction medium, we could isolate an intermediate **95** which was the uncyclized form, and also, characterize it with HRMS and NMR. Due to the existence of intermediate, we could propose a reaction mechanism in which the first step may be the nucleophilic substitution at boron atom by the salicylaldehyde cesium salt giving prochiral intermediate or its *Cl*-congener. Then, the deprotonation of α -methyl groups of intermediate or its *Cl*-congener would be conducted by the excess aryloxy base generating the carbanion which would attack the formyl unit. Then, secondary alkoxide reactive intermediate was formed and as a final step, oxyanion would substitute the remaining halogen on the boron center in order to give BODIPY **96** in a stereospecific manner (Figure 26). Moreover, the second reaction mechanism would be initiated with the trapping of the benzylic oxygen that would form upon a reaction between α -methyl deprotonated and salicylaldehyde **74**. Unfortunately, this mechanism would require a rigorous quantum chemical calculation.

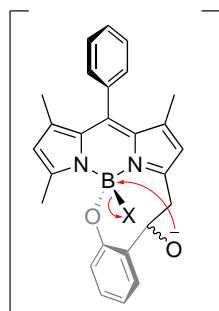


Figure 26. Proposed reactive intermediate

2.4.1 Spectroscopic Properties

In order to examine the spectroscopic properties of BODIPY **96**, we took the dye's UV-vis electronic absorption and emission spectra in different solvents with varying

degrees of polarity (Figure 27a and b). Also, among all solvents, for MeCN, CHCl₃, toluene, and *n*-hexane, the fluorescence quantum yields, weighed lifetimes, molar absorptivities, absorption, and emission maxima of the dye were given (Table 9).

Table 9. Optical characterization of BODIPY **96** in various solvents

solvent	λ_{abs} [nm]	ϵ [M ⁻¹ cm ⁻¹]	λ_{em} [nm]	τ_{avg}^a [ns]	Φ_{fl}^b [10 ⁻³]
MeCN	503	62500	522	0.15	0.62
CHCl ₃	508	62500	524	0.13	1.93
toluene	510	66500	524	0.23	0.72
<i>n</i> -hexane	508	61500	520	0.28	0.38

^a The weighed mean fluorescence lifetime. ^b Relative fluorescence quantum yields were determined using fluorescein as the standard ($\Phi_{\text{fl}} = 0.85$ in 0.1 M NaOH).¹³⁷

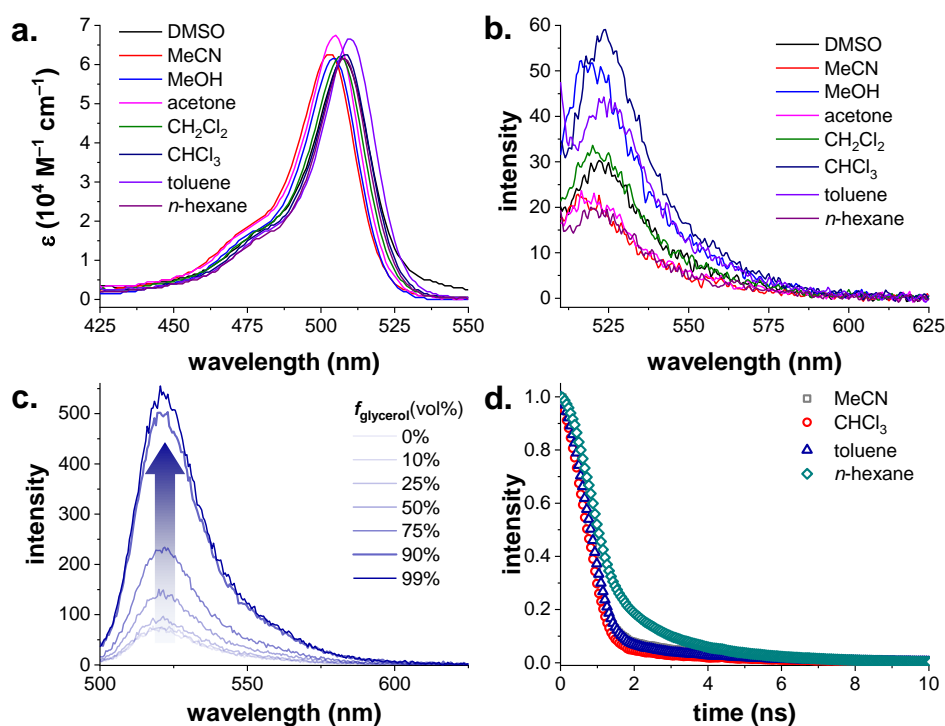


Figure 27. Spectroscopic analyses of BODIPY **96**

Absorption and emission maxima of the BODIPY dyes are generally not affected significantly by double oxynucleophile substitution at the boron center, but these

substitutions improve the quantum yields.^{78,79,100,102} When compared to **53b**, small bathochromic shifts (approximately 10 nm) were observed in both absorption and emission spectra of BODIPY **96**, which carrying one alkoxy and one aryloxy unit on the boron center. Also, BODIPY **96** showed very low solvent-dependent chromofluorogenicity in UV-vis and fluorescence analyses. More interestingly, the quantum yields of the BODIPY **96** were smaller than 1% in all the solvents tested (Table 9). This result showed that BODIPY **96** displayed considerably attenuated emission contrast to **53b** and O-BODIPYs.^{78,79,100} Recognizably, a seven-fold enhancement in the emission intensity of the BODIPY **96** in ethanol-glycerol mixtures with different viscosities was observed by an increase in the percentage of glycerol (Figure 27c). Though this indicated that the nonradiative deactivation, supposedly through intramolecular vibrational relaxations, had a significant contribution to the quenching process, it does not account for all of the quenching. So, the excited-state lifetimes of the BODIPY **96** were measured (Figure 27d and Table 9). Different from the typical BODIPYs,⁷⁹ BODIPY **96** had very fast decays with the possibility of intersystem crossing to a triplet manifold (S_1-T_1) in the excited state. However, no phosphorescence was observed in the MeCN, $CHCl_3$, toluene, and *n*-hexane solutions of BODIPY **96** at room temperature. We could conclude that the reason for the weak fluorescence of BODIPY **96** was attributed to the nonradiative vibrational relaxations and probably the S_1-T_1 transition processes which contribute more significantly.

To explain the unusual fluorescence emission and to ensure the complex molecular structure, X-ray analysis was conducted with the crystals of BODIPY **96** formed by slow evaporation from methanol. In the X-ray crystal structure, the planarity of the C_9BN_2 framework was destroyed by an 18.7° dihedral angle between the two pyrrole rings (Figure 28).

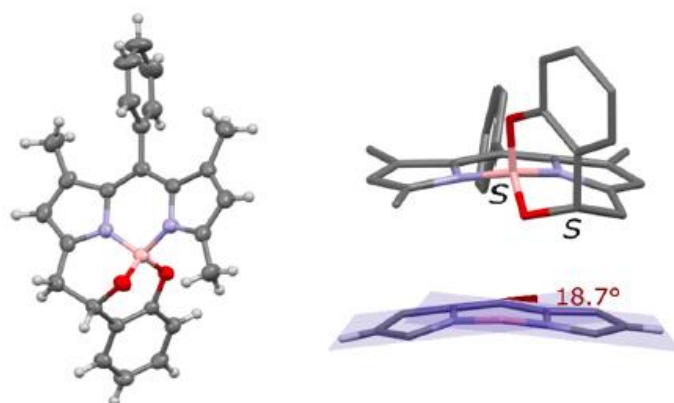
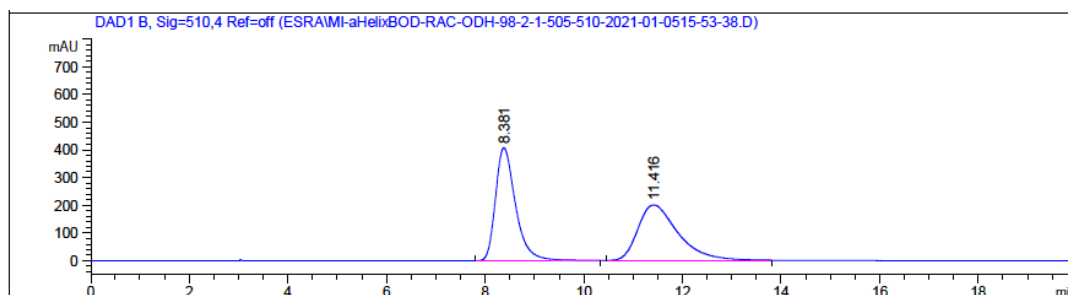


Figure 28. X-Ray Structure of BODIPY **96**

Moreover, the C-C and C-N bond lengths of the C₉BN₂ framework were 1.365 to 1.445 Å and 1.336 to 1.403 Å, respectively. No distinction between single and double bonds was an indication of a strong delocalized π -system. Large molar absorptivity constants (Table 9) were also another important evidence for the π -conjugation for BODIPY **96** although it had the bending of the core by 18.7°. On the contrary, the 18.7° dihedral angle could be the reason for the weak fluorescence of BODIPY **96** as there are BODIPYs for which such quenched fluorescence is closely related to distortion from planarity leading to spin-orbit coupling.¹⁴⁵

2.4.2 Resolution of BODIPY **96**

After characterization of the structure of BODIPY **96**, this novel compound was resolved well into its enantiomers on chiral stationary-phase high performance liquid chromatography (HPLC) using an analytical Chiralcel OD-H column under isocratic conditions (*n*-Hexane/Isopropanol; 98:2). The separated two peaks with an equal area showed the expected enantiomerism (Figure 29). Also, the kinetic resolution of BODIPY **96** at mg quantities was conducted by a semipreparative Kromasil 10-Cellucoat column. The chromatograms of the separated enantiomers are shown in Figures 30 and 31, respectively.



Signal 2: DAD1 B, Sig=510,4 Ref=off

Peak #	RetTime [min]	Type	Width [min]	Area [mAU*s]	Height [mAU]	Area %
1	8.381	BB	0.4249	1.15018e4	407.37750	50.4564
2	11.416	BB	0.6799	1.12937e4	200.26288	49.5436

Figure 29. The separation of enantiomers of BODIPY 96 on chiral HPLC

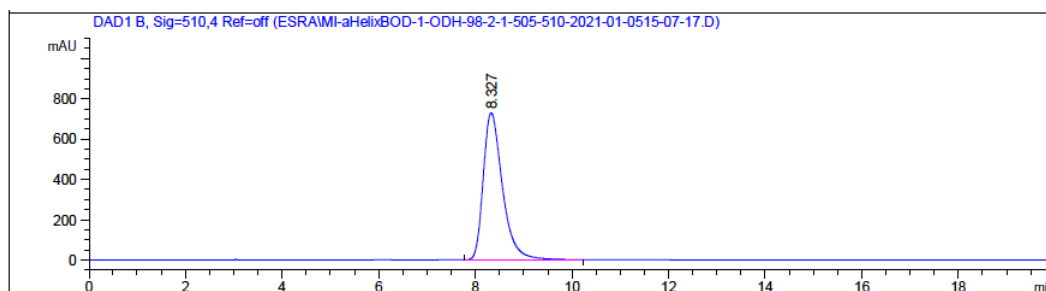


Figure 30. The HPLC chromatogram of fast-eluting enantiomer

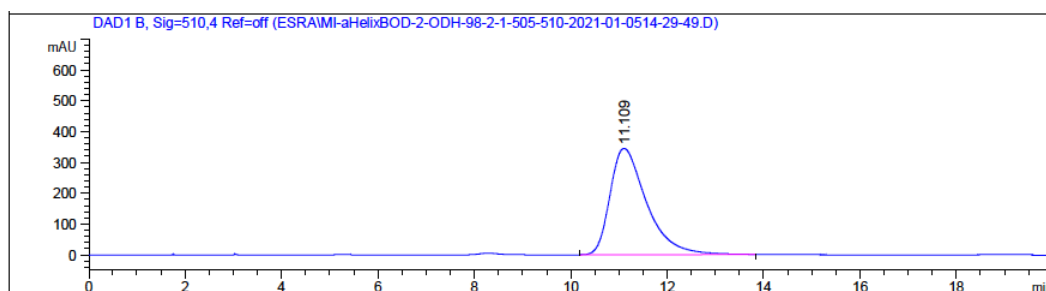


Figure 31. The HPLC chromatogram of slow-eluting enantiomer

Moreover, optical activities of separated enantiomers were tested. For the fast-eluting enantiomer, a large counterclockwise specific rotation was observed as -567.9° and $+617.3^\circ$ for the slow-eluting one. Almost equal but opposite directions in rotating plane-polarized light was a supporting evidence for enantiomeric relationship. For point-chiral small organic molecules, these kind of large specific rotations were not usually observed.

2.4.3 Chiroptical and Electrochemical Properties of BODIPY **96**

In order to investigate the chiroptical properties, ECD spectra (Figure 32) of the enantiomers of BODIPY **96** were recorded in $50\mu\text{M}$ solutions prepared in chloroform. The ECD spectra of the enantiomers had a similar shape and appearance to UV spectra as well as shared mirror symmetry characteristics across the entire region of the electromagnetic radiation. The strongest Cotton effect was observed with a monosignate nature in the visible region at 508 nm due to boron dipyrromethene chromophore which was responsible for the absorption of light in that region. Chirality was induced to the chromophore very efficiently at least in its ground state by the central chirality created at boron & carbon, and perhaps more so the bent geometry adopted as a result of the imposed stereoelectronic constraints or these factors makes it now an “inherently chiral” small organic molecular chromophore. Due to their highly symmetrical structure, transferring chirality to BODIPY dyes is a substantial concept. As a result, it is worth noting clear Cotton absorptions in the visible region with moderate dissymmetry factors ($|g_{abs}|$ 2.11×10^{-4} for (+)-BODIPY **96**; 1.76×10^{-4} for (–)-BODIPY **96**) recorded for the enantiomers.¹⁴⁵ Since BODIPY **96** had weak emission behavior, CPL analysis was not conducted.

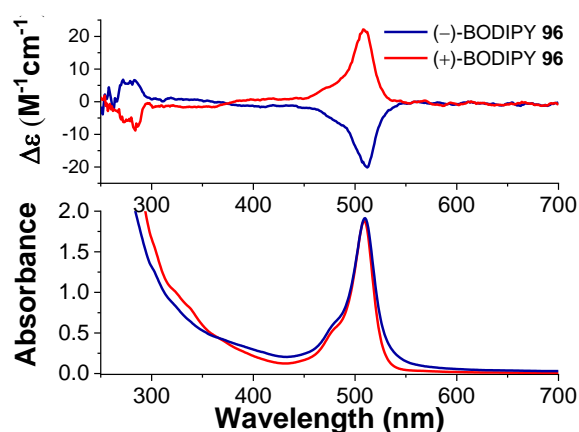


Figure 32. ECD and UV spectra of enantiomers of BODIPY **96**

Moreover, cyclic voltammetry (CV) and differential pulse voltammetry (DPV) analyses were conducted to investigate the electrochemical properties of BODIPY **96** (Figure 33). The analysis was performed *vs.* Ag/AgCl in an anhydrous and degassed CH₃CN solution containing [Bu₄N⁺][PF₆⁻] (0.1 M) as a supporting electrolyte. It could be concluded that oxidation and reduction processes of BODIPY **96** were reversible from looping CV and symmetric DPV spectra.

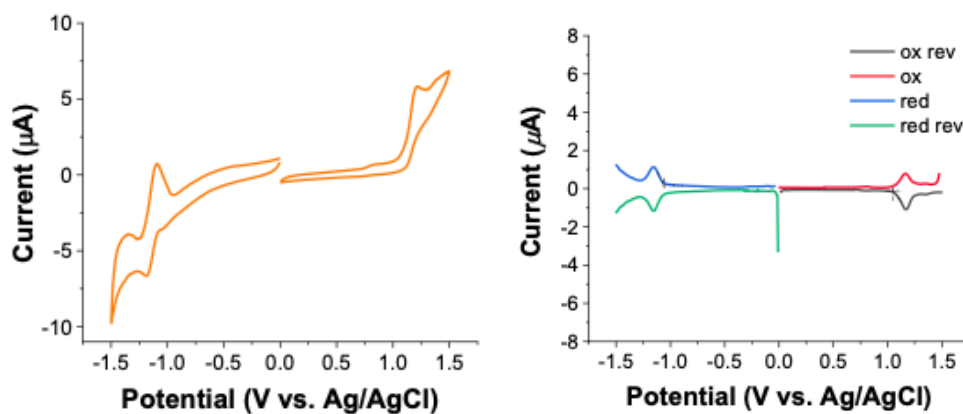


Figure 33. CV (left) and DPV (right) of BODIPY **96**

In addition to CV and DPV analyses, HOMO, LUMO, and E_{gap} values of BODIPY **96** were calculated (Table 10).

Table 10. Electrochemical Properties of BODIPY **96**

	$E_{\text{ox}}^{\text{onset}}$ (eV) ^a	$E_{\text{red}}^{\text{onset}}$ (eV) ^a	E_{HOMO} (eV) ^b	E_{LUMO} (eV) ^c	E_{gap} (eV) ^d
BODIPY 96	1.05	-1.06	-5.76	-3.65	2.1

^a Calculated from the DPV ^b Calculated with E_{HOMO} : - (4.71 + $E_{\text{ox}}^{\text{onset}}$) ^c Calculated with E_{LUMO} : - (4.71 + $E_{\text{red}}^{\text{onset}}$) ^d Calculated with E_{gap} : $E_{\text{LUMO}} - E_{\text{HOMO}}$

2.4.4 Stability Tests

Due to its unique structure, BODIPY **96** was investigated about thermal and (photo)chemical stability. BODIPY **96** dye was firstly tested to be thermally vulnerable to epimerization because of its tetrahedrally arranged boron center which consists of three covalent and one dative bond. For this purpose, 0.1mM xylene solutions of the fast-eluting enantiomer of (-)-BODIPY **96** were prepared and heated at 50, 75, 100, 125, and 150 °C for one hour. These first four reactions were conducted in closed vessels but the last one in an open-air atmosphere. Any epimerization was not observed in all runs with HPLC analysis. The results were indicative of high configurational stability (See pages 151-155, Appendices B, for HPLC chromatograms).

Moreover, the racemic form of BODIPY **96** was tested for acid-base stability. 1mM DCM solutions of the dye were prepared and these solutions were stirred with equal moles of acids (acetic acid and trifluoroacetic acid)/bases (triethylamine and piperidine) at room temperature. Even after one week of stirring, the BODIPY **96** did not show any observable deterioration except in the trifluoroacetic acid case. In the trifluoroacetic acid experiment, after 1 h, color change, from brownish-orange to maroon, was observed and a new spot was formed on TLC. The removal of the boron bridge was proved with LC-MS analysis (Figure 34).

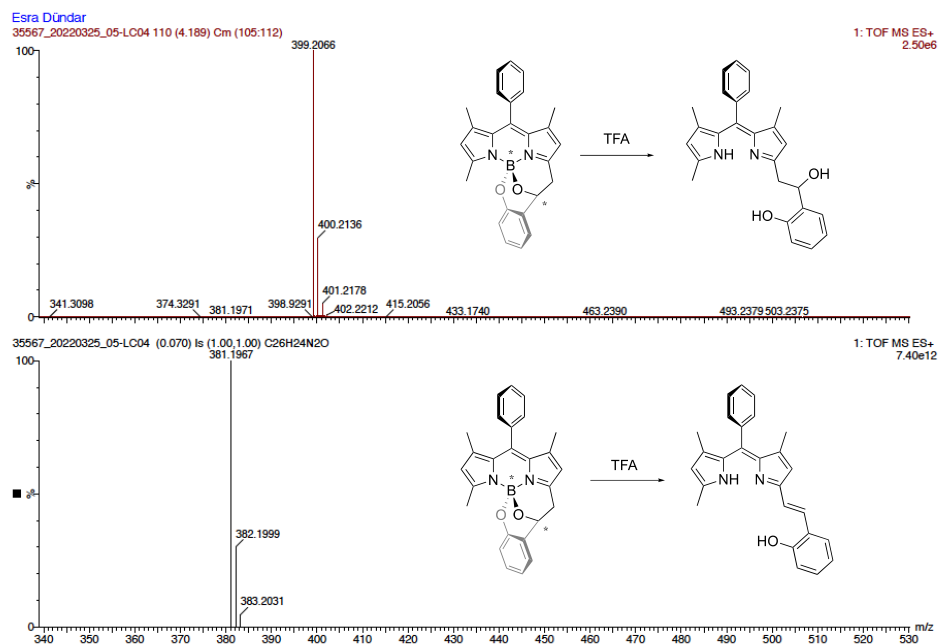


Figure 34. LC-MS analysis after TFA addition

As a final stability test, the photochemical stability of BODIPY **96** was examined. The dye in methanol was irradiated with a light pulse (λ_{ex} 490 nm) for 1h at 10 second intervals and recorded its fluorescence. Due to almost constant fluorescence (<1% decomposition) over that period, it could be concluded that racemic BODIPY **96** was considerably photostable (Figure 35).

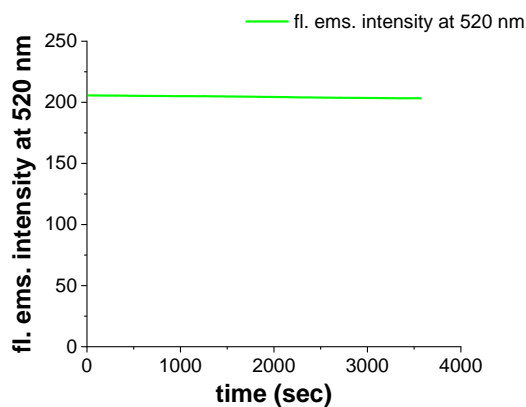


Figure 35. Time-dependent fluorescence intensity profile of BODIPY **96**

CHAPTER 3

EXPERIMENTAL

3.1 Materials and Methods

In this thesis, ^1H and ^{13}C NMR spectra of products were recorded in Bruker Spectroscopin Avance DPX 400 spectrometer with CDCl_3 and DMSO-d_6 as solvents. Also, an Agilent-Premium Compact (600 MHz, 14.1 Tesla) was used for taking high-resolution NMR spectra at Çankırı Karatekin University. Spin multiplicities were stated as bs (broad singlet), s (singlet), d (doublet), dd (doublet of doublet), t (triplet), and m (multiplet). Chemical shift values were reported in ppm with TMS as a reference, and coupling constants of compounds were specified in Hertz (Hz). All ^1H and ^{13}C NMR spectra of products were given in Appendices part A.

HPLC analyses were conducted both on Thermo-Finnigan and Agilent HPLC systems with the usage of Daicel Chiralpak OD-H, AD-H, AS-H, and OJ-H columns at room temperatures. For the analyses, different *n*-Hexane/Isopropanol systems were used as mobile phases. HPLC chromatograms of products were given in Appendices part B. Also, preparative separations of enantiomers were done on an Agilent Technologies Preparative HPLC-1200 Series with a diode array detector (DAD) using a Kromasil® 10-Cellucoat column (1.0 cm.Å~25 cm) in Unam, Bilkent University.

The measurement of optical rotations was done by Rudolph Scientific Autopol III polarimeter and specific rotations were reported as $[\alpha]_{\text{D}}^{25}$ (*c* in g/100 mL, solvent). The conversions of products were controlled with Thermo Scientific DSQ II Single Quadrupole GC-MS. Moreover, HRMS data were recorded with Agilent 6224 TOF LC-MS in Unam, Bilkent University. Also, LC-MS analyses were done on a UPLC:

Waters Acquity & MS: Waters SYNAPT G1 MS System equipped with ACQUITY UPLC BEH C18 1.7 μ m column (1.0.Å~100 mm) in Central Laboratory at METU.

For functional group determination, FTIR analyses were conducted on Bruker Alpha Platinum ATR, and band positions were reported in cm^{-1} .

Melting points of solid products were measured on a MEL-TEMP 1002D apparatus. For spectroscopic analyses, absorption spectra of compounds were recorded by Shimadzu UV-2450 UV-VIS spectrophotometer. Besides, emission spectra of compounds were analyzed with a Perkin Elmer fluorescence spectrometer. For all absorption and emission analyses, a quartz cell with a 1 cm path length was used. Also, in order to conduct the fluorescence decay experiments, Horiba Jobin-Yvon Time-Resolved Fluorometer, Fluorolog FL-1057, equipped with HORIBA NanoLED-495 light source, was used in Unam, Bilkent University. To analyze the chiroptical properties of products, ECD spectra were taken by JASCO J-1500 CD Spectrometers, and for the electrochemical properties, Gamry PCI4/300 Potentiostat/Galvanostat was used in analyses.

X-ray data were collected on a four-circle Rigaku R-AXIS RAPID-S Diffractometer in Erzurum Atatürk University.

All reactions were monitored by Merck Silica Gel 60 F₂₅₄ TLC using precoated silica gel plates, which were visualized by UV light. Also, flash column chromatography was done by silica gel 60 F₂₅₄ with mesh sizes 200-400 and 60-200.

Bifunctional organocatalysts **23-25**⁴¹ & **28-30**⁴² were synthesized according to the literature procedure.

3.2 General Procedure for Friedel-Crafts Alkylation of Indoles **33 with Nitroolefins **16****

For racemic synthesis;

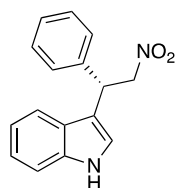
Indole derivative **33** (0.2 mmol), the nitroolefin derivative **16** (0.2 mmol), Zn(OAc)₂ · 2H₂O (0.02 mmol), and cyclohexane (1.3 mL) were mixed at 80 °C for 12-24 h. The reaction was monitored by TLC and after completion, the solvent was

evaporated under a vacuum. Then, the product was extracted with ethyl acetate and organic layers were dried over anhydrous Na₂SO₄. Ethyl acetate was evaporated under reduced pressure, and the residue was purified by column chromatography with *n*-hexane/ethyl acetate solvents systems to afford the pure product.¹⁴⁶

For asymmetric synthesis;

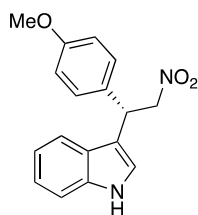
Indole derivative **33** (0.2 mmol) and *trans*- β -nitrostyrene derivative **16** (0.2 mmol) were added to a solution of bifunctional organocatalyst **30** (0.004 mmol, 1.89 mg) in DCM (0.5 mL) at room temperature. The reaction was monitored by TLC and then, the crude mixture was purified with flash column chromatography, using *n*-hexane/ethyl acetate solvent systems (1:5 to 1:8) to afford the products **34**.

3.2.1 Synthesis of 3-(2-nitro-1-phenylethyl)-1*H*-indole **34aa**



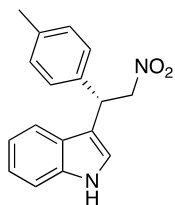
With the general procedure, chiral product **34aa** was obtained as a white solid with 45% conversion in 24 h. HPLC analysis (AD-H, *n*-Hexane/Isopropanol, 90:10, 1 mL/min, 254 nm) $t_{\text{minor}} = 24$ min and $t_{\text{major}} = 26$ min, 91% ee, $[\alpha]_{\text{D}}^{25} = +23.73$ (c 0.8, CH₂Cl₂). ¹H NMR (400 MHz, CDCl₃) δ 8.12 (bs, 1H), 7.48 (d, $J = 8.0$ Hz, 1H), 7.42 – 7.27 (m, 6H), 7.23 (t, $J = 7.6$ Hz, 1H), 7.11 (t, $J = 7.2$, 1H), 7.06 (s, 1H), 5.23 (t, $J = 8.0$ Hz, 1H), 5.10 (dd, $J = 12.5, 7.6$ Hz, 1H), 4.98 (dd, $J = 12.4, 8.4$ Hz, 1H). ¹³C NMR (101 MHz, CDCl₃) δ 139.1, 136.4, 128.8, 127.7, 127.5, 126.0, 122.6, 121.5, 119.9, 118.8, 114.2, 111.4, 79.4, 41.5 ppm.

3.2.2 Synthesis of 3-(1-(4-methoxyphenyl)-2-nitroethyl)-1H-indole 34ab



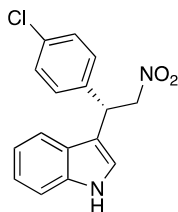
With the general procedure, chiral product **34ab** was obtained as a white solid with 27% conversion in 44 h. HPLC analysis (OD-H, *n*-Hexane/Isopropanol, 85:15, 1 mL/min, 254 nm) $t_{\text{major}} = 70$ min and $t_{\text{minor}} = 84$ min, 85% ee, $[\alpha]_{\text{D}}^{25} = +9.80$ (*c* 0.4, CH₂Cl₂). ¹H NMR (400 MHz, DMSO-*d*₆) δ 11.04 (bs, 1H), 7.48 (d, *J* = 7.9 Hz, 1H), 7.41 – 7.29 (m, 4H), 7.06 (t, *J* = 7.5 Hz, 1H), 6.94 (t, *J* = 7.4 Hz, 1H), 6.84 (d, *J* = 8.6 Hz, 2H), 5.37 – 5.16 (m, 2H), 4.99 (t, *J* = 8.2 Hz, 1H), 3.69 (s, 3H). ¹³C NMR (101 MHz, DMSO) δ 158.1, 136.2, 132.6, 128.9, 126.0, 122.1, 121.3, 118.6, 118.5, 113.8, 113.8, 111.5, 79.4, 55.0, 40.0 ppm.

3.2.3 Synthesis of 3-(2-nitro-1-(*p*-tolyl)ethyl)-1H-indole 34ac



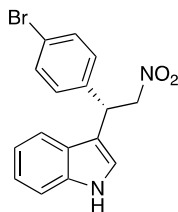
With the general procedure, chiral product **34ac** was obtained as a white solid with 38% conversion in 46 h. HPLC analysis (AD-H, *n*-Hexane/Isopropanol, 95:5, 1 mL/min, 254 nm) $t_{\text{minor}} = 49$ min and $t_{\text{major}} = 57$ min, 91% ee, $[\alpha]_{\text{D}}^{25} = +16.60$ (*c* 0.5, CH₂Cl₂). ¹H NMR (400 MHz, Chloroform-*d*) δ 8.08 (bs, 1H), 7.46 (d, *J* = 8.0 Hz, 1H), 7.35 (d, *J* = 8.2 Hz, 1H), 7.27 – 7.06 (m, 6H), 7.01 (s, 1H), 5.16 (t, *J* = 8.0 Hz, 1H), 5.06 (dd, *J* = 12.4, 7.6 Hz, 1H), 4.93 (dd, *J* = 12.3, 8.4 Hz, 1H), 2.32 (s, 3H). ¹³C NMR (101 MHz, CDCl₃) δ 137.1, 136.4, 136.1, 129.5, 127.5, 126.0, 122.6, 121.5, 119.8, 118.9, 114.5, 111.3, 79.5, 41.1, 20.9 ppm.

3.2.4 Synthesis of 3-(1-(4-chlorophenyl)-2-nitroethyl)-1H-indole 34ad



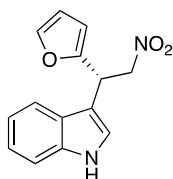
With the general procedure, chiral product **34ad** was obtained as a white solid with 32% conversion in 49 h. HPLC analysis (AD-H, *n*-Hexane/Isopropanol, 90:10, 1 mL/min, 254 nm) $t_{\text{minor}} = 23$ min and $t_{\text{major}} = 30$ min, 87% ee, $[\alpha]_{\text{D}}^{25} = +9.43$ (*c* 0.6, CH_2Cl_2). ^1H NMR (400 MHz, Chloroform-*d*) δ 8.16 (bs, 1H), 7.41 (t, $J = 9.1$ Hz, 2H), 7.34 – 7.28 (m, 4H), 7.24 (t, $J = 7.7$ Hz, 1H), 7.11 (t, $J = 7.6$ Hz, 1H), 7.05 (d, $J = 2.2$ Hz, 1H), 5.20 (t, $J = 8.0$ Hz, 1H), 5.08 (dd, $J = 12.5, 7.4$ Hz, 1H), 4.93 (dd, $J = 12.6, 8.6$ Hz, 1H). ^{13}C NMR (101 MHz, CDCl_3) δ 137.8, 136.6, 133.5, 129.2, 129.2, 126.0, 122.9, 121.6, 120.1, 118.8, 114.0, 111.6, 79.3, 41.0 ppm.

3.2.5 Synthesis of 3-(1-(4-bromophenyl)-2-nitroethyl)-1H-indole 34ae



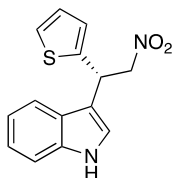
With the general procedure, chiral product **34ae** was obtained as a white solid with 22% conversion in 51 h. HPLC analysis (AD-H, *n*-Hexane/Isopropanol, 90:10, 1 mL/min, 254 nm) $t_{\text{minor}} = 25$ min and $t_{\text{major}} = 33$ min, 89% ee, $[\alpha]_{\text{D}}^{25} = +4.43$ (*c* 0.8, CH_2Cl_2). ^1H NMR (400 MHz, Chloroform-*d*) δ 8.15 (bs, 1H), 7.47 (dd, $J = 8.4, 1.7$ Hz, 2H), 7.41 (dd, $J = 16.8, 8.1$ Hz, 2H), 7.27 – 7.20 (m, 3H), 7.12 (t, $J = 7.5$ Hz, 1H), 7.03 (d, $J = 2.4$ Hz, 1H), 5.18 (t, $J = 8.0$ Hz, 1H), 5.07 (dd, $J = 12.5, 7.4$ Hz, 1H), 4.93 (dd, $J = 12.5, 8.6$ Hz, 1H). ^{13}C NMR (101 MHz, CDCl_3) δ 138.4, 136.6, 132.1, 129.6, 125.9, 122.9, 121.6, 121.6, 120.1, 118.8, 113.8, 111.6, 79.3, 41.1 ppm.

3.2.6 Synthesis of 3-(1-(furan-2-yl)-2-nitroethyl)-1H-indole 34af



With the general procedure, chiral product **34af** was obtained as a light brown solid with 74% conversion in 28 h. HPLC analysis (OJ-H, *n*-Hexane/Isopropanol, 70:30, 1 mL/min, 254 nm) $t_{\text{minor}} = 54$ min and $t_{\text{major}} = 63$ min, 87% ee, $[\alpha]_{\text{D}}^{25} = -5.80$ (*c* 0.2, CH₂Cl₂). ¹H NMR (400 MHz, Chloroform-*d*) δ 8.09 (bs, 1H), 7.55 (d, *J* = 7.9 Hz, 1H), 7.38 – 7.29 (m, 2H), 7.21 (t, *J* = 7.5 Hz, 1H), 7.13 (t, *J* = 7.5 Hz, 1H), 7.07 (d, *J* = 2.5 Hz, 1H), 6.30 (dd, *J* = 3.3, 1.9 Hz, 1H), 6.15 (d, *J* = 3.26, 1H), 5.24 (t, *J* = 7.8 Hz, 1H), 5.04 (dd, *J* = 12.5, 8.2 Hz, 1H), 4.90 (dd, *J* = 12.5, 7.4 Hz, 1H). ¹³C NMR (101 MHz, CDCl₃) δ 151.2, 141.2, 135.3, 124.7, 121.7, 121.6, 119.1, 117.7, 110.6, 110.5, 109.5, 106.4, 76.9, 34.7 ppm.

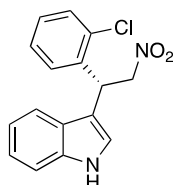
3.2.7 Synthesis of 3-(2-nitro-1-(thiophen-2-yl)ethyl)-1H-indole 34ag



With the general procedure, chiral product **34ag** was obtained as a yellow solid with 78% conversion in 30 h. HPLC analysis (AD-H, *n*-Hexane/Isopropanol, 90:10, 1 mL/min, 254 nm) $t_{\text{minor}} = 23$ min and $t_{\text{major}} = 27$ min, 56% ee, $[\alpha]_{\text{D}}^{25} = +9.44$ (*c* 0.5, CH₂Cl₂). ¹H NMR (400 MHz, Chloroform-*d*) δ 8.10 (bs, 1H), 7.54 (d, *J* = 8.0 Hz, 1H), 7.36 (d, *J* = 8.2 Hz, 1H), 7.26 – 7.18 (m, 2H), 7.14 (t, *J* = 7.5 Hz, 1H), 7.08 (d, *J* = 2.5 Hz, 1H), 7.00 (d, *J* = 3.5 Hz, 1H), 6.96 (dd, *J* = 5.1, 3.5 Hz, 1H), 5.48 (t, *J* = 7.9 Hz, 1H), 5.05 (dd, *J* = 12.5, 7.6 Hz, 1H), 4.99 (dd, *J* = 12.5, 8.2 Hz, 1H). ¹³C

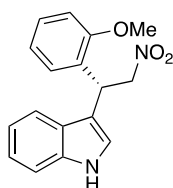
NMR (101 MHz, CDCl₃) δ 143.0, 136.5, 127.0, 125.8, 125.3, 124.9, 122.8, 122.0, 120.1, 118.9, 114.1, 111.6, 80.1, 37.0 ppm.

3.2.8 Synthesis of 3-(1-(2-chlorophenyl)-2-nitroethyl)-1H-indole 34ah



With the general procedure, chiral product **34ah** was obtained as a white solid with 80% conversion in 47 h. HPLC analysis (AD-H, *n*-Hexane/Isopropanol, 90:10, 1 mL/min, 254 nm) $t_{\text{minor}} = 18$ min and $t_{\text{major}} = 20$ min, 90% ee, $[\alpha]_{\text{D}}^{25} = +45.60$ (*c* 1.3, CH₂Cl₂). ¹H NMR (400 MHz, Chloroform-*d*) δ 8.14 (bs, 1H), 7.44 (d, *J* = 7.9 Hz, 2H), 7.37 (d, *J* = 8.2 Hz, 1H), 7.24 – 7.12 (m, 5H), 7.08 (t, *J* = 7.5 Hz, 1H), 5.75 (t, *J* = 7.8 Hz, 1H), 5.06 – 4.92 (m, 2H). ¹³C NMR (101 MHz, CDCl₃) δ 136.6, 136.5, 133.9, 130.2, 129.0, 128.9, 127.3, 126.2, 122.8, 122.0, 120.1, 119.0, 113.3, 111.5, 77.8, 38.0 ppm.

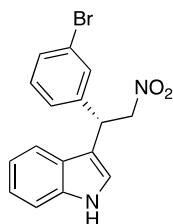
3.2.9 Synthesis of 3-(1-(2-methoxyphenyl)-2-nitroethyl)-1H-indole 34ai



With the general procedure, chiral product **34ai** was obtained as a white solid with 78% conversion in 50 h. HPLC analysis (OD-H, *n*-Hexane/Isopropanol, 80:20, 1 mL/min, 254 nm) $t_{\text{minor}} = 20$ min and $t_{\text{major}} = 24$ min, 80% ee, $[\alpha]_{\text{D}}^{25} = +34.42$ (*c* 1.0, CH₂Cl₂). ¹H NMR (400 MHz, Chloroform-*d*) δ 8.14 (bs, 1H), 7.52 (d, *J* = 8.0 Hz, 1H), 7.40 (d, *J* = 8.2 Hz, 1H), 7.31 – 7.21 (m, 2H), 7.19 – 7.08 (m, 3H), 6.97 (d, *J* = 8.2 Hz, 1H), 6.88 (t, *J* = 7.5 Hz, 1H), 5.66 (t, *J* = 7.9 Hz, 1H), 5.09 (dd, *J* = 12.5, 6.7

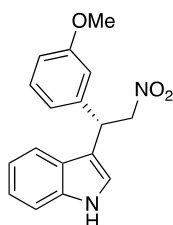
Hz, 1H), 5.02 (dd, $J = 12.5, 9.1$ Hz, 1H), 3.97 (s, 3H). ^{13}C NMR (101 MHz, CDCl_3) δ 157.0, 136.5, 129.0, 128.7, 127.3, 126.6, 122.5, 122.1, 120.9, 119.8, 119.1, 114.0, 111.4, 110.9, 78.2, 55.6, 35.6 ppm.

3.2.10 Synthesis of 3-(1-(3-bromophenyl)-2-nitroethyl)-1H-indole 34aj



With the general procedure, chiral product **34aj** was obtained as an oil with 57% conversion in 42 h. HPLC analysis (AD-H, *n*-Hexane/Isopropanol, 90:10, 1 mL/min, 254 nm) $t_{\text{minor}} = 19$ min and $t_{\text{major}} = 21$ min, 74% ee, $[\alpha]_{\text{D}}^{25} = +12.68$ (c 0.7, CH_2Cl_2). ^1H NMR (400 MHz, Chloroform-*d*) δ 8.13 (bs, 1H), 7.49 (t, $J = 1.7$ Hz, 1H), 7.44 (d, $J = 8.0$ Hz, 1H), 7.42 – 7.33 (m, 2H), 7.29 (d, $J = 7.8$ Hz, 1H), 7.25 – 7.16 (m, 2H), 7.11 (t, $J = 7.5$ Hz, 1H), 7.00 (d, $J = 2.3$ Hz, 1H), 5.16 (t, $J = 7.7$ Hz, 1H), 5.04 (dd, $J = 12.7, 7.5$ Hz, 1H), 4.91 (dd, $J = 12.6, 8.4$ Hz, 1H). ^{13}C NMR (101 MHz, CDCl_3) δ 140.6, 135.5, 129.8, 129.8, 129.5, 125.4, 124.9, 122.0, 121.9, 120.6, 119.1, 117.7, 112.6, 110.5, 78.1, 40.1 ppm.

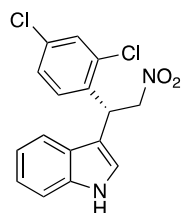
3.2.11 Synthesis of 3-(1-(3-methoxyphenyl)-2-nitroethyl)-1H-indole 34ak



With the general procedure, chiral product **34ak** was obtained as an oil with 37% conversion in 47 h. HPLC analysis (OD-H, *n*-Hexane/Isopropanol, 80:20, 1 mL/min,

254 nm) $t_{\text{major}} = 42$ min and $t_{\text{minor}} = 60$ min, 92% ee, $[\alpha]_{\text{D}}^{25} = +9.30$ (c 1.0, CH_2Cl_2). ^1H NMR (400 MHz, Chloroform- d) δ 8.08 (bs, 1H), 7.48 (d, $J = 8.0$ Hz, 1H), 7.31 (d, $J = 8.2$ Hz, 1H), 7.25 – 7.16 (m, 2H), 7.08 (t, $J = 7.5$ Hz, 1H), 6.96 (d, $J = 2.3$ Hz, 1H), 6.93 (d, $J = 7.7$, 1H), 6.90 – 6.86 (m, 1H), 6.80 (dd, $J = 8.2, 2.3$, 1H), 5.16 (t, $J = 8.0$ Hz, 1H), 5.03 (dd, $J = 12.5, 7.6$ Hz, 1H), 4.92 (dd, $J = 12.5, 8.4$ Hz, 1H), 3.75 (s, 3H). ^{13}C NMR (101 MHz, CDCl_3) δ 158.9, 139.9, 135.5, 128.9, 125.1, 121.6, 120.6, 119.0, 118.9, 117.9, 113.2, 113.0, 111.5, 110.4, 78.4, 54.2, 40.5 ppm.

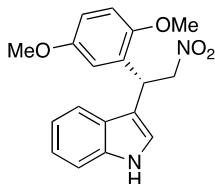
3.2.12 Synthesis of 3-(1-(2,4-dichlorophenyl)-2-nitroethyl)-1H-indole 34al



With the general procedure, chiral product **34al** was obtained as a white solid with 33% isolated yield in 24 h. HPLC analysis (OD-H, n -Hexane/Isopropanol, 70:30, 1 mL/min, 254 nm) $t_{\text{minor}} = 21$ min and $t_{\text{major}} = 31$ min, 77% ee, $[\alpha]_{\text{D}}^{25} = +31.70$ (c 0.8, CH_2Cl_2). ^1H NMR (400 MHz, Chloroform- d) δ 8.15 (bs, 1H), 7.47 (s, 1H), 7.42 (d, $J = 8.0$ Hz, 1H), 7.35 (d, $J = 8.2$ Hz, 1H), 7.23 (t, $J = 7.7$ Hz, 1H), 7.15 – 7.08 (m, 3H), 7.07 (d, $J = 2.3$ Hz, 1H), 5.7 (t, $J = 7.9$ Hz, 1H), 4.99 (dd, $J = 12.9, 8.8$ Hz, 1H), 4.92 (dd, $J = 12.9, 7.0$ Hz, 1H). ^{13}C NMR (101 MHz, CDCl_3) δ 136.5, 135.2, 134.5, 134.1, 130.0, 130.0, 127.7, 126.0, 123.0, 122.0, 120.2, 118.8, 112.8, 111.6, 77.5, 37.6 ppm.

3.2.13 Synthesis of 3-(1-(2,5-dimethoxyphenyl)-2-nitroethyl)-1*H*-indole

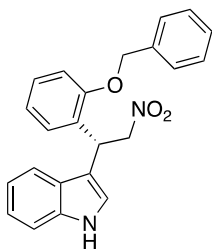
34am



With the general procedure, chiral product **34am** was obtained as a white solid with 49% isolated yield in 54 h. HPLC analysis (AD-H, *n*-Hexane/Isopropanol, 80:20, 1 mL/min, 254 nm) $t_{\text{minor}} = 10$ min and $t_{\text{major}} = 13$ min, 76% ee, $[\alpha]_{\text{D}}^{25} = +10.72$ (c 1.3, CH_2Cl_2). ^1H NMR (400 MHz, Chloroform-*d*) δ 8.13 (bs, 1H), 7.52 (d, $J = 7.9$ Hz, 1H), 7.31 (d, $J = 8.1$ Hz, 1H), 7.19 (t, $J = 7.7$ Hz, 1H), 7.12 – 7.03 (m, 2H), 6.87 (d, $J = 8.8$ Hz, 1H), 6.76 (dd, $J = 8.8, 3.1$ Hz, 1H), 6.71 (d, $J = 3.0$ Hz, 1H), 5.60 (dd, $J = 9.0, 6.8$ Hz, 1H), 5.03 (dd, $J = 12.5, 6.7$ Hz, 1H), 4.96 (dd, $J = 12.5, 9.1$ Hz, 1H), 3.88 (s, 3H), 3.66 (s, 3H). ^{13}C NMR (101 MHz, CDCl_3) δ 153.6, 151.2, 136.4, 128.6, 126.5, 122.5, 122.0, 119.8, 119.0, 116.0, 113.6, 112.2, 111.8, 111.4, 78.2, 56.1, 55.6, 35.6 ppm.

3.2.14 Synthesis of 3-(1-(2-(benzyloxy)phenyl)-2-nitroethyl)-1*H*-indole

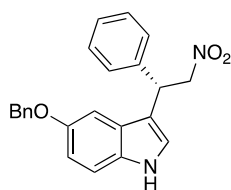
34an



With the general procedure, chiral product **34an** was obtained as a colorless oil with 79% isolated yield in 54 h. HPLC analysis (AD-H, *n*-Hexane/Isopropanol, 80:20, 1 mL/min, 254 nm) $t_{\text{minor}} = 10$ min and $t_{\text{major}} = 20$ min, 69% ee, $[\alpha]_{\text{D}}^{25} = +43.10$ (c 2.1, CH_2Cl_2). ^1H NMR (400 MHz, Chloroform-*d*) δ 8.08 (bs, 1H), 7.46 (d, $J = 7.6$ Hz,

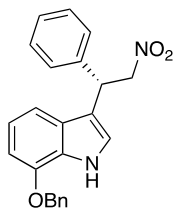
3H), 7.43 – 7.30 (m, 4H), 7.25 – 7.15 (m, 3H), 7.07 (t, $J = 7.5$ Hz, 1H), 7.03 (d, $J = 2.3$ Hz, 1H), 7.01 (d, $J = 8.2$ Hz, 1H), 6.88 (t, $J = 7.4$ Hz, 1H), 5.70 (t, $J = 8.3$ Hz, 1H), 5.18 (s, 2H), 5.10 (dd, $J = 12.5, 6.9$ Hz, 1H), 4.99 (dd, $J = 12.4, 8.9$ Hz, 1H). ^{13}C NMR (101 MHz, CDCl_3) δ 156.0, 136.9, 136.4, 129.1, 128.7, 128.1, 127.7, 127.3, 126.5, 122.5, 122.2, 121.2, 119.8, 119.2, 113.8, 112.3, 111.4, 78.1, 70.3, 35.9 ppm. IR (neat): 3419, 3059, 3032, 2915, 1598, 1546, 1489, 1452, 1376, 1288, 1239, 1104, 1010, 850, 739, 697, 594, 498, 424 cm^{-1} . HRMS (ESI-TOF) m/z : $[\text{M-H}]^-$ Calcd. for $\text{C}_{23}\text{H}_{19}\text{N}_2\text{O}_3$ 371.1396; Found 371.2351.

3.2.15 Synthesis of 5-(benzyloxy)-3-(2-nitro-1-phenylethyl)-1H-indole 34ba



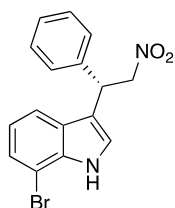
With the general procedure, chiral product **34ba** was obtained as a white solid with 63% isolated yield in 46 h. HPLC analysis (AD-H, *n*-Hexane/Isopropanol, 80:20, 1 mL/min, 254 nm) $t_{\text{minor}} = 15$ min and $t_{\text{major}} = 19$ min, 73% ee, $[\alpha]_{\text{D}}^{25} = -32.82$ (c 0.9, CH_2Cl_2). ^1H NMR (400 MHz, CDCl_3) δ 8.02 (bs, 1H), 7.47 – 7.37 (m, 4H), 7.36 – 7.25 (m, 7H), 7.06 – 6.89 (m, 3H), 5.14 (t, $J = 7.9$ Hz, 1H), 5.08 – 5.00 (m, 3H), 4.94 (dd, $J = 12.4, 8.5$ Hz, 1H). ^{13}C NMR (101 MHz, CDCl_3) δ 153.2, 139.0, 137.3, 131.7, 128.8, 128.5, 127.8, 127.7, 127.6, 127.5, 126.4, 122.3, 113.9, 113.3, 112.1, 102.4, 79.3, 70.8, 41.4 ppm.

3.2.16 Synthesis of 7-(benzyloxy)-3-(2-nitro-1-phenylethyl)-1H-indole 34ca



With the general procedure, chiral product **34ca** was obtained as a white solid with 55% isolated yield in 46 h. HPLC analysis (AD-H, *n*-Hexane/Isopropanol, 80:20, 1 mL/min, 254 nm) $t_{\text{minor}} = 17$ min and $t_{\text{major}} = 26$ min, 67% ee, $[\alpha]_{\text{D}}^{25} = +9.31$ (c 0.4, CH_2Cl_2). ^1H NMR (400 MHz, CDCl_3) δ 8.38 (bs, 1H), 7.51 – 7.27 (m, 11H), 7.09 (d, $J = 8.0$ Hz, 1H), 7.04 – 7.00 (m, 1H), 6.75 (d, $J = 7.6$ Hz, 1H), 5.26 – 5.15 (m, 3H), 5.09 (dd, $J = 12.4, 7.5$ Hz, 1H), 4.97 (dd, $J = 12.4, 8.5$ Hz, 1H). ^{13}C NMR (101 MHz, CDCl_3) δ 145.3, 139.1, 136.8, 128.8, 128.5, 128.1, 127.7, 127.6, 127.4, 127.4, 127.2, 121.1, 120.3, 114.8, 111.7, 103.6, 79.4, 70.2, 41.6 ppm. IR (neat): 3421, 3030, 2922, 2853, 1713, 1628, 1577, 1547, 1496, 1453, 1375, 1260, 1227, 1178, 1092, 1060, 1019, 979, 910, 845, 781, 731, 695, 584, 469 cm^{-1} . HRMS (ESI-TOF) m/z : $[\text{M}+\text{H}]^+$ Calcd. for $\text{C}_{23}\text{H}_{21}\text{N}_2\text{O}_3$ 373.1552; Found 373.1556.

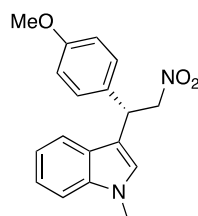
3.2.17 Synthesis of 7-bromo-3-(2-nitro-1-phenylethyl)-1H-indole 34da



With the general procedure, chiral product **34da** was obtained as a colorless oil with 43% isolated yield in 47 h. HPLC analysis (AS-H, *n*-Hexane/Isopropanol, 90:10, 1 mL/min, 254 nm) $t_{\text{major}} = 22$ min and $t_{\text{minor}} = 28$ min, >99% ee, $[\alpha]_{\text{D}}^{25} = +40.00$ (c 0.08, CH_2Cl_2). ^1H NMR (400 MHz, CDCl_3) δ 8.32 (bs, 1H), 7.44 – 7.26 (m, 7H), 7.15 (s, 1H), 6.98 (t, $J = 7.8$ Hz, 1H), 5.20 (t, $J = 7.9$ Hz, 1H), 5.08 (dd, $J = 12.4, 8.0$

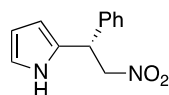
Hz, 1H), 4.97 (dd, $J = 12.4, 8.1$ Hz, 1H). ^{13}C NMR (101 MHz, CDCl_3) δ 138.7, 135.1, 128.9, 127.6, 127.2, 125.0, 122.0, 121.1, 118.2, 115.6, 104.8, 79.3, 41.5 ppm. IR (neat): 3386, 3062, 3027, 2918, 1713, 1618, 1544, 1488, 1453, 1432, 1406, 1376, 1335, 1276, 1259, 1193, 1142, 1090, 1048, 1025, 983, 910, 882, 852, 818, 807, 781, 750, 736, 697, 655, 610, 582, 528, 504, 469 cm^{-1} . HRMS (ESI-TOF) m/z : $[\text{M}-\text{H}]^-$ Calcd. for $\text{C}_{16}\text{H}_{12}\text{BrN}_2\text{O}_2$ 343.0082; Found 343.0079.

3.2.18 Synthesis of 3-(1-(4-methoxyphenyl)-2-nitroethyl)-1-methyl-1H-indole 34eb



With the general procedure, chiral product **34eb** was obtained as a white solid with 15% isolated yield in 24 h. HPLC analysis (AS-H, *n*-Hexane/Isopropanol, 90:10, 1 mL/min, 254 nm) $t_{\text{minor}} = 18$ min and $t_{\text{major}} = 22$ min, 18% ee. ^1H NMR (400 MHz, CDCl_3) δ 7.36 (d, $J = 8.0$ Hz, 1H), 7.23 – 7.11 (m, 4H), 6.99 (t, $J = 7.5$ Hz, 1H), 6.77 (d, $J = 7.1$, 3H), 5.04 (t, $J = 8.0$ Hz, 1H), 4.94 (dd, $J = 12.3, 7.4$ Hz, 1H), 4.80 (dd, $J = 12.3, 8.6$ Hz, 1H), 3.68 (s, 3H), 3.65 (s, 3H). ^{13}C NMR (101 MHz, CDCl_3) δ 158.9, 137.3, 131.4, 128.8, 126.6, 126.3, 122.2, 119.4, 119.1, 114.3, 113.2, 109.5, 79.8, 55.3, 40.9, 32.8 ppm.

3.2.19 Synthesis of 2-(2-nitro-1-phenylethyl)-1H-pyrrole 86



With the general procedure, chiral product **86** was obtained as a light brown solid with 32% isolated yield in 46 h. HPLC analysis (AD-H, *n*-Hexane/Isopropanol, 95:5,

1 mL/min, 254 nm) $t_{\text{minor}} = 14$ min and $t_{\text{major}} = 16$ min, 50% ee, $[\alpha]_{\text{D}}^{25} = +24.47$ (c 0.3, CH₂Cl₂). ¹H NMR (400 MHz, CDCl₃) δ 7.87 (bs, 1H), 7.41 – 7.33 (m, 3H), 7.29 – 7.24 (m, 2H), 6.72 (dd, $J = 3.9, 2.5$ Hz, 1H), 6.20 (dd, $J = 5.9, 2.8$ Hz, 1H), 6.12 (s, 1H), 5.02 (dd, $J = 12.0, 7.3$ Hz, 1H), 4.93 (t, $J = 7.4$ Hz, 1H), 4.84 (dd, $J = 12.0, 7.6$ Hz, 1H). ¹³C NMR (101 MHz, CDCl₃) δ 137.9, 129.1, 128.8, 128.0, 127.8, 118.1, 108.6, 105.7, 79.1, 42.8 ppm.

3.3 Synthesis of BODIPYs 53

Synthesis of BODIPY 53a

For BODIPY **53a**, firstly, 3,5-dimethylpyrrole-2-carbaldehyde (**52**) was synthesized from 2,4-dimethylpyrrole (**51**) via the Vilsmeier-Haack reaction. For that purpose, POCl₃ (5.9 mL, 63 mmol) was added dropwise to DMF (4.9 mL, 63 mmol) at 0 °C. Then, the reaction mixture was warmed to room temperature and stirred for 15 min. After that, 30 mL of 1,2-dichloroethane was added to the reaction mixture at 0 °C. At this temperature, a solution of 2,4-dimethylpyrrole (**51**) (5.0 g, 52.5 mmol) in 50 mL of 1,2-dichloroethane was added dropwise over 20 min. When the solution was added, the reaction mixture was refluxed for 30 min and then cooled to room temperature. After the addition of a solution of NaOAc (23.7 g, 289 mmol) in 100 mL of water, the reaction mixture was again refluxed for 30 min. For the work-up process, the cooled mixture was washed with water (1x100 mL), saturated Na₂CO₃ solution (2x50 mL), and brine (1x50 mL). The organic layer was dried over Na₂SO₄ and then the solvent was removed under vacuum. The residue was purified by flash chromatography using *n*-hexane/ethyl acetate solvent systems (1:5). 3,5-dimethylpyrrole-2-carbaldehyde (**52**) was obtained as a light yellow solid (5.8 g, 89% isolated yield).

After purification, 3,5-dimethylpyrrole-2-carbaldehyde (**52**) (246 mg, 2mmol) was dissolved in 10 mL DCM and then POCl₃ (0.22 mL, 2.4 mmol) was added dropwise over 1 min at 0 °C. The solution was warmed to room temperature slowly and stirred

for 12h. Then, Et₃N (1.4 mL, 10 mmol) was added dropwise over 5 min at 0 °C. After stirring for 15 min, BF₃OEt₂ (2.0 mL, 16 mmol) was added dropwise to the solution over 5 min. The reaction was warmed to room temperature and stirred for 12 h. In order to remove the polar impurities, the reaction mixture was passed through a short pad of silica gel eluting with DCM. The solvent was removed under vacuum and then the residue was dissolved in DCM. With the addition of water, the reaction mixture was stirred at room temperature overnight to decompose excess BF₃OEt₂ and other impurities. For the work-up process, the organic layer was washed with water, brine and then dried over Na₂SO₄. Then, the solvent was removed under vacuum and the residue was purified by flash chromatography using *n*-hexane/ethyl acetate solvent systems (1:20). BODIPY **53a** was obtained as a red solid (229 mg, 92% isolated yield). Analytical data matched previously reported value in the literature.¹⁰⁵

Synthesis of BODIPY 53b

2,4-dimethylpyrrole (**51**) (2 mL, 19 mmol), benzoyl chloride (**87**) (1.15 mL, 9.5 mmol), and DCM (50 mL) were mixed overnight at room temperature under N₂ atmosphere. Then, NEt₃ (10 mL) was added dropwise to the solution in ice bath. After stirring for about 30 min, BF₃OEt₂ (10 mL) was added dropwise and then the mixture was stirred overnight again at room temperature under N₂ atmosphere. For the work-up process, the organic phase was washed with saturated NaHCO₃ solution (100 mL), and water for three times. Then, solvent was dried over Na₂SO₄ and concentrated under vacuum. The product was purified by flash chromatography using *n*-hexane/ethyl acetate solvent systems (1:20). BODIPY **53b** was obtained as an orange solid (1.2 g, 38% isolated yield). Analytical data matched previously reported value in the literature.¹³⁴

Isatin derivatives **72** were synthesized according to literature procedure.¹³⁵

3.4 General Procedure for Addition of BODIPYs **53** to Isatin Derivatives

72

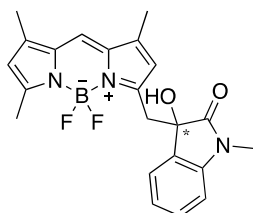
For racemic synthesis;

DBU was added to a solution of BODIPY derivative **53** (0.1 mmol) and isatin derivative **72** (0.2 mmol) in DCM (0.2 mL). Then, the reaction was stirred for 5-15 minutes at room temperature. After evaporation of DCM, the crude mixture was directly loaded on flash column chromatography using *n*-hexane/ethyl acetate solvent systems (1:5 to 1:2).

For asymmetric synthesis;

BODIPY derivative **53** (0.1 mmol), isatin derivative **72** (0.2 mmol) and bifunctional organocatalyst **29** (0.02 mmol) were stirred in DCM (0.2 mL) at room temperature for 5-13 days. All reactions were monitored by TLC and then, purified with column chromatography using *n*-hexane/ethyl acetate solvent systems (1:5 to 1:2).

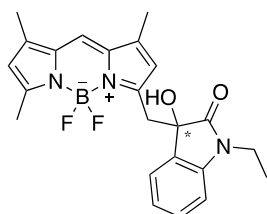
3.4.1 Synthesis of chiral BODIPY **73aa**



With the general procedure, chiral BODIPY **73aa** was obtained as an orange solid with 10% isolated yield in 7 days. Melting Point: 164-168 °C. HPLC analysis (AD-H, *n*-Hexane/Isopropanol, 80:20, 1 mL/min, 254 nm) $t_{\text{major}} = 15$ min and $t_{\text{minor}} = 23$ min, 53% ee, $[\alpha]_{\text{D}}^{25} = -105.8$ (c 0.1, CH_2Cl_2). $^1\text{H-NMR}$ (400 MHz, Chloroform- d) δ 7.34 – 7.26 (m, 2H), 7.09 (s, 1H), 7.03 (t, $J = 7.5$ Hz, 1H), 6.83 (d, $J = 7.7$ Hz, 1H), 6.25 (s, 1H), 6.07 (s, 1H), 3.86 (bs, 1H), 3.59 (d, $J = 15.0$ Hz, 1H), 3.31 (d, $J = 15.0$ Hz, 1H), 3.21 (s, 3H), 2.51 (s, 3H), 2.29 (s, 3H), 2.26 (s, 3H). $^{13}\text{C-NMR}$ (101 MHz, CDCl_3) δ 177.1, 158.6, 151.9, 143.1, 142.6, 140.1, 134.0, 132.8, 129.9, 129.6, 124.5,

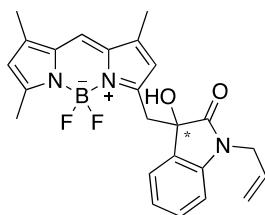
122.7, 120.6, 119.7, 119.5, 108.2, 75.2, 36.6, 26.2, 14.8, 11.3, 11.12 ppm. IR (neat): 3380, 2917, 1699, 1600, 1507, 1469, 1376, 1351, 1314, 1247, 1193, 1150, 1065, 1029, 964, 898, 829, 751, 702, 671, 579, 537, 479, 423 cm^{-1} . HRMS (ESI-TOF) m/z : $[\text{M}]^+$ Calcd. for $\text{C}_{22}\text{H}_{22}\text{BF}_2\text{N}_3\text{O}_2$ 409.1773; Found 409.1776.

3.4.2 Synthesis of chiral BODIPY 73ab



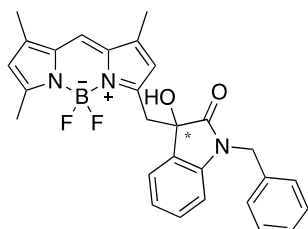
With the general procedure, chiral BODIPY **73ab** was obtained as an orange solid with 17% isolated yield in 7 days. Melting Point: 184-186 °C (decomposed). HPLC analysis (AD-H, *n*-Hexane/Isopropanol, 80/20, 1 mL/min, 510 nm) $t_{\text{major}}=15$ min and $t_{\text{minor}}=22$ min, 45% ee, $[\alpha]_{\text{D}}^{25} = -99.0$ (c 0.1, CH_2Cl_2). $^1\text{H-NMR}$ (400 MHz, Chloroform- d) δ 7.33 – 7.27 (m, 2H), 7.09 (s, 1H), 7.03 (t, $J = 7.5$ Hz, 1H), 6.85 (d, $J = 7.7$ Hz, 1H), 6.22 (s, 1H), 6.07 (s, 1H), 3.86 – 3.65 (m, 3H), 3.59 (d, $J = 15.1$, 1H), 3.32 (d, $J = 15.1$ Hz, 1H), 2.51 (s, 3H), 2.27 (d, $J = 8.8$ Hz, 6H), 1.28 (t, $J = 7.2$ Hz, 3H). $^{13}\text{C-NMR}$ (101 MHz, CDCl_3) δ 176.6, 158.6, 151.8, 142.6, 142.2, 140.1, 134.0, 132.8, 130.1, 129.5, 124.7, 122.5, 120.6, 119.7, 119.5, 108.4, 75.1, 36.7, 34.7, 14.8, 12.4, 11.3, 11.2 ppm. IR (neat): 3382, 2919, 1712, 1602, 1512, 1470, 1431, 1367, 1312, 1241, 1211, 1174, 1152, 1133, 1076, 1032, 966, 898, 878, 819, 753, 700, 673, 613, 575, 498, 473 cm^{-1} . HRMS (ESI-TOF) m/z : $[\text{M-H}]^-$ Calcd. for $\text{C}_{23}\text{H}_{23}\text{BF}_2\text{N}_3\text{O}_2$ 422.1851; Found 422.1881.

3.4.3 Synthesis of chiral BODIPY 73ac



With the general procedure, chiral BODIPY **73ac** was obtained as an orange solid with 12% isolated yield in 5 days. Melting Point: 212-214 °C (decomposed). HPLC analysis (AD-H, *n*-Hexane/Isopropanol, 80/20, 1 mL/min, 254 nm) $t_{\text{major}} = 15$ min and $t_{\text{minor}} = 22$ min, 55% ee, $[\alpha]_{\text{D}}^{25} = -161.5$ (*c* 0.1, CH₂Cl₂). ¹H-NMR (400 MHz, Chloroform-*d*) δ 7.34 – 7.27 (m, 2H), 7.09 (s, 1H), 7.03 (t, *J* = 7.4 Hz, 1H), 6.83 (d, *J* = 7.7 Hz, 1H), 6.22 (s, 1H), 6.08 (s, 1H), 5.91 – 5.79 (m, 1H), 5.24 (t, *J* = 14.1 Hz, 2H), 4.44 (d, *J* = 16.3 Hz, 1H), 4.23 (d, *J* = 16.2 Hz, 1H), 3.80 (bs, 1H), 3.62 (d, *J* = 15.0 Hz, 1H), 3.35 (d, *J* = 15.0 Hz, 1H), 2.52 (s, 3H), 2.27 (d, *J* = 8.0 Hz, 6H). ¹³C-NMR (101 MHz, CDCl₃) δ 176.8, 158.7, 151.7, 142.6, 142.3, 140.1, 134.1, 132.8, 131.2, 129.9, 129.5, 124.6, 122.7, 120.6, 119.7, 119.5, 117.7, 109.1, 75.1, 42.4, 36.8, 14.8, 11.3, 11.2 ppm. IR (neat): 3399, 2960, 2918, 2851, 1714, 1601, 1511, 1469, 1428, 1357, 1250, 1199, 1174, 1150, 1076, 973, 931, 896, 875, 817, 799, 756, 703, 672, 610, 580, 558, 472 cm⁻¹. HRMS (ESI-TOF) *m/z*: [M+Na]⁺ Calcd for C₂₄H₂₄BF₂N₃NaO₂ 458.1827; Found 458.1837.

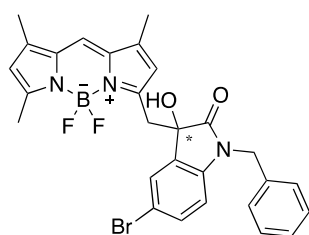
3.4.4 Synthesis of chiral BODIPY 73ad



With the general procedure, chiral BODIPY **73ad** was obtained as an orange solid with 10% isolated yield in 7 days. Melting Point: 211-213 °C (decomposed). HPLC

analysis (AS-H, *n*-Hexane/Isopropanol, 75/25, 1 mL/min, 510 nm) $t_{\text{minor}}=22$ min and $t_{\text{major}}=33$ min, 60% ee, $[\alpha]_{\text{D}}^{25} = -127.4$ (c 0.1, CH_2Cl_2). ^1H NMR (400 MHz, Chloroform-*d*) δ 7.37 – 7.23 (m, 6H), 7.19 (t, $J = 7.8$ Hz, 1H), 7.09 (s, 1H), 7.01 (t, $J = 7.5$ Hz, 1H), 6.71 (d, $J = 7.8$ Hz, 1H), 6.16 (s, 1H), 6.08 (s, 1H), 5.01 (d, $J = 15.7$ Hz, 1H), 4.79 (d, $J = 15.7$ Hz, 1H), 3.90 (bs, 1H), 3.69 (d, $J = 15.0$ Hz, 1H), 3.41 (d, $J = 14.9$ Hz, 1H), 2.53 (s, 3H), 2.26 (s, 6H). ^{13}C NMR (101 MHz, CDCl_3) δ 177.3, 158.8, 151.5, 142.7, 142.3, 140.1, 135.5, 134.1, 132.8, 129.9, 129.5, 128.7, 127.5, 127.3, 124.6, 122.8, 120.6, 119.8, 119.4, 109.3, 75.2, 43.8, 36.8, 14.8, 11.3, 11.2 ppm. IR (neat): 3354, 2960, 2921, 2852, 1691, 1599, 1583, 1529, 1511, 1494, 1469, 1444, 1408, 1381, 1302, 1254, 1235, 1194, 1169, 1149, 1068, 972, 903, 795, 746, 727, 707, 691, 672, 622, 582, 546, 479, 456 cm^{-1} . HRMS (ESI-TOF) m/z : $[\text{M}+\text{Na}]^+$ Calcd for $\text{C}_{28}\text{H}_{26}\text{BF}_2\text{N}_3\text{NaO}_2$ 508.1984; Found 508.1984.

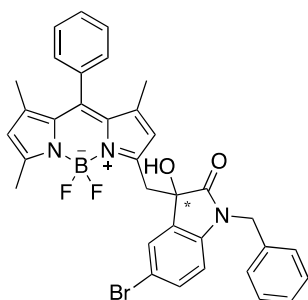
3.4.5 Synthesis of chiral BODIPY 73ae



With the general procedure, chiral BODIPY **73ae** was obtained as an orange solid with 9% isolated yield in 10 days. Melting Point: 190-195 °C (decomposed). HPLC analysis (OD-H, *n*-Hexane/Isopropanol, 90/10, 1 mL/min, 510 nm) $t_{\text{minor}}=22$ min and $t_{\text{major}}=46$ min, 52% ee, $[\alpha]_{\text{D}}^{25} = -109.2$ (c 0.1, CH_2Cl_2). ^1H NMR (400 MHz, Chloroform-*d*) δ 7.42 (d, $J = 1.7$ Hz, 1H), 7.36 – 7.27 (m, 6H), 7.12 (s, 1H), 6.57 (d, $J = 8.3$ Hz, 1H), 6.11 (d, $J = 2.6$ Hz, 2H), 4.98 (d, $J = 15.7$ Hz, 1H), 4.78 (d, $J = 15.7$ Hz, 1H), 4.11 (bs, 1H), 3.68 (d, $J = 14.9$ Hz, 1H), 3.32 (d, $J = 14.9$ Hz, 1H), 2.55 (s, 3H), 2.28 (s, 6H). ^{13}C NMR (101 MHz, CDCl_3) δ 176.8, 159.4, 150.3, 143.2, 141.2, 140.0, 135.0, 134.3, 132.8, 132.3, 131.9, 128.8, 128.1, 127.7, 127.2, 120.8, 120.1, 119.4, 115.4, 110.8, 75.2, 43.9, 36.7, 14.8, 11.3, 11.3 ppm. IR (neat): 3258, 2920,

2851, 1689, 1603, 1531, 1507, 1483, 1450, 1431, 1410, 1370, 1342, 1307, 1293, 1241, 1216, 1192, 1170, 1153, 1122, 1078, 1016, 973, 920, 897, 871, 806, 758, 699, 627, 606, 557, 533, 468 cm^{-1} . HRMS (ESI-TOF) m/z : $[\text{M}+\text{Na}]^+$ Calcd for $\text{C}_{28}\text{H}_{25}\text{BBrF}_2\text{N}_3\text{NaO}_2$ 586.1089; Found 586.1088.

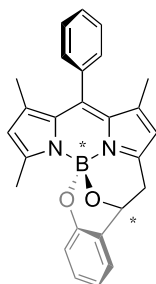
3.4.6 Synthesis of chiral BODIPY 73be



With the general procedure, chiral BODIPY **73ae** was obtained as an orange solid with 10% isolated yield in 13 days. Melting Point: 111-114 °C (decomposed). HPLC analysis (AD-H, *n*-Hexane/Isopropanol, 90/10, 1 mL/min, 254 nm) $t_{\text{major}} = 23$ min and $t_{\text{minor}} = 40$ min, 45% ee, $[\alpha]_{\text{D}}^{25} = -42$ (c 0.1, CH_2Cl_2). ^1H NMR (400 MHz, Chloroform-*d*) δ 7.55 – 7.48 (m, 3H), 7.43 (d, $J = 1.9$ Hz, 1H), 7.36 – 7.26 (m, 8H), 6.57 (d, $J = 8.3$ Hz, 1H), 6.05 (d, $J = 11.6$ Hz, 2H), 5.01 (d, $J = 15.7$ Hz, 1H), 4.78 (d, $J = 15.7$ Hz, 1H), 3.73 (d, $J = 15.0$ Hz, 1H), 3.36 (d, $J = 15.0$ Hz, 1H), 2.57 (s, 3H), 1.40 (s, 6H), OH peak could not be observed. ^{13}C NMR (101 MHz, CDCl_3) δ 176.9, 157.9, 149.1, 145.1, 142.5, 142.0, 141.2, 135.0, 134.6, 132.2, 132.0, 129.2, 129.1, 129.0, 128.9, 128.8, 128.1, 127.7, 127.7, 127.2, 122.1, 121.7, 115.4, 110.8, 75.2, 43.9, 36.6, 14.8, 14.4, 14.3 ppm. IR (neat): 3506, 3379, 2956, 2925, 2856, 1724, 1707, 1609, 1541, 1505, 1481, 1454, 1431, 1407, 1364, 1312, 1260, 1184, 1154, 1077, 1043, 1025, 980, 883, 839, 809, 722, 697, 627, 603, 560, 532, 506, 488, 473 cm^{-1} . HRMS (ESI-TOF) m/z : $[\text{M}+\text{Na}]^+$ Calcd for $\text{C}_{34}\text{H}_{29}\text{BBrF}_2\text{N}_3\text{NaO}_2$ 662.1402; Found 662.1445.

3.5 Procedure for Synthesis of BODIPY 96

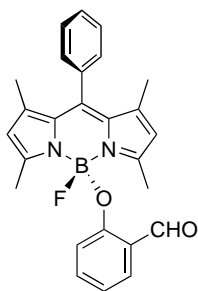
1 eq. BCl_3 (154 μL , 1.0 M in *n*-hexane) was added dropwise to the DCM solution (5 mL) of BODIPY **53b** (50 mg) placed in 10 mL vial while stirring at room temperature. In another 25 mL round-bottom flask, 3.6 eq. cesium carbonate (179 mg, 550 μmol), 3.25 eq. salicylaldehyde (61mg, 500 μmol) and anhydrous DMF (3 mL) were left to stir at room temperature. After 1 hour mixed separately, the former solution was poured over the latter and then, combined solution was stirred an additional hour. For the work-up process, 50 mL DCM was added to reaction mixture and the mixture was washed with water (3 x 50 mL) and brine (1 x 25 mL). The organic phase was dried over anhydrous Na_2SO_4 , filtered and then concentrated under vacuum. The residue was purified by FCC with DCM as eluent.



With the procedure, BODIPY **96** was obtained as an orange solid with 18% isolated yield in 2 h. Melting Point: 214-217 °C. HPLC analysis (OD-H, *n*-Hexane/Isopropanol, 98/2, 1 mL/min, 505 nm) t_{R1} = 8.38 min and t_{R2} = 11.42 min, $[\alpha]_D^{25} = -567.9$ (*c* 4.05 x 10⁻³, CHCl_3) for fast-eluting enantiomer, 99.5% ee, (-) BODIPY **96**; $[\alpha]_D^{25} = +617.3$ (*c* 4.05 x 10⁻³, CHCl_3) for slow-eluting enantiomer, 98.5% ee, (+) BODIPY **96**. ^1H NMR (600 MHz, CDCl_3) δ 7.52 – 7.42 (m, 4H), 7.24 – 7.19 (m, 1H), 7.11 – 7.06 (m, 1H), 7.02 (dd, *J* = 7.5, 1.3 Hz, 1H), 6.82 (d, *J* = 7.9 Hz, 1H), 6.78 (td, *J* = 7.4, 0.9 Hz, 1H), 5.98 (s, 1H), 5.88 (s, 1H), 5.45 (bs, 1H), 3.51 (dd, *J* = 18.5, 6.3 Hz, 1H), 2.95 (d, *J* = 18.5 Hz, 1H), 2.53 (s, 3H), 1.44 (s, 3H), 1.37 (s, 3H). ^{13}C NMR (151 MHz, CDCl_3) δ 155.9, 154.2, 151.7, 144.1, 142.8, 142.3, 134.9, 131.5, 129.8, 129.0, 128.9, 128.8, 128.3, 128.2, 128.1, 128.0, 125.3, 120.9, 118.3, 118.2, 118.1, 70.3, 35.6, 29.7, 14.9, 13.9 ppm. IR (neat): 3052, 2955, 2922,

2885, 1607, 1581, 1548, 1538, 1514, 1500, 1488, 1426, 1406, 1380, 1361, 1348, 1329, 1308, 1282, 1243, 1217, 1191, 1153, 1051 cm^{-1} . HRMS (ESI-TOF) m/z : $[\text{M}-\text{H}]^-$ Calcd for $\text{C}_{26}\text{H}_{22}\text{BN}_2\text{O}_2$ 405.1774; Found 405.1786.

3.5.1 The reaction intermediate **95**



The reaction intermediate **95** was isolated as an orange solid with 3% chemical yield. Melting Point: 185-189 °C. ^1H NMR (600 MHz, CDCl_3) δ 10.69 (s, 1H), 7.76 (dd, $J = 7.7, 1.8$ Hz, 1H), 7.56 – 7.47 (m, 3H), 7.34 – 7.20 (m, 3H), 6.83 (dd, $J = 13.4, 5.9$ Hz, 1H), 6.32 (d, $J = 8.4$ Hz, 1H), 5.93 (s, 2H), 2.44 (s, 6H), 1.40 (s, 6H). ^{13}C NMR (151 MHz, CDCl_3) δ 191.4, 159.9, 159.8, 155.9, 143.7, 141.8, 135.7, 134.7, 131.5, 129.2, 129.2, 129.1, 128.0, 127.9, 127.8, 121.8, 121.8, 119.5, 117.2, 14.8, 14.8, 14.5 ppm. HRMS (ESI-TOF) m/z : $[\text{M}\cdot]^-$ Calcd for $\text{C}_{26}\text{H}_{24}\text{BFN}_2\text{O}_2$ 426.1914; Found 426.1920.

3.6 The experimental calculation of fluorescence quantum yield

The most reliable method for calculating fluorescence quantum yield is the relative method¹³⁶ of Williams et al. which involves the use of characterized reference with known Φ_{fl} .

In practice, the experimental measurement of quantum yield is complicated because a number of considerations should be taken into such as concentration effects, the use of different solvents, and validity of reference and its Φ_{fl} value. To overcome these considerations, it is important to acquire a set of data in different absorbance

and ensure linearity across the concentration range, include the refractive index and cross-calibrating the reference with the sample.

Also, as experimental considerations, a reference that emits in a similar fashion to the sample should be chosen. Also, in this analysis, in order to minimize the re-absorption effects, absorbances should never exceed 0.1 at and above the excitation wavelength. Above this level, non-linear effects could be observed due to inner filter effects and resulted in incorrect quantum yield values. Besides, in fluorescence analysis, constant slit widths and a single excitation wavelength should be used for both sample and reference.

For the analysis, firstly, UV-vis absorbance spectrum of the solvent for the sample should be recorded at the excitation wavelength. Then, its fluorescence emission spectra should be taken, and this intensity should be converted to integrated fluorescence intensity. There should be six solutions whose absorbances at the excitation wavelength of $\sim 0/\text{solvent}$, 0.02, 0.04, 0.06, 0.08, and 0.1. After conducting the fluorescence analysis of these solutions, a plot of integrated fluorescence intensity vs absorbance should be drawn. In this graph, R^2 value should be higher 0.99 and intercept should be equal to zero. This procedure should be repeated for the reference. After getting two lines for sample and reference, following equation was used to calculate Φ_{fl} :

$$\Phi_s = \Phi_r \left(\frac{m_s}{m_r} \right) \left(\frac{n_s}{n_r} \right)^2$$

Where Φ denotes fluorescence quantum yield, m : gradient of the plot of integrated fluorescence intensity against absorbance, n : refractive index of the solution, and subscripts r and s denotes reference and sample, respectively.

In this study, the relative fluorescence quantum yields (Φ_{fl}) of the dyes were calculated by taking aqueous alkaline solutions of fluorescein as the reference (λ_{ex} 490 nm in 0.1 N NaOH, $\Phi_{fl} = 0.85$ according to the literature).

CHAPTER 4

CONCLUSION

In this study, the enantioselective synthesis of 2-indolyl-1-nitro derivatives **34** and BODIPY dyes **73** was conducted in the presence of 2-aminoDMAP **23-25** and quinine-based **28-30** bifunctional organocatalysts.

In the first chapter of the study, asymmetric Friedel-Crafts alkylation of indoles **33** with nitroolefins **16** was carried out with 2 mol% *tert*-butyl squaramide/quinine organocatalyst **30**. 19 different 2-indolyl-1-nitro derivatives **34** were synthesized with acceptable to excellent enantioselectivities (up to >99% ee) and high yields (up to 80%).

In the second chapter, the enantioselective addition of BODIPY **53** to *N*-substituted isatin derivatives **72** was conducted with 20 mol% 2-adamantyl squaramide/quinine organocatalyst **29**. The six novel chiral BODIPYs **73** were synthesized with acceptable enantioselectivities (up to 60% ee). This part of the study is the most valuable one because this kind of enantioselective addition will be *the first in the literature*. For the spectroscopic analyses, high emissions were observed in fluorescence analyses with all derivatives. As a representative example, the quantum yield of **73aa** was calculated as 0.78 in CHCl₃. However, very low ECD activity was observed in the analyses of BODIPY **73aa** in different concentrations.

In the last chapter, a novel BODIPY point chiral at boron and carbon, BODIPY **96**, was synthesized through a two-pot, one-step procedure. The resolved enantiomers showed a strong Cotton effect in the visible region in ECD spectra. Also, chiral dye **96** was thermally stable to epimerization but showed very weak fluorescence emission due to nonradiative decay involving vibrational relaxation, intersystem crossing to the triplet manifold and bent-shaped molecular geometry.

REFERENCES

- (1) Ahrendt, K. A.; Borths, C. J.; MacMillan, D. W. C. *J. Am. Chem. Soc.* **2000**, *122*, 4243-4244.
- (2) List, B.; Lerner, R. A.; Barbas, C. F. *J. Am. Chem. Soc.* **2000**, *122*, 2395-2396.
- (3) Negishi, E. *J. Syn. Org. Chem., Jpn.* **2011**, *69*, 1201-1201.
- (4) Retrieved from <https://www.nobelprize.org/prizes/chemistry/2021/press-release/>. (Last accessed on 07.01.2022)
- (5) Alemán, J.; Cabrera, S. *Chem. Soc. Rev.* **2013**, *42*, 774-793.
- (6) Berkessel, A.; Gröger, H. *Asymmetric Organocatalysis-From Biomimetic Concepts to Applications in Asymmetric Synthesis*; Wiley-VCH: Weinheim, Germany, 2005.
- (7) Moyano, A.; Rios, R. *Chem. Rev.* **2011**, *111*, 4703-4832.
- (8) Takemoto, Y. *Org. Biomol. Chem.*, **2005**, *3*, 4299-4306.
- (9) MacMillan, D. W. C. *Nature* **2008**, *455*, 304-308.
- (10) Mukherjee, S.; Yang, J. W.; Hoffmann, S.; List, B. *Chem. Rev.* **2007**, *107*, 5471-5569.
- (11) Erkkilä, A.; Majander, I.; Pihko, P. M. *Chem. Rev.* **2007**, *107*, 5416-5470.
- (12) Notz, W.; List, B. *J. Am. Chem. Soc.* **2000**, *122*, 7386-7387.
- (13) List, B. *J. Am. Chem. Soc.* **2000**, *122*, 9336-9337.
- (14) Hechavarria Fonseca, M. T.; List, B. *Angew. Chem. Int. Ed.* **2004**, *43*, 3958-3960.
- (15) Danishefsky, S.; Cain, P. *J. Am. Chem. Soc.* **1976**, *98*, 4975-4983.
- (16) Agami, C.; Meynier, F.; Puchot, C.; Guilhem, J.; Pascard, C. *Tetrahedron* **1984**, *40*, 1031-1038.
- (17) Marigo, M.; Wabnitz, T. C.; Fielenbach, D.; Jørgensen, K. A. *Angew. Chem. Int. Ed.* **2005**, *44*, 794-797.
- (18) Hayashi, Y.; Gotoh, H.; Hayashi, T.; Shoji, M. *Angew. Chem. Int. Ed.* **2005**, *44*, 4212-4215.
- (19) Sakakura, A.; Suzuki, K.; Ishihara, K. *Adv. Synth. Catal.* **2006**, *348*, 2457-2465.
- (20) Ishihara, K.; Nakano, K. *J. Am. Chem. Soc.* **2005**, *127*, 10504-10505.

- (21) Yu, X.; Wang, W. *Chem. Asian J.* **2008**, *3*, 516-532.
- (22) Doyle, A. G.; Jacobsen, E. N. *Chem. Rev.* **2007**, *107*, 5713-5743.
- (23) Schreiner, P. R. *Chem. Soc. Rev.* **2003**, *32*, 289-296.
- (24) Huang, Y.; Unni, A. K.; Thadani, A. N.; Rawal, V. H. *Nature* **2003**, *424*, 146-146.
- (25) Uraguchi, D.; Sorimachi, K.; Terada, M. *J. Am. Chem. Soc.* **2004**, *126*, 11804-11805.
- (26) Akiyama, T.; Itoh, J.; Yokota, K.; Fuchibe, K. *Angew. Chem. Int. Ed.* **2004**, *43*, 1566-1568.
- (27) Wang, Y.; Deng, L. *Catalytic Asymmetric Synthesis*; Ojima, I., Ed.; John Wiley & Sons, Inc.: Hoboken, NJ, USA, 2010.
- (28) Hiemstra, H.; Wynberg, H. *J. Am. Chem. Soc.* **1981**, *103*, 417-430.
- (29) Okino, T.; Hoashi, Y.; Takemoto, Y. *J. Am. Chem. Soc.* **2003**, *125*, 12672-12673.
- (30) Hou, X.; Du, D. *Adv. Synth. Catal.* **2020**, *362*, 4487-4512.
- (31) Malerich, J. P.; Hagihara, K.; Rawal, V. H. *J. Am. Chem. Soc.* **2008**, *130*, 14416-14417.
- (32) Alemán, J.; Parra, A.; Jiang, H.; Jørgensen, K. A. *Chem. Eur. J.* **2011**, *17*, 6890-6899.
- (33) Quiñonero, D.; Prohens, R.; Garau, C.; Frontera, A.; Ballester, P.; Costa, A.; Deyà, P. M. *Chem. Phys. Lett.* **2002**, *351*, 115-120.
- (34) Tomàs, S.; Prohens, R.; Vega, M.; Rotger, M. C.; Deyà, P. M.; Ballester, P.; Costa, A. *J. Org. Chem.* **1996**, *61*, 9394-9401.
- (35) Okino, T.; Hoashi, Y.; Furukawa, T.; Xu, X.; Takemoto, Y. *J. Am. Chem. Soc.* **2005**, *127*, 119-125.
- (36) Li, X.; Deng, H.; Zhang, B.; Li, J.; Zhang, L.; Luo, S.; Cheng, J.-P. *Chem. Eur. J.* **2010**, *16*, 450-455.
- (37) Jakab, G.; Tancon, C.; Zhang, Z.; Lippert, K. M.; Schreiner, P. R. *Org. Lett.* **2012**, *14*, 1724-1727.
- (38) Ni, X.; Li, X.; Wang, Z.; Cheng, J.-P. *Org. Lett.* **2014**, *16*, 1786-1789.
- (39) Zhao, B.; Li, J.; Du, D. *Chem. Rec.* **2017**, *17*, 994-1018.
- (40) Chauhan, P.; Mahajan, S.; Kaya, U.; Hack, D.; Enders, D. *Adv. Synth. Catal.* **2015**, *357*, 253-281.
- (41) Işık, M.; Unver, M. Y.; Tanyeli, C. *J. Org. Chem.* **2015**, *80*, 828-835.

- (42) Kanberoğlu, E.; Tanyeli, C. *Asian J. Org. Chem.* **2016**, *5*, 114-119.
- (43) Susam, D.; Tanyeli, C. *New. J. Chem.* **2017**, *41*, 3555-3561.
- (44) Karahan, S.; Tanyeli, C. *New. J. Chem.* **2017**, *41*, 9192-9202.
- (45) Hasilcioğulları, D.; Tanyeli, C. *Tetrahedron Lett.* **2018**, *59*, 1414-1416.
- (46) İşibol, D.; Karahan, S.; Tanyeli, C. *Tetrahedron Lett.* **2018**, *59*, 541-545.
- (47) Karahan, S.; Tanyeli, C. *Org. Biomol. Chem.*, **2020**, *18*, 479-487.
- (48) Susam, Z. D.; Bozdemir, M.; Gündoğdu, G.; Tanyeli, C. *New. J. Chem.* **2022**, *46*, 599-606.
- (49) Olah, G. A.; Krishnamurthy, R.; Prakash, G. K. S. *Comprehensive Organic Synthesis*, First edition.; Fleming, I., Ed.; Pergamon: Oxford, United Kingdom, 1991.
- (50) Manabe, K.; Aoyama, N.; Kobayashi, S. *Adv. Synth. Catal.* **2001**, *343*, 174-176.
- (51) Kim, H. Y.; Kim, S.; Oh, K. *Angew. Chem. Int. Ed.* **2010**, *49*, 4476-4478.
- (52) Li, W.-J. *Catal. Commun.* **2014**, *52*, 53-56.
- (53) Tanaka, K.; Sakuragi, K.; Ozaki, H.; Takada, Y. *Chem. Commun.* **2018**, *54*, 6328-6331.
- (54) Jia, Y.-X.; Zhu, S.-F.; Yang, Y.; Zhou, Q.-L. *J. Org. Chem.* **2006**, *7*, 75-80.
- (55) Venkatanna, K.; Yeswanth Kumar, S.; Karthick, M.; Padmanaban, R.; Ramaraj Ramanathan, C. *Org. Biomol. Chem.*, **2019**, *17*, 4077-4086.
- (56) Arai, T.; Tsuchida, A.; Miyazaki, T.; Awata, A. *Org. Lett.* **2017**, *19*, 758-761.
- (57) Ganesh, M.; Seidel, D. *J. Am. Chem. Soc.* **2008**, *130*, 16464-16465.
- (58) Fan, Y.; Kass, S. R. *J. Org. Chem.* **2017**, *82*, 13288-13296.
- (59) Ma, J.; Kass, S. R. *J. Org. Chem.* **2019**, *84*, 11125-11134.
- (60) Didaskalou, C.; Kupai, J.; Cseri, L.; Barabas, J.; Vass, E.; Holtzl, T.; Szekeley, G. *ACS Catal.* **2018**, *8*, 743-7438.
- (61) Zhang, G. *Inorg. Chem. Commun.* **2014**, *40*, 1-4.
- (62) Herrera, R. P.; Sgarzani, V.; Bernardi, L.; Ricci, A. *Angew. Chem. Int. Ed.* **2005**, *44*, 6576-6579.
- (63) Zhuang, W.; Hazell, R. G.; Jørgensen, K. A. *Org. Biomol. Chem.*, **2005**, *3*, 2566-2571.

- (64) Fleming, E. M.; McCabe, T.; Connon, S. J. *Tetrahedron Lett.* **2006**, *47*, 7037-7042.
- (65) Itoh, J.; Fuchibe, K.; Akiyama, T. *Angew. Chem. Int. Ed.* **2008**, *47*, 4016-4018.
- (66) Tang, H.-Y.; Zhang, Z.-B. *Phosphorus Sulfur Silicon Relat. Elem.* **2011**, *186*, 2038-2046.
- (67) Huang, K.; Pei, X.; Yin, X.; Chen, Z. *Asian J. Chem.* **2017**, *29*, 595-600.
- (68) Austin, J. F.; MacMillan, D. W. C. *J. Am. Chem. Soc.* **2002**, *124*, 1172-1173.
- (69) Sundberg, R. *The Chemistry of Indoles*; Academic Press, 1970.
- (70) Ono, N. *The Nitro Group in Organic Synthesis*; John Wiley & Sons, Inc.: New York, USA, 2001.
- (71) Bandini, M.; Eichholzer, A. *Angew. Chem. Int. Ed.* **2009**, *48*, 9608-9644.
- (72) Fînaru, A.; Berthault, A.; Besson, T.; Guillaumet, G.; Berteina-Raboin, S. *Tetrahedron Lett.* **2002**, *43*, 787-790.
- (73) Laine, A.; Lood, C.; Koskinen, A. *Molecules* **2014**, *19*, 1544-1567.
- (74) Paulvannan, K.; Hale, R.; Mesis, R.; Chen, T. *Tetrahedron Lett.* **2002**, *43*, 203-207.
- (75) Jandu, K. S.; Barrett, V.; Brockwell, M.; Cambridge, D.; Farrant, D. R.; Foster, C.; Giles, H.; Glen, R. C.; Hill, A. P.; Hobbs, H.; Honey, A.; Martin, G. R.; Salmon, J.; Smith, D.; Woollard, P.; Selwood, D. L. *J. Med. Chem.* **2001**, *44*, 681-693.
- (76) Leitch, J. A.; Bhonoah, Y.; Frost, C. G. *ACS Catal.* **2017**, *7*, 5618-5627.
- (77) Boens, N.; Leen, V.; Dehaen, W. *Chem. Soc. Rev.* **2012**, *41*, 1130-1172.
- (78) Loudet, A.; Burgess, K. *Chem. Rev.* **2007**, *107*, 4891-4932.
- (79) Ulrich, G.; Ziesel, R.; Harriman, A. *Angew. Chem. Int. Ed.* **2008**, *47*, 1184-1201.
- (80) Treibs, A.; Kreuzer, F.-H. *Justus Liebigs Ann. Chem.* **1968**, *718*, 208-223.
- (81) Boens, N.; Verbelen, B.; Dehaen, W. *Eur. J. Org. Chem.* **2015**, 6577-6595.
- (82) Boyer, J. H.; Haag, A. M.; Sathyamoorthi, G.; Soong, M.-L.; Thangaraj, K.; Pavlopoulos, T. G. *Heteroat. Chem.* **1993**, *4*, 39-49.
- (83) Yogo, T.; Urano, Y.; Ishitsuka, Y.; Maniwa, F.; Nagano, T. *J. Am. Chem. Soc.* **2005**, *127*, 12162-12163.
- (84) Shah, M.; Thangaraj, K.; Soong, M.-L.; Wolford, L. T.; Boyer, J. H.; Politzer, I. R.; Pavlopoulos, T. G. *Heteroat. Chem.* **1990**, *1*, 389-399.

- (85) Rurack, K.; Kollmannsberger, M.; Daub, J. *New. J. Chem.* **2001**, *25*, 289-292.
- (86) Dost, Z.; Atilgan, S.; Akkaya, E. U. *Tetrahedron* **2006**, *62*, 8484-8488.
- (87) Buyukcakil, O.; Bozdemir, O. A.; Kolemen, S.; Erbas, S.; Akkaya, E. U. *Org. Lett.* **2009**, *11*, 4644-4647.
- (88) Bura, T.; Hablot, D.; Ziesel, R. *Tetrahedron Lett.* **2011**, *52*, 2370-2374.
- (89) Rurack, K.; Kollmannsberger, M.; Daub, J. *Angew. Chem. Int. Ed.* **2001**, *40*, 385-387.
- (90) Baruah, M.; Qin, W.; Flors, C.; Hofkens, J.; Vallée, R. A. L.; Beljonne, D.; van der Auweraer, M.; de Borggraeve, W. M.; Boens, N. *J. Phys. Chem. A* **2006**, *110*, 5998-6009.
- (91) Negishi, E. *Handbook of Organopalladium Chemistry for Organic Synthesis*; Negishi, E., Ed.; John Wiley & Sons, Inc.: New York, USA, 2002.
- (92) Li, F.; Yang, S. I.; Ciringh, Y.; Seth, J.; Martin, C. H.; Singh, D. L.; Kim, D.; Birge, R. R.; Bocian, D. F.; Holten, D.; Lindsey, J. S. *J. Am. Chem. Soc.* **1998**, *120*, 10001-10017.
- (93) Thivierge, C.; Bandichhor, R.; Burgess, K. *Org. Lett.* **2007**, *9*, 2135-2138.
- (94) Gómez-Durán, C. F. A.; García-Moreno, I.; Costela, A.; Martin, V.; Sastre, R.; Bañuelos, J.; López Arbeloa, F.; López Arbeloa, I.; Peña-Cabrera, E. *Chem. Commun.* **2010**, *46*, 5103-5105.
- (95) Osorio-Martínez, C. A.; Urías-Benavides, A.; Gómez-Durán, C. F. A.; Bañuelos, J.; Esnal, I.; López Arbeloa, I.; Peña-Cabrera, E. *J. Org. Chem.* **2012**, *77*, 5434-5438.
- (96) Leen, V.; Yuan, P.; Wang, L.; Boens, N.; Dehaen, W. *Org. Lett.* **2012**, *14*, 6150-6153.
- (97) Goze, C.; Ulrich, G.; Mallon, L. J.; Allen, B. D.; Harriman, A.; Ziesel, R. *J. Am. Chem. Soc.* **2006**, *128*, 10231-10239.
- (98) Rousseau, T.; Cravino, A.; Bura, T.; Ulrich, G.; Ziesel, R.; Roncali, J. *Chem. Commun.* **2009**, 1673-1675.
- (99) Ulrich, G.; Goze, C.; Goeb, S.; Retailleau, P.; Ziesel, R. *New. J. Chem.* **2006**, *30*, 982-986.
- (100) Tahtaoui, C.; Thomas, C.; Rohmer, F.; Klotz, P.; Duportail, G.; Mély, Y.; Bonnet, D.; Hibert, M. *J. Org. Chem.* **2007**, *72*, 269-272.
- (101) Jiang, X.-D.; Zhang, J.; Furuyama, T.; Zhao, W. *Org. Lett.* **2012**, *14*, 248-251.

- (102) Bodio, E.; Goze, C. *Dyes Pigm.* **2019**, *160*, 700-710.
- (103) van Koeveringe, J. A.; Lugtenburg, J. *Recl. Trav. Chim. Pays-Bas* **1977**, *96*, 55-57.
- (104) de Wael, E. V.; Pardoën, J. A.; van Koeveringe, J. A.; Lugtenburg, J. *Recl. Trav. Chim. Pays-Bas* **1977**, *96*, 306-309.
- (105) Wu, L.; Burgess, K. *Chem. Commun.* **2008**, 4933-4935.
- (106) Lu, H.; Mack, J.; Nyokong, T.; Kobayashi, N.; Shen, Z. *Coord. Chem. Rev.* **2016**, *318*, 1-15.
- (107) Gossauer, A.; Fehr, F.; Nydegger, F.; Stöckli-Evans, H. *J. Am. Chem. Soc.* **1997**, *119*, 1599-1608.
- (108) Móczár, I.; Huszthy, P.; Maidics, Z.; Kádár, M.; Klára Tóth. *Tetrahedron* **2009**, *65*, 8250-8258.
- (109) Sánchez-Carnerero, E. M.; Moreno, F.; Maroto, B. L.; Agarrabeitia, A. R.; Bañuelos, J.; Arbeloa, T.; López-Arbeloa, I.; Ortiz, M. J.; Moya, S. de la. *Chem. Commun.* **2013**, *49*, 11641-11643.
- (110) Beer, G.; Niederal, C.; Grimme, S.; Daub, J. *Angew. Chem.* **2000**, *39*, 3252-3255.
- (111) Beer, G.; Daub, J.; Rurack, K. *Chem. Commun.* **2001**, *12*, 1138-1139.
- (112) Nagai, A.; Kokado, K.; Miyake, J.; Chujo, Y. *Polym. J.* **2010**, *42*, 37-42.
- (113) Sánchez-Carnerero, E. M.; Moreno, F.; Maroto, B. L.; Agarrabeitia, A. R.; Ortiz, M. J.; Vo, B. G.; Muller, G.; Moya, S. de la. *J. Am. Chem. Soc.* **2014**, *136*, 3346-3349.
- (114) Wang, Y.-W.; Descalzo, A. B.; Shen, Z.; You, X.-Z.; Rurack, K. *Chem. Eur. J.* **2010**, *16*, 2887-2903.
- (115) Lerrick, R. I.; Winstanley, T. P. L.; Haggerty, K.; Wills, C.; Clegg, W.; Harrington, R. W.; Bultinck, P.; Herrebout, W.; Benniston, A. C.; Hall, M. J. *Chem. Commun.* **2014**, *50*, 4714-4716.
- (116) Kolemen, S.; Cakmak, Y.; Kostereli, Z.; Akkaya, E. U. *Org. Lett.* **2014**, *16*, 660-663.
- (117) Guerrero-Corella, A.; Asenjo-Pascual, J.; Pawar, T. J.; Díaz-Tendero, S.; Martín-Sómer, A.; Gómez, C. V.; Belmonte-Vázquez, J. L.; Ramírez-Ornelas, D. E.; Peña-Cabrera, E.; Fraile, A.; Cruz, D. C.; Alemán, J. *Chem. Sci.* **2019**, *10*, 4346-4351.
- (118) Rigotti, T.; Asenjo-Pascual, J.; Martín-Sómer, A.; Milán Rois, P.; Cordani, M.; Díaz-Tendero, S.; Somoza, Á.; Fraile, A.; Alemán, J. *Adv. Synth. Catal.* **2020**, *362*, 1345-1355.

- (119) Meazza, M.; Cruz, C. M.; Ortuño, A. M.; Cuerva, J. M.; Crovetto, L.; Rios, R. *Chem. Sci.* **2021**, *12*, 4503-4508.
- (120) Kwon, Y.-D.; Byun, Y.; Kim, H.-K. *Nucl. Med. Biol.* **2021**, *93*, 22-36.
- (121) Ametamey, S. M.; Honer, M.; Schubiger, P. A. *Chem. Rev.* **2008**, *108*, 1501-1516.
- (122) Jacobson, O.; Kiesewetter, D. O.; Chen, X. *Bioconjugate Chem.* **2015**, *26*, 1-18.
- (123) Kobayashi, H.; Ogawa, M.; Alford, R.; Choyke, P. L.; Urano, Y. *Chem. Rev.* **2010**, *110*, 2620-2640.
- (124) Colas, K.; Doloczi, S.; Posada Urrutia, M.; Dyrager, C. *Eur. J. Org. Chem.* **2021**, 2133-2144.
- (125) Poddar, M.; Misra, R. *Coord. Chem. Rev.* **2020**, *421*, 213462.
- (126) Squeo, B. M.; Gregoriou, V. G.; Avgeropoulos, A.; Baysec, S.; Allard, S.; Scherf, U.; Chochos, C. L. *Prog. Polym. Sci.* **2017**, *71*, 26-52.
- (127) Isik, M.; Tanyeli, C. *J. Org. Chem.* **2013**, *78*, 1604-1611.
- (128) Vakulya, B.; Varga, S.; Csámpai, A.; Soós, T. *Org. Lett.* **2005**, *7*, 1967-1969.
- (129) Busschaert, N.; Park, S.-H.; Baek, K.-H.; Choi, Y. P.; Park, J.; Howe, E. N. W.; Hiscock, J. R.; Karagiannidis, L. E.; Marques, I.; Félix, V.; Namkung, W.; Sessler, J. L.; Gale, P. A.; Shin, I. *Nat. Chem.* **2017**, *9*, 667-675.
- (130) Ganesh, M.; Seidel, D. *J. Am. Chem. Soc.* **2008**, *130*, 16464-16465.
- (131) Venkatanna, K.; Yeswanth Kumar, S.; Karthick, M.; Padmanaban, R.; Ramaraj Ramanathan, C. *Org. Biomol. Chem.* **2019**, *17*, 4077-4086.
- (132) Islam, M. S.; al Majid, A. M. A.; Al-Othman, Z. A.; Barakat, A. *Tetrahedron: Asymmetry* **2014**, *25*, 245-251.
- (133) Chittoory, A. K.; Kumari, G.; Mohapatra, S.; Kundu, P. P.; Maji, T. K.; Narayana, C.; Rajaram, S. *Tetrahedron* **2014**, *70*, 3459-3465.
- (134) Emrullohoğlu, M.; Üçüncü, M.; Karakuş, E. *Chem. Commun.* **2013**, *49*, 7836-7838.
- (135) Furdas, S. D.; Shekfeh, S.; Kannan, S.; Sippl, W.; Jung, M. *MedChemComm* **2012**, *3*, 305-311.
- (136) Williams, A. T. R.; Winfield, S. A.; Miller, J. N. *Analyst* **1983**, *108*, 1067-1071.
- (137) Sunahara, H.; Urano, Y.; Kojima, H.; Nagano, T. *J. Am. Chem. Soc.* **2007**, *129*, 5597-5604.

- (138) Jiménez, J.; Sánchez-Camacho, J.; Moreno, F.; Agarrabeitia, A. R.; Arbeloa, T.; Cabrerros, T. A.; Muller, G.; Bañuelos, J.; Maroto, B. L.; Moya, S. de la. In *The 23rd International Electronic Conference on Synthetic Organic Chemistry*; MDPI: Basel Switzerland, 2020; p 53.
- (139) Avello, M. G.; de la Torre, M. C.; Guerrero-Martínez, A.; Sierra, M. A.; Gornitzka, H.; Hemmert, C. *Eur. J. Inorg. Chem.* **2020**, 4045-4053.
- (140) Haefele, A.; Zedde, C.; Retailleau, P.; Ulrich, G.; Ziesel, R. *Org. Lett.* **2010**, *12*, 1672-1675.
- (141) Jiménez, V. G.; Santos, F. M. F.; Castro-Fernández, S.; Cuerva, J. M.; Gois, P. M. P.; Pischel, U.; Campaña, A. G. *J. Org. Chem.* **2018**, *83*, 14057-14062.
- (142) Mori, T. *Chem. Rev.* **2021**, *121*, 2373-2412.
- (143) Zhou, Z.; Zhou, J.; Gai, L.; Yuan, A.; Shen, Z. *Chem. Commun.* **2017**, *53*, 6621-6624.
- (144) Lundrigan, T.; Crawford, S. M.; Cameron, T. S.; Thompson, A. *Chem. Commun.* **2012**, *48*, 1003-1005.
- (145) Tanaka, H.; Inoue, Y.; Mori, T. *ChemPhotoChem* **2018**, *2*, 386-402.
- (146) Ji, X.; Tong, H.; Yuan, Y. *Synth. Commun.* **2011**, *41*, 372-379.

APPENDICES

A. NMR SPECTRA

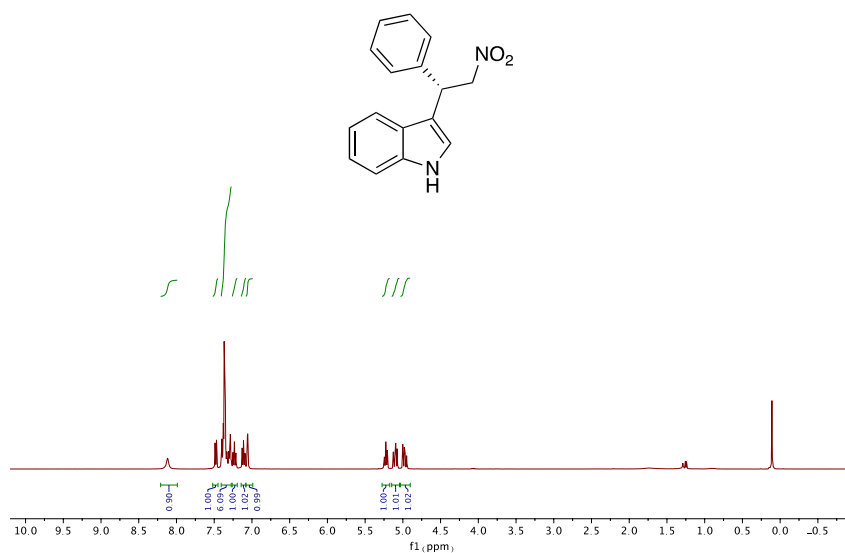


Figure A. 1. ¹H NMR spectrum of **34aa**

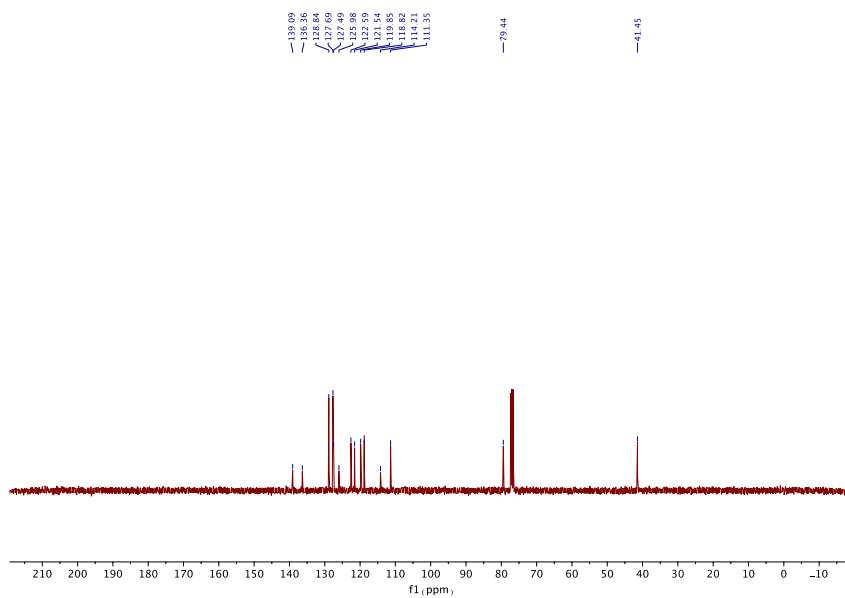


Figure A. 2. ¹³C NMR spectrum of **34aa**

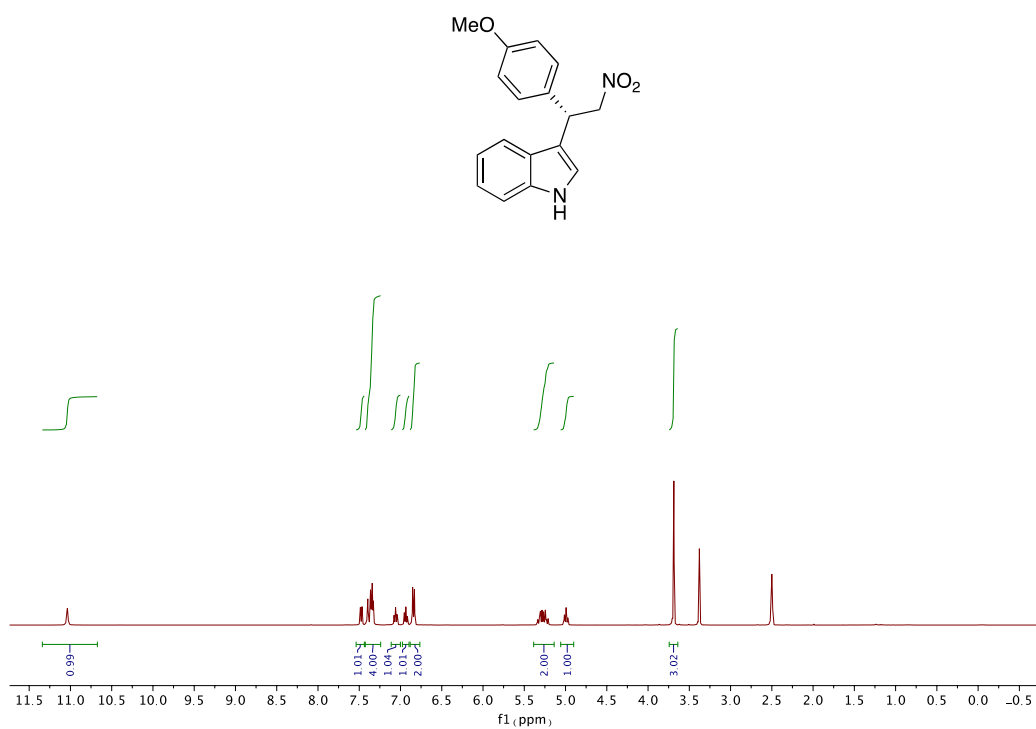


Figure A. 3. ¹H NMR spectrum of **34ab**

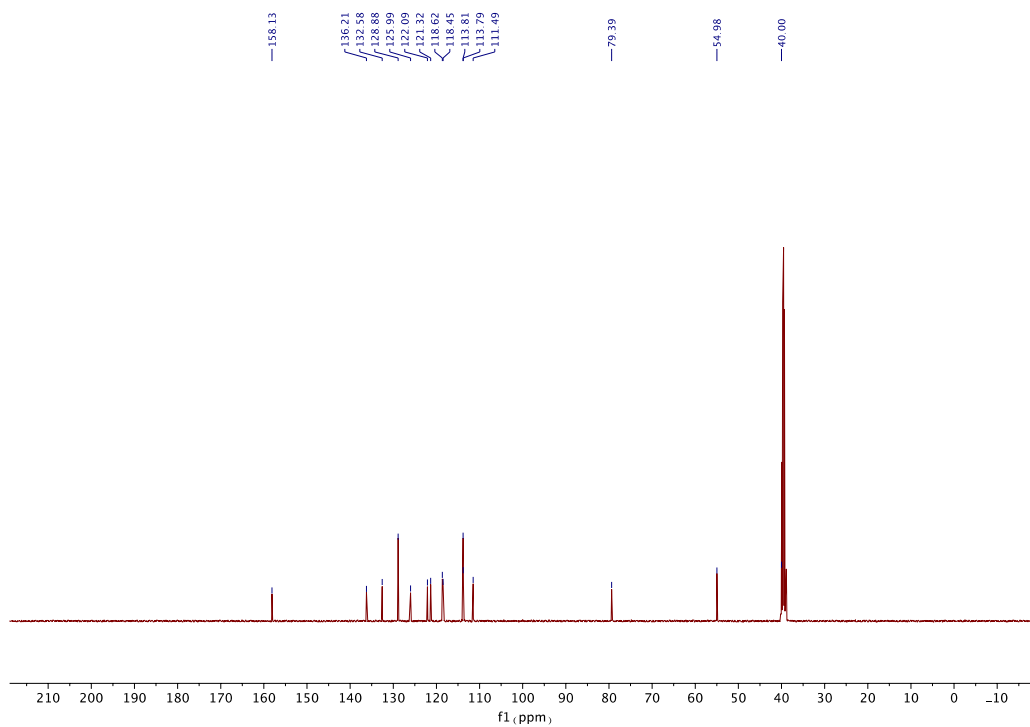


Figure A. 4. ¹³C NMR spectrum of **34ab**

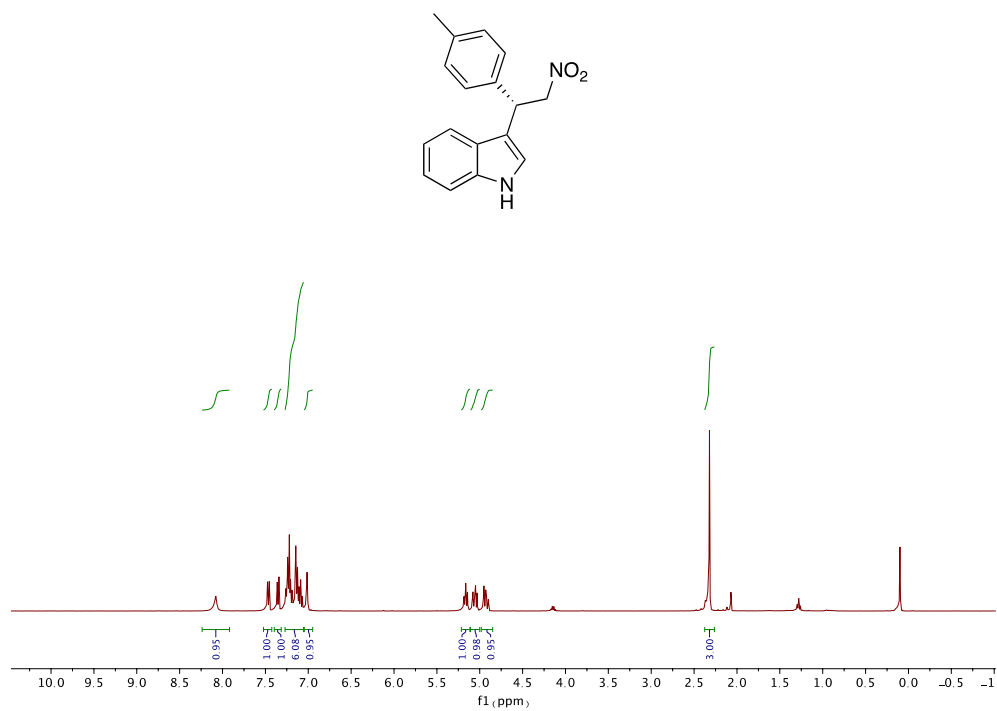


Figure A. 5. ^1H NMR spectrum of **34ac**

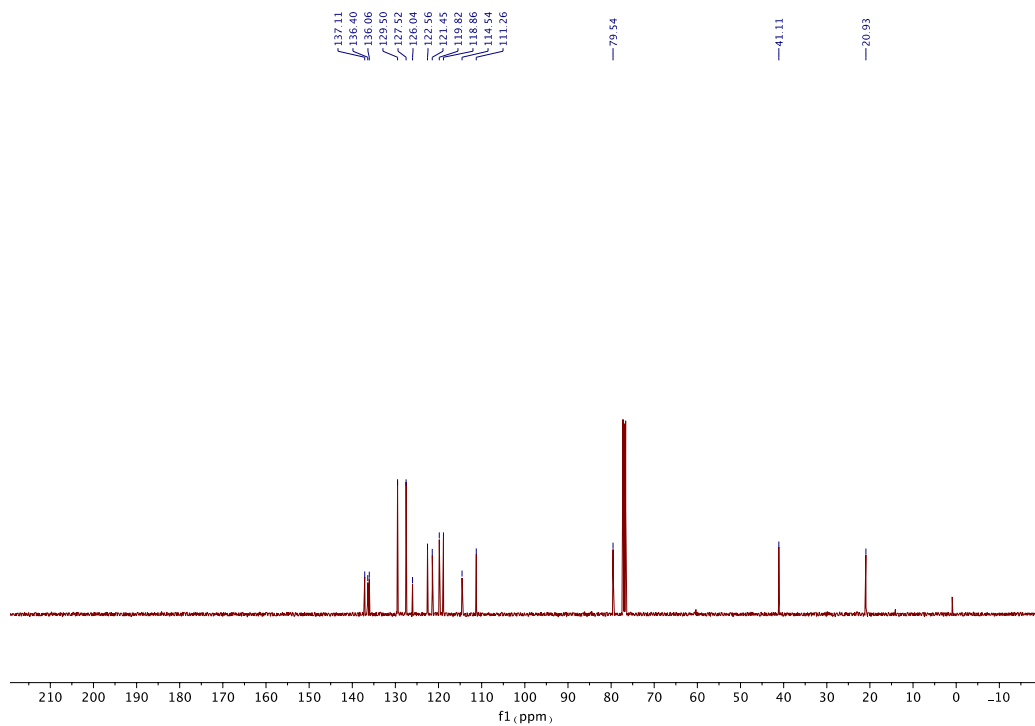


Figure A. 6. ^{13}C NMR spectrum of **34ac**

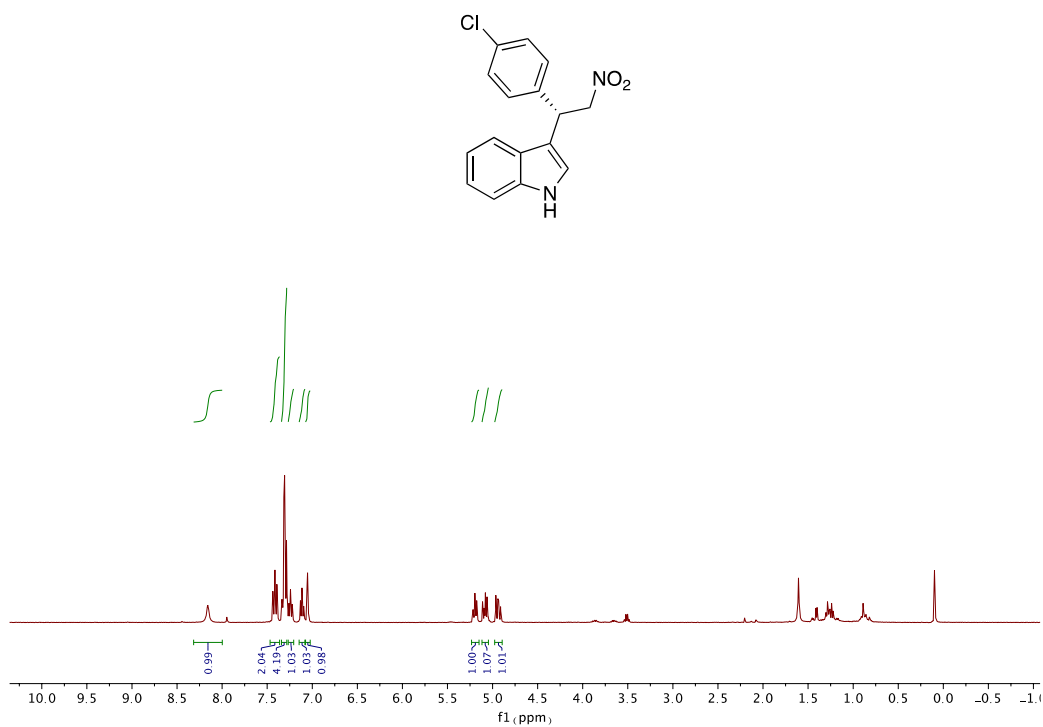


Figure A. 7. ¹H NMR spectrum of **34ad**

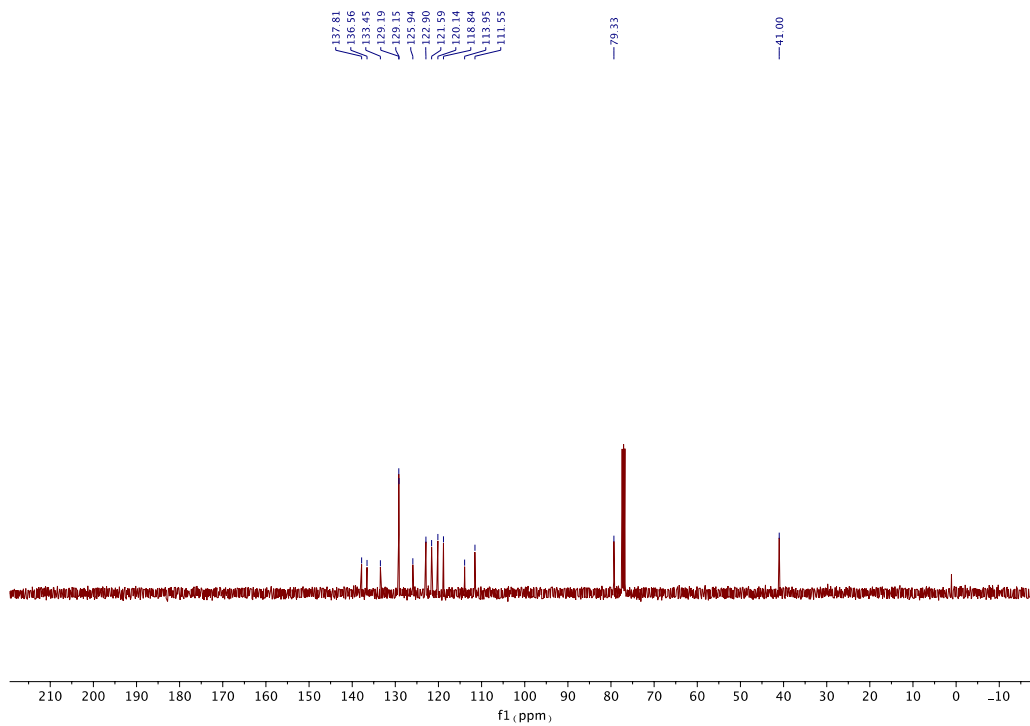


Figure A. 8. ¹³C NMR spectrum of **34ad**

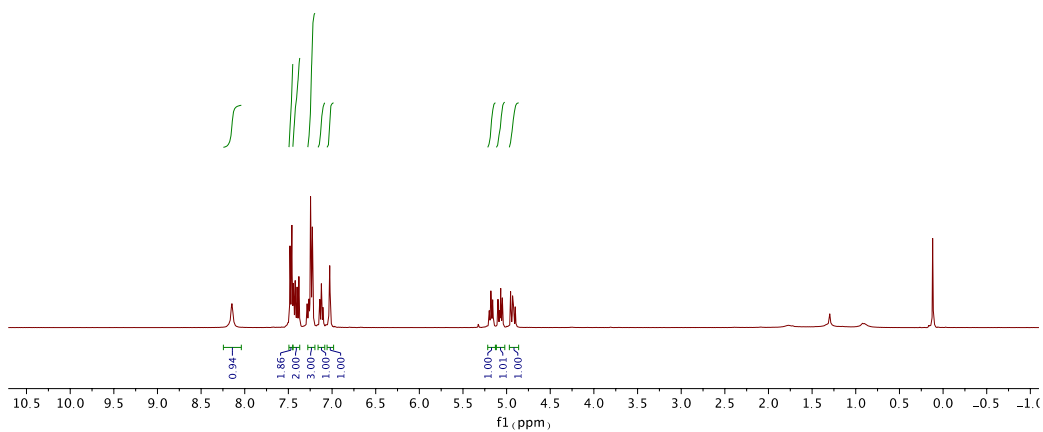
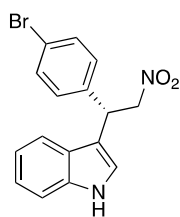


Figure A. 9. ^1H NMR spectrum of **34ae**

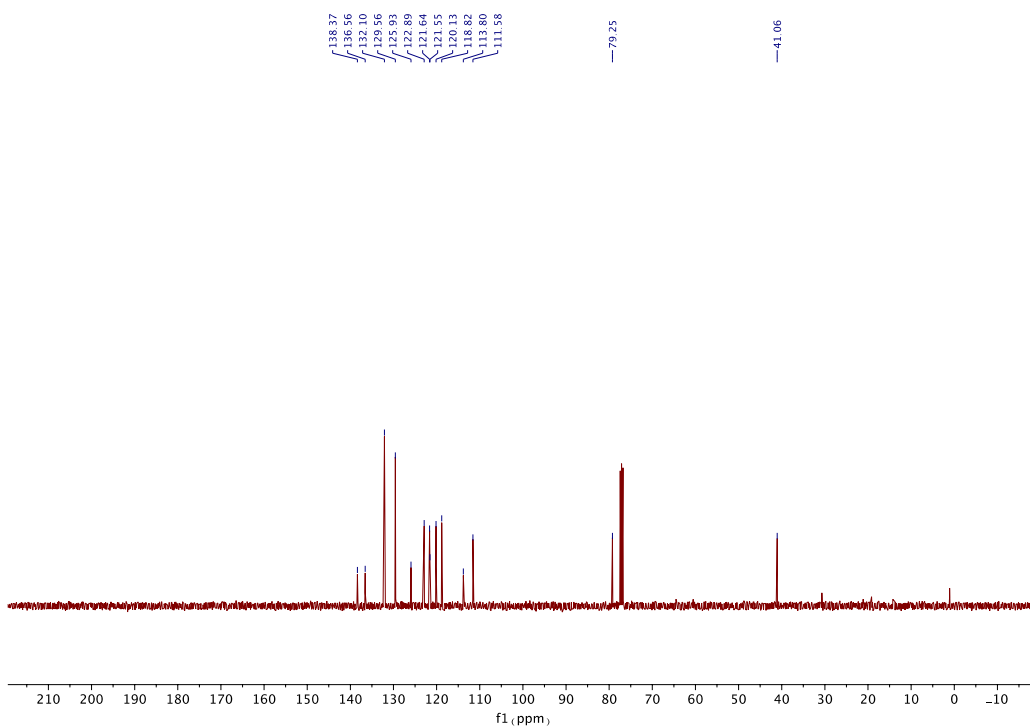


Figure A. 10. ^{13}C NMR spectrum of **34ae**

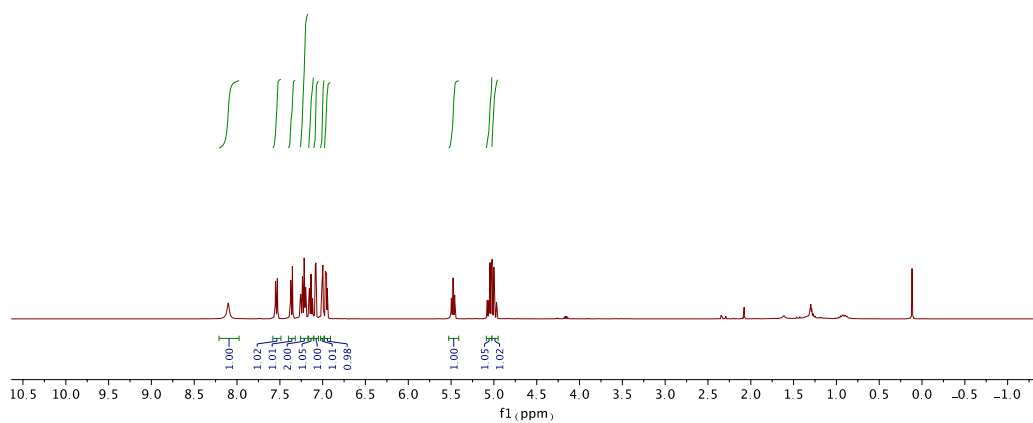
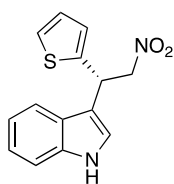


Figure A. 13. ¹H NMR spectrum of **34ag**

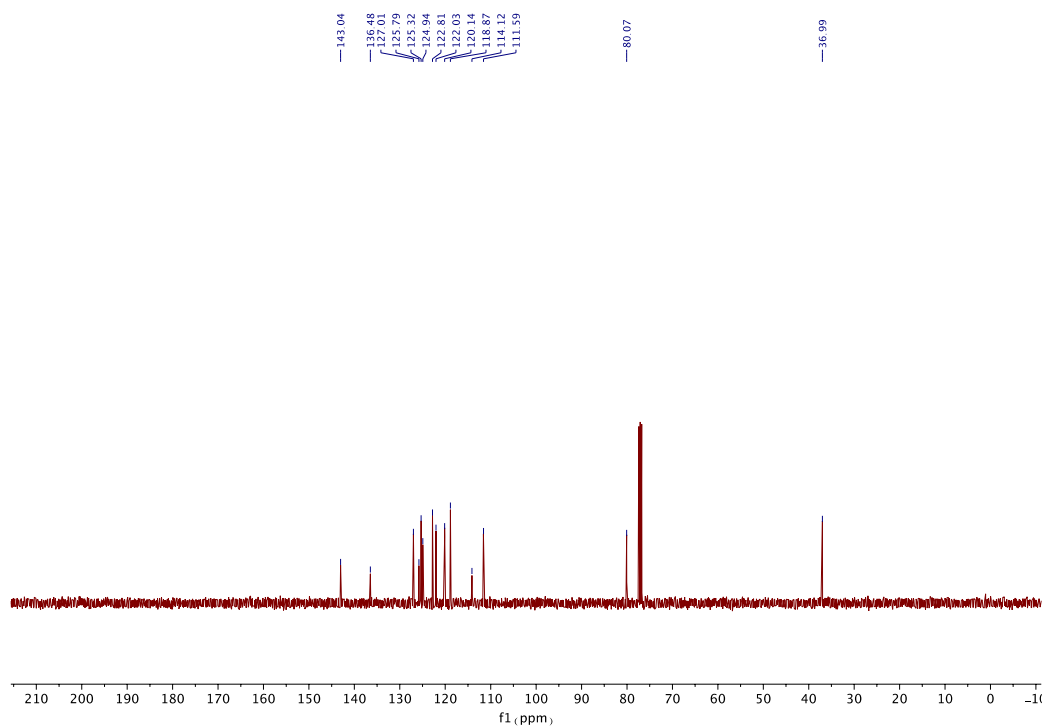


Figure A. 14. ¹³C NMR spectrum of **34ag**

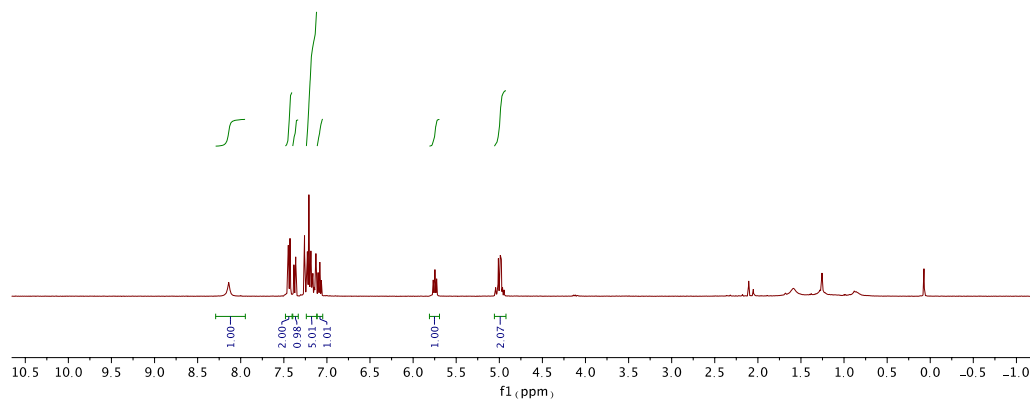
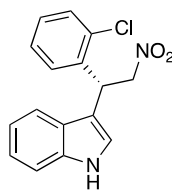


Figure A. 15. ^1H NMR spectrum of **34ah**

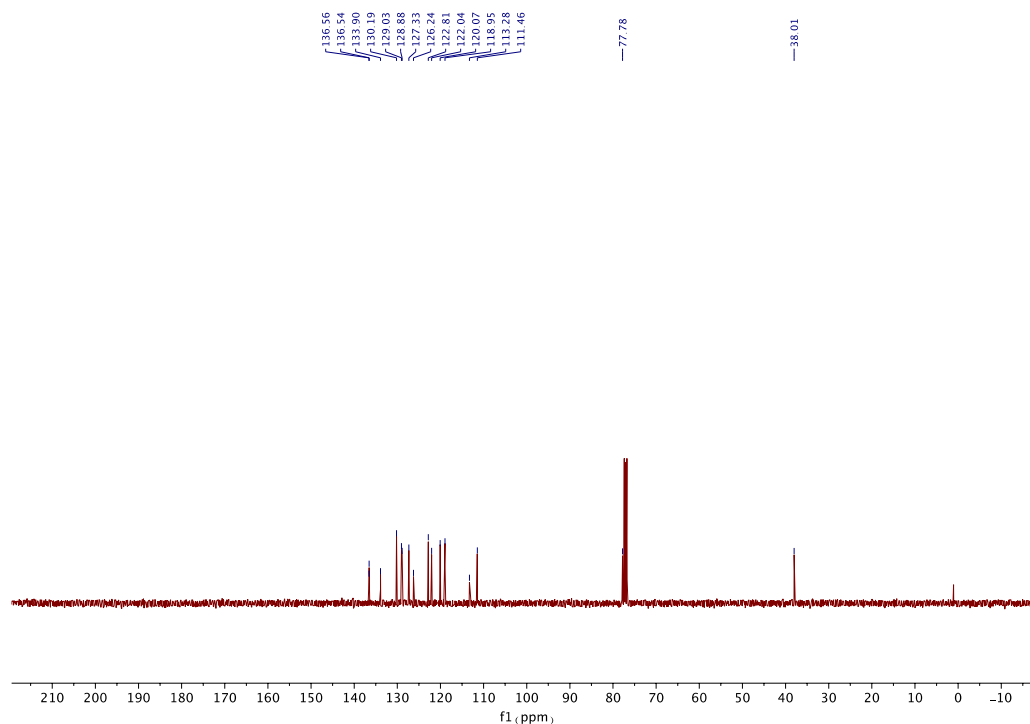


Figure A. 16. ^{13}C NMR spectrum of **34ah**

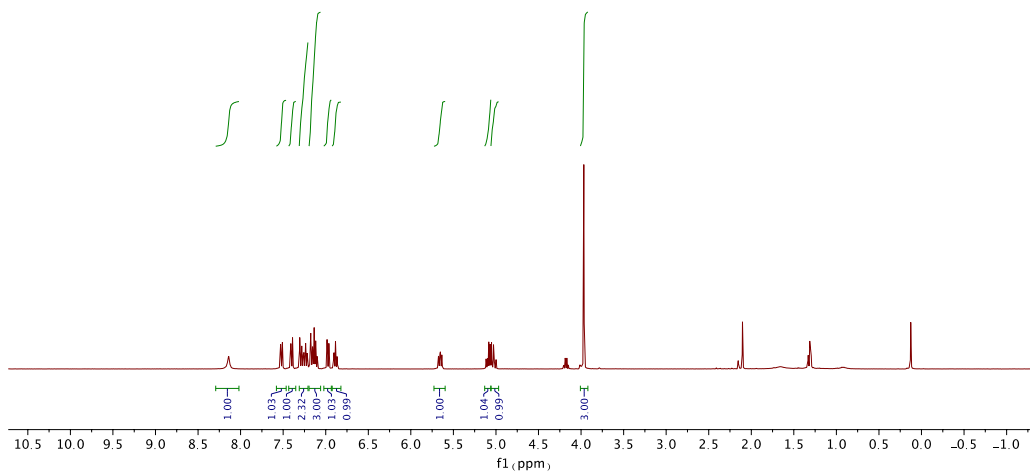
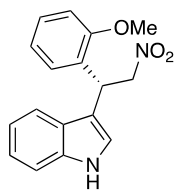


Figure A. 17. ^1H NMR spectrum of **34ai**

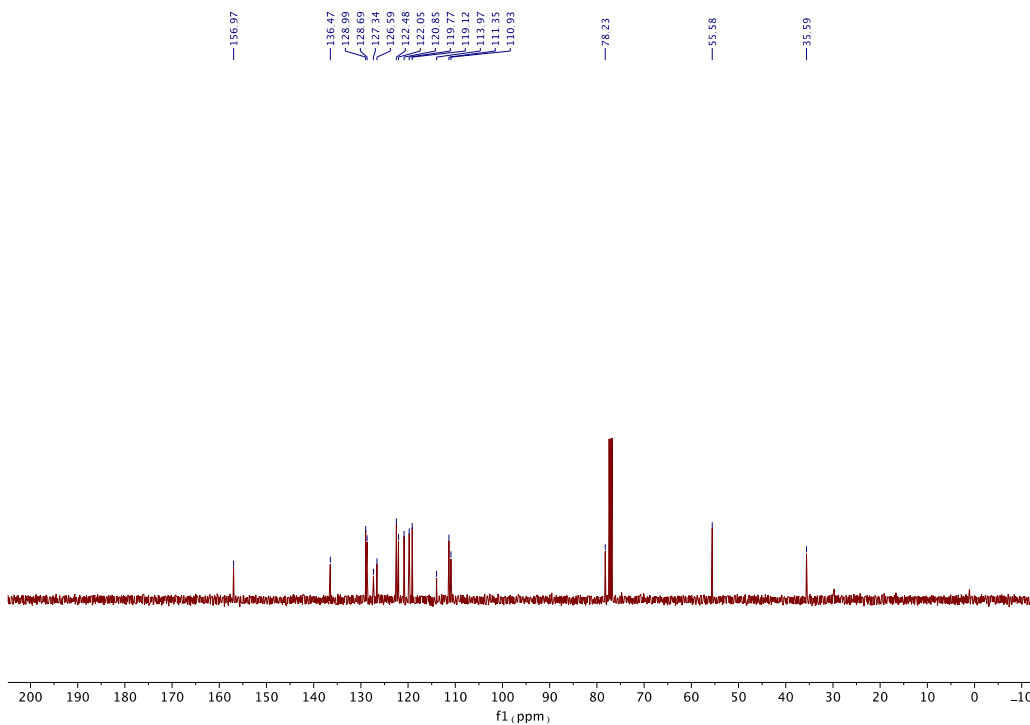


Figure A. 18. ^{13}C NMR spectrum of **34ai**

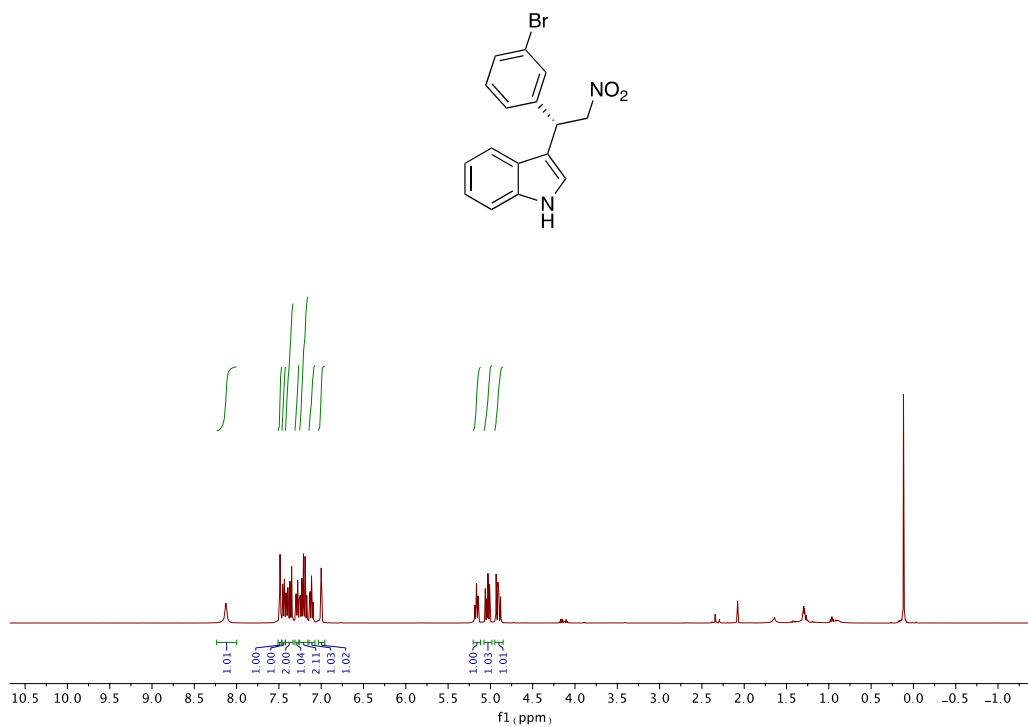


Figure A. 19. ¹H NMR spectrum of **34aj**

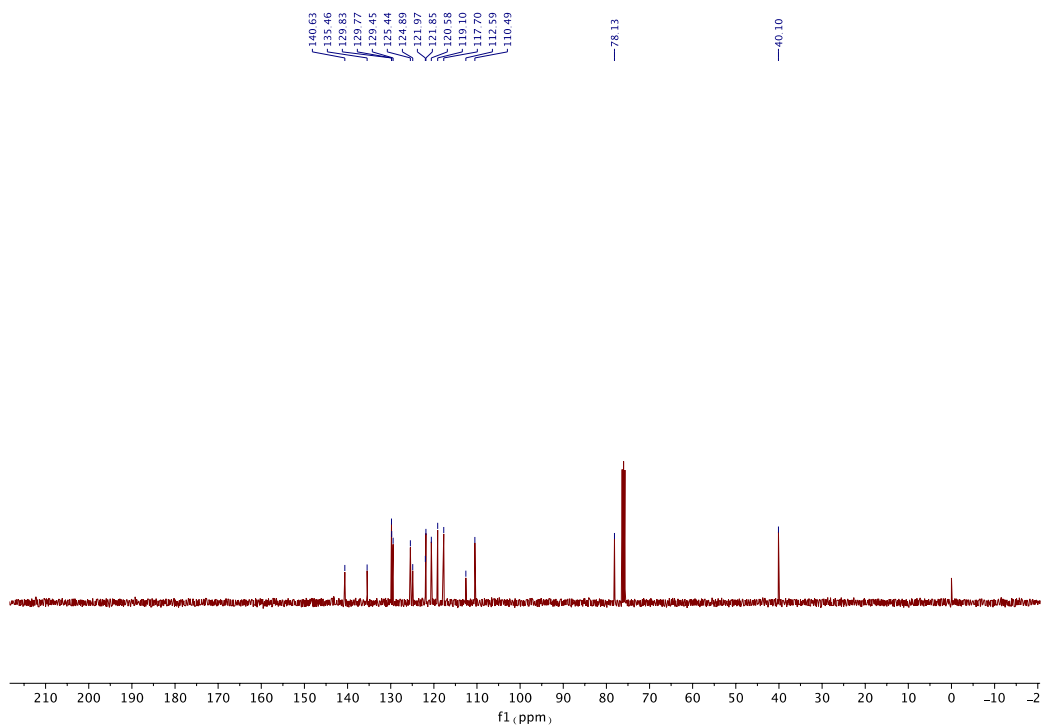


Figure A. 20. ¹³C NMR spectrum of **34aj**

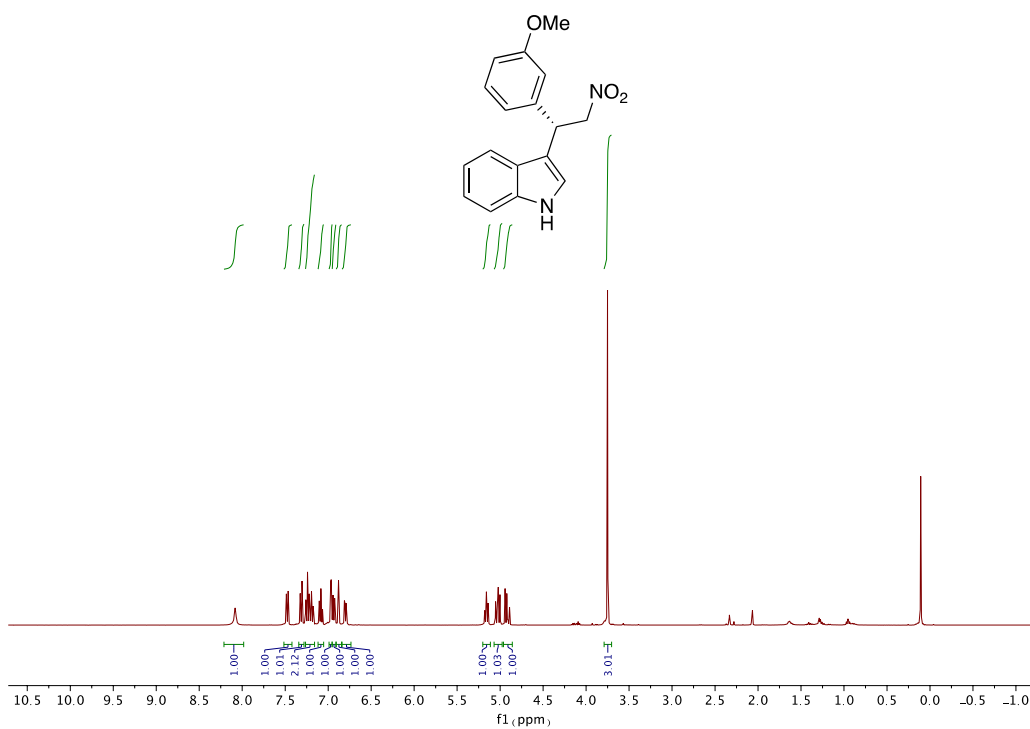


Figure A. 21. ¹H NMR spectrum of **34ak**

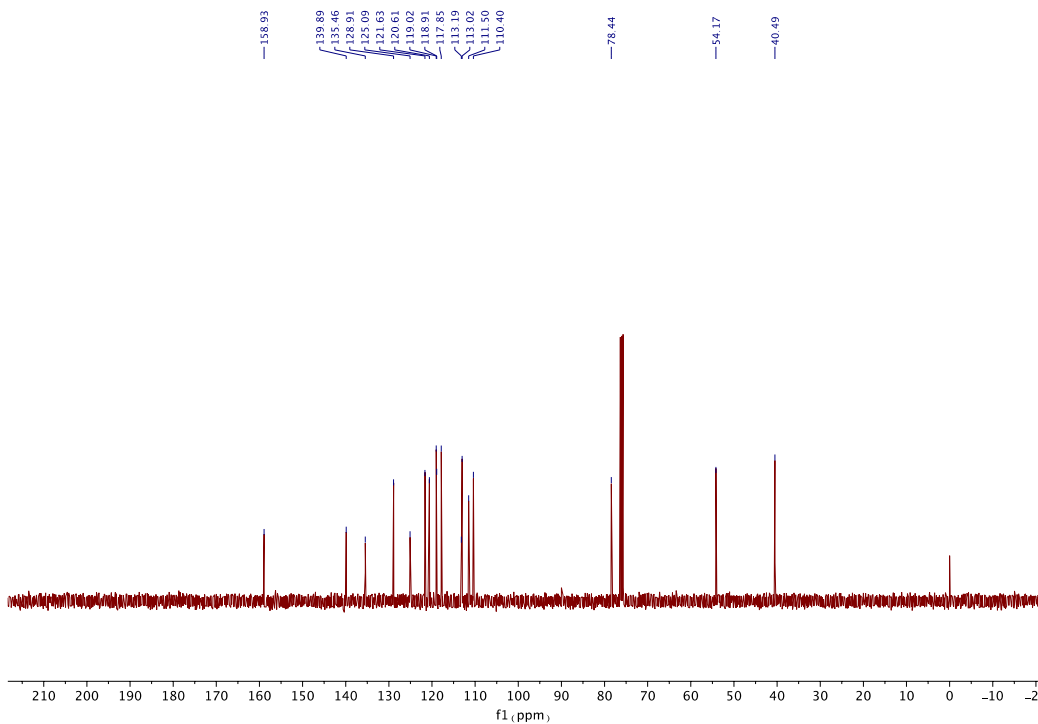


Figure A. 22. ¹³C NMR spectrum of **34ak**

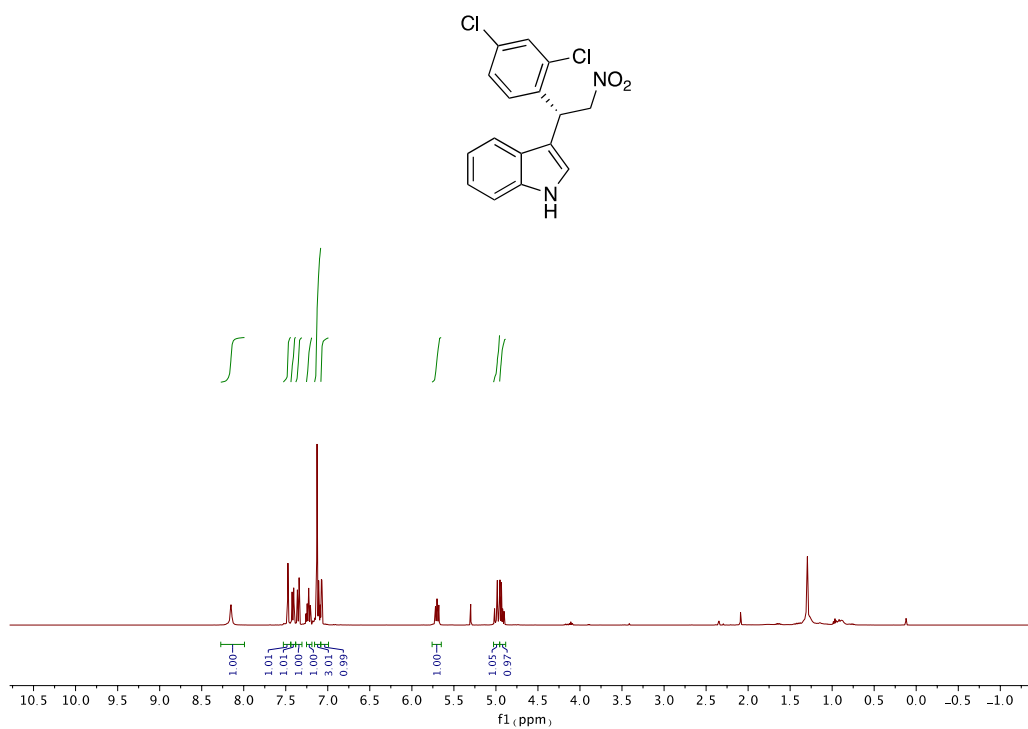


Figure A. 23. ¹H NMR spectrum of **34al**

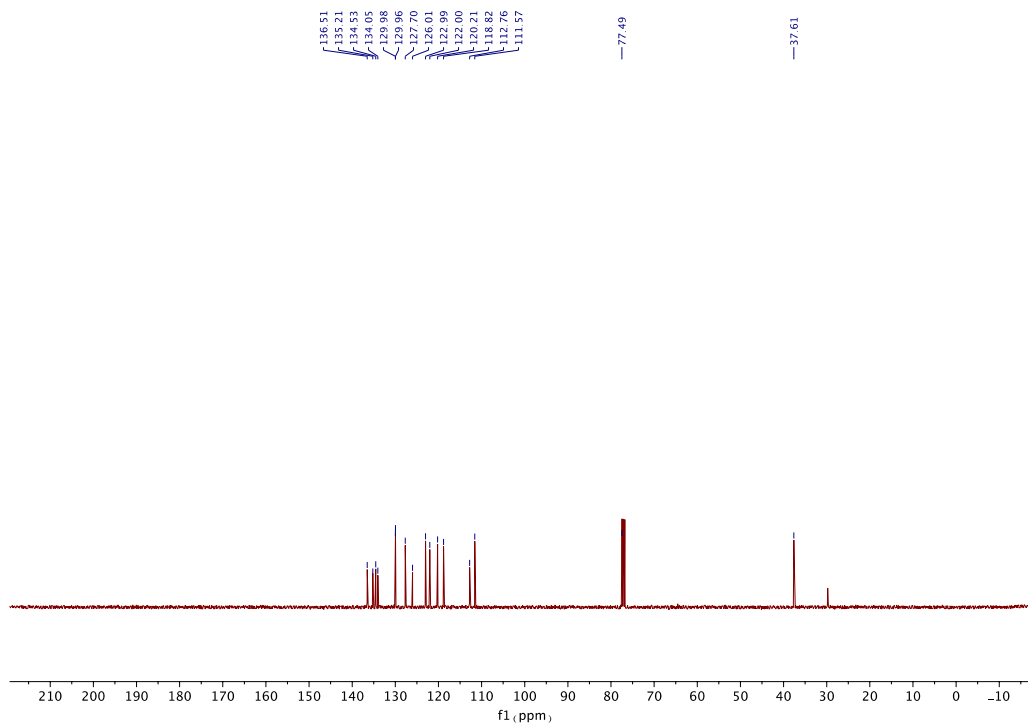


Figure A. 24. ¹³C NMR spectrum of **34al**

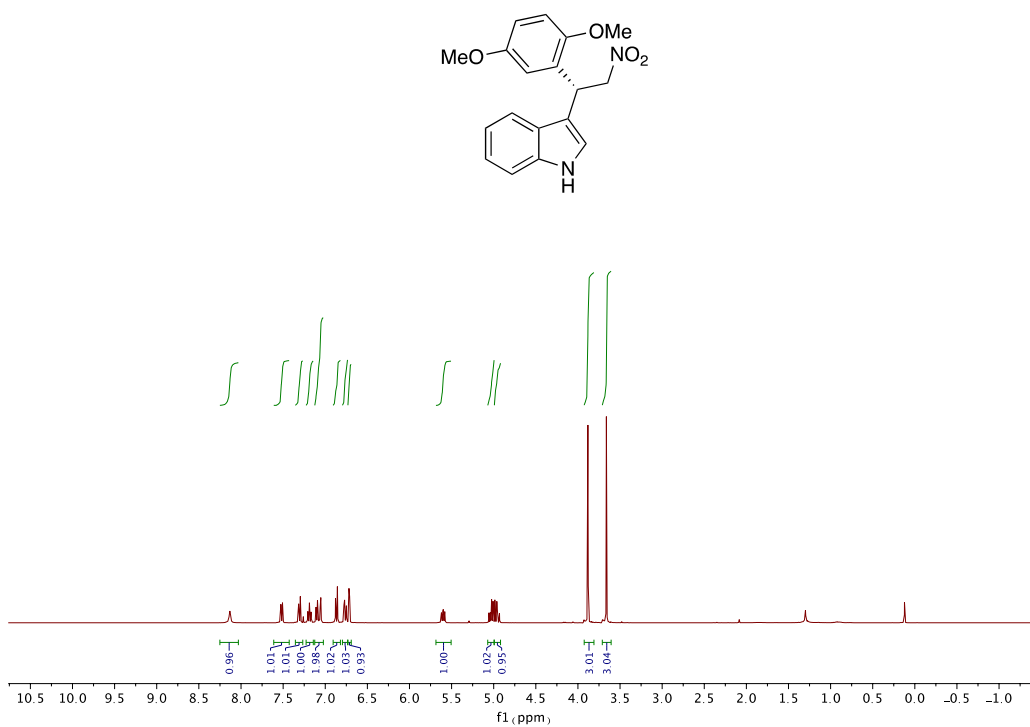


Figure A. 25. $^1\text{H NMR}$ spectrum of **34am**

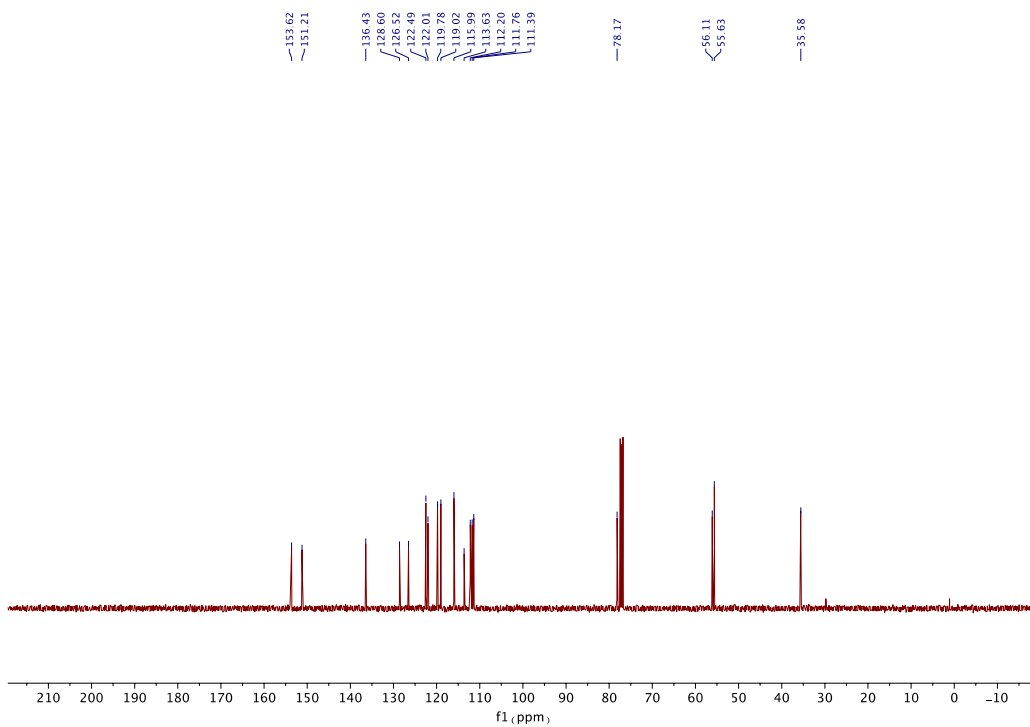


Figure A. 26. $^{13}\text{C NMR}$ spectrum of **34am**

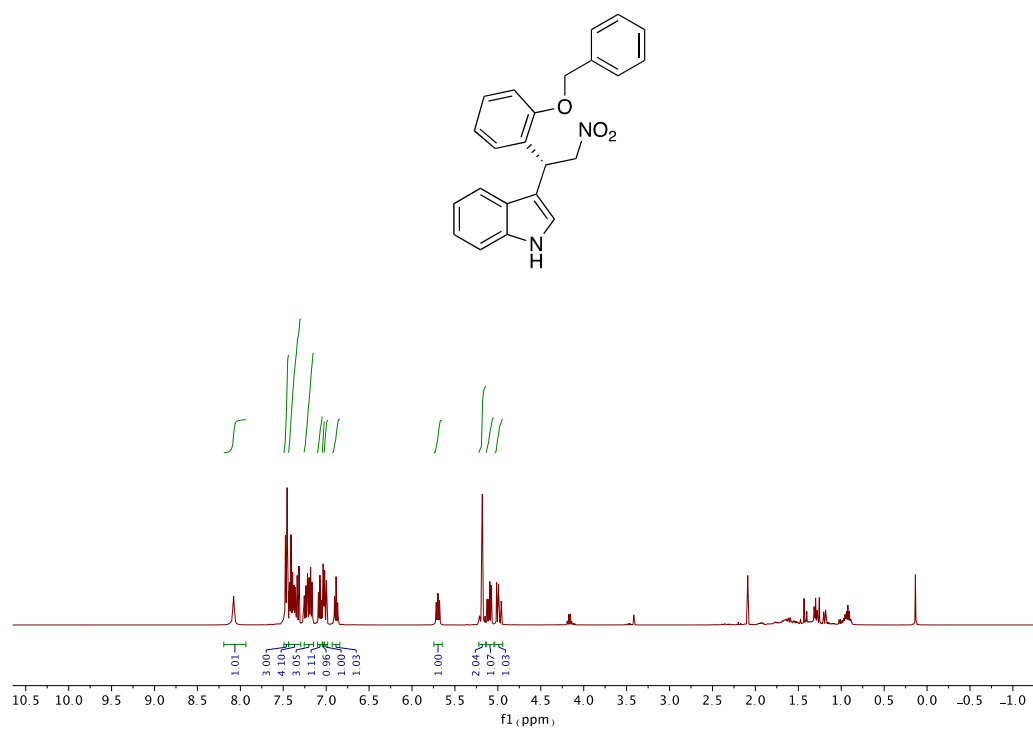


Figure A. 27. ¹H NMR spectrum of **34an**

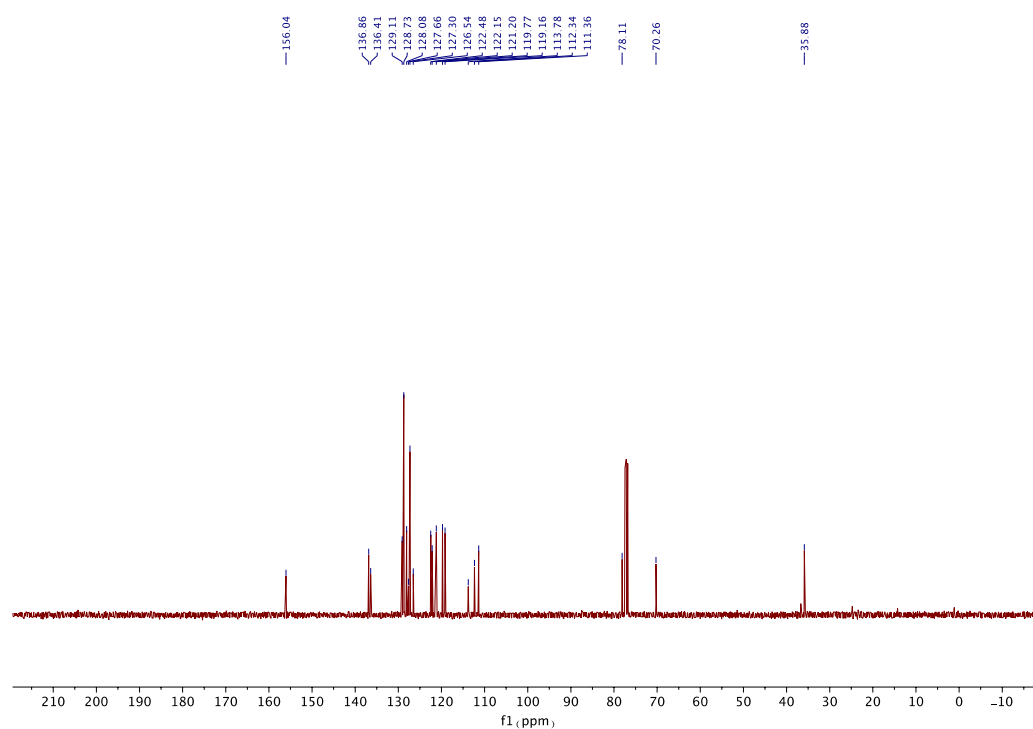


Figure A. 28. ¹³C NMR spectrum of **34an**

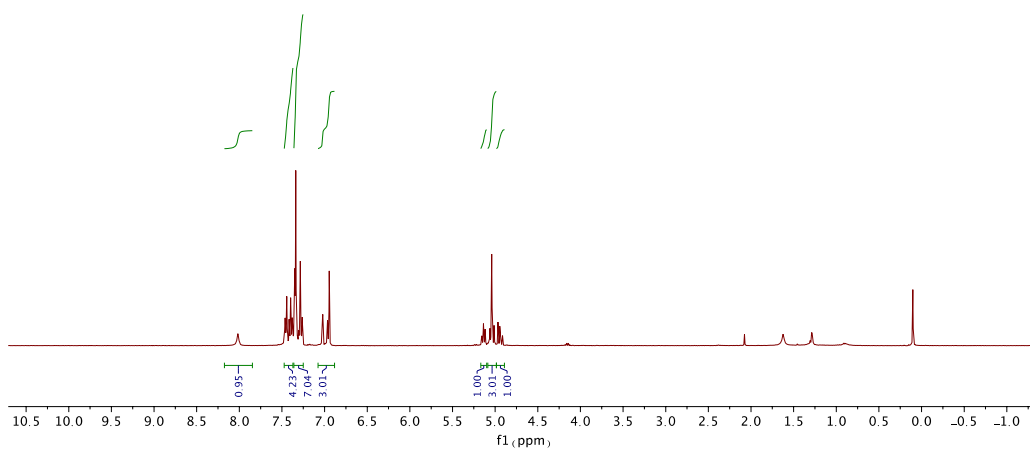
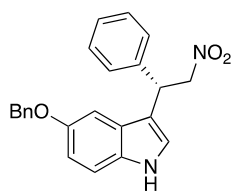


Figure A. 29. ^1H NMR spectrum of **34ba**

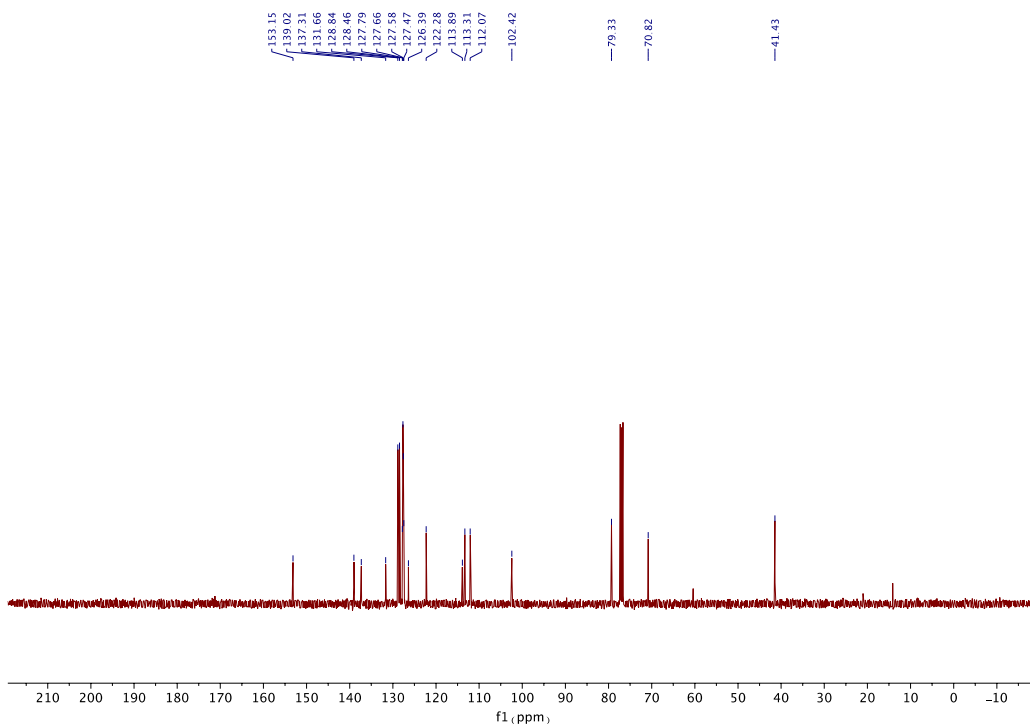


Figure A. 30. ^{13}C NMR spectrum of **34ba**

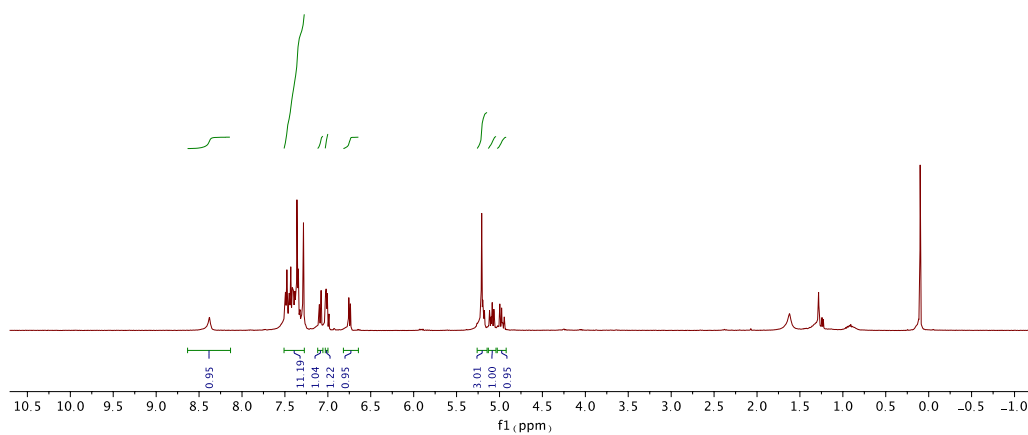
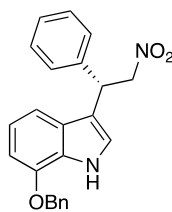


Figure A. 31. ^1H NMR spectrum of **34ca**

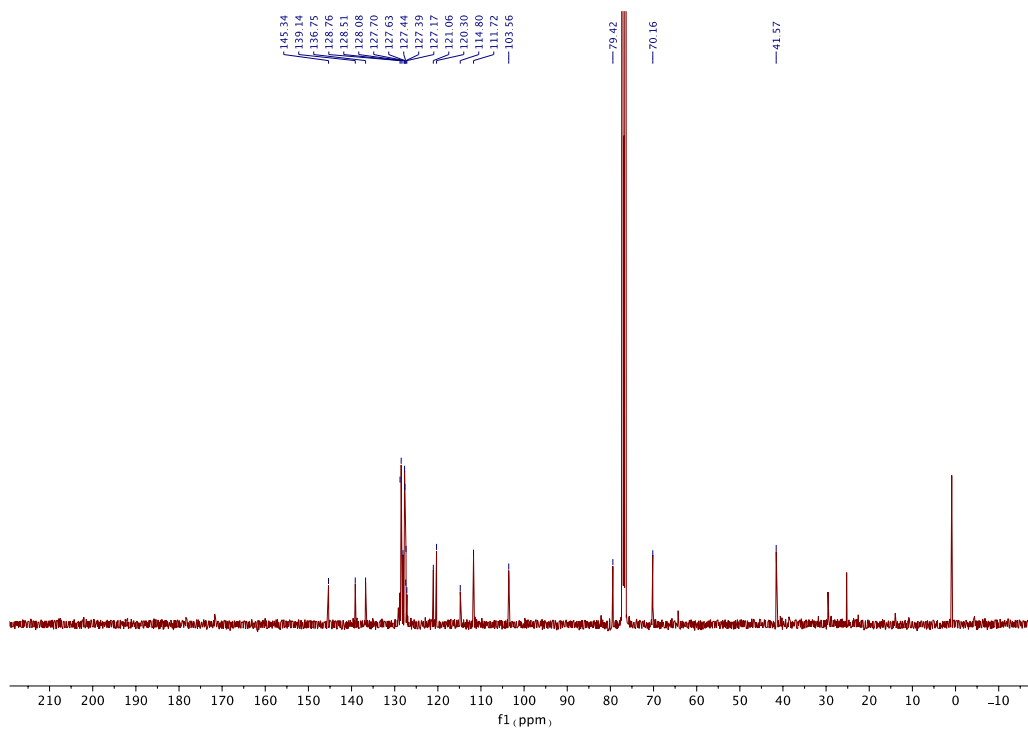


Figure A. 32. ^{13}C NMR spectrum of **34ca**

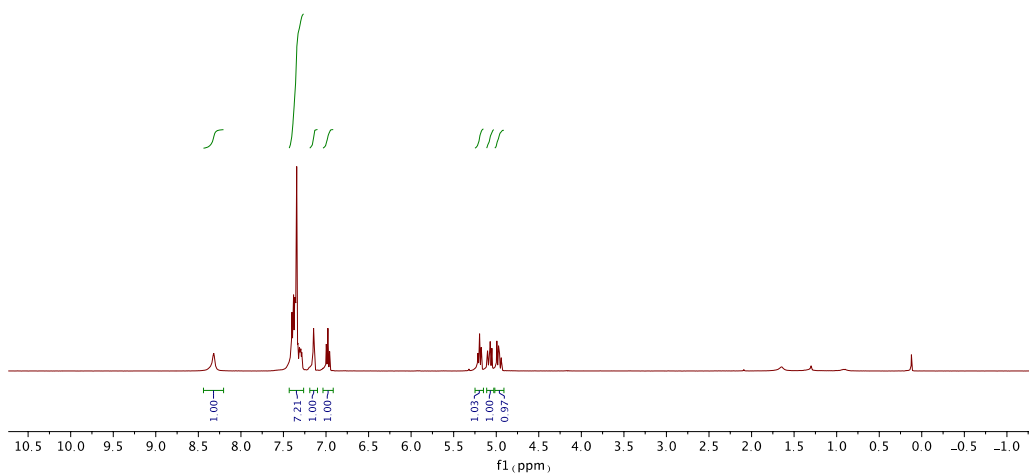
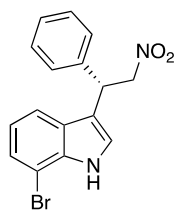


Figure A. 33. ^1H NMR spectrum of **34da**

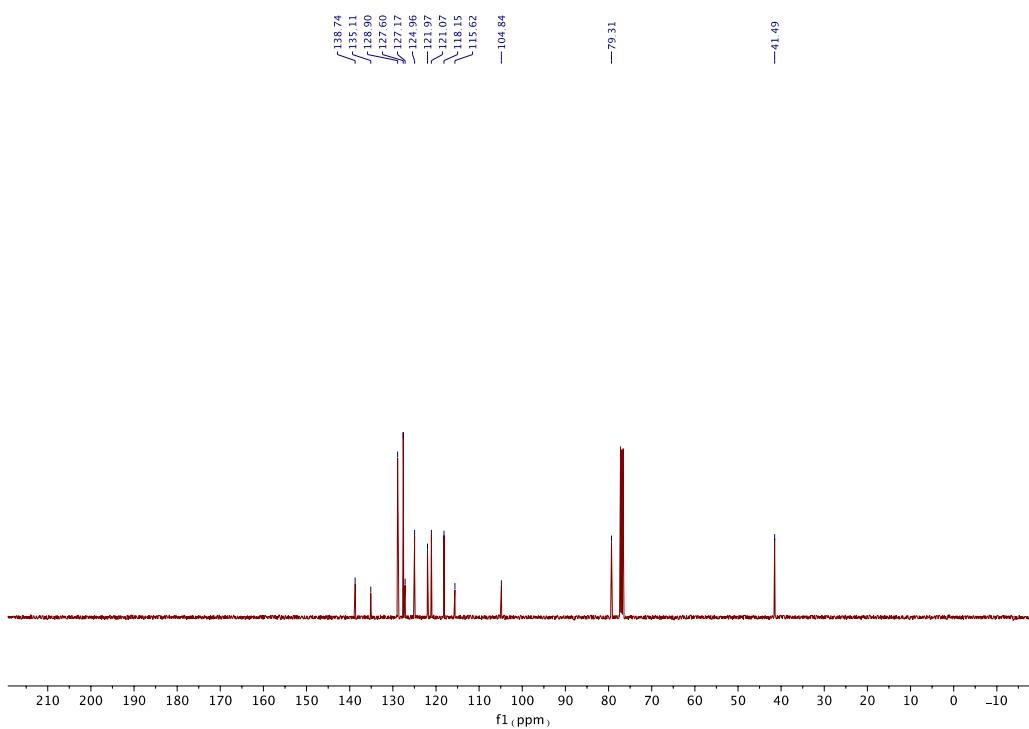


Figure A. 34. ^{13}C NMR spectrum of **34da**

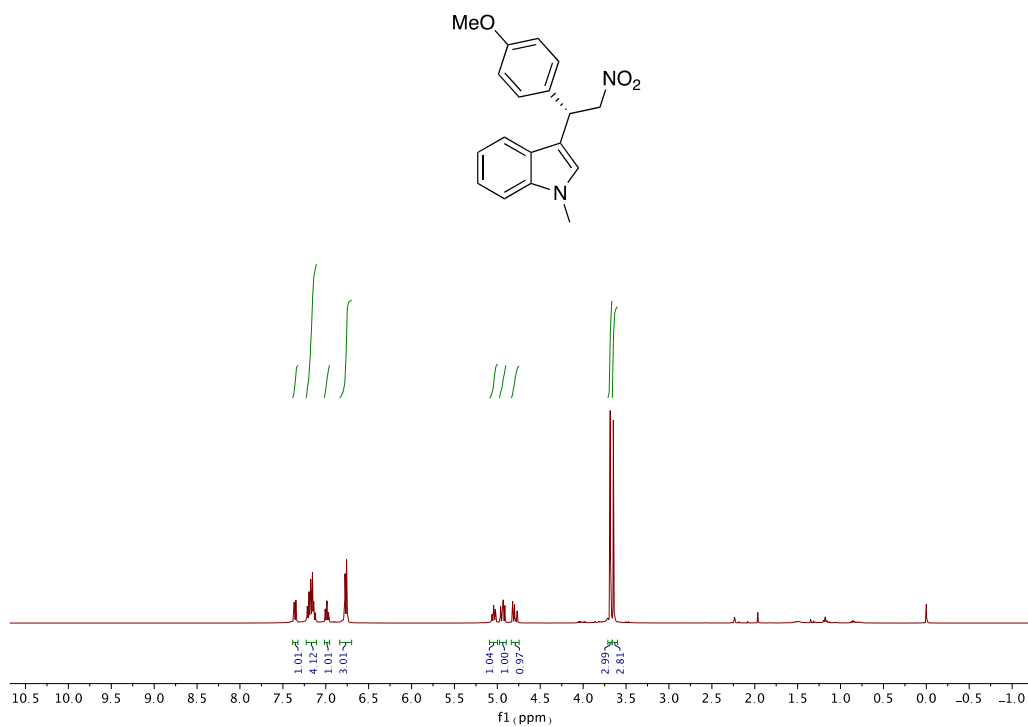


Figure A. 35. ¹H NMR spectrum of **34eb**

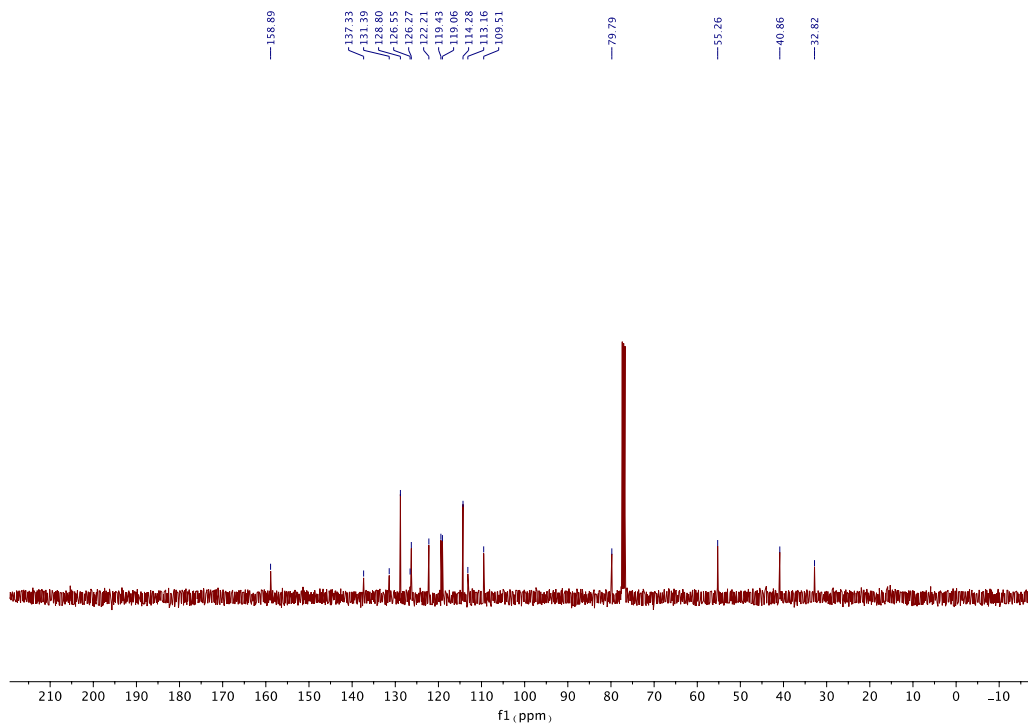


Figure A. 36. ¹³C NMR spectrum of **34eb**

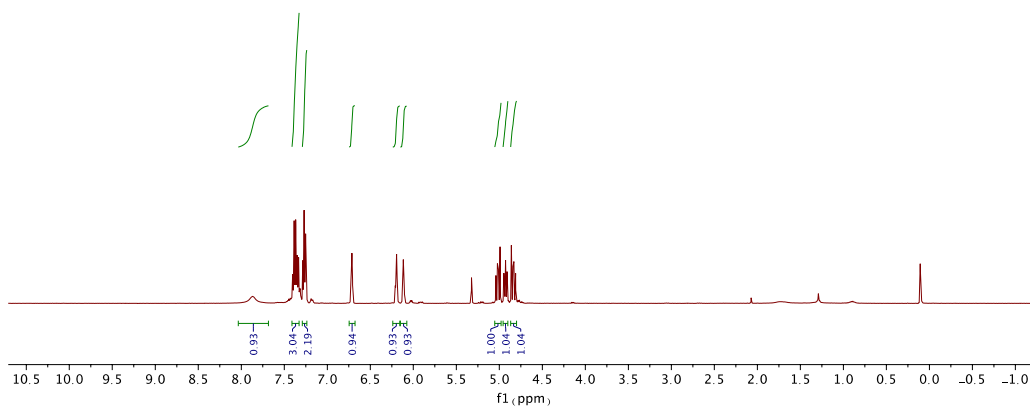
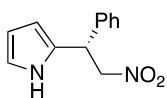


Figure A. 37. ^1H NMR spectrum of **86**

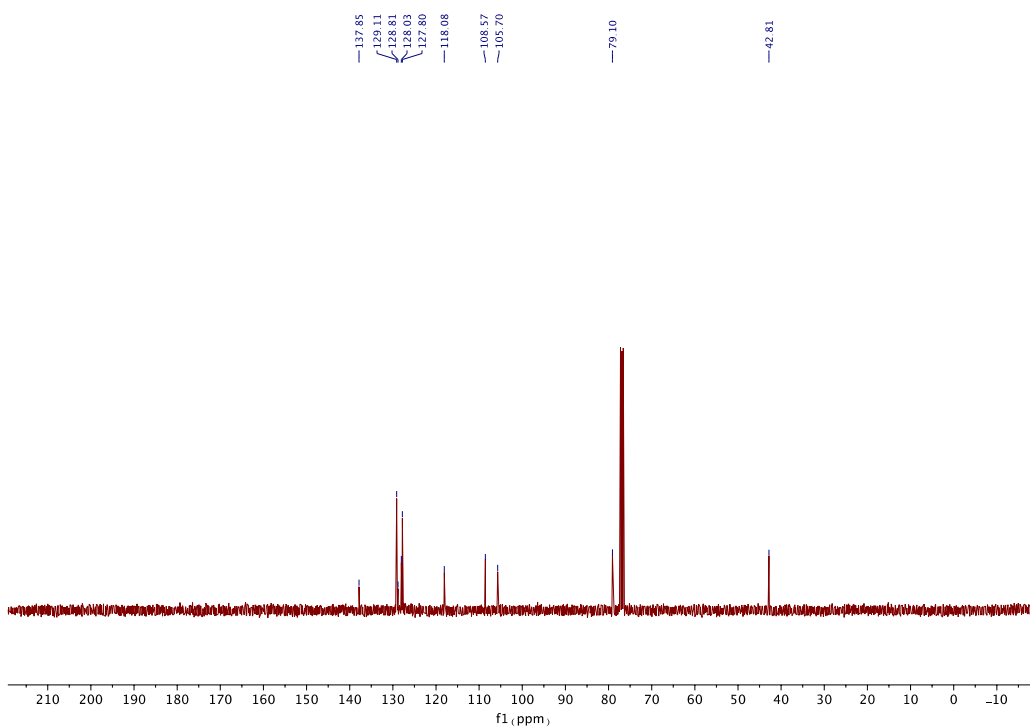


Figure A. 38. ^{13}C NMR spectrum of **86**

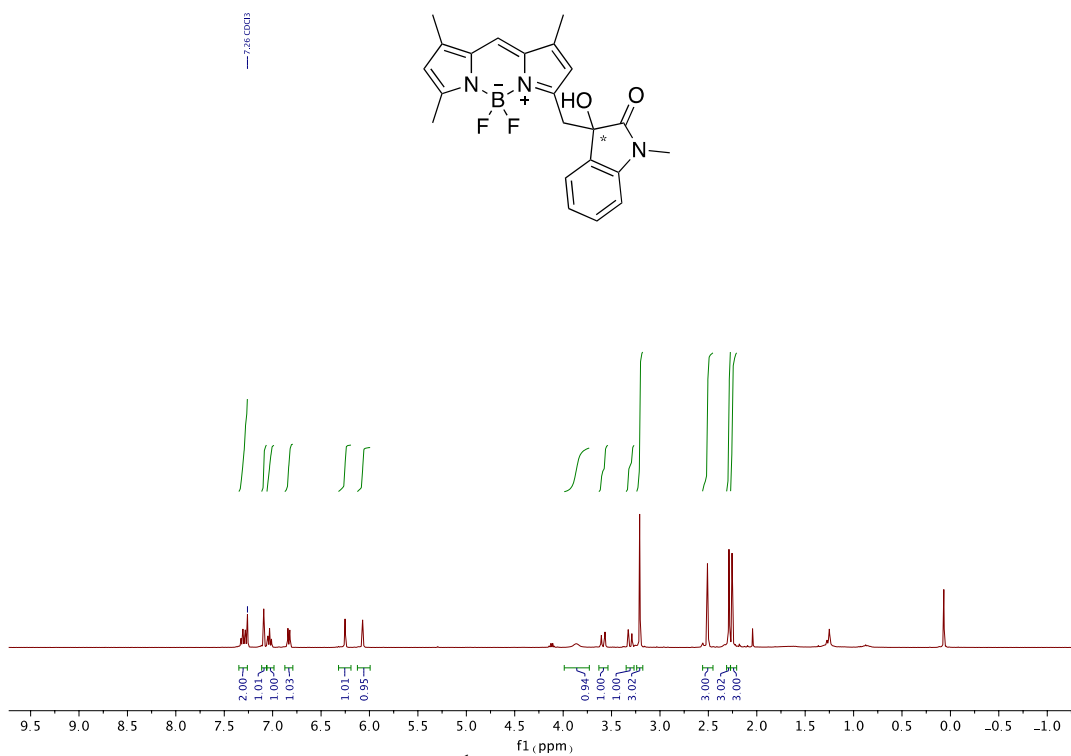


Figure A. 39. ^1H NMR spectrum of **73aa**

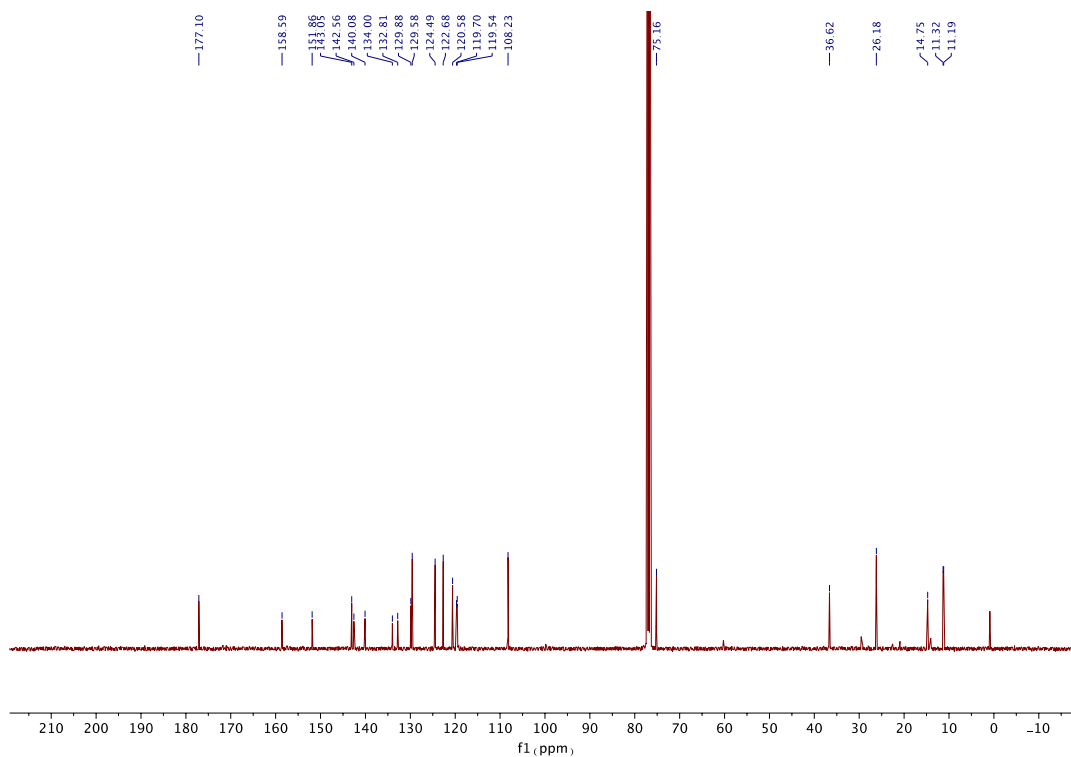


Figure A. 40. ^{13}C NMR spectrum of **73aa**

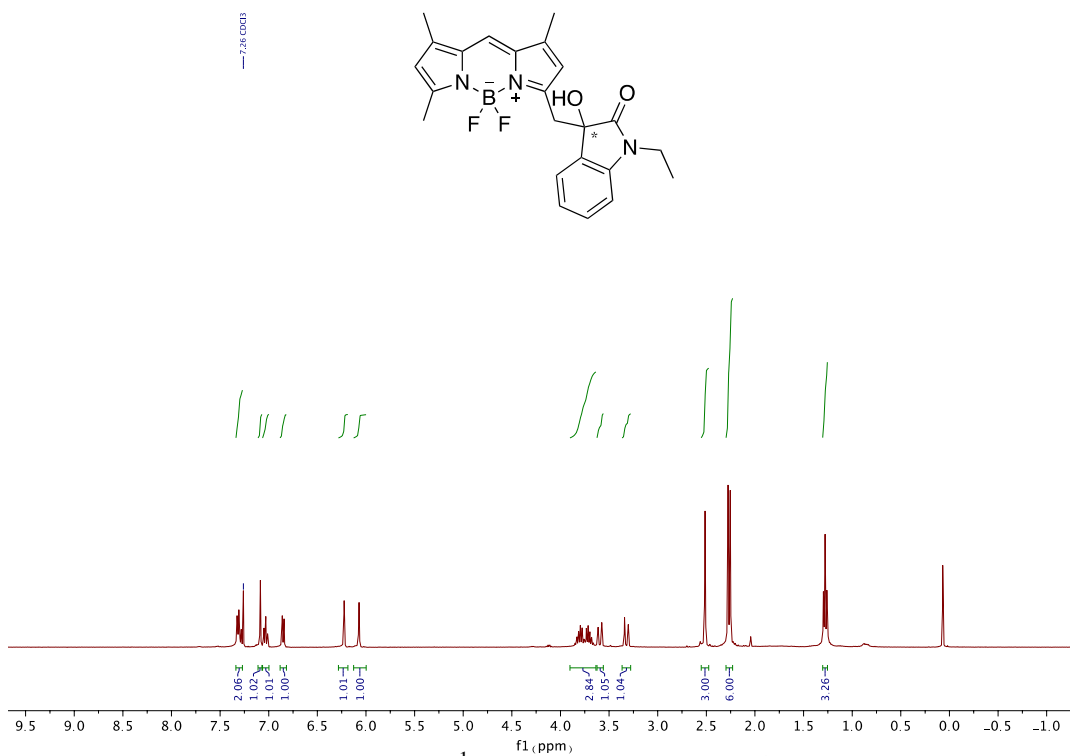


Figure A. 41. ¹H NMR spectrum of **73ab**

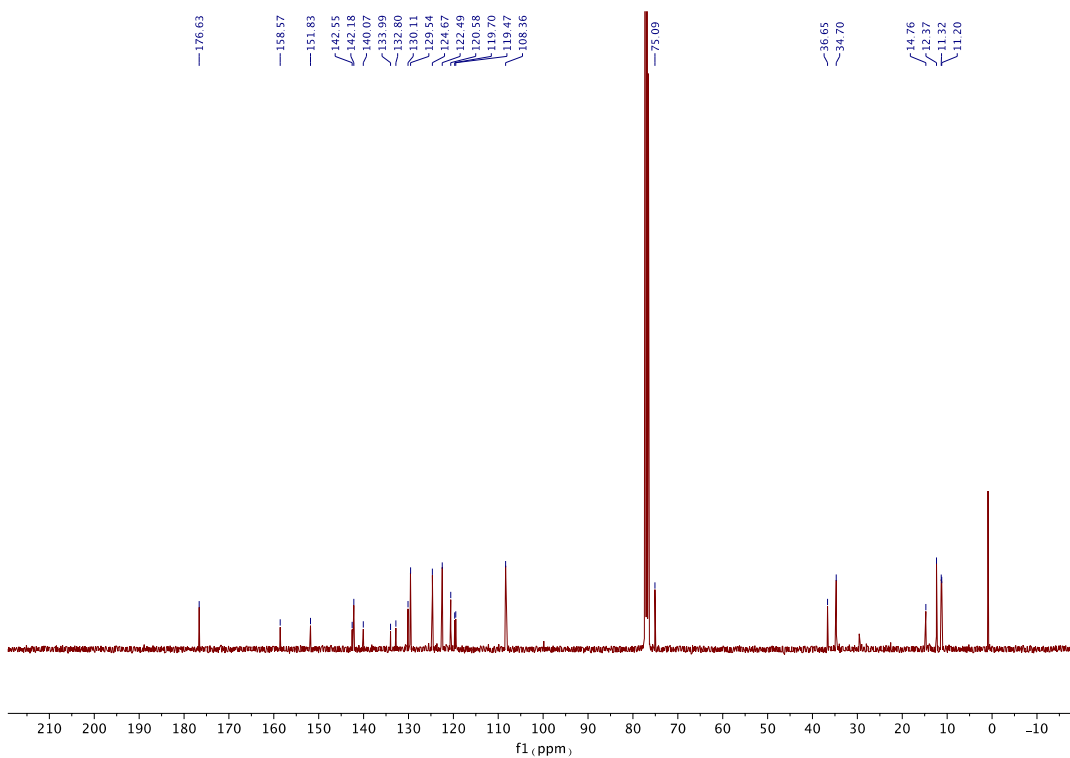


Figure A. 42. ¹³C NMR spectrum of **73ab**

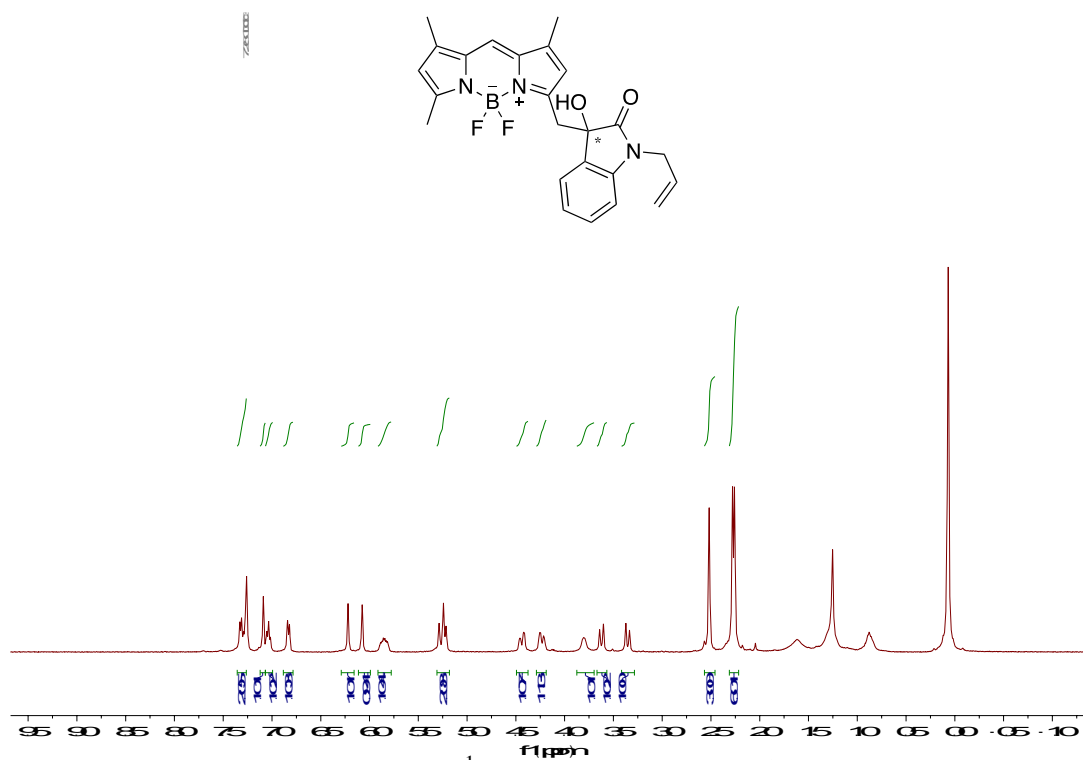


Figure A. 43. ^1H NMR spectrum of **73ac**

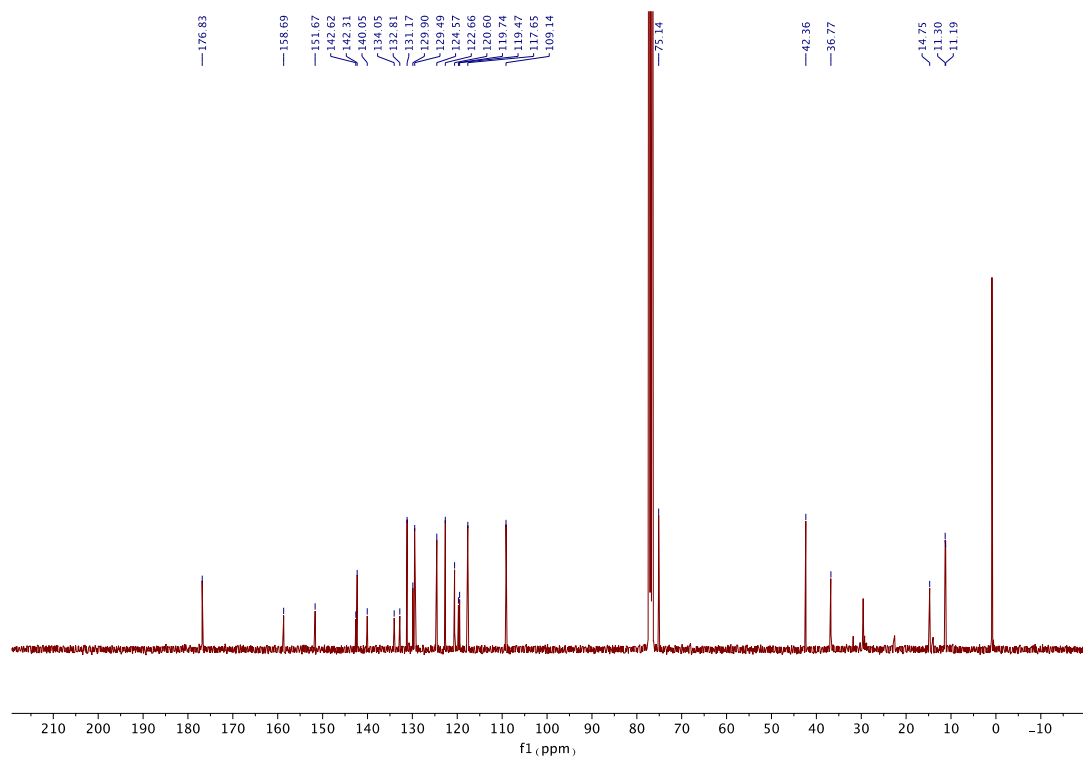


Figure A. 44. ^{13}C NMR spectrum of **73ac**

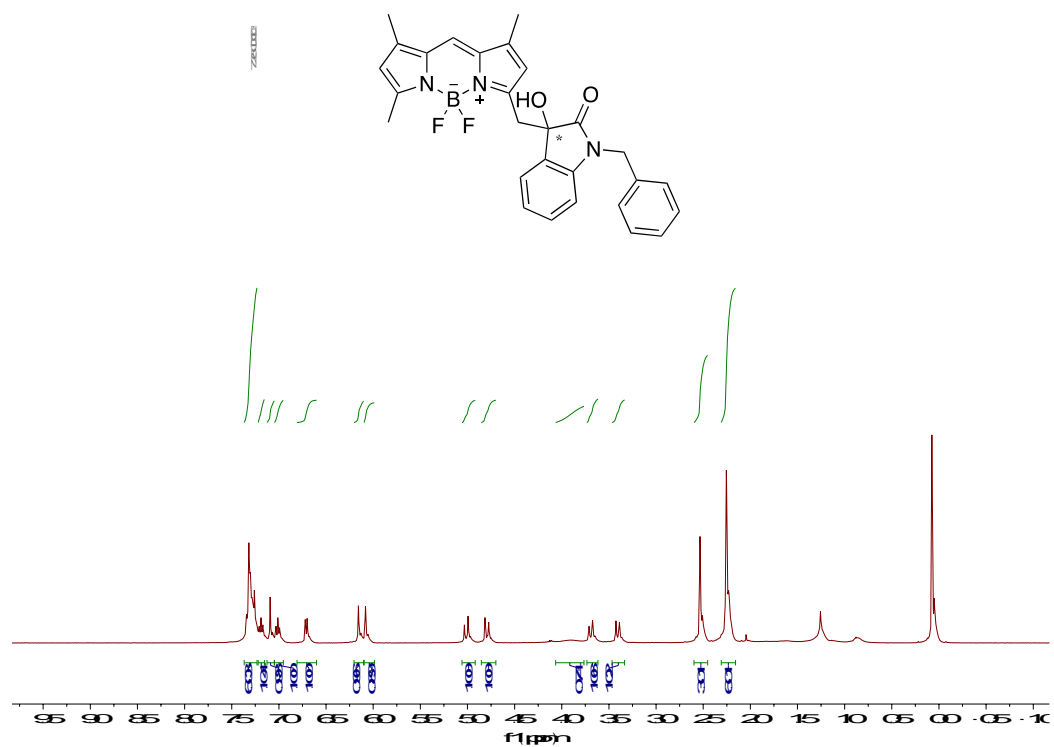


Figure A. 45. ^1H NMR spectrum of **73ad**

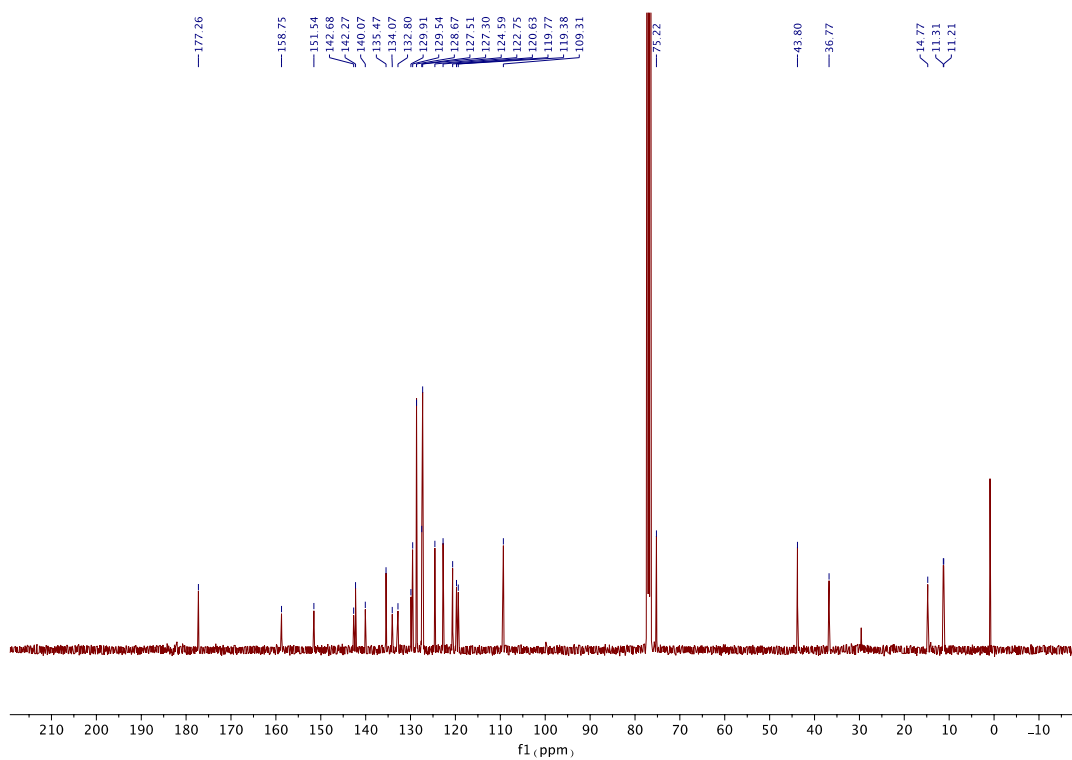
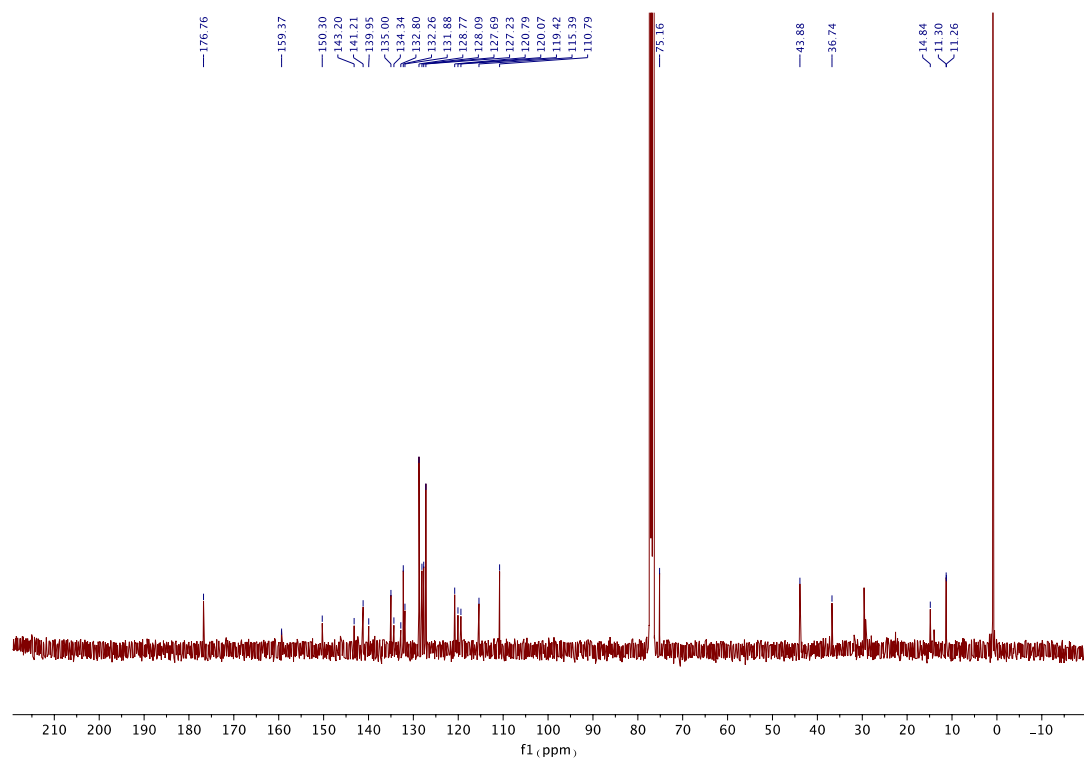
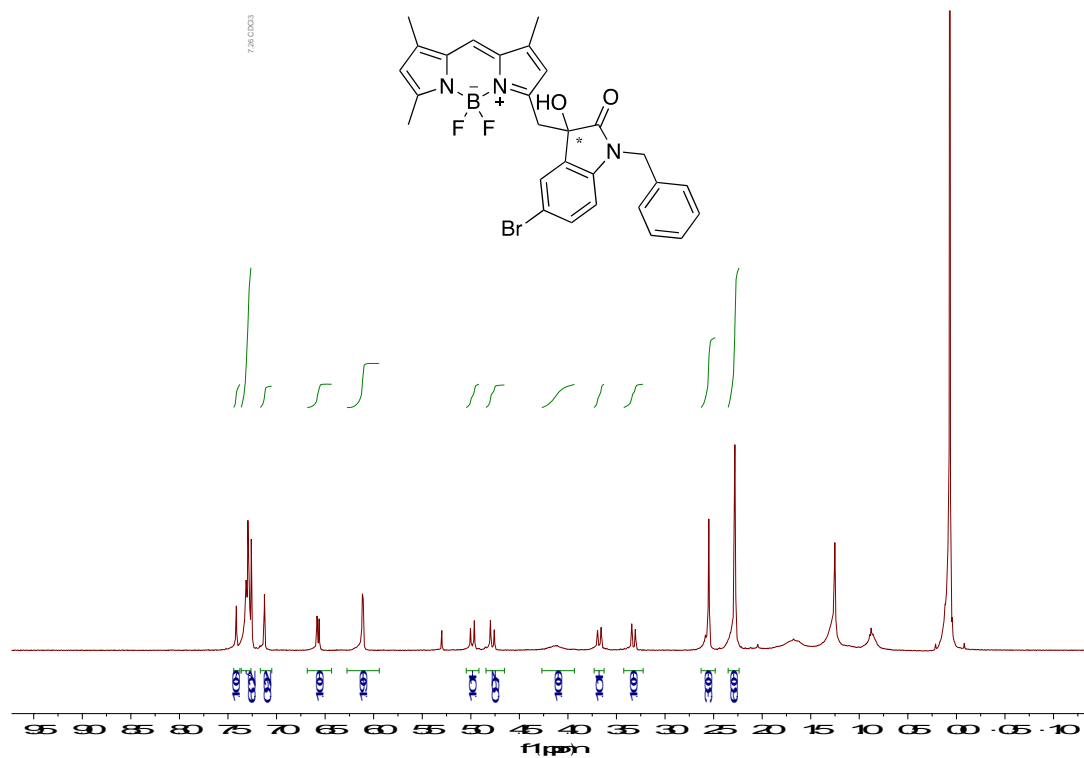
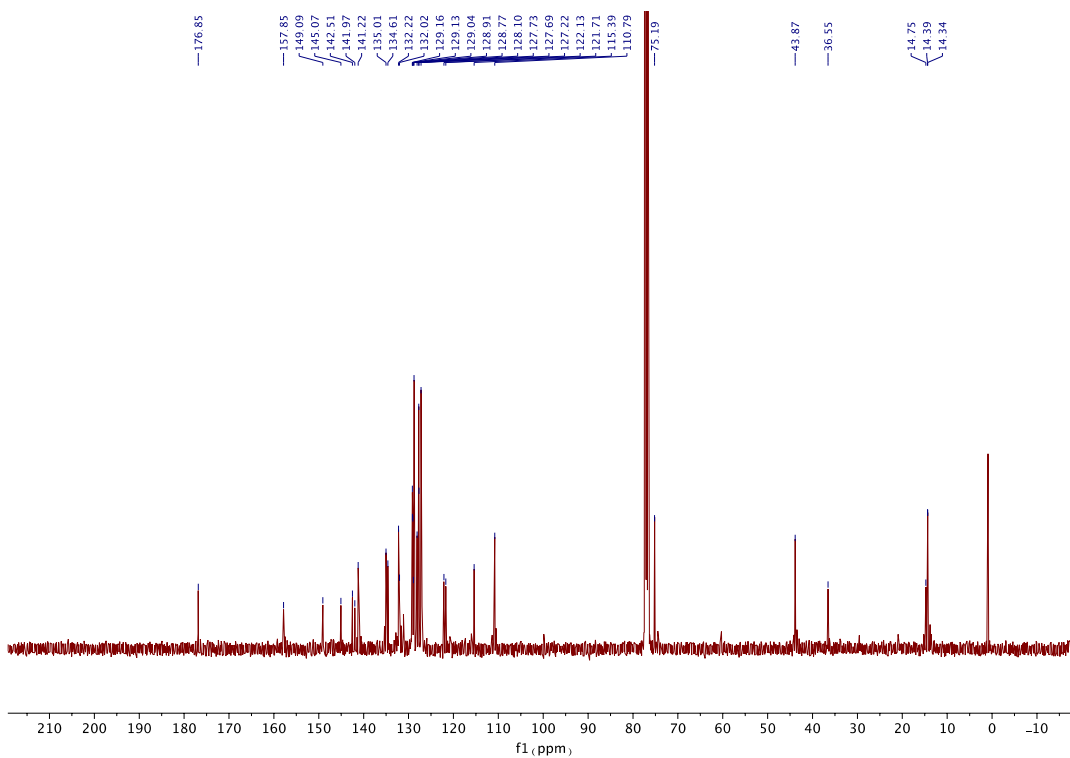
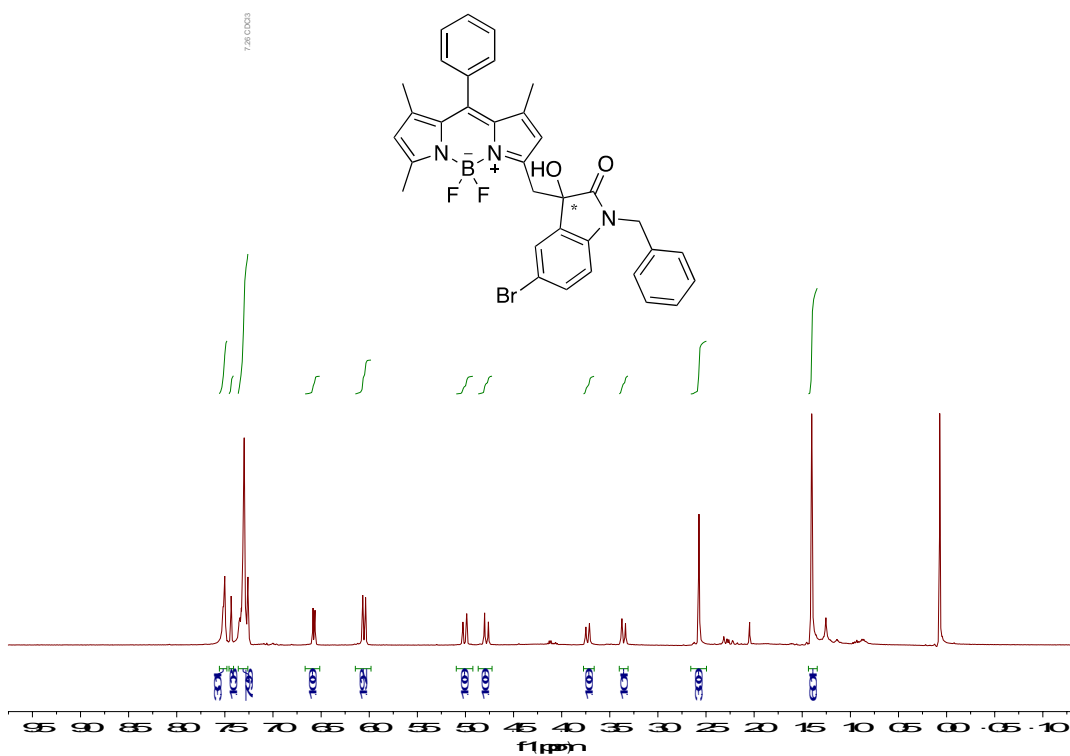


Figure A. 46. ^{13}C NMR spectrum of **73ad**





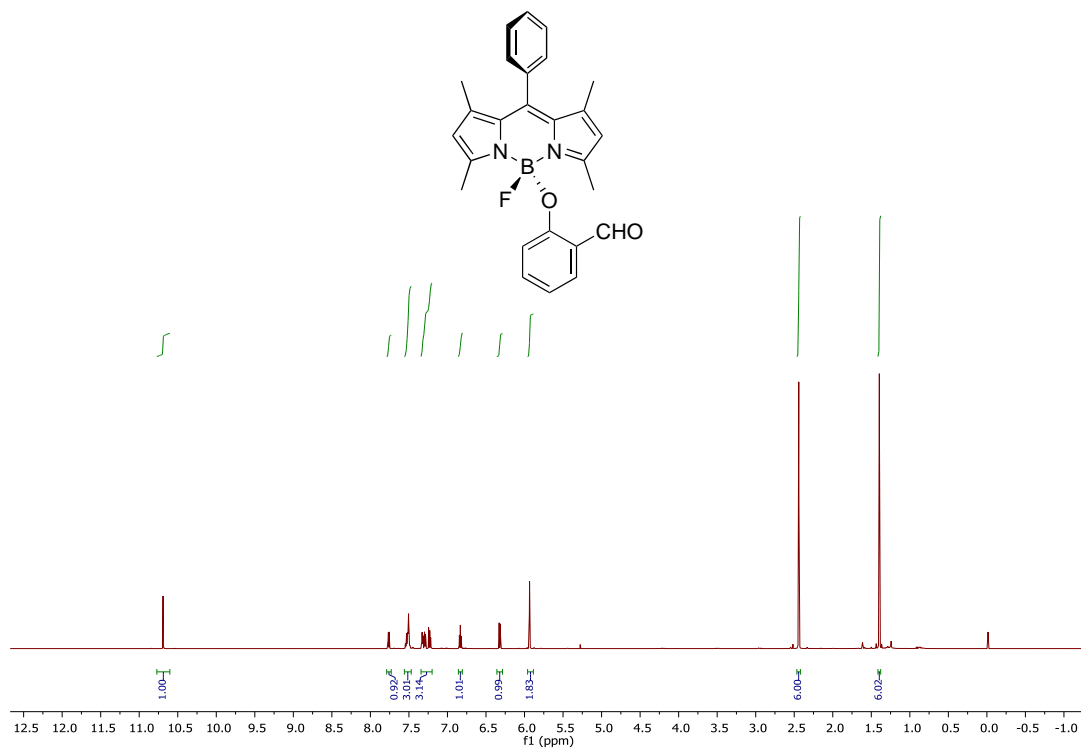


Figure A. 51. ¹H NMR spectrum of **95**

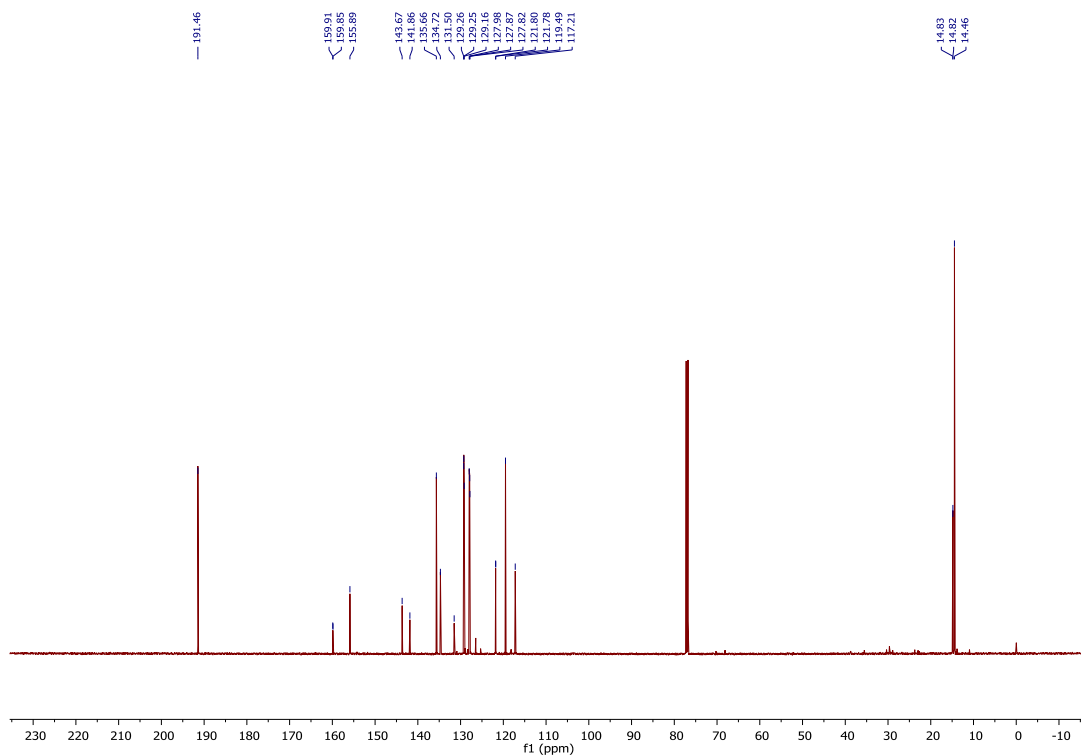


Figure A. 52. ¹³C NMR spectrum of **95**

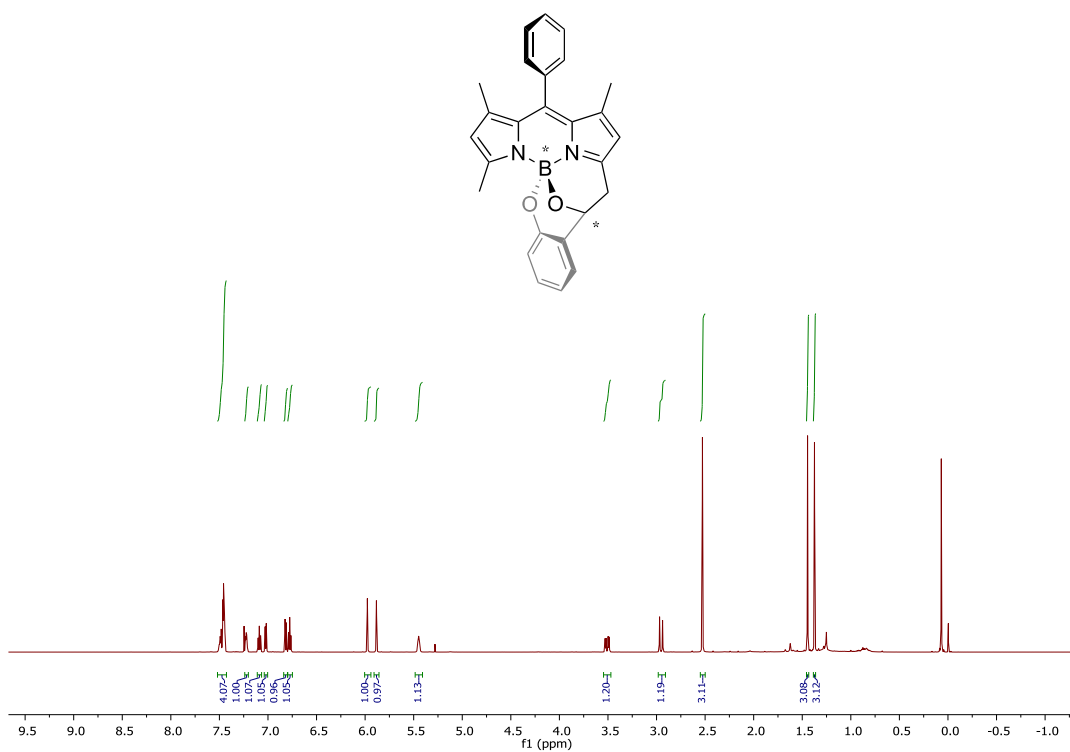


Figure A. 53. ^1H NMR spectrum of BODIPY 96

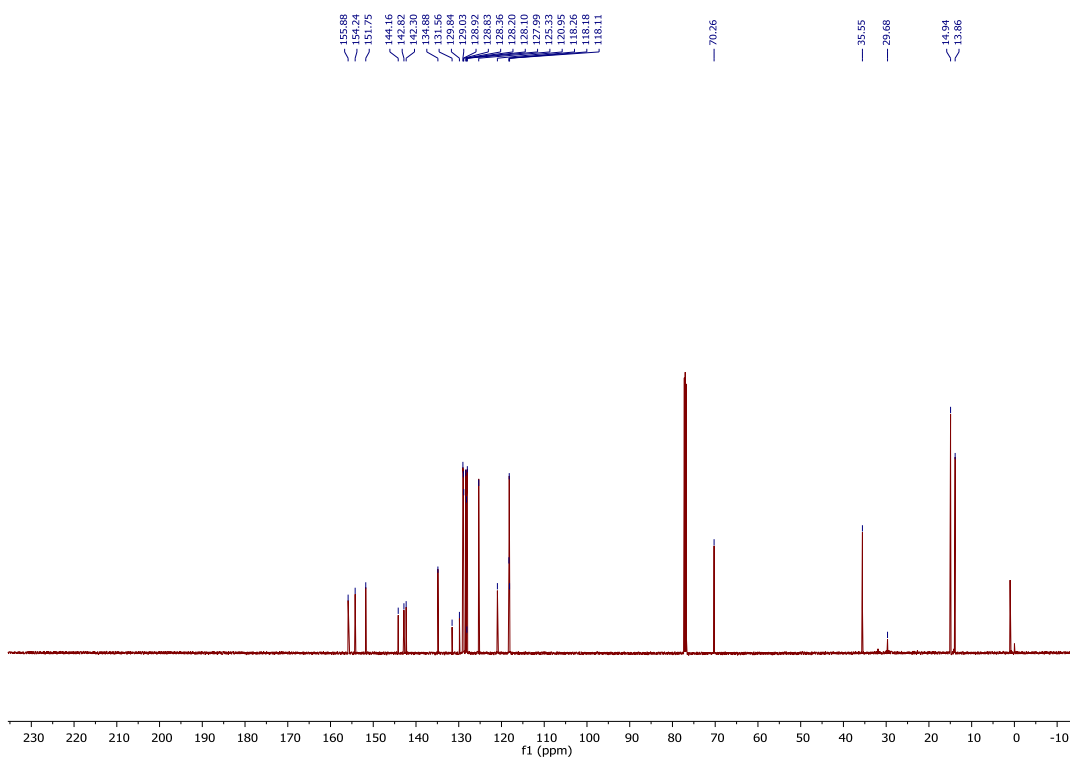


Figure A. 54. ^{13}C NMR spectrum of BODIPY 96

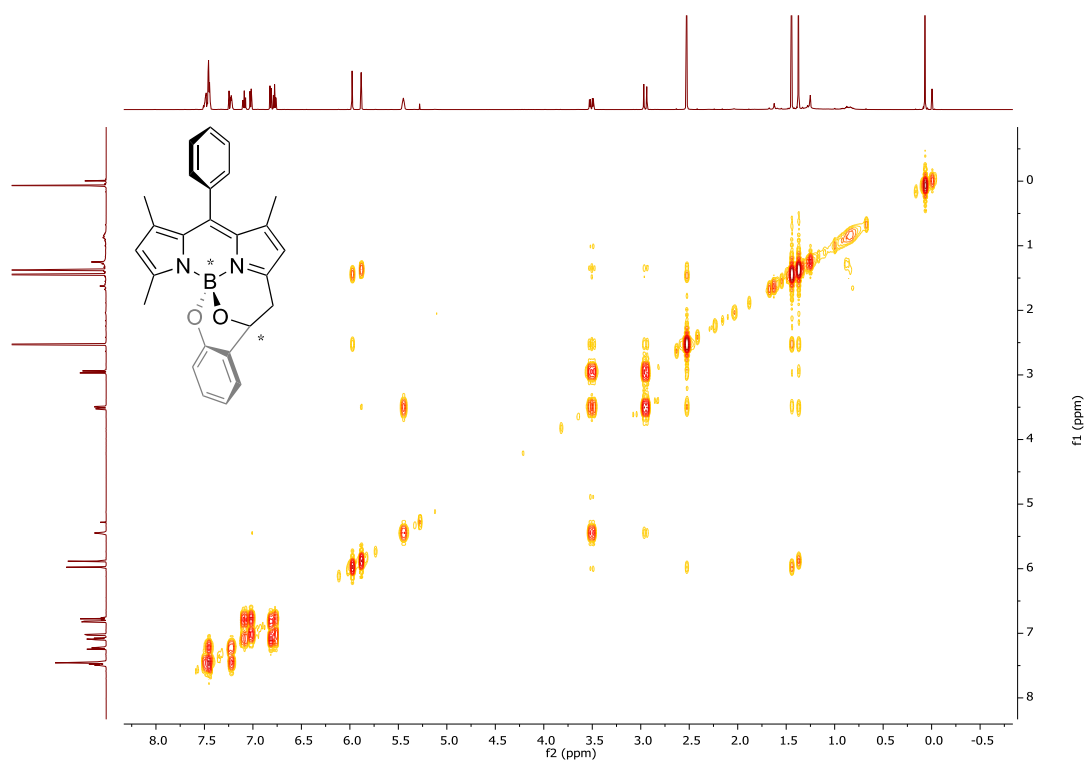


Figure A. 55. ^1H - ^1H COSY NMR spectrum of BODIPY **96**

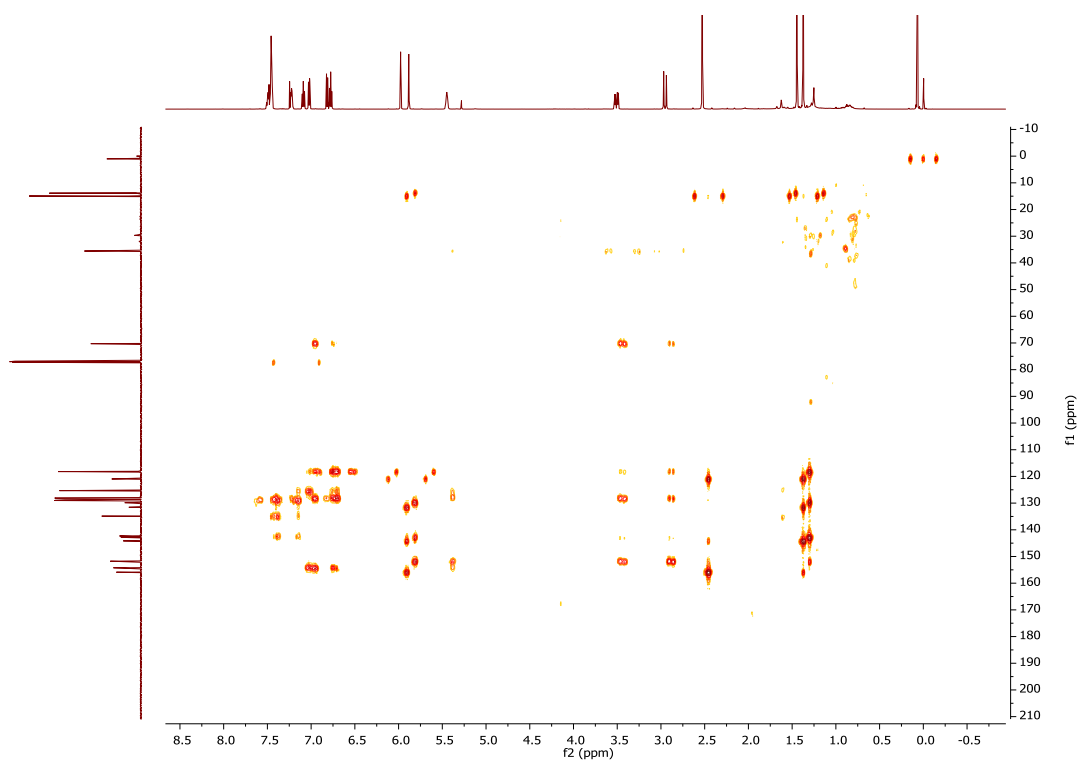


Figure A. 56. HMBC NMR spectrum of BODIPY **96**

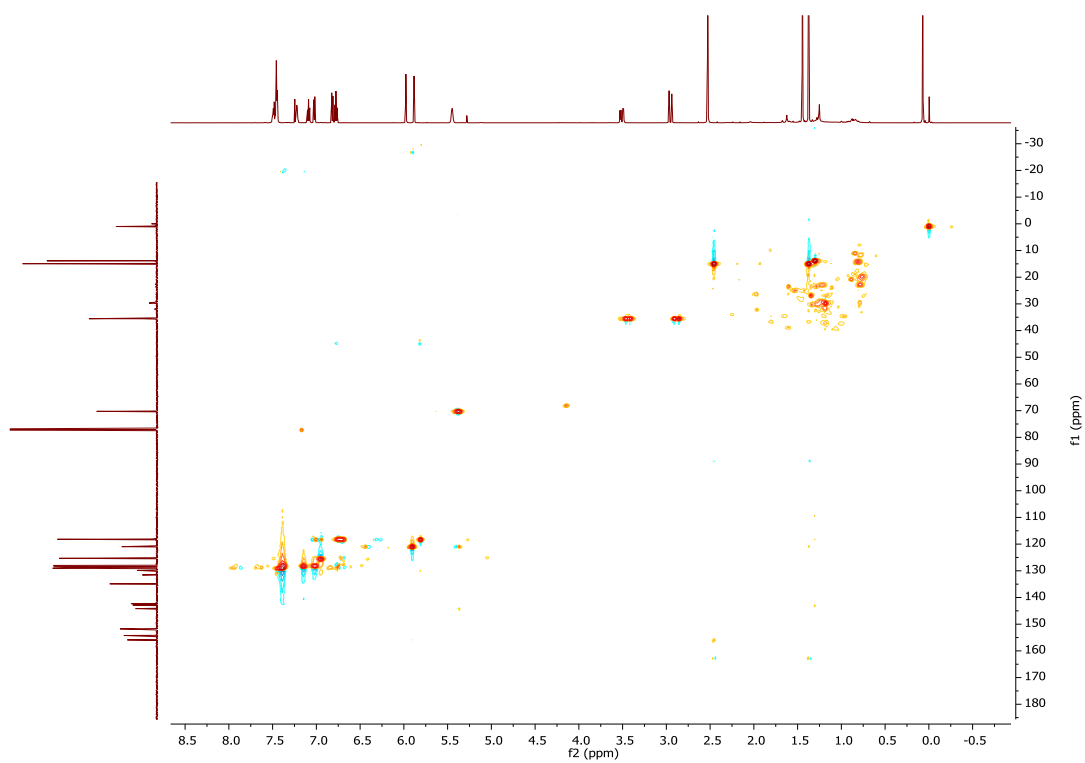


Figure A. 57. HSQC NMR spectrum of BODIPY **96**

B. HPLC CHROMATOGRAMS

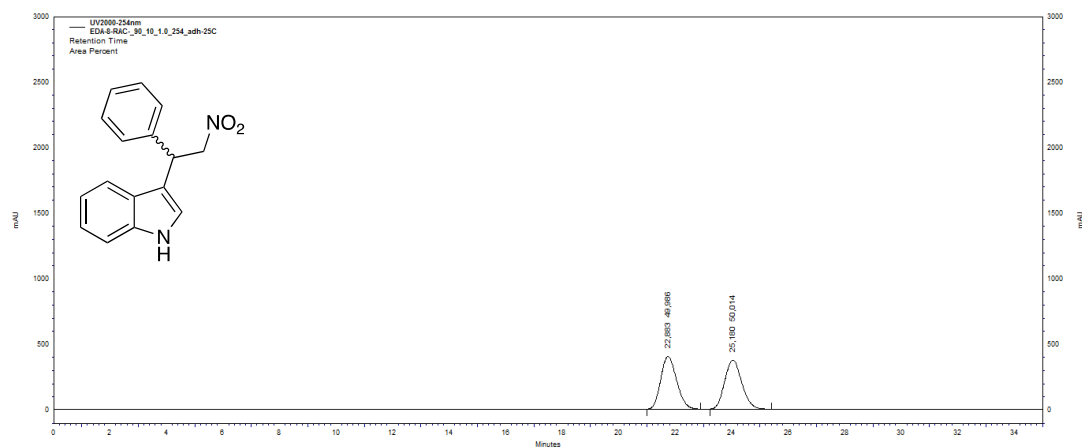


Figure B. 1. HPLC chromatogram of *rac*-**34aa**

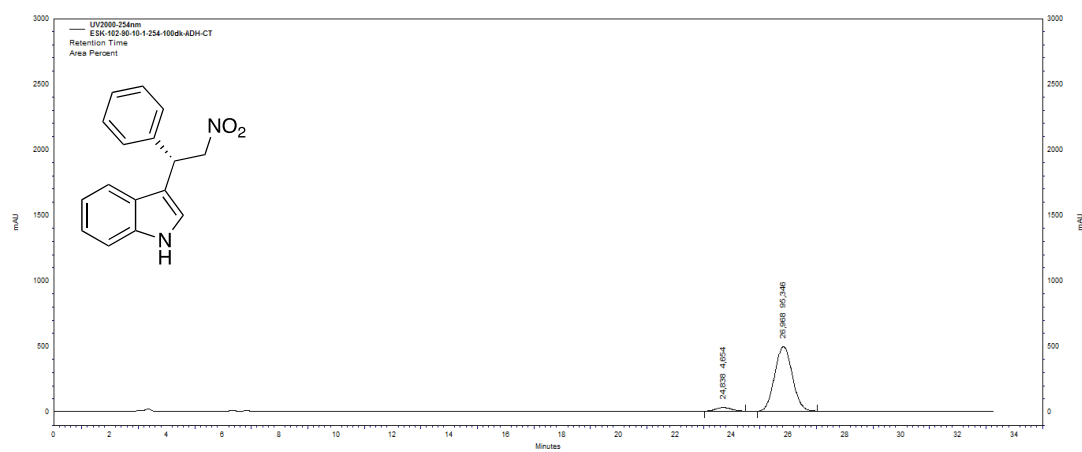


Figure B. 2. HPLC chromatogram of enantiomerically enriched **34aa**

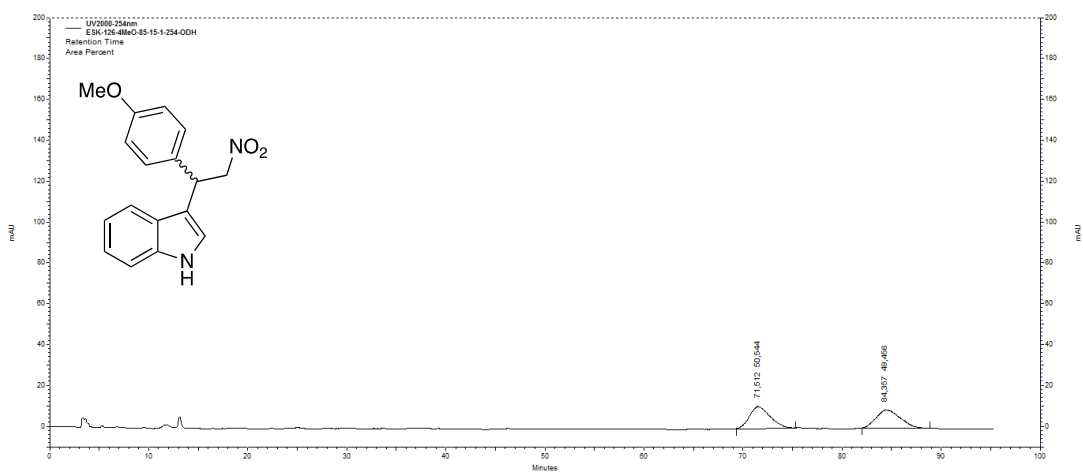


Figure B. 3. HPLC chromatogram of *rac*-**34ab**

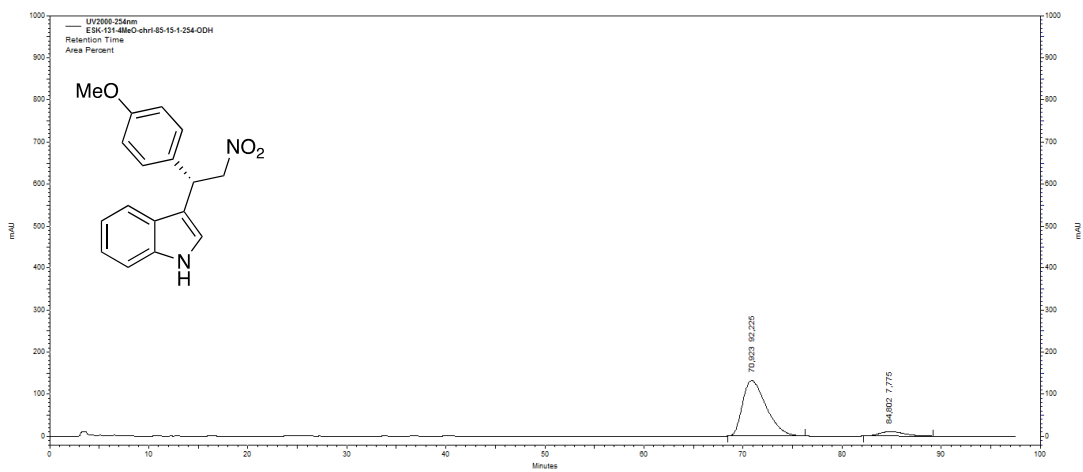


Figure B. 4. HPLC chromatogram of enantiomerically enriched **34ab**

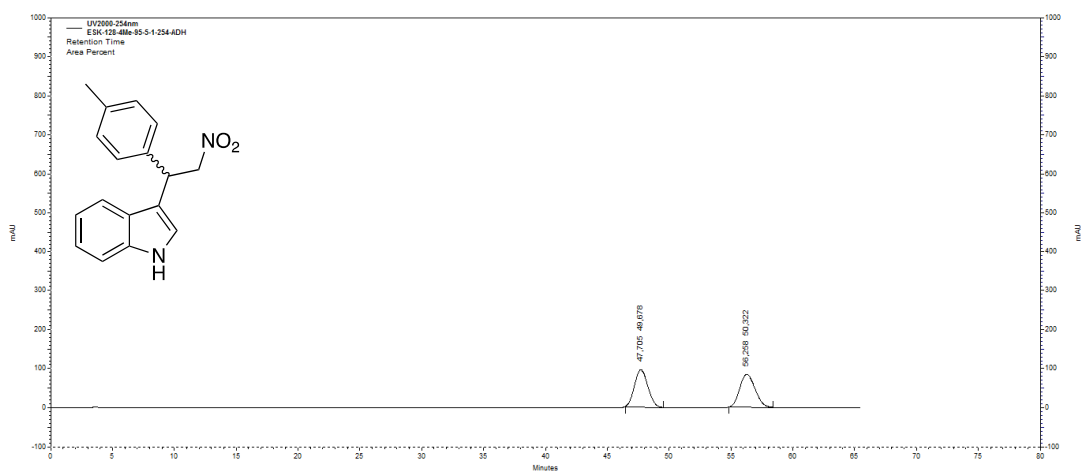


Figure B. 5. HPLC chromatogram of *rac*-34ac

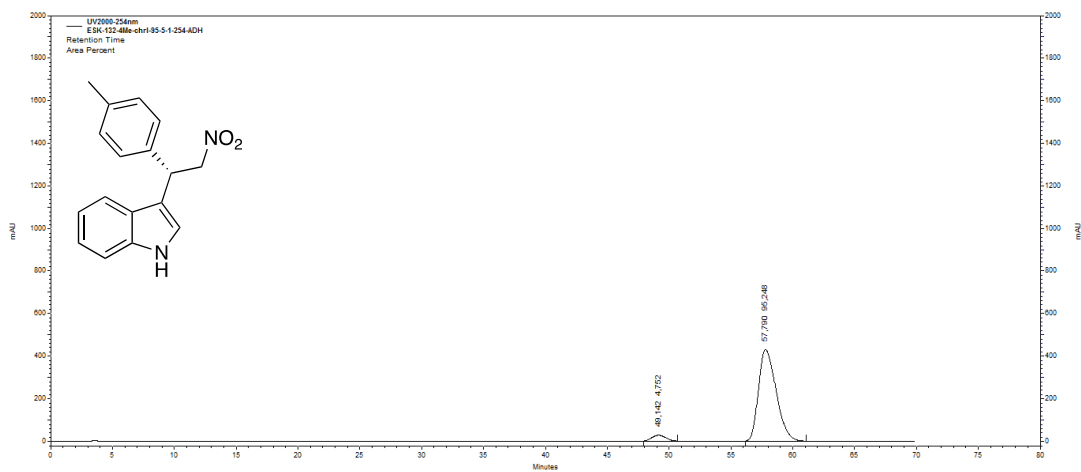


Figure B. 6. HPLC chromatogram of enantiomerically enriched 34ac

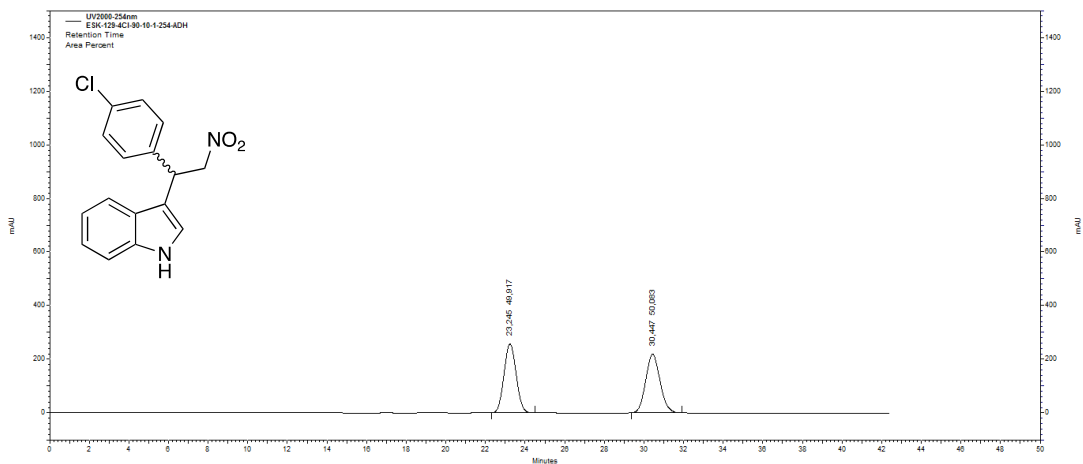


Figure B. 7. HPLC chromatogram of *rac*-34ad

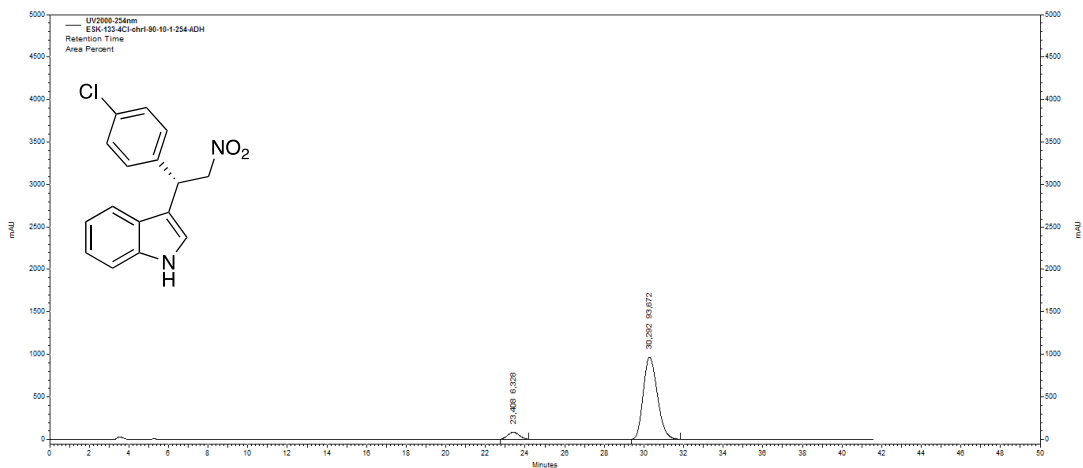


Figure B. 8. HPLC chromatogram of enantiomerically enriched 34ad

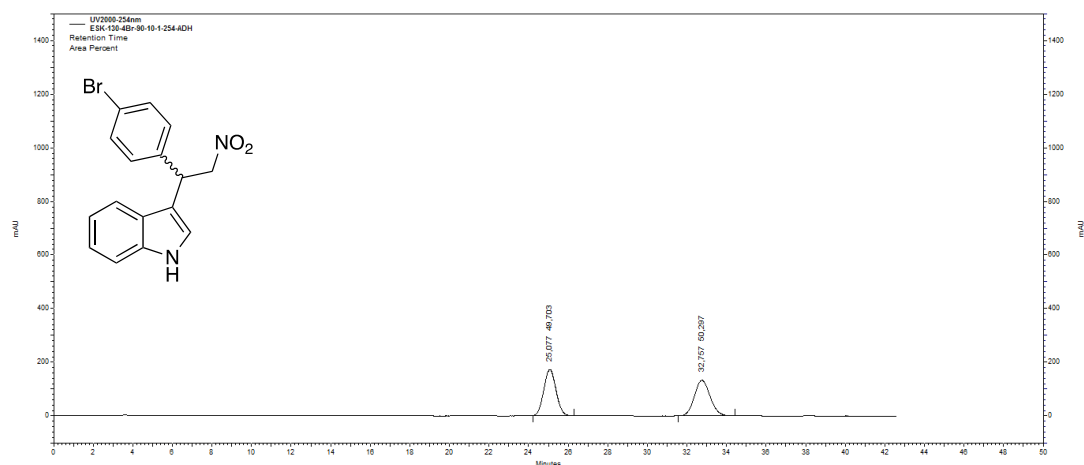


Figure B. 9. HPLC chromatogram of *rac*-**34ae**

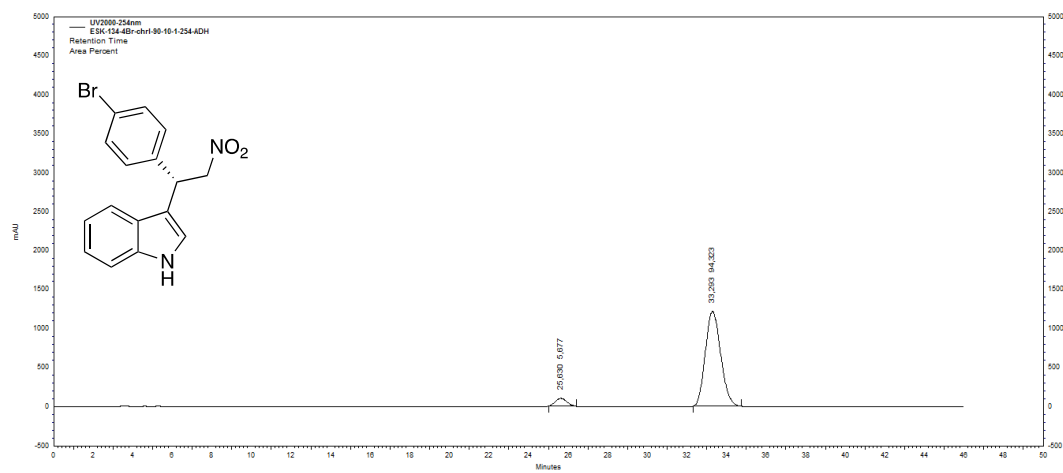


Figure B. 10. HPLC chromatogram of enantiomerically enriched **34ae**

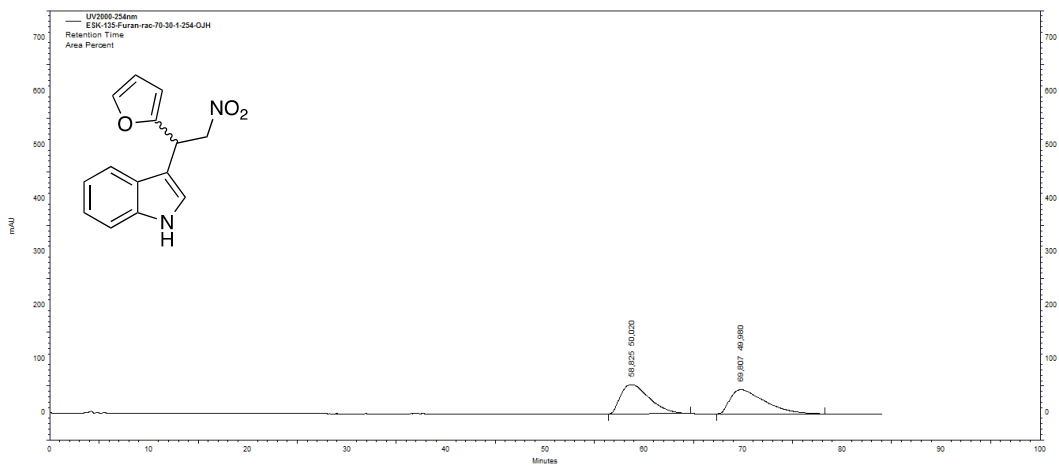


Figure B. 11. HPLC chromatogram of *rac*-**34af**

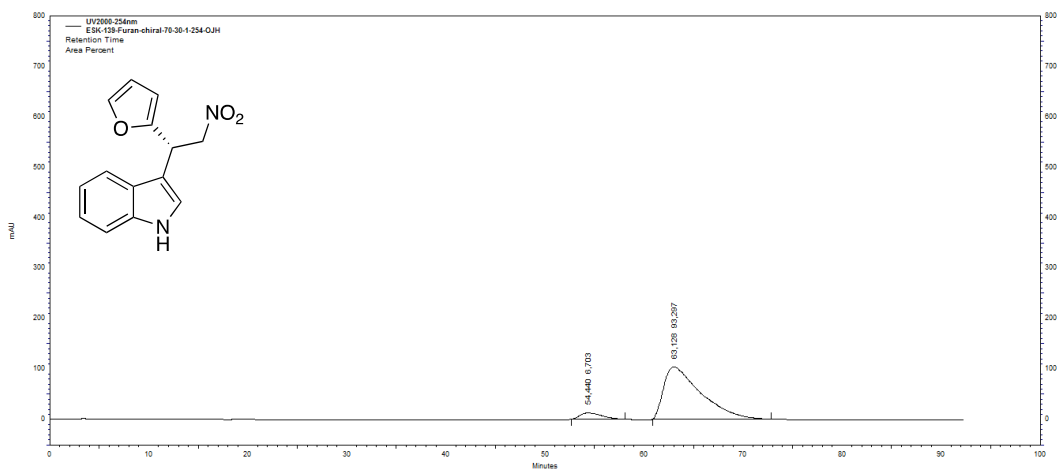


Figure B. 12. HPLC chromatogram of enantiomerically enriched **34af**

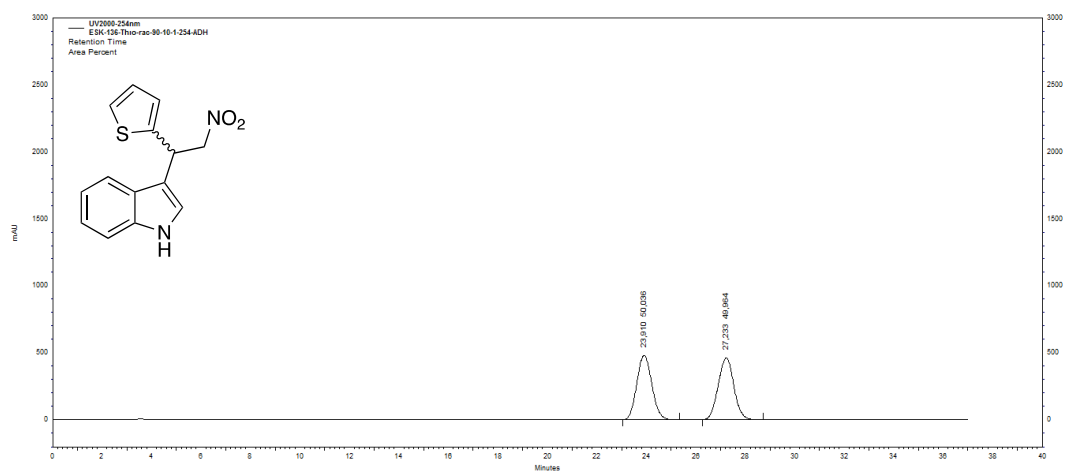


Figure B. 13. HPLC chromatogram of *rac*-**34ag**

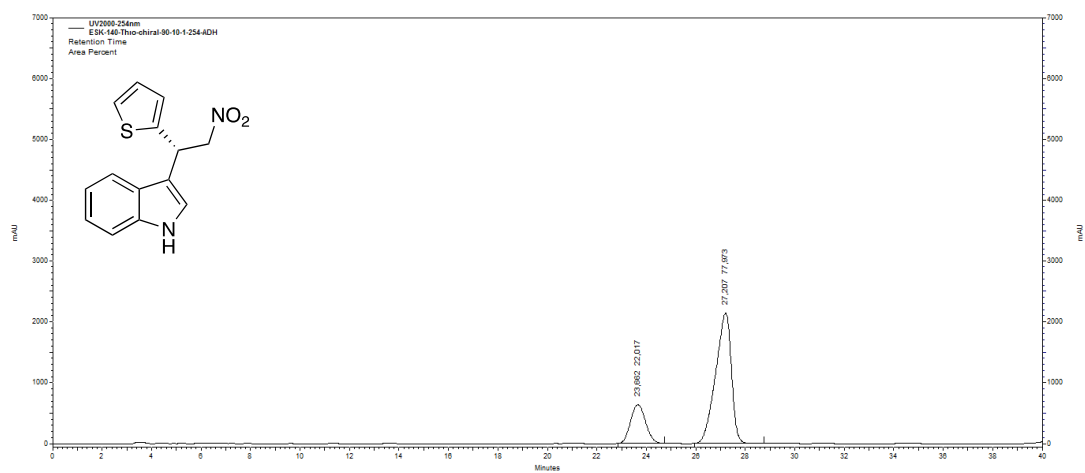


Figure B. 14. HPLC chromatogram of enantiomerically enriched **34ag**

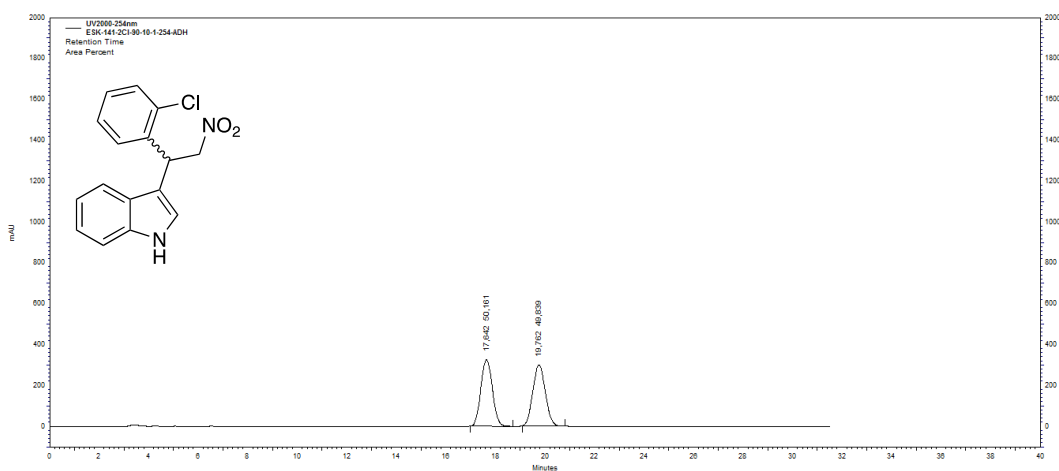


Figure B. 15. HPLC chromatogram of *rac*-34ah

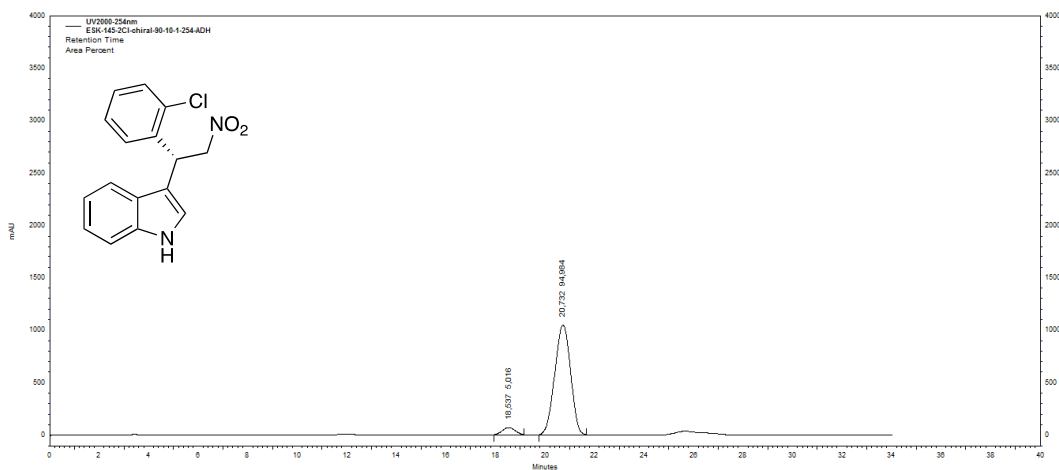


Figure B. 16. HPLC chromatogram of enantiomerically enriched 34ah

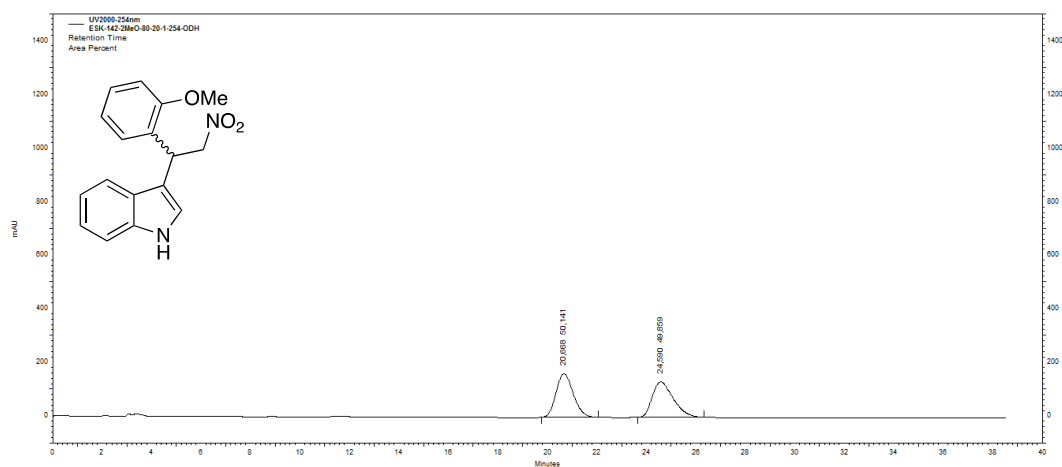


Figure B. 17. HPLC chromatogram of *rac*-**34ai**

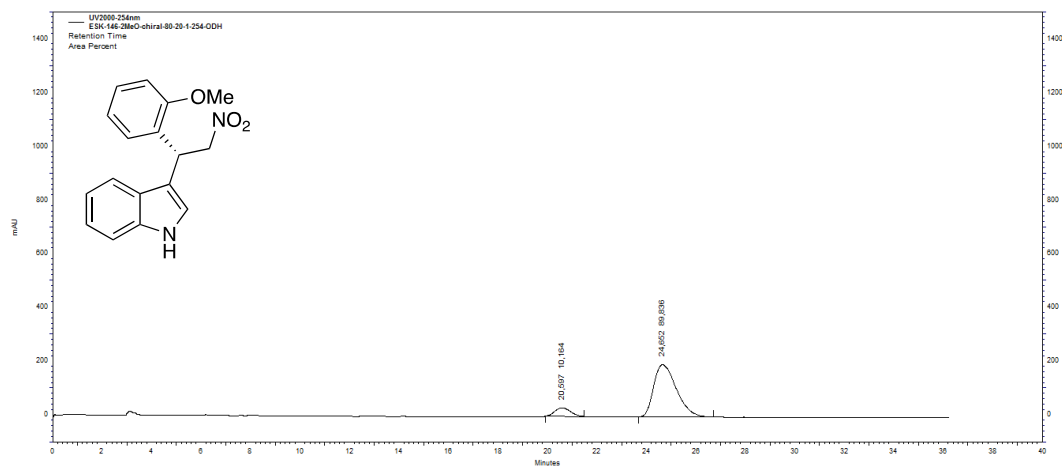


Figure B. 18. HPLC chromatogram of enantiomerically enriched **34ai**

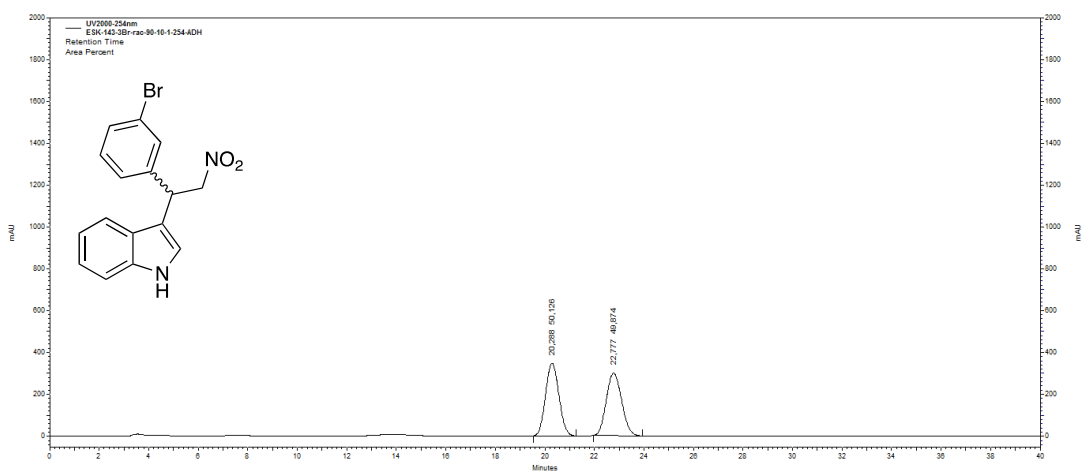


Figure B. 19. HPLC chromatogram of *rac*-**34aj**

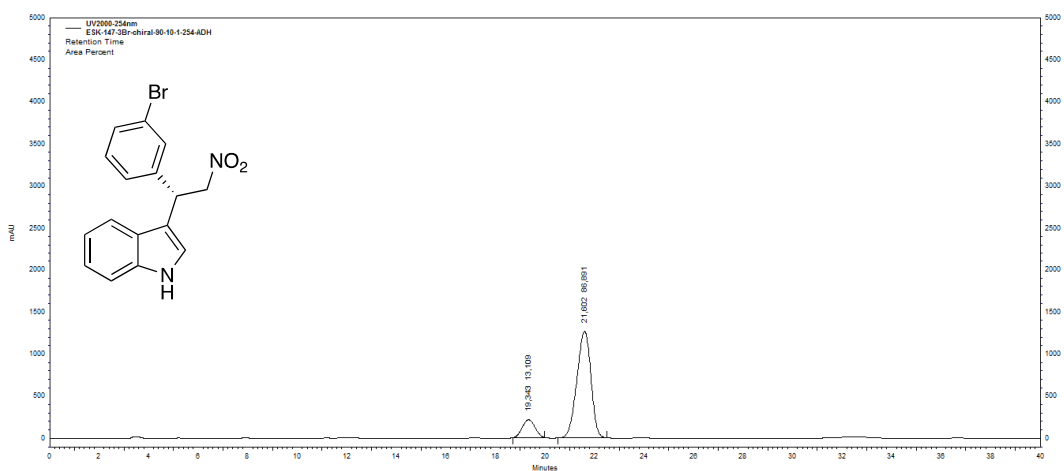


Figure B. 20. HPLC chromatogram of enantiomerically enriched **34aj**

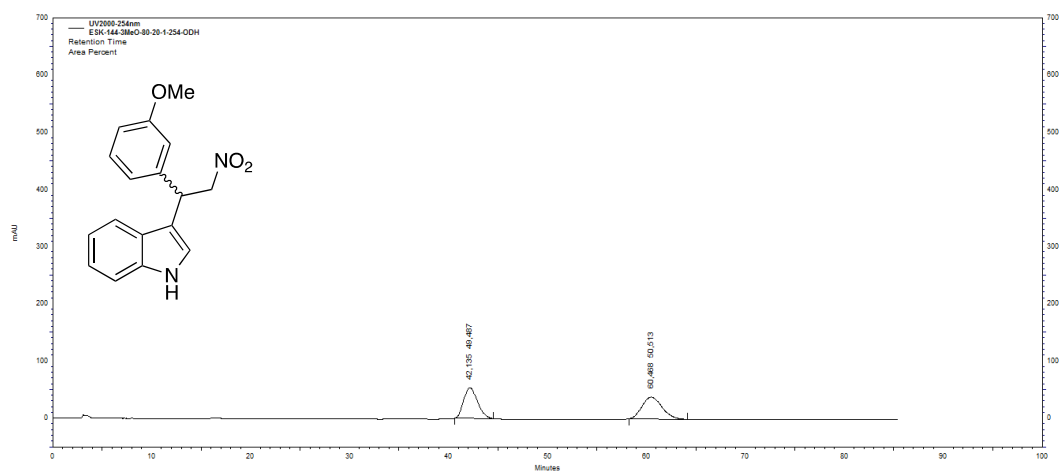


Figure B. 21. HPLC chromatogram of *rac*-**34ak**

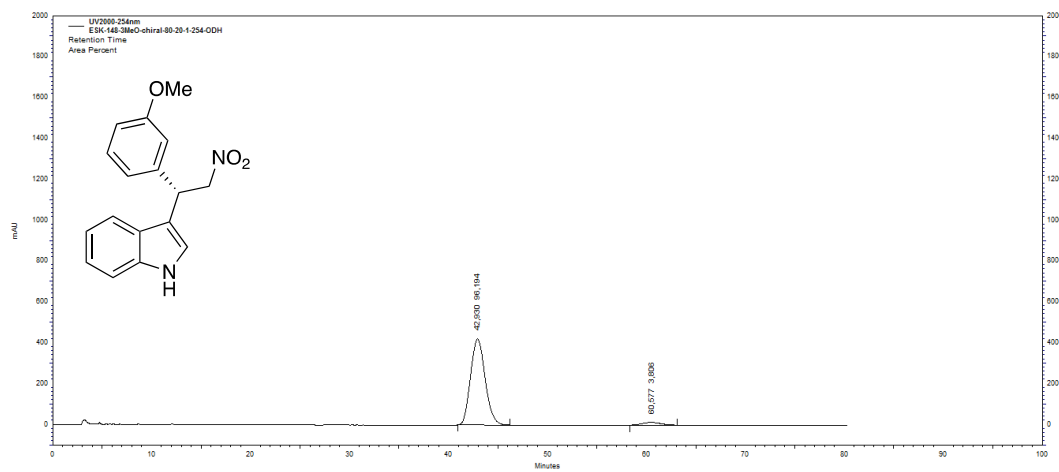
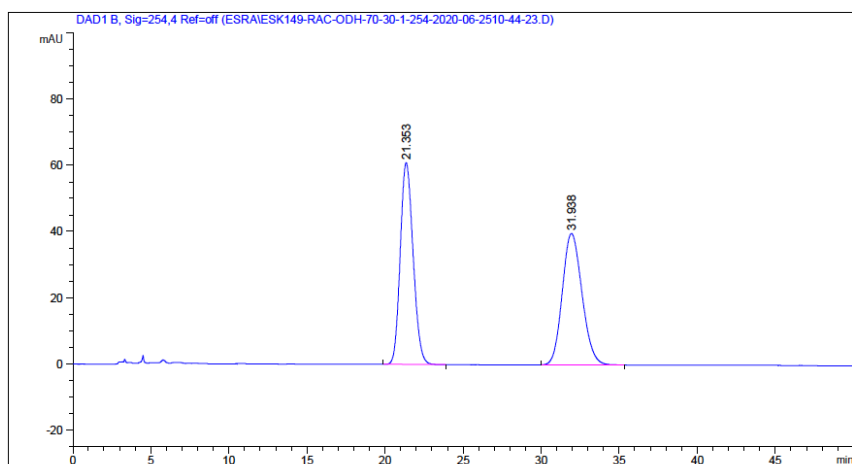


Figure B. 22. HPLC chromatogram of enantiomerically enriched **34ak**



Signal 1: DAD1 B, Sig=254,4 Ref=off

Peak #	RetTime [min]	Type	Width [min]	Area [mAU*s]	Height [mAU]	Area %
1	21.353	BB	0.8892	3485.40601	60.94368	49.9780
2	31.938	BB	1.3205	3488.47876	39.72559	50.0220

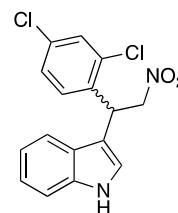
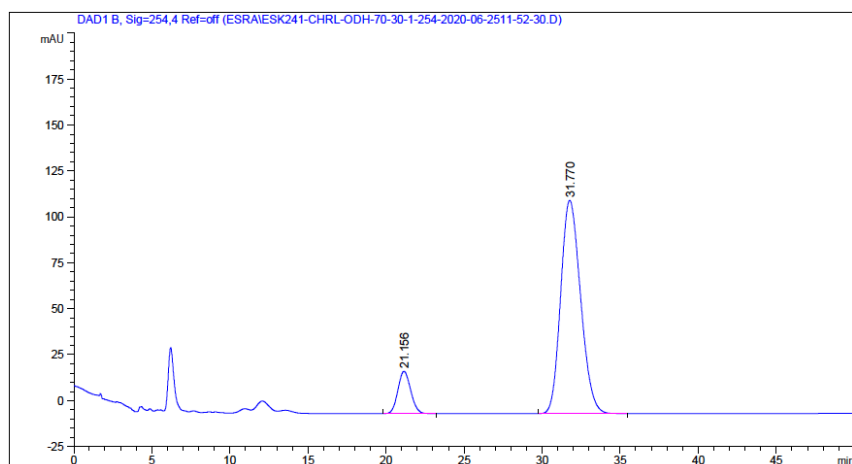


Figure B. 23. HPLC chromatogram of *rac*-34al



Signal 1: DAD1 B, Sig=254,4 Ref=off

Peak #	RetTime [min]	Type	Width [min]	Area [mAU*s]	Height [mAU]	Area %
1	21.156	BB	0.8750	1314.84045	22.99977	11.3326
2	31.770	BB	1.3684	1.02874e4	116.02837	88.6674

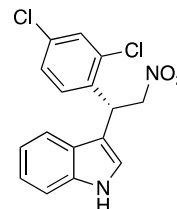
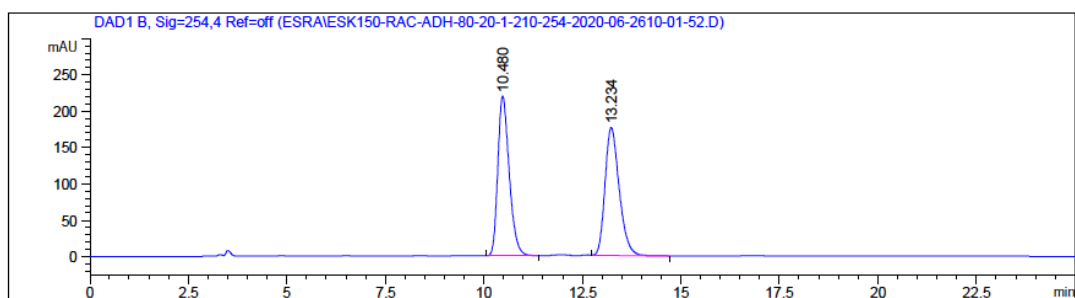


Figure B. 24. HPLC chromatogram of enantiomerically enriched 34al



Signal 1: DAD1 B, Sig=254,4 Ref=off

Peak #	RetTime [min]	Type	Width [min]	Area [mAU*s]	Height [mAU]	Area %
1	10.480	BB	0.3063	4414.46143	219.80779	50.1540
2	13.234	BB	0.3812	4387.35205	175.78143	49.8460

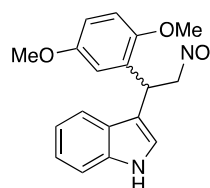
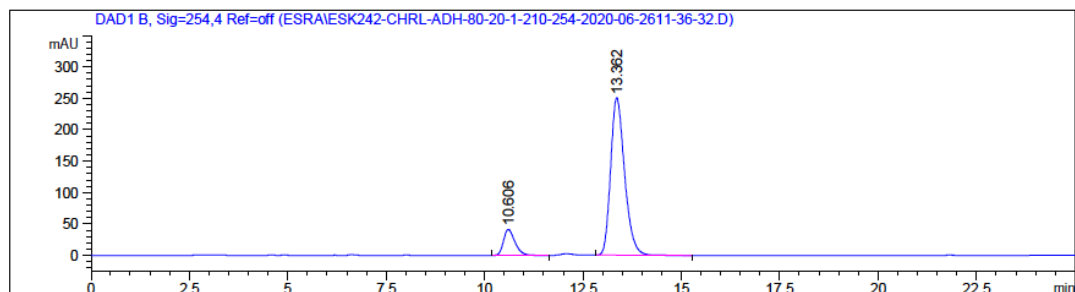


Figure B. 25. HPLC chromatogram of *rac*-**34am**



Signal 1: DAD1 B, Sig=254,4 Ref=off

Peak #	RetTime [min]	Type	Width [min]	Area [mAU*s]	Height [mAU]	Area %
1	10.606	BB	0.3088	831.63507	41.32728	11.8480
2	13.362	BB	0.3756	6187.55518	250.97047	88.1520

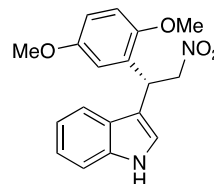
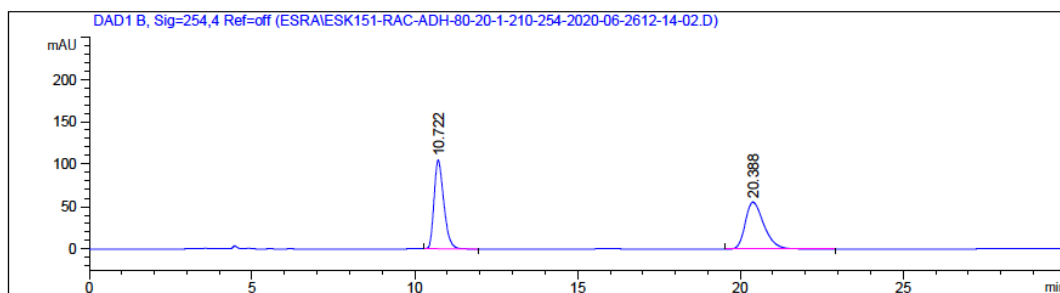


Figure B. 26. HPLC chromatogram of enantiomerically enriched **34am**



Signal 1: DAD1 B, Sig=254,4 Ref=off

Peak #	RetTime [min]	Type	Width [min]	Area [mAU*s]	Height [mAU]	Area %
1	10.722	BB	0.3172	2161.97583	104.57887	49.6076
2	20.388	BB	0.6064	2196.17432	55.41263	50.3924

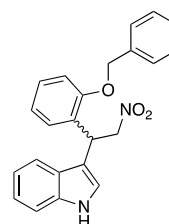
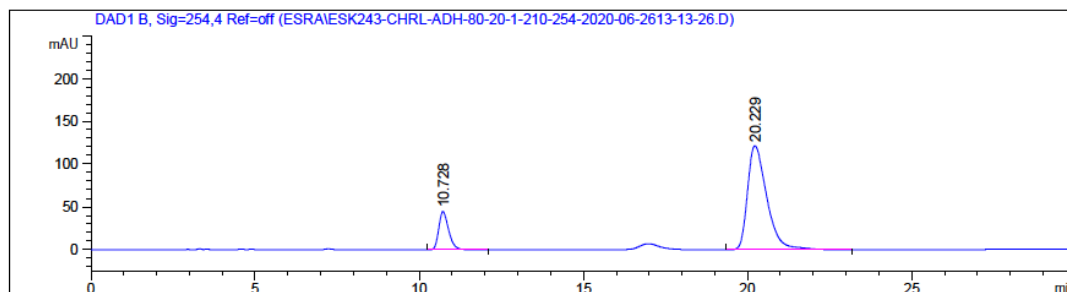


Figure B. 27. HPLC chromatogram of *rac*-**34an**



Signal 1: DAD1 B, Sig=254,4 Ref=off

Peak #	RetTime [min]	Type	Width [min]	Area [mAU*s]	Height [mAU]	Area %
1	10.728	BB	0.3149	923.20789	44.71656	15.6982
2	20.229	BB	0.6222	4957.76367	121.46062	84.3018

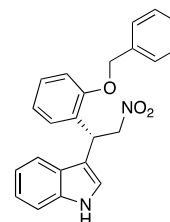
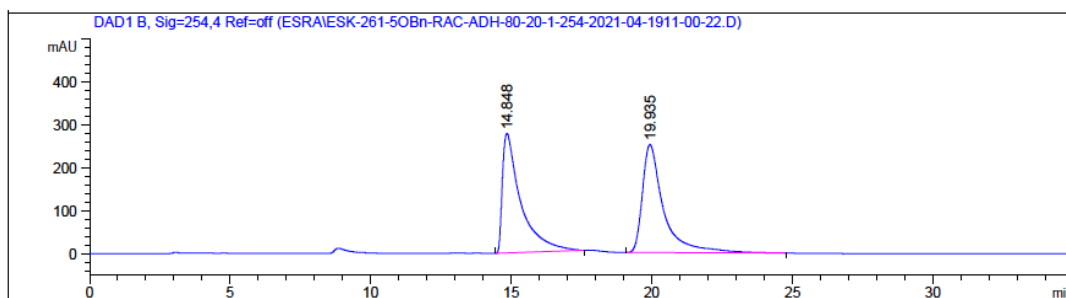


Figure B. 28. HPLC chromatogram of enantiomerically enriched **34an**



Signal 2: DAD1 B, Sig=254,4 Ref=off

Peak #	RetTime [min]	Type	Width [min]	Area [mAU*s]	Height [mAU]	Area %
1	14.848	BB	0.6364	1.26065e4	278.58795	48.7553
2	19.935	BB	0.7492	1.32502e4	252.08261	51.2447

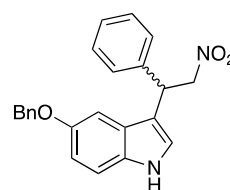
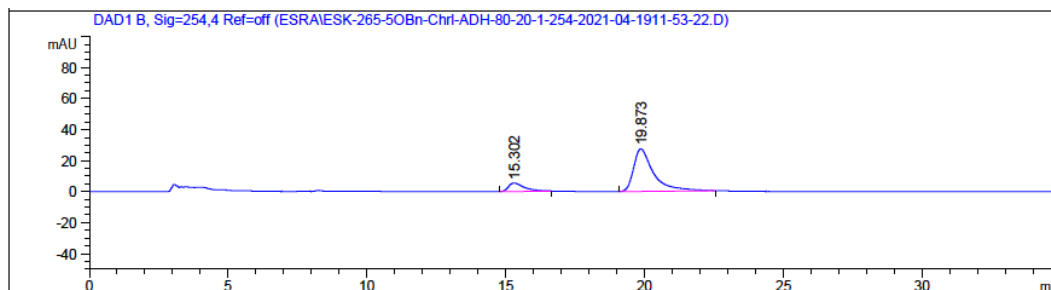


Figure B. 29. HPLC chromatogram of *rac*-**34ba**



Signal 2: DAD1 B, Sig=254,4 Ref=off

Peak #	RetTime [min]	Type	Width [min]	Area [mAU*s]	Height [mAU]	Area %
1	15.302	BB	0.4630	210.79732	5.35174	13.4168
2	19.873	BB	0.5838	1360.34875	27.39546	86.5832

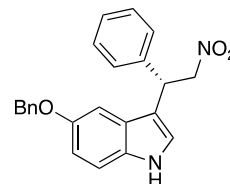
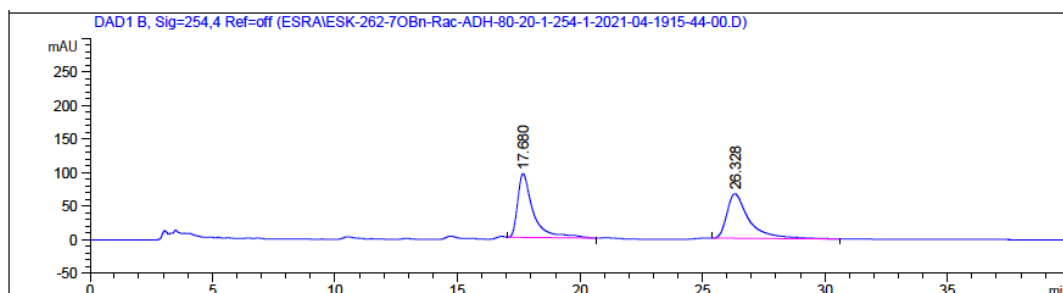


Figure B. 30. HPLC chromatogram of enantiomerically enriched **34ba**



Signal 2: DAD1 B, Sig=254,4 Ref=off

Peak #	RetTime [min]	Type	Width [min]	Area [mAU*s]	Height [mAU]	Area %
1	17.680	BB	0.6227	4200.61572	95.12856	50.1209
2	26.328	BB	0.7872	4180.34424	66.56180	49.8791

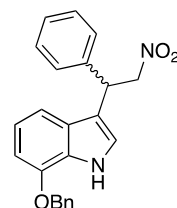
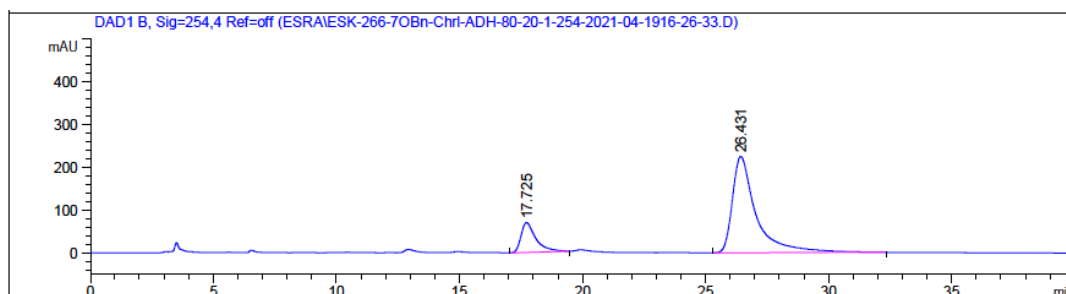


Figure B. 31. HPLC chromatogram of *rac*-**34ca**



Signal 2: DAD1 B, Sig=254,4 Ref=off

Peak #	RetTime [min]	Type	Width [min]	Area [mAU*s]	Height [mAU]	Area %
1	17.725	BB	0.5845	2922.39453	69.51305	16.1925
2	26.431	BB	0.9380	1.51255e4	225.08141	83.8075

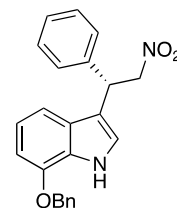
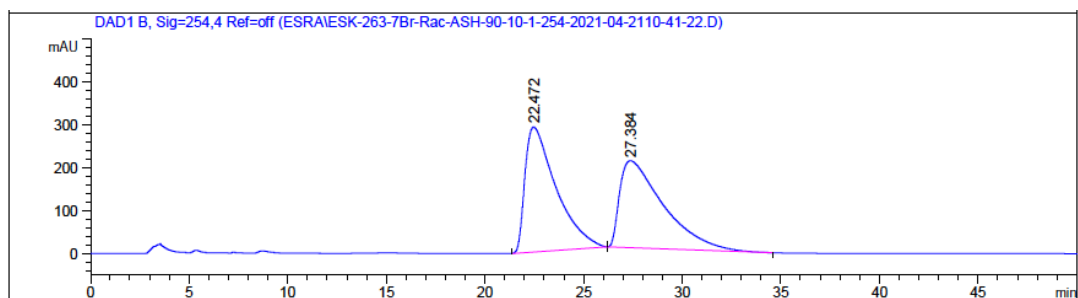


Figure B. 32. HPLC chromatogram of enantiomerically enriched **34ca**



Signal 2: DAD1 B, Sig=254,4 Ref=off

Peak #	RetTime [min]	Type	Width [min]	Area [mAU*s]	Height [mAU]	Area %
1	22.472	BB	1.3037	3.19204e4	290.89813	50.4174
2	27.384	BB	1.8062	3.13919e4	202.98941	49.5826

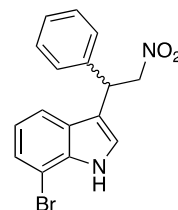
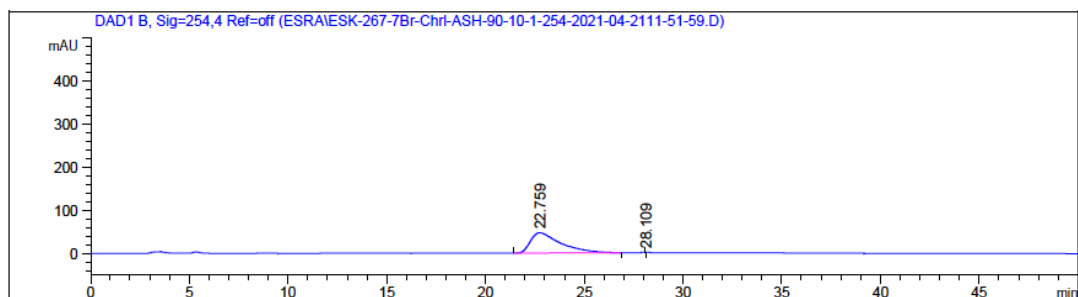


Figure B. 33. HPLC chromatogram of *rac*-**34da**



Signal 2: DAD1 B, Sig=254,4 Ref=off

Peak #	RetTime [min]	Type	Width [min]	Area [mAU*s]	Height [mAU]	Area %
1	22.759	BBA	1.2659	5062.20117	46.85888	99.9992
2	28.109	BB	0.0287	4.28389e-2	1.97986e-2	8.462e-4

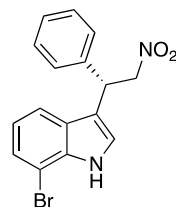


Figure B. 34. HPLC chromatogram of enantiomerically enriched **34da**

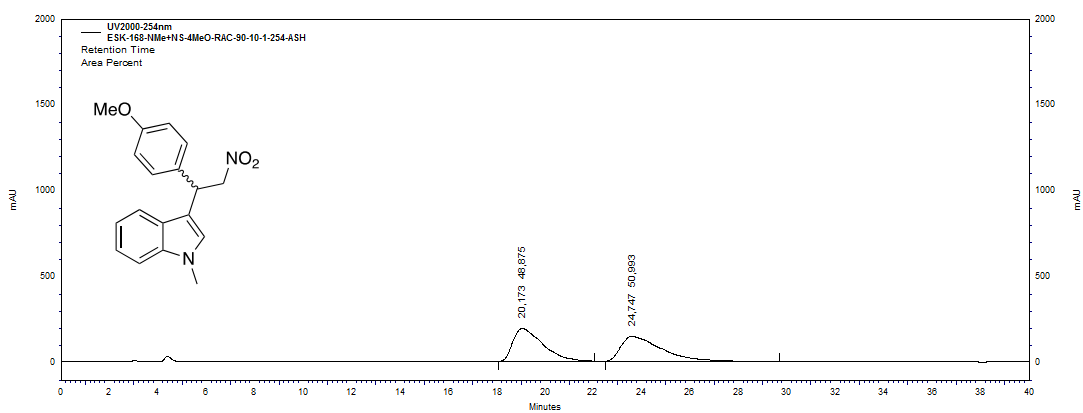


Figure B. 35. HPLC chromatogram of *rac*-**34eb**

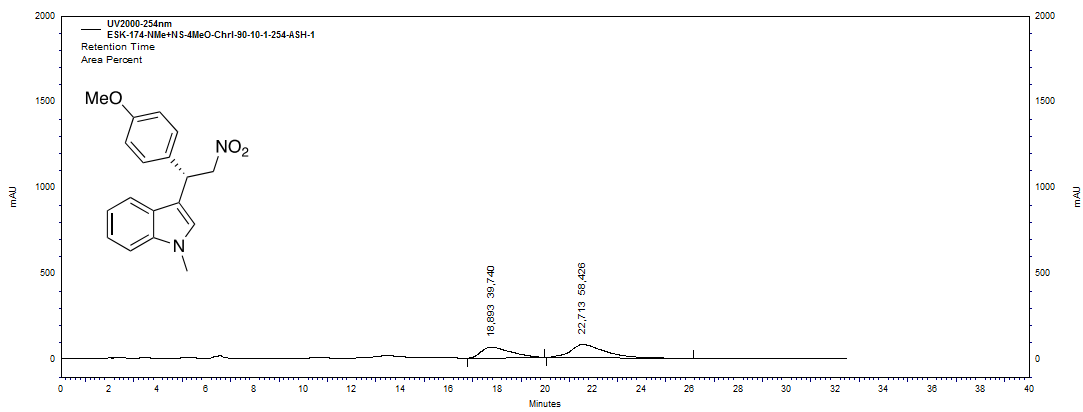
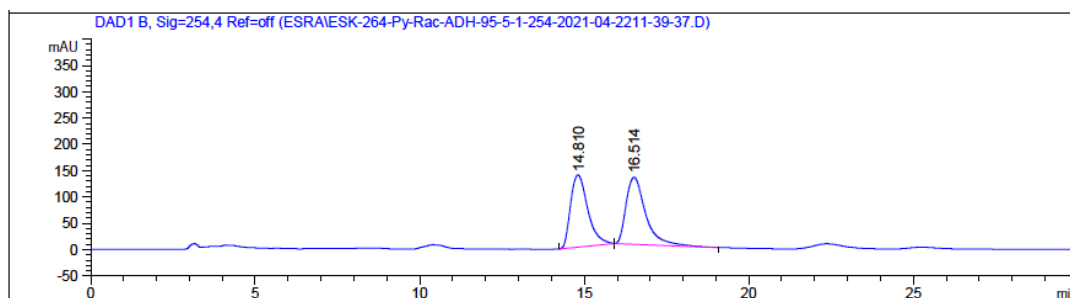


Figure B. 36. HPLC chromatogram of enantiomerically enriched **34eb**



Signal 2: DAD1 B, Sig=254,4 Ref=off

Peak #	RetTime [min]	Type	Width [min]	Area [mAU*s]	Height [mAU]	Area %
1	14.810	BB	0.5643	4988.34180	137.16852	48.7688
2	16.514	BB	0.6228	5240.20020	127.28893	51.2312

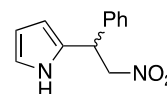
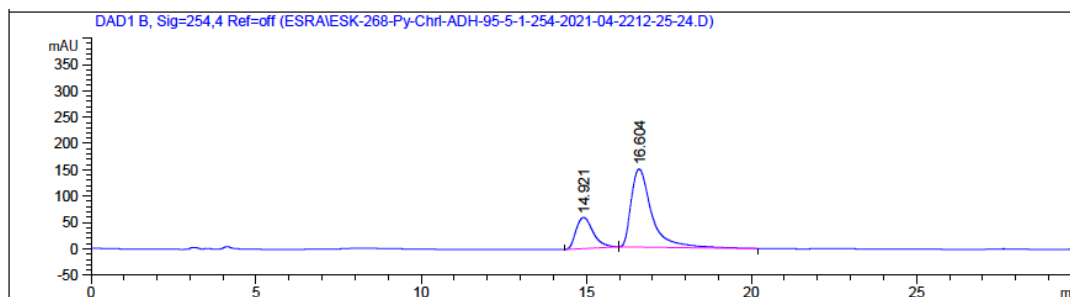


Figure B. 37. HPLC chromatogram of *rac*-86



Signal 2: DAD1 B, Sig=254,4 Ref=off

Peak #	RetTime [min]	Type	Width [min]	Area [mAU*s]	Height [mAU]	Area %
1	14.921	BB	0.5444	2127.42261	59.04294	24.8428
2	16.604	BB	0.6459	6436.10742	148.41667	75.1572

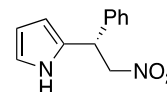
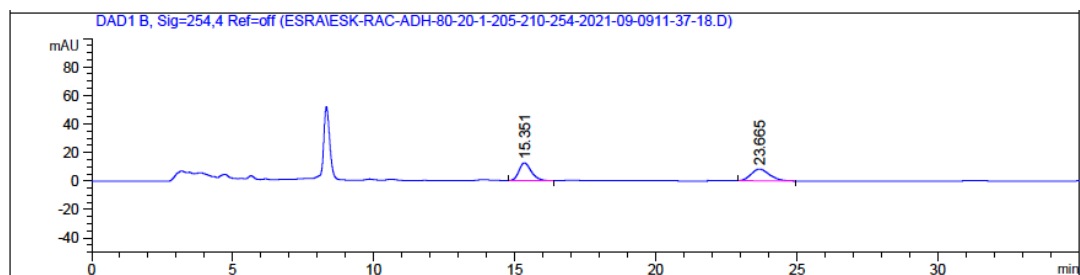


Figure B. 38. HPLC chromatogram of enantiomerically enriched 86



Signal 2: DAD1 B, Sig=254,4 Ref=off

Peak #	RetTime [min]	Type	Width [min]	Area [mAU*s]	Height [mAU]	Area %
1	15.351	BB	0.3580	377.56326	12.46240	50.9973
2	23.665	BB	0.5278	362.79602	8.05729	49.0027

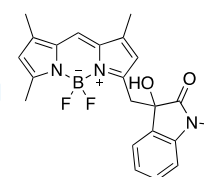
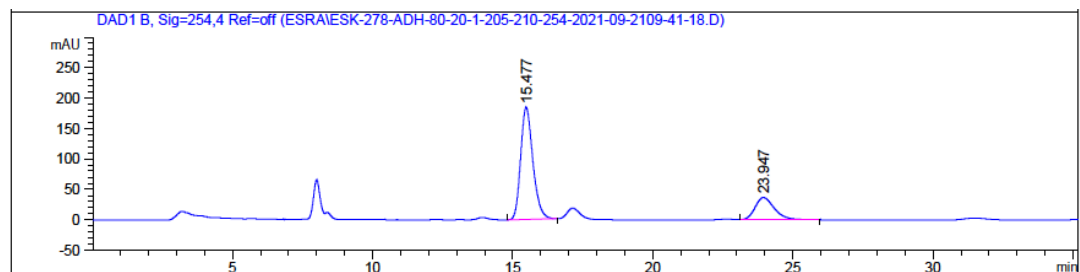


Figure B. 39. HPLC chromatogram of *rac*-73aa



Signal 2: DAD1 B, Sig=254,4 Ref=off

Peak #	RetTime [min]	Type	Width [min]	Area [mAU*s]	Height [mAU]	Area %
1	15.477	BB	0.4598	5593.32861	184.18770	76.4617
2	23.947	BB	0.5762	1721.87231	36.31173	23.5383

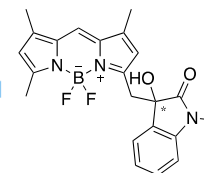
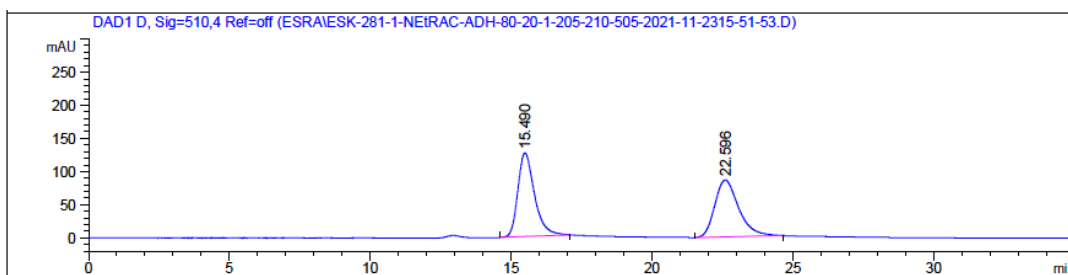


Figure B. 40. HPLC chromatogram of enantiomerically enriched 73aa



Signal 4: DAD1 D, Sig=510,4 Ref=off

Peak #	RetTime [min]	Type	Width [min]	Area [mAU*s]	Height [mAU]	Area %
1	15.490	VV R	0.4848	5202.46631	126.23048	50.7041
2	22.596	BV R	0.6960	5057.96924	85.77293	49.2959

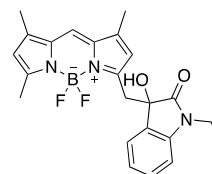
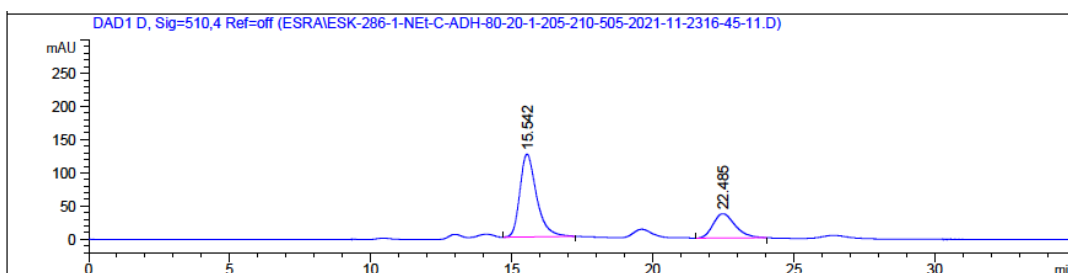


Figure B. 41. HPLC chromatogram of *rac*-**73ab**



Signal 4: DAD1 D, Sig=510,4 Ref=off

Peak #	RetTime [min]	Type	Width [min]	Area [mAU*s]	Height [mAU]	Area %
1	15.542	VV R	0.5115	5153.97363	124.89008	72.1403
2	22.485	VV R	0.6364	1990.40210	36.74969	27.8597

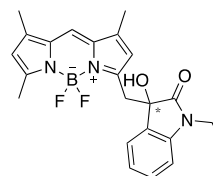
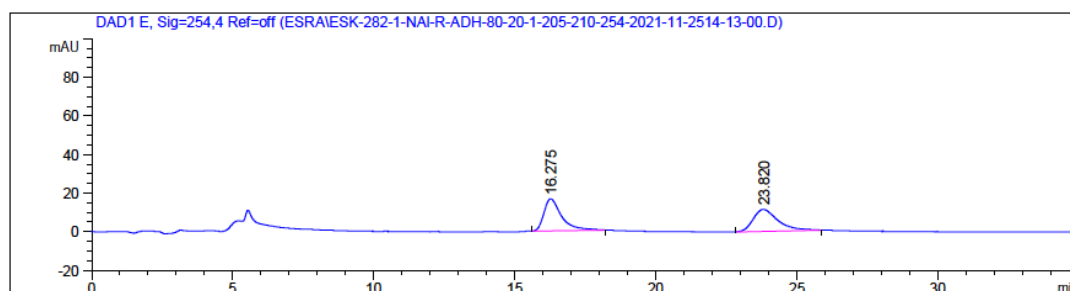


Figure B. 42. HPLC chromatogram of enantiomerically enriched **73ab**



Signal 5: DAD1 E, Sig=254,4 Ref=off

Peak #	RetTime [min]	Type	Width [min]	Area [mAU*s]	Height [mAU]	Area %
1	16.275	BB	0.5173	727.18878	16.64234	51.3155
2	23.820	BB	0.7144	689.90491	11.32939	48.6845

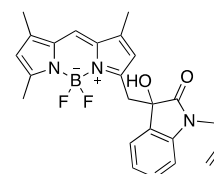
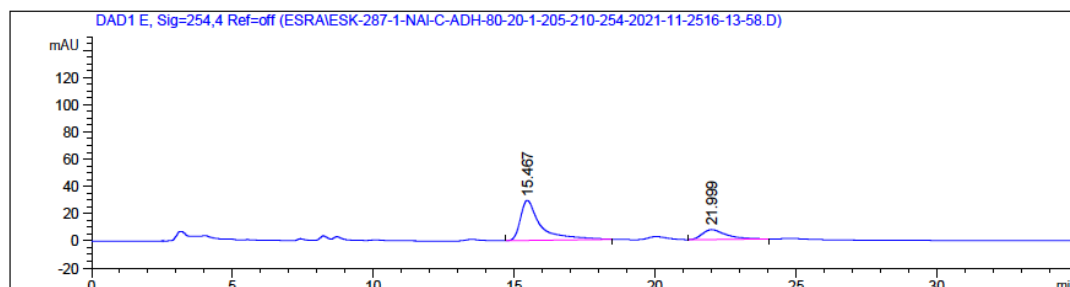


Figure B. 43. HPLC chromatogram of *rac*-73ac



Signal 5: DAD1 E, Sig=254,4 Ref=off

Peak #	RetTime [min]	Type	Width [min]	Area [mAU*s]	Height [mAU]	Area %
1	15.467	BB	0.5982	1472.54126	29.55941	77.6944
2	21.999	BB	0.6894	422.75748	7.17993	22.3056

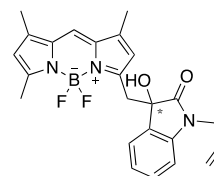
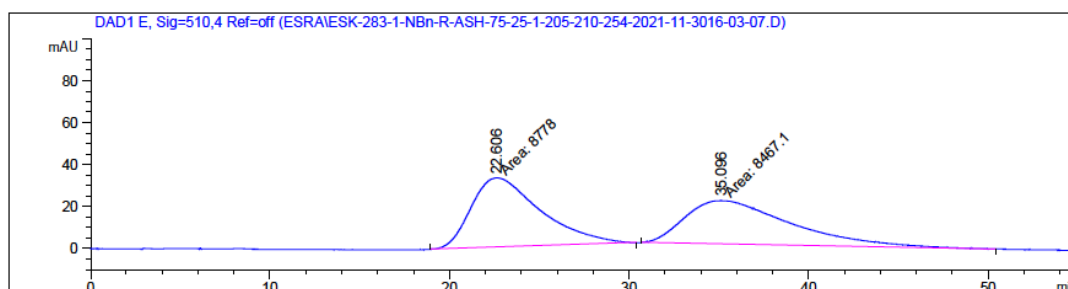


Figure B. 44. HPLC chromatogram of enantiomerically enriched 73ac



Signal 5: DAD1 E, Sig=510,4 Ref=off

Peak #	RetTime [min]	Type	Width [min]	Area [mAU*s]	Height [mAU]	Area %
1	22.606	MM	4.4330	8778.00293	33.00220	50.9014
2	35.096	MM	6.8287	8467.09668	20.66540	49.0986

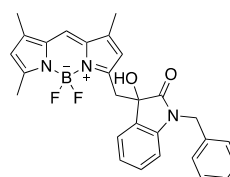
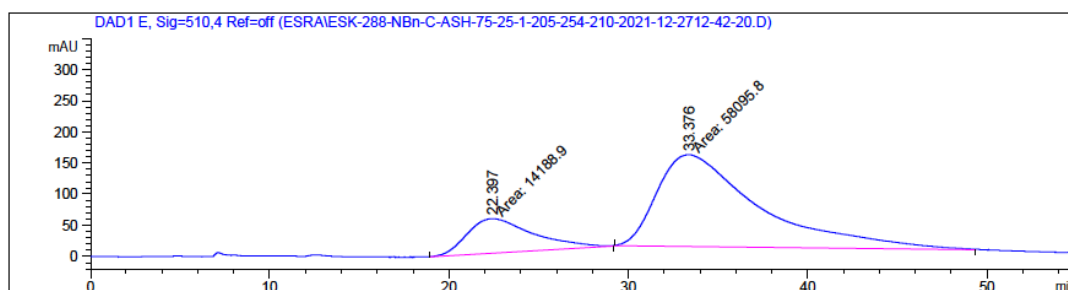


Figure B. 45. HPLC chromatogram of *rac*-73ad



Signal 5: DAD1 E, Sig=510,4 Ref=off

Peak #	RetTime [min]	Type	Width [min]	Area [mAU*s]	Height [mAU]	Area %
1	22.397	MM	4.2453	1.41889e4	55.70435	19.6292
2	33.376	MM	6.5680	5.80958e4	147.42049	80.3708

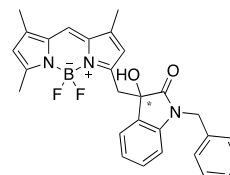
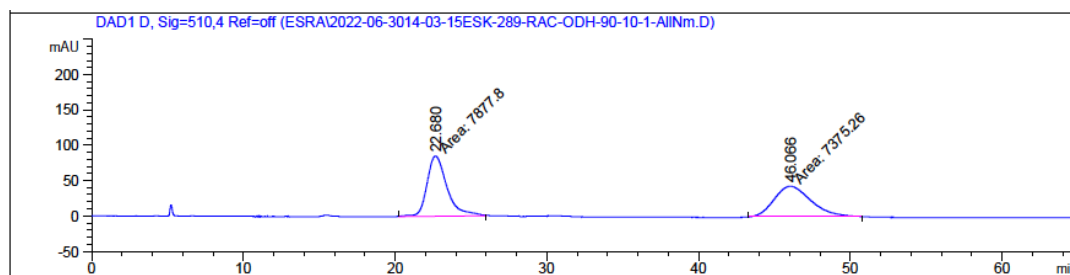


Figure B. 46. HPLC chromatogram of enantiomerically enriched 73ad



Signal 4: DAD1 D, Sig=510,4 Ref=off

Peak #	RetTime [min]	Type	Width [min]	Area [mAU*s]	Height [mAU]	Area %
1	22.680	MM	1.5370	7877.80420	85.42406	51.6473
2	46.066	MM	2.8459	7375.26367	43.19309	48.3527

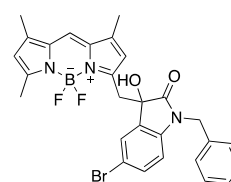
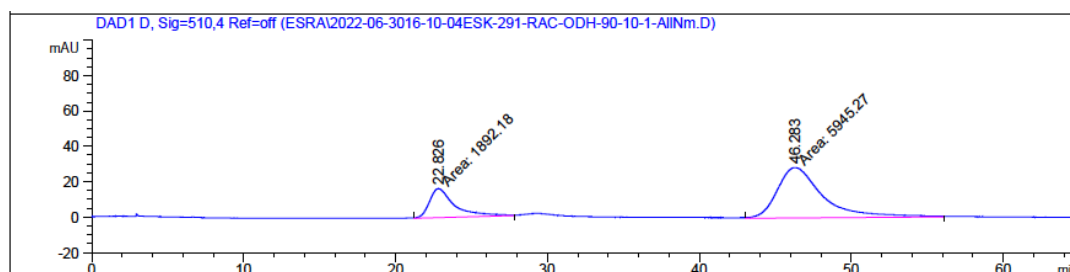


Figure B. 47. HPLC chromatogram of *rac*-73ae



Signal 4: DAD1 D, Sig=510,4 Ref=off

Peak #	RetTime [min]	Type	Width [min]	Area [mAU*s]	Height [mAU]	Area %
1	22.826	MM	1.9267	1892.18140	16.36839	24.1428
2	46.283	MM	3.4824	5945.27148	28.45380	75.8572

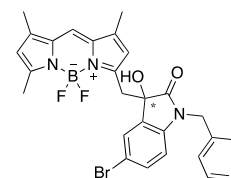
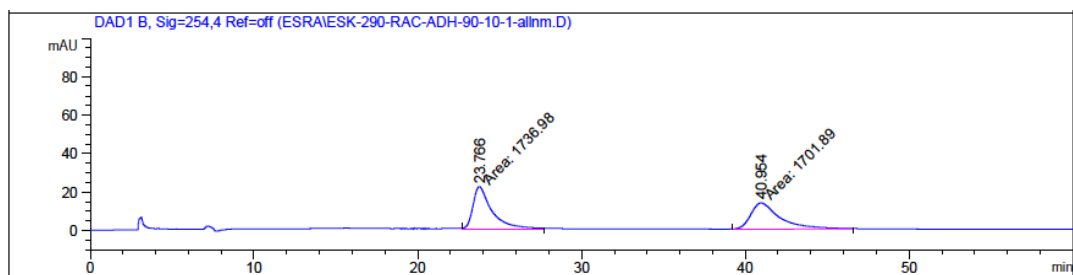


Figure B. 48. HPLC chromatogram of enantiomerically enriched 73ae



Signal 2: DAD1 B, Sig=254,4 Ref=off

Peak #	RetTime [min]	Type	Width [min]	Area [mAU*s]	Height [mAU]	Area %
1	23.766	MM	1.3273	1736.98438	21.81134	50.5103
2	40.954	MM	2.0686	1701.88831	13.71236	49.4897

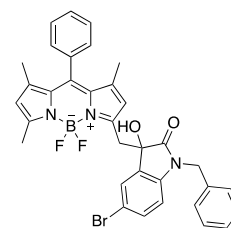
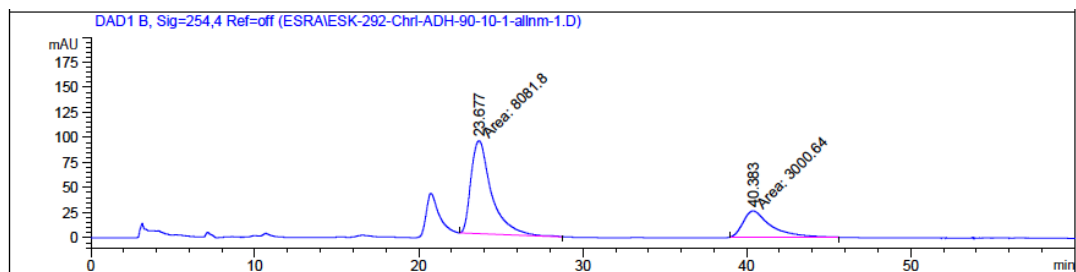


Figure B. 49. HPLC chromatogram of *rac*-73be



Signal 2: DAD1 B, Sig=254,4 Ref=off

Peak #	RetTime [min]	Type	Width [min]	Area [mAU*s]	Height [mAU]	Area %
1	23.677	MM	1.4579	8081.79834	92.39211	72.9244
2	40.383	MM	1.9298	3000.63843	25.91506	27.0756

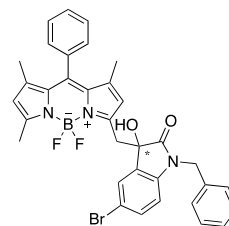
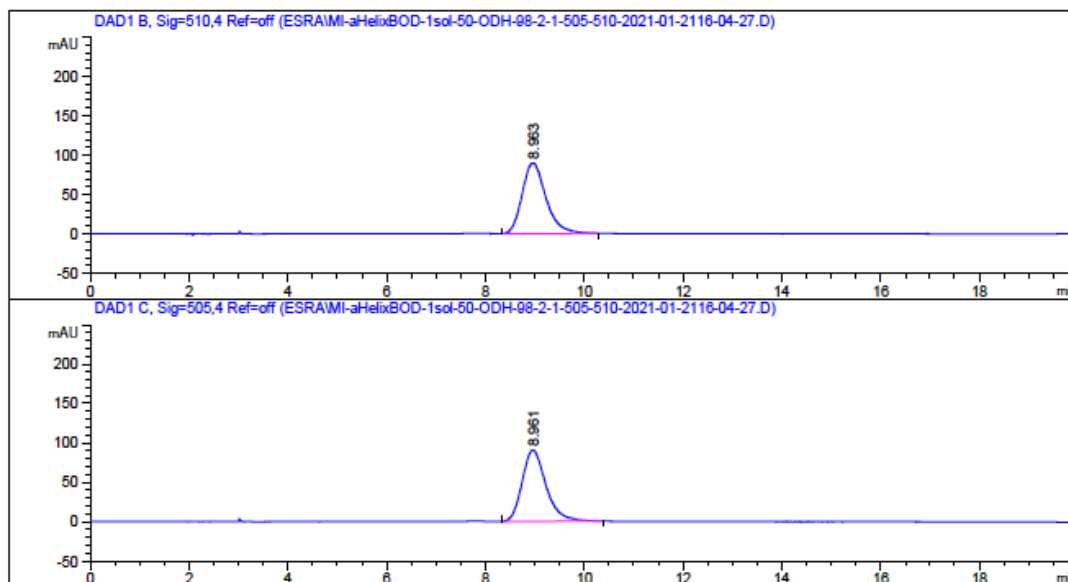


Figure B. 50. HPLC chromatogram of enantiomerically enriched 73be



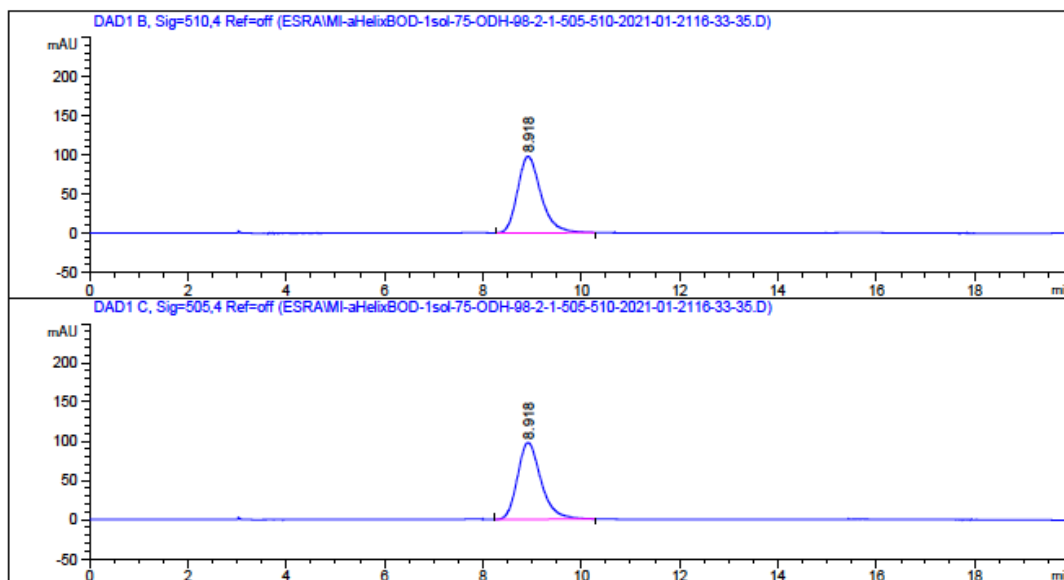
Signal 1: DAD1 B, Sig=510,4 Ref=off

Peak #	RetTime [min]	Type	Width [min]	Area [mAU*s]	Height [mAU]	Area %
1	8.963	BB	0.4515	3003.61328	89.73844	100.0000

Signal 2: DAD1 C, Sig=505,4 Ref=off

Peak #	RetTime [min]	Type	Width [min]	Area [mAU*s]	Height [mAU]	Area %
1	8.961	BB	0.4640	3037.00146	90.27879	100.0000

Figure B. 51. HPLC Chromatogram of (-)-BODIPY **96** at 50 °C



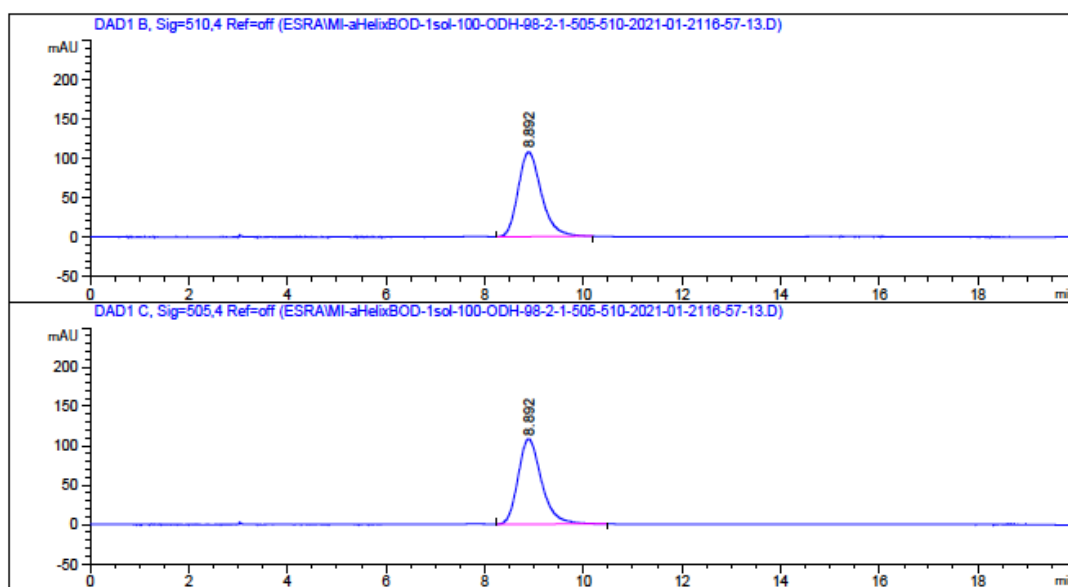
Signal 1: DAD1 B, Sig=510,4 Ref=off

Peak #	RetTime [min]	Type	Width [min]	Area [mAU*s]	Height [mAU]	Area %
1	8.918	BB	0.4621	3227.66431	97.40687	100.0000

Signal 2: DAD1 C, Sig=505,4 Ref=off

Peak #	RetTime [min]	Type	Width [min]	Area [mAU*s]	Height [mAU]	Area %
1	8.918	BB	0.4222	3244.37427	97.88682	100.0000

Figure B. 52. HPLC Chromatogram of (-)-BODIPY **96** at 75 °C



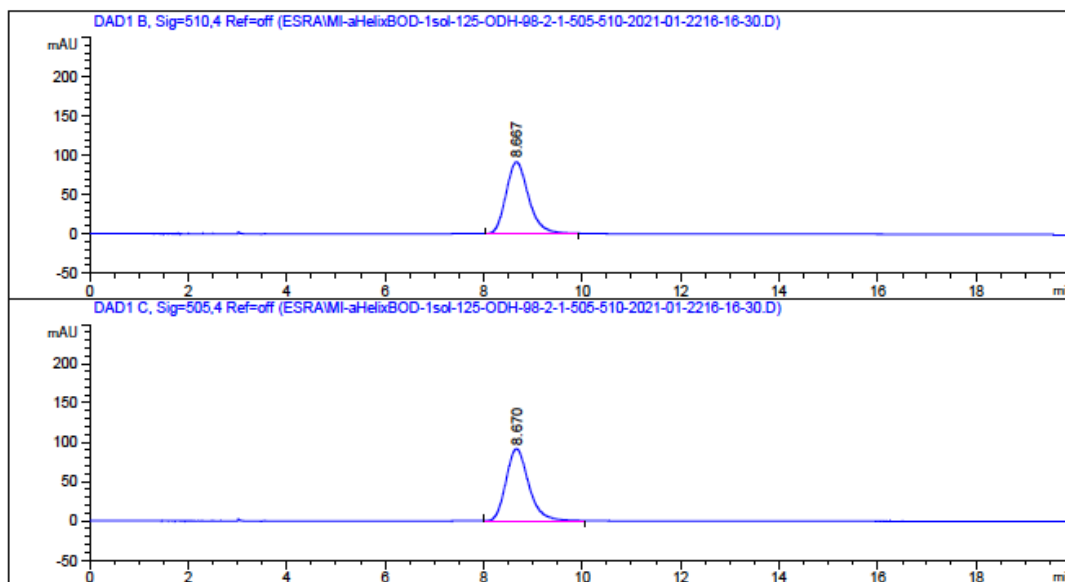
Signal 1: DAD1 B, Sig=510,4 Ref=off

Peak #	RetTime [min]	Type	Width [min]	Area [mAU*s]	Height [mAU]	Area %
1	8.892	BB	0.4313	3534.71582	107.46067	100.0000

Signal 2: DAD1 C, Sig=505,4 Ref=off

Peak #	RetTime [min]	Type	Width [min]	Area [mAU*s]	Height [mAU]	Area %
1	8.892	BB	0.4581	3590.99292	108.21491	100.0000

Figure B. 53. HPLC Chromatogram of (-)-BODIPY 96 at 100 °C



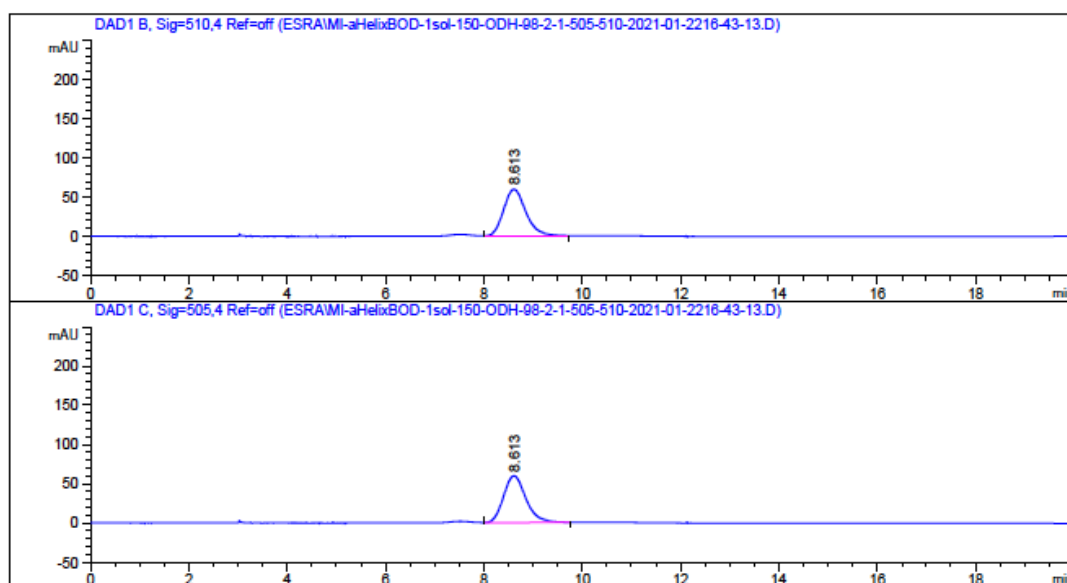
Signal 1: DAD1 B, Sig=510,4 Ref=off

Peak #	RetTime [min]	Type	Width [min]	Area [mAU*s]	Height [mAU]	Area %
1	8.667	BB	0.4343	2898.66748	91.06919	100.0000

Signal 2: DAD1 C, Sig=505,4 Ref=off

Peak #	RetTime [min]	Type	Width [min]	Area [mAU*s]	Height [mAU]	Area %
1	8.670	BB	0.4387	2928.68408	91.55736	100.0000

Figure B. 54. HPLC Chromatogram of (-)-BODIPY **96** at 125 °C



Signal 1: DAD1 B, Sig=510,4 Ref=off

Peak #	RetTime [min]	Type	Width [min]	Area [mAU*s]	Height [mAU]	Area %
1	8.613	BB	0.3761	1868.30725	59.45347	100.0000

Signal 2: DAD1 C, Sig=505,4 Ref=off

Peak #	RetTime [min]	Type	Width [min]	Area [mAU*s]	Height [mAU]	Area %
1	8.613	BB	0.3900	1873.17346	59.62061	100.0000

Figure B. 55. HPLC Chromatogram of (-)-BODIPY **96** at 150 °C

C. HRMS DATA

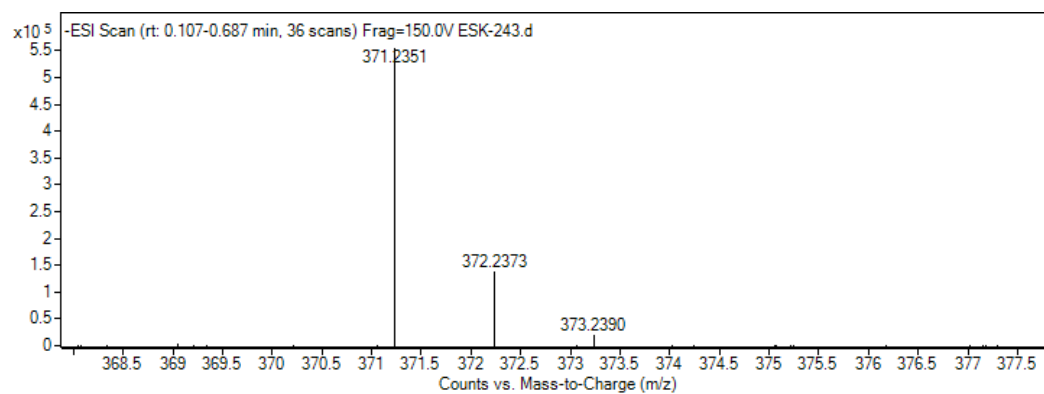


Figure C. 1. Mass Spectrum of **34an**

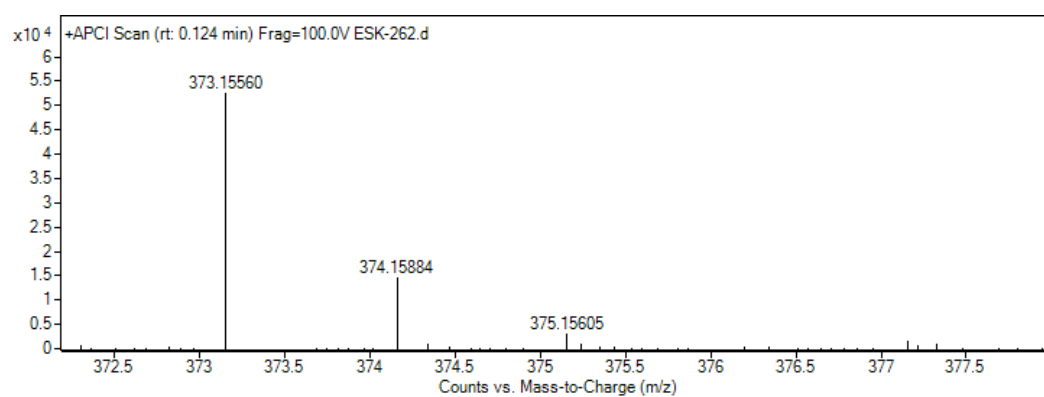


Figure C. 2. Mass Spectrum of **34ca**

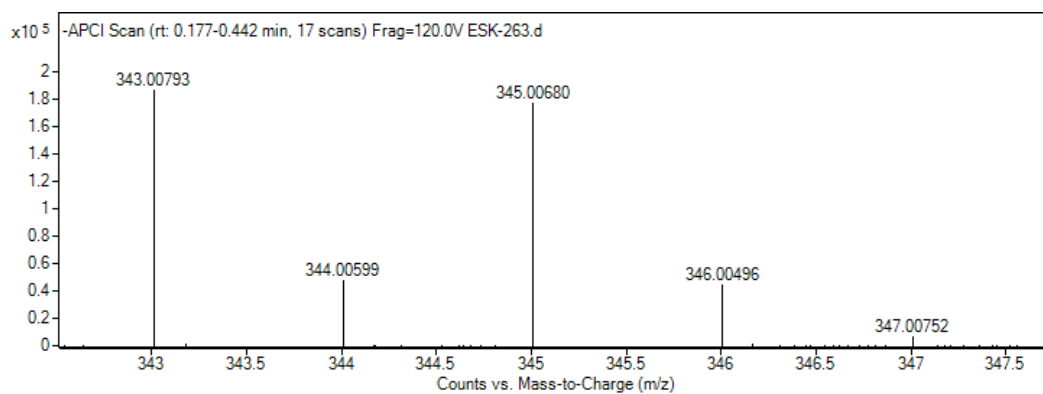


Figure C. 3. Mass Spectrum of **34da**

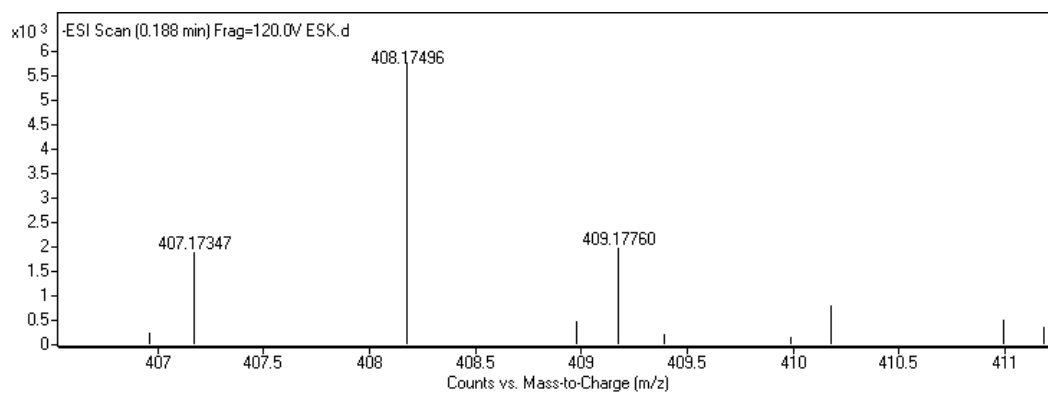


Figure C. 4. Mass Spectrum of **73aa**

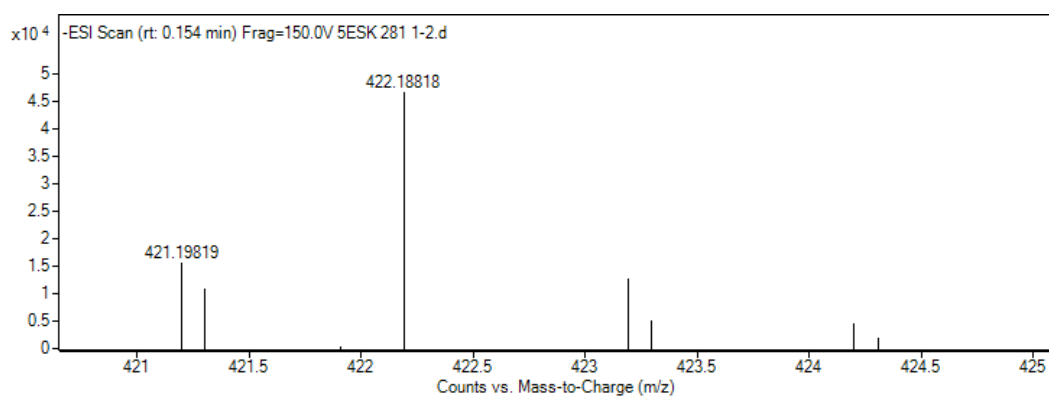


Figure C. 5. Mass Spectrum of **73ab**

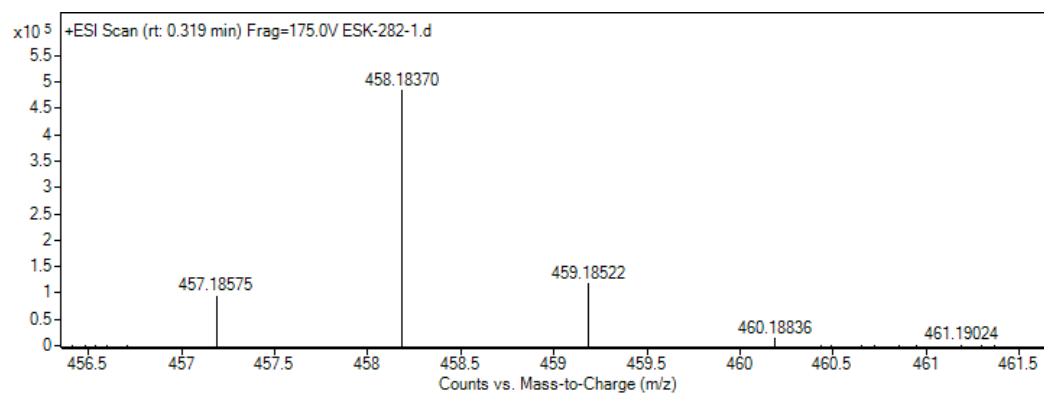


Figure C. 6. Mass Spectrum of **73ac**

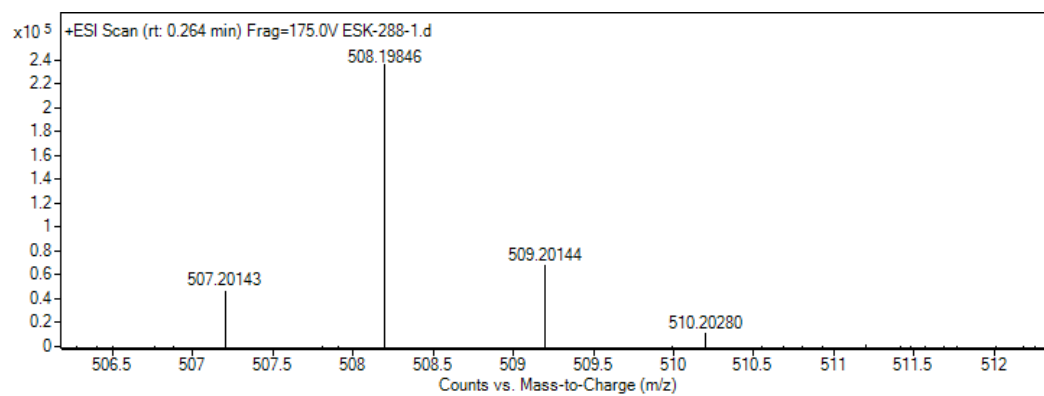


Figure C. 7. Mass Spectrum of **73ad**

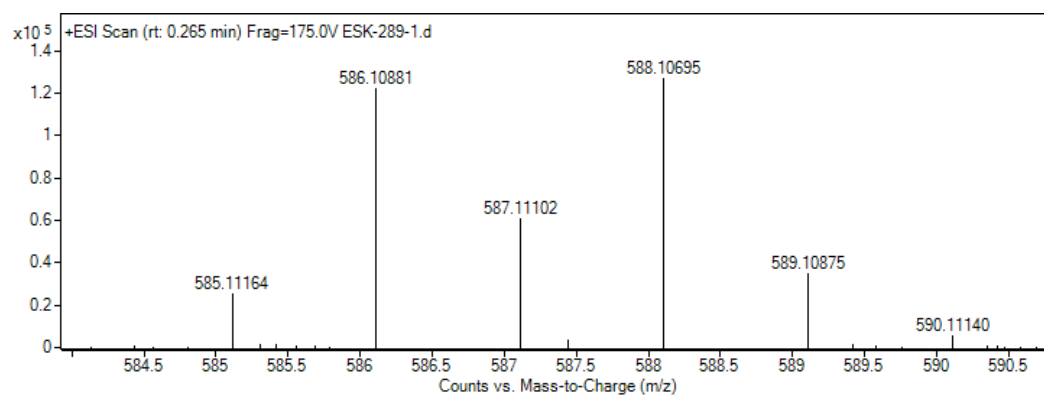


Figure C. 8. Mass Spectrum of **73ae**

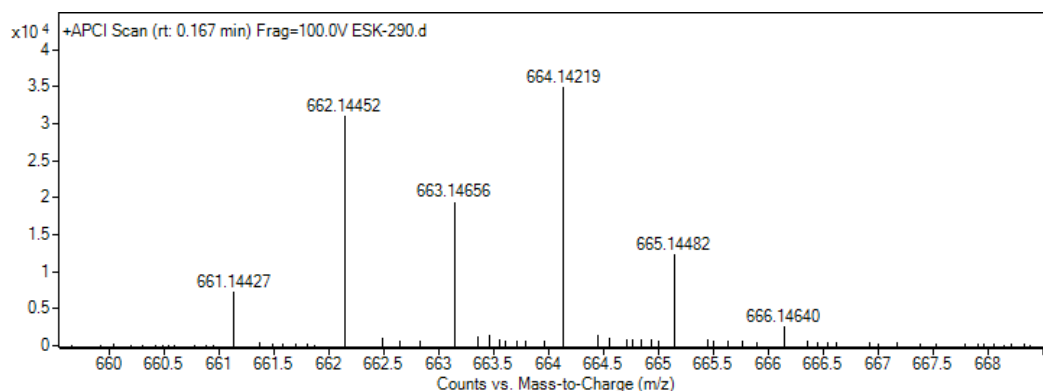


Figure C. 9. Mass Spectrum of **73be**

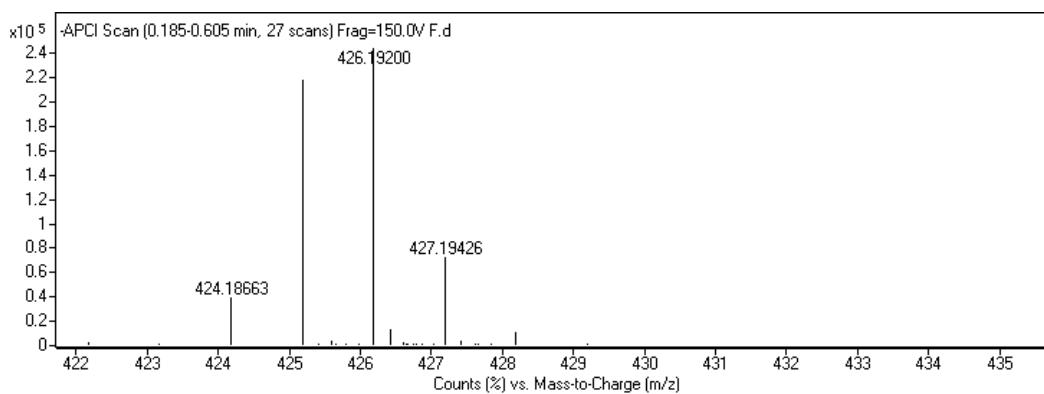


Figure C. 10. Mass Spectrum of **95**

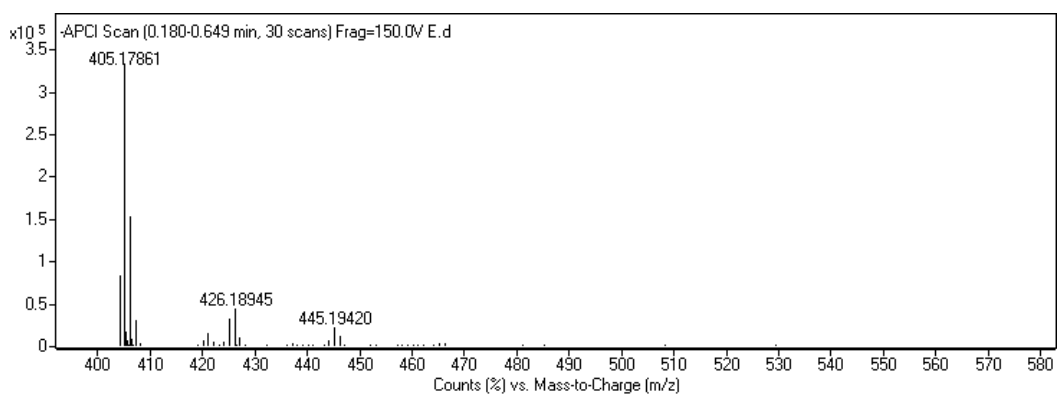


Figure C. 11. Mass Spectrum of **96**

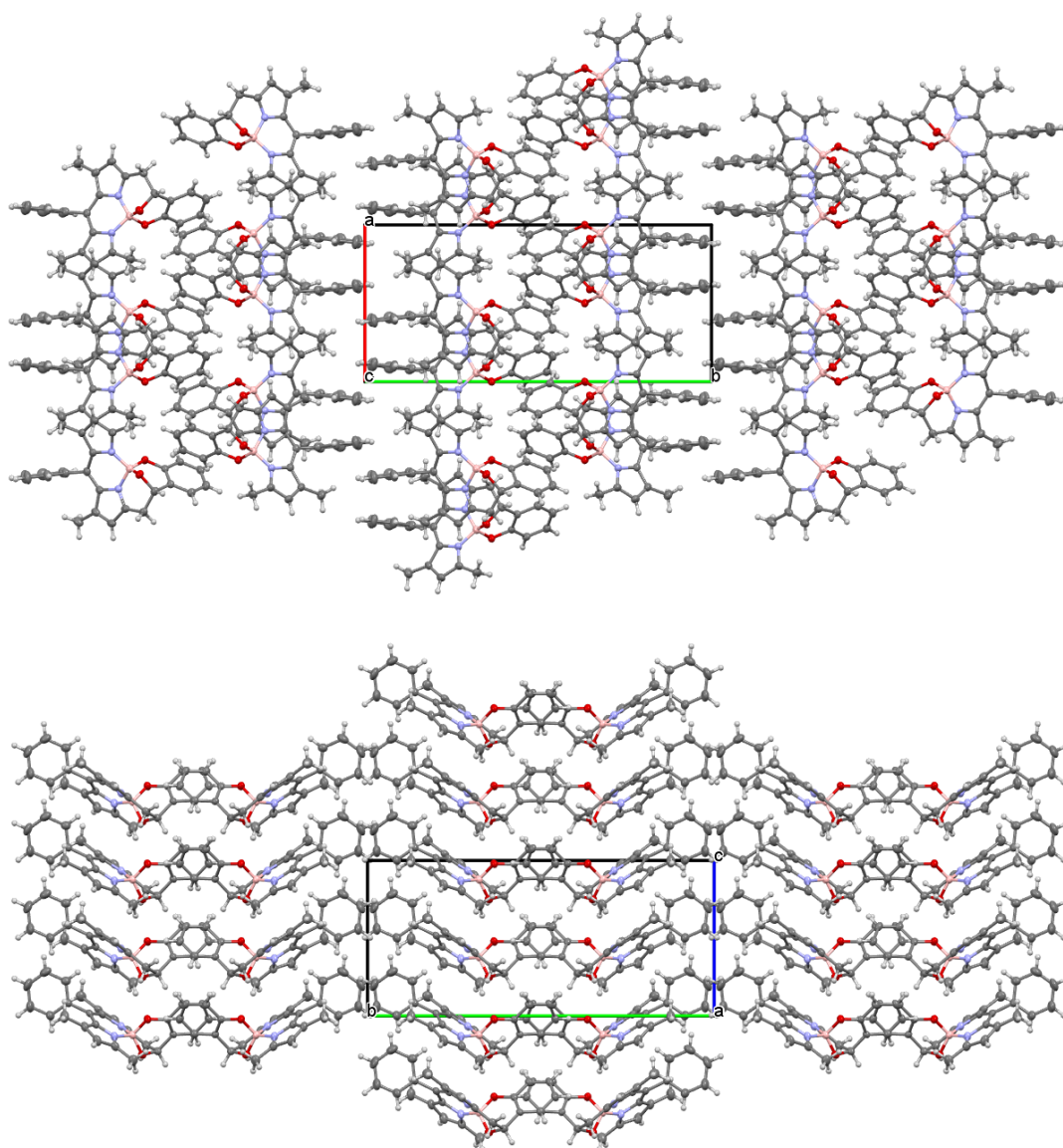
D. X-RAY DATA

X-RAY Data for BODIPY 96

For the crystal structure determination, single-crystal of the compound BODIPY 96 was used for data collection on a four-circle Rigaku R-AXIS RAPID-S diffractometer (equipped with a two-dimensional area IP detector). Graphite-monochromated Mo-K α radiation ($\lambda = 0.71073 \text{ \AA}$) and oscillation scans technique with $\Delta\omega = 5^\circ$ for one image were used for data collection. The lattice parameters were determined by the least-squares methods on the basis of all reflections with $F^2 > 2\sigma(F^2)$. Integration of the intensities, correction for Lorentz and polarization effects and cell refinement were performed using CrystalClear (Rigaku/MSI Inc., 2005) software. The structures were solved by direct methods using SHELXS-97 which allowed for the location of most of the heaviest atoms, with the remaining non-hydrogen atoms being located from different Fourier maps calculated from successive full-matrix least squares refinement cycles on F^2 using SHELXL-97. All non-hydrogen atoms were refined using anisotropic displacement parameters. Hydrogens attached to carbons were located at their geometric positions using appropriate HFIX instructions in SHELXL. The final difference Fourier maps showed no peaks of chemical significance.

Crystal data for BODIPY 96: C₂₆H₂₃N₂O₂B, crystal system, space group: orthorhombic, Pca2₁; (no:29); unit cell dimensions: $a = 9.8114(5)$, $b = 21.6884(8)$, $c = 9.7138(6) \text{ \AA}$, $\alpha = 90$, $\beta = 90$, $\gamma = 90^\circ$; volume; $2067.0(3) \text{ \AA}^3$, $Z=4$; calculated density: 1.306 g/cm^3 ; absorption coefficient: 0.082 mm^{-1} ; $F(000)$: 856; θ -range for data collection $2.4\text{--}26.0^\circ$; refinement method: full matrix least-square on F^2 ; data/parameters: 4026/285; goodness-of-fit on F^2 : 1.060; final R -indices [$I > 2\sigma(I)$]: $R_1 = 0.043$, $wR_2 = 0.103$; largest diff. peak and hole: 0.177 and $-0.164 \text{ e \AA}^{-3}$.

CCDC-2095290 number contains the supplementary crystallographic data for this structure. These data are provided free of charge via the joint CCDC/FIZ Karlsruhe deposition service www.ccdc.cam.ac.uk/structures



Stacking of the molecules with the unit cell viewed down along the (top) c -axis and the (bottom) a -axis. Note: The strongest intermolecular interaction is the X-H \cdots Cg (Pi-Ring) interaction [C26-H \cdots C20/C25(ring centroid) 3.585(4) Å]. The π - π stacking interactions are relatively weak, for which the ring centroids are found to be in the range of 4.90–5.95 Å.

CURRICULUM VITAE

PERSONAL INFORMATION

Surname, Name: Dündar, Esra
Nationality: Turkish (TC)
Date and Place of Birth: 18 August 1988, Rize
Marital Status: Married
Phone: +90 312 210 76 09
email: ekanber@metu.edu.tr

EDUCATION

Degree	Institution	Year of Graduation
MS	METU Chemistry	2015
BS	METU Chemistry Education	2012
High School	Anatolian Teacher High School, Rize	2006

WORK EXPERIENCE

Year	Place	Enrollment
2015-Present	METU Chemistry	Research and Teaching Assistant
2011-2012 Spring	Mehmet Emin Resulzade Anatolian High School	Intern Chemistry Teacher
2011-2012 Fall	METU Development Foundation Private High School	Intern Chemistry Teacher

FOREIGN LANGUAGES

Advanced English

PUBLICATIONS

1. Işık, M.; **Dündar, E.**; Şahin, E.; Tanyeli, C. *Chem. Commun.*, **2022**, 58, 7188-7191.
2. **Dündar, E.**; Tanyeli, C. *Tetrahedron Lett.* **2021**, 73, 153153.
3. **Kanberoğlu, E.**; Tanyeli, C. *Asian J. Org. Chem.* **2016**, 5, 114-119.